DIFFERENTIAL ROLES FOR HEDGEHOG SIGNALING IN MOTOR NEURON DEVELOPMENT

_____

A Dissertation
Presented to
The Faculty of the Graduate School
University of Missouri-Columbia

_____

In Partial Fulfillment
of the Requirements for the Degree

Doctor of Philosophy

_____

by
GARY VANDERLAAN

Dr. Anand Chandrasekhar, Dissertation Advisor

July, 2006

The undersigned, appointed by the Dean of the Graduate School, have

examined the thesis entitled

DIFFERENTIAL ROLES FOR HEDGEHOG SIGNALING
IN MOTOR NEURON DEVELOPMENT

Presented by Gary Vanderlaan

A candidate for the degree of Doctor of Philosophy of Biological Sciences

And hereby certify that in their opinion it is worthy of acceptance.

_____
Professor Anand Chandrasekhar

_____
Professor Steve Alexander

_____
Professor Karen Bennett

_____
Professor Mannie Liscum

_____
Professor Steve Nothwehr

ACKNOWLEDGEMENTS

LIST OF TABLES

LIST OF FIGURES

ABSTRACT

Induction of neurons in the correct number and location is essential for the proper development and function of a nervous system. Signaling mediated by the Hedgehog (Hh) family of secreted proteins plays an important role in the induction of the vertebrate branchiomotor neurons (BMNs), which are located in the brainstem and regulate chewing, swallowing, and sound production. Numerous disorders result from aberrant Hh signaling ranging from skin or brain cancers to neurodegenerative disorders.

The Gli family of zinc-finger transcription factors mediates Hedgehog (Hh) signaling in all vertebrates. However, the role of the Gli genes in ventral neural tube patterning, in particular motor neuron induction, has diverged across species. For instance, zebrafish *gli1* is required for the development of motor neurons in the brainstem but not in the spinal cord, whereas the mouse *gli* genes appear to be dispensable for motor neuron formation. Furthermore, the expression of some Hh-regulated genes (e.g. *ptc1*, *net1a*, *gli1*) is mostly unaffected in the *detour* (*gli1⁻*) mutant hindbrain, suggesting that other Gli transcriptional activators may be involved. To better define the roles of the zebrafish *gli* genes in motor neuron induction and in Hh-regulated gene expression, we examined these processes in *you-too* (*yot*) mutants, which encode dominant repressor forms of Gli2 (Gli2^{DR}), and following morpholino-mediated knockdown of *gli3* function. Motor neuron induction at all axial levels was reduced in *yot* (*gli2^{DR}*) mutant embryos. In addition, Hh target gene expression at all axial levels except in rhombomere 4 was also reduced,

suggesting an interference with the function of other Glis. Indeed, morpholino-mediated knockdown of Gli2^{DR} protein in *yot* mutants led to a suppression of the defective motor neuron phenotype, suggesting that mutant Gli2^{DR} protein functions by a dominant negative mechanism to repress motor neuron induction. Further, *gli2* knockdown in wild type embryos generated no discernable motor neuron phenotype, while *gli3* knockdown reduced motor neuron induction in the hindbrain and spinal cord. Significantly, *gli2* or *gli3* knockdown in *detour* (*gli1*⁻) mutants revealed roles for Gli2 and Gli3 activator functions in *ptc1* expression and spinal motor neuron induction. Similarly, *gli1* or *gli3* knockdown in *yot* (*gli2^{DR}*) mutants resulted in severe or complete loss of motor neurons, and of *ptc1* and *net1a* expression, in the hindbrain and spinal cord. In addition, *gli1* expression, a known Hh-regulated gene, was greatly reduced in *yot* mutants following *gli3*, but not *gli1*, knockdown, suggesting that Gli3 activator function is specifically required for *gli1* expression. These observations demonstrate that Gli activator function (encoded by *gli1*, *gli2*, and *gli3*) is essential for motor neuron induction and Hh-regulated gene expression in zebrafish.

Although many genes required for Hedgehog (Hh)-mediated specification of vertebrate motor neurons have been characterized, much less is known about the temporal aspect of the specification event itself. We utilized cyclopamine, a potent inhibitor of Hh signaling, to examine the temporal requirement for Hh signaling during specification of different populations of branchiomotor (BMN) or somatomotor neurons in the zebrafish head and trunk. Remarkably, while the Hh signal is continuously expressed in midline tissue between 10-30 hpf at all axial

levels, Hh signaling is required at different times for the specification of motor

neurons at all axial levels. For instance, spinal motor neurons, a somatomotor

neuron population, require Hh signaling over a long period, from 10-27 hpf. By

contrast, the nVI abducens somatomotor neuron and the nVII facial BMN

populations in the hindbrain appear to be completely specified by 21 hpf.

Furthermore, in the anterior hindbrain, some nV trigeminal BMNs require Hh

signaling prior to 15 hpf. Birth date analysis using BrdU labeling also reveals that

different BMN populations enter S-phase en masse at different times. Our

results demonstrate that different populations of motor neurons are specified by

Hh signals at different times during development, and suggest that these

differences may generate subtype identities.

CHAPTER 1

INTRODUCTION

1.1   EARLY EVENTS IN NERVOUS SYSTEM DEVELOPMENT

1.1.1   Neuronal Differentiation Paradigm

     To understand neuronal differentiation, it is helpful to define the different stages an undifferentiated cell might traverse through while acquiring a cell fate program: (1) competence, (2) specification, (3) commitment, and (4) differentiation (Wilson and Edlund, 2001). A cell's competence defines its capability of acquiring progenitor status, so long as appropriate cues and morphogens are made available at critical periods in development. These cues transform naïve cells and specify a progenitor status that is not yet stable. Specified progenitor cells are sensitive to specification blockers that, if present, could delay or reverse the differentiation program. Commitment then is a state in which cells have acquired progenitor status, but are no longer sensitive to specification reversal. As neural progenitors exit the cell cycle, new, fate-specific combinatorial transcription factor codes facilitate the differentiation program. Finally, the story of neuronal development is one of synergy amongst several

signaling pathways, used and re-used at different times, and places in development.

1.1.2   Neural Plate Induction

To get differentiated neurons, an embryo must first build the structures conducive for neuronal specification. This is not a trivial task, albeit deceptively routine, as an embryo must specify first neuroectoderm from naïve ectoderm in order to create a neural plate, a sheet of neuroepithelium in which neurogenesis is made possible.

Neural induction was first demonstrated in 1938 by Hans Spemann by grafting the dorsal lip blastopore of an early blastula stage Xenopus embryo to the ventral side of a host gastrula (Spemann, 1938). In doing so, an ectopic, secondary axis complete with neural tube is formed demonstrating that the Spemann organizer is sufficient for neural induction of the animal pole, a mass of naïve ectoderm. The molecular mechanism for this neural induction was discovered using simple animal cap assays (Wilson and Edlund, 2001). Cultured animal cap explants differentiate into epidermis, a tissue with shared lineage to neuroectoderm. However, when dissociated, cultured animal caps differentiated into neural tissue, suggesting that the default differentiation path of naïve ectoderm is neuronal. Dissociated animal caps treated with BMP generate epidermis, while BMP antagonists generate neural tissue (Wilson and Edlund, 2001). Thus, the Neural-Default model suggests that naïve ectoderm will

differentiate into neural tissue naturally, but BMP signaling is sufficient to convert ectoderm into epidermis (Wilson and Edlund, 2001).

The molecular basis for BMP antagonism from the Spemann Organizer for neuroectoderm induction is now well described. Neural ectoderm can be induced from many different BMP antagonists: Follistatin (Hemmati-Brivanlou et al., 1994), Noggin (Knecht et al., 1995; Lamb and Harland, 1995), Chordin (Sasai et al., 1995), Xnr3 (Hansen et al., 1997), Cerberus (Bouwmeester et al., 1996), and Gremlin (Hsu et al., 1998). Although each of these BMP antagonists is sufficient to induce neural plate formation of anterior character, the Spemann Organizer itself is dispensable for neural plate formation (Wilson and Edlund, 2001). Mice with mutations in *HNF3B* (Ang and Rossant, 1994) or *arkadia* (Episkopou et al., 2001) fail to form the Spemann Organizer, yet can still form a neural plate (Klingensmith et al., 1999)().

The earliest demonstration of neural induction originates at the blastula stage, well before Node/Organizer formation. FGF signaling derived from organizer precursor cells, the posterior cells of Koller's Sickle, is sufficient to induce neuroectoderm (Streit et al., 2000), suggesting that FGF signaling rather than BMP antagonism might initiate neural tissue induction. This is further bolstered by differences between dorsal and ventral ectoderm at late blastula stages, where transcripts of the early neural marker Sox3 are enriched in dorsal ectoderm while activated, phosphorylated forms of Smad proteins, the BMP effectors, are enriched in the ventral ectoderm (Kurata et al., 2001; Penzel et al., 1997). Thus, neuroectoderm induction involves at least FGF signaling and BMP

antagonism, with the strong possibility that FGF signaling initiates the induction event (Streit et al., 2000).

Positional axis information, anterior/posterior and dorsal/ventral, is further specified by multiple signaling pathways. Both BMP antagonism and retinoic acid are each sufficient to generate anterior neural plate (Bouwmeester et al., 1996; Durston et al., 1989; Hansen et al., 1997; Hemmati-Brivanlou et al., 1994; Hsu et al., 1998; Knecht et al., 1995; Lamb and Harland, 1995; Sasai et al., 1995). FGF signaling is necessary and sufficient to induce posterior neural plate (Cox and Hemmati-Brivanlou, 1995; Kengaku and Okamoto, 1995; Lamb and Harland, 1995; Ribisi et al., 2000). BMP signaling, from the lateral edges of the neural plate, dorsalizes the neural plate (Lee and Jessell, 1999) while Shh signaling, from axial mesoderm / notochord, ventralizes the neural plate (Jessell, 2000).

1.1.3   Neurulation

Two morphological mechanisms of neurulation, the conversion of the neural plate into a neural tube, have been described (Copp et al., 2003; Lowery and Sive, 2004). Primary and secondary neurulation differ mainly in starting cell character, either epithelial or mesenchymal, respectively (Criley, 1969; Griffith et al., 1992; Lowery and Sive, 2004).

In primary neurulation, epithelial sheets columnarize, and sink at the midline while neural folds elevate along the lateral edges (Figure 1A-B) (Copp et

4

al., 2003; Lowery and Sive, 2004; Schmitz et al., 1993). Apical (outside)

surfaces of the neural plate then converge at the midline in a process known as

fusion or apposition (Figure 1C). Convergent-extension movements facilitate the

bending of the neural plate for the formation of the neural groove (Figure 1D).

Fusion of the lateral edges of the neural groove completes the formation of the

neural plate, and as a consequence, a lumen or neurocoele is formed (Figure

1E) (Copp et al., 2003; Lowery and Sive, 2004). Non-neural ectoderm from the

distal, lateral edges of the original neural plate subsequently covers the neural

plate (Copp et al., 2003). Secondary neurulation begins with mesenchymal cells

which condense into a rod-like structure called a medullary cord (Lowery and

Sive, 2004), followed by the appearance of a lumen.

Neural tube formation in zebrafish is a subtle variation of primary

neurulation (Lowery and Sive, 2004; Papan and Campos-Ortega, 1993), the

difference arising in how the lumen is created. After fusion of the neural plate in

teleosts, a neural keel (Figure 1D-(i)) is generated followed by a neural rod

(Figure 1D-(ii)). Apoptotic-driven cavitation then generates a lumen (Figure 1D-

(iii), 1E) (Lowery and Sive, 2004; Papan and Campos-Ortega, 1993). As the

substrate for neural tube formation is epithelial in character, zebrafish embryos

therefore undergo primary neurulation (Criley, 1969; Griffith et al., 1992).

A
Neuroectoderm

B
Neural Plate

C
Dorsal
Ventral

D
Neural Groove

D-(i)
Neural Keel

D-(ii)   D-(iii)
Neural Rod
Lumenal Apoptosis

E
Neural Tube

6
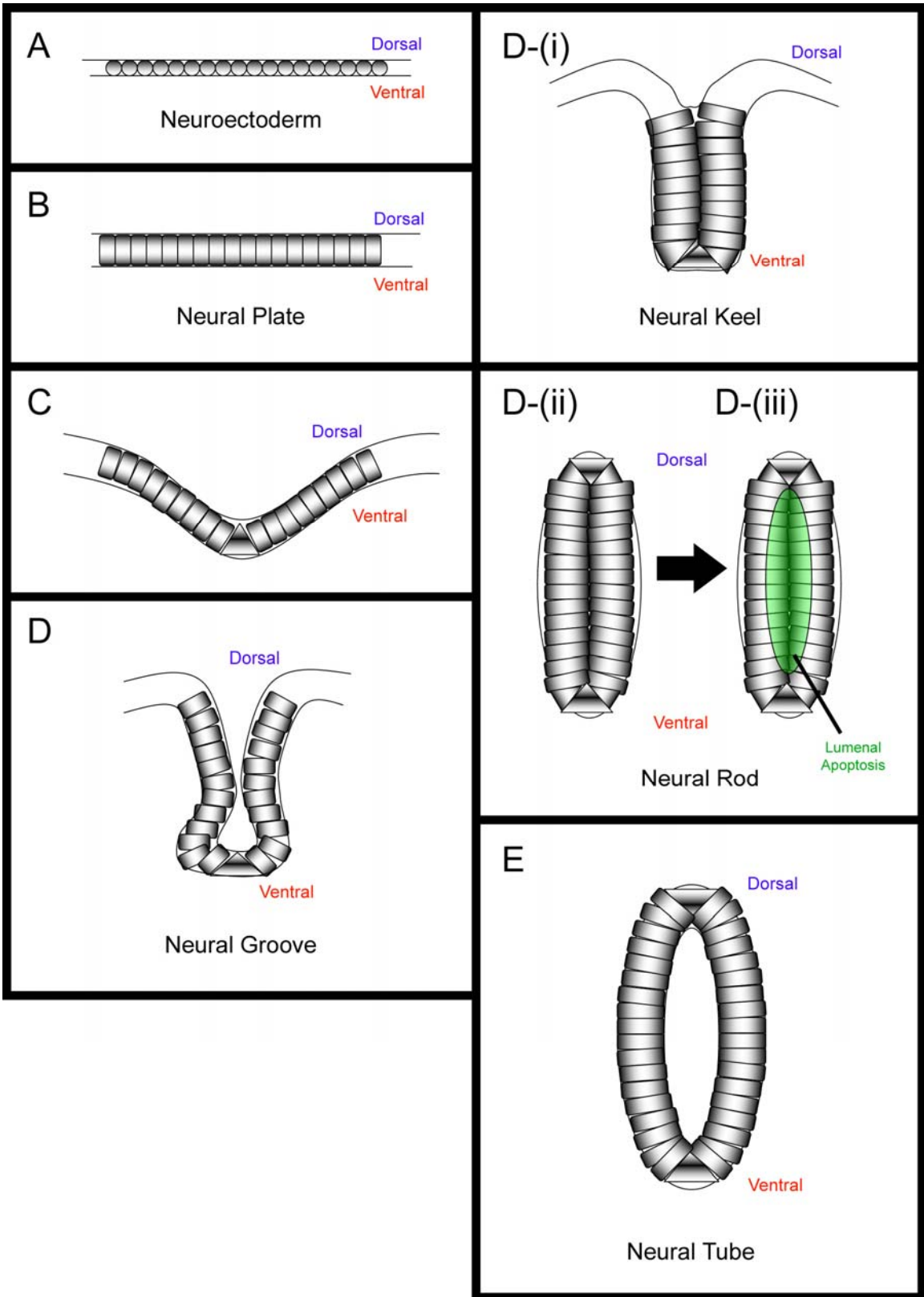
FIGURE 1. Primary Neurulation in Mouse and Zebrafish

(A): In mouse and zebrafish, neuroectoderm (gray circles) initially presumptive neural plate as uncondensed sheets. **(B):** In all vertebrates, neuroectoderm (gray rectangles) columnarizes into neuroepithelium to form the neural plate. **(C):** The ventral side of the neural plate invaginates as lateral edges rise for apposition and fusion using convergent-extension mechanisms. Floor plate (gray triangle) emerges at this time. **(D)** and **(E):** In mouse, fusion of the lateral edges of the neural plate generates the neural tube with a central lumen, called a neurocoele. (**D-(i)**): In zebrafish, ongoing fusion of lateral neural plate generates the neural keel, a structure lacking a neurocoele. (**D-(ii)**): In zebrafish, a neural rod is formed which resembles a neural plate except for the missing neurocoele. (**D-(iii)**): Zebrafish neural rods form neurocoeles by an apoptotic-driven cavitation event (red shading). **(E):** Both mouse and zebrafish neural tubes are characterized by a central lumen, a ventrally located floor plate (gray triangle), and a dorsally located roof plate (inverted gray triangle).

The mechanism for neural tube formation is best understood in rodents. Mutations arising in the non-canonical Wnt signaling pathway (Planar Cell Polarity Pathway) eliminate neural tube closure. For instance, *flamingo*, *strabismus*, *scribbled*, and *dishevelled2* are all necessary for neural tube closure (Curtin et al., 2003; Hamblet et al., 2002; Murdoch et al., 2001; Murdoch et al., 2003). Failure to initiate closure of the neural tube is followed by massive neurodegeneration, a process known as anencephaly (Copp et al., 2003).

1.1.4   Neurogenesis

Neurogenesis is the process by which neural progenitors are specified from a common pool of neuroectodermal cells. Notch signaling controls acquisition of neural determination via lateral inhibition (Figure 2), whereby activated Notch signaling in neighboring cells blocks proneural development thereby promoting neuroectodermal status (Baker, 2000; Gridley, 1997).

In cells that produce the greatest amount of Delta, proneural bHLH expression is not expressed and these cells acquire neuronal progenitor status (Figure 2) (Artavanis-Tsakonas et al., 1999). In teleost and amphibian gain-of-function experiments, misexpression of *delta* throughout the embryo is sufficient to severely reduce primary neuron formation (Appel and Eisen, 1998; Chitnis et al., 1995; Haddon et al., 1998b). Similarly, misexpression of a constitutively-active truncated *notch1* receptor in frogs is sufficient to reduce neuronal differentiation (Coffman et al., 1993). Conversely, in both zebrafish and frogs,

8

misexpression of a dominant-negative *delta1* ligand, in which the intracellular domain is deleted, is sufficient to induce supernumerary primary neurons in the spinal cord (Appel et al., 1999; Chitnis et al., 1995).

Within neuroectoderm, clusters of proneural cells express a set of proneural bHLH-class transcription factors of the Achaete-Scute-Complex (ASC) (Figure 3D) (Baker, 2000). In flies, proneural genes include *achaete*, *scute*, *lethal of scute*, and *atonal*, and are required for neuronal determination (Baker, 2000). Numerous examples in vertebrates exist where neural precursors are also eliminated in proneural mutants. For instance, in mouse, mutations in the vertebrate ortholog to *atonal*, *neurogenin1*, disrupt neural progenitor development in the proximal cranial sensory ganglia (Ma et al., 1998). Likewise, *neurogenin2* knockout mice lack neural precursors for epibranchial placode-derived sensory neurons (Fode et al., 1998), while mutations in the proneural mouse *achaete-scute-complex* (*mash1*) result in severe reductions in olfactory neuron cell number (Cau et al., 1997). In zebrafish, the proneural gene *neurogenin1* drives expression of *deltaA* and *deltaD*, ligands for the Notch signaling pathway (Appel and Eisen, 1998; Haddon et al., 1998b). Proneural genes confer neural progenitor status by promoting production of Delta ligand and therefore activation of Notch signaling in neighboring neuroectodermal cells (Figure 3) (Baker, 2000; Gridley, 1997).

Key	
▬▬	Delta (ligand)
➡	Notch (receptor)
🟡	Neuronal Fate
🔵	Neuroectoderm

(Modified from Baker, 2000)
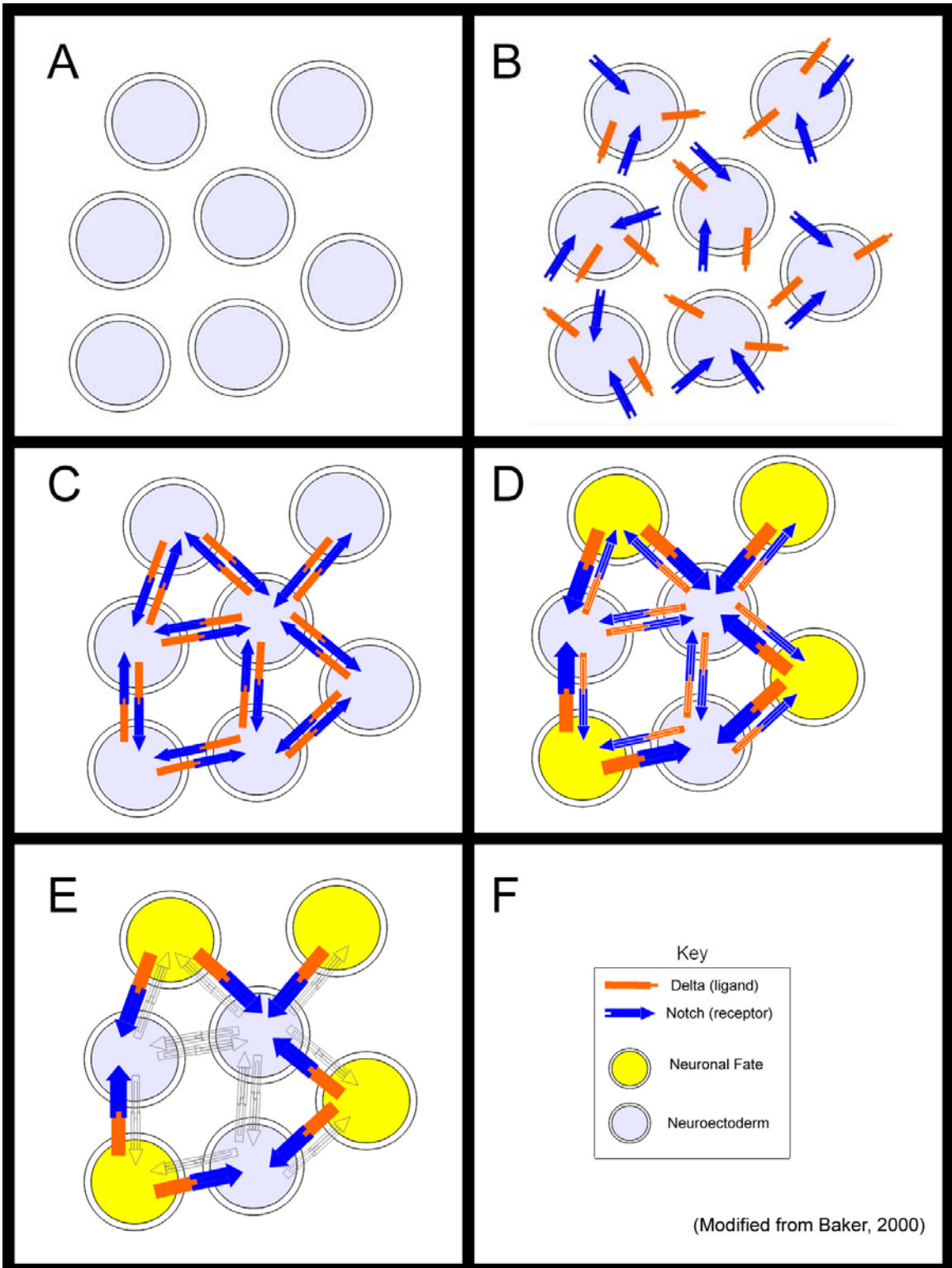
FIGURE 2. Notch-Delta Signaling and Lateral Inhibition

(A): Neuroectoderm (light blue circles) initially exists in a naive state. **(B):** Neuroectoderm cells produce and insert into the membranes, Delta ligands (orange) and Notch receptors (dark blue).

(C): As receptors and ligands are transmembrane proteins, protein-protein interactions are limited to neighboring neuroectodermal cells only. **(D)** and **(E):** Activation of Notch signaling inhibits proneural development through a negative feedback loop. Cells receiving the most Notch signaling (center three cells, light blue) progressively fail to generate Delta ligands over time, and therefore fail to become neuronal, remaining as neuroectoderm. Cells that receive the least amount of Notch signaling (distal three cells, yellow) adopt a proneural program.

As both ligand and receptor are membrane proteins, Notch signaling is a contact-dependent pathway (Figure 2C-E; see also Figure 3). Delta is a single pass membrane bound ligand for the Notch receptor (Baker, 2000; Gridley, 1997). The Notch receptor is first generated as a single precursor peptide which undergoes several cleavage events for activation (Figure 3C) (Baker, 2000; Gridley, 1997). Mammalian precursor Notch peptide must first be cleaved by a Furin-like convertase to generate two receptor fragments (Kidd and Lieber, 2002; Logeat et al., 1998). Both fragments heterodimerize and become inserted into the plasma membrane as a mature receptor, with an extracellular domain (ECD) and an intracellular domain (ICD) (Artavanis-Tsakonas et al., 1999; Gridley, 1997). Delta ligands, presented by proneural cells, bind to the extracellular fragment of the Notch receptor (Figure 3B-C) (Artavanis-Tsakonas et al., 1999). Upon binding of Delta ligand to Notch receptor, several cleavage events occur to generate the active Notch signaling fragment (Notch^{ICD}). First, Delta binding to Notch permits TNFα-converting enzyme (TACE) metalloprotease-mediated cleavage of the mature Notch receptor (Figure 3C) (Brou et al., 2000). Cleavage by TACE metalloprotease occurs in the Notch^{ECD} fragment, permitting internalization of Delta-Notch^{ECD} complexes by cells presenting Delta ligand (Figure 3C-D) (Brou et al., 2000). Endocytosis of Delta-bound Notch^{ECD} fragments is a critical step in the activation of Notch signaling and requires ubiquitination of Delta (Itoh et al., 2003; Parks et al., 2000). In temperature-sensitive dynamin mutants grown at restrictive temperatures, endocytosis of Notch^{ECD} fails to occur (Parks et al., 2000). Likewise, chemical-mediated

removal of the Notch^{ECD} from the Notch^{ICD} fragment is sufficient to activate Notch

reporter gene expression (Rand et al., 2000). After removal of Delta-Notch^{ECD},

the remaining fragment of the Notch receptor is cleaved inside the

transmembrane domain by γ-secretases to generate the active Notch^{ICD} signaling

peptide (Figure 3C-D) (De Strooper et al., 1999). In cell culture, Presenilin-1 is

required for γ-secretase cleavage activity. In *presenelin-1* deficient cells,

generation of Notch^{ICD} fragments is severely reduced (De Strooper et al., 1999).

Upon cleavage by γ-secretase, Notch^{ICD} free to enter the nucleus to complex with

the transcriptional activator, Su(H), for the induction of Notch target genes

(Figure 3D) (Artavanis-Tsakonas et al., 1999; Baker, 2000).

Notch-regulated genes include a second set of bHLH transcription factors

of the Enhancer of Split (E(Spl)/HES) family (Figure 3D) (Artavanis-Tsakonas et

al., 1999; Baker, 2000). Once transcribed, E(Spl) factors recruit the

transcriptional corepressor Groucho to inhibit expression of the proneural bHLH

ASC genes (Figure 3D). Misexpression of *her4*, an E(Spl) ortholog, is sufficient

to reduce both *neurogenin1* expression and primary neuron cell number in

zebrafish embryos (Takke et al., 1999). Decreased expression of *ngn1* results in

reduced levels of *delta* expression (Ma et al., 1998), and hence an attenuated

capacity to initiate Notch signaling in neighboring cells (Artavanis-Tsakonas et

al., 1999). Thus, the consequence of Notch signaling is suppression of both

Delta ligand production and proneural bHLH gene expression (Figure 3D) (Baker,

2000).
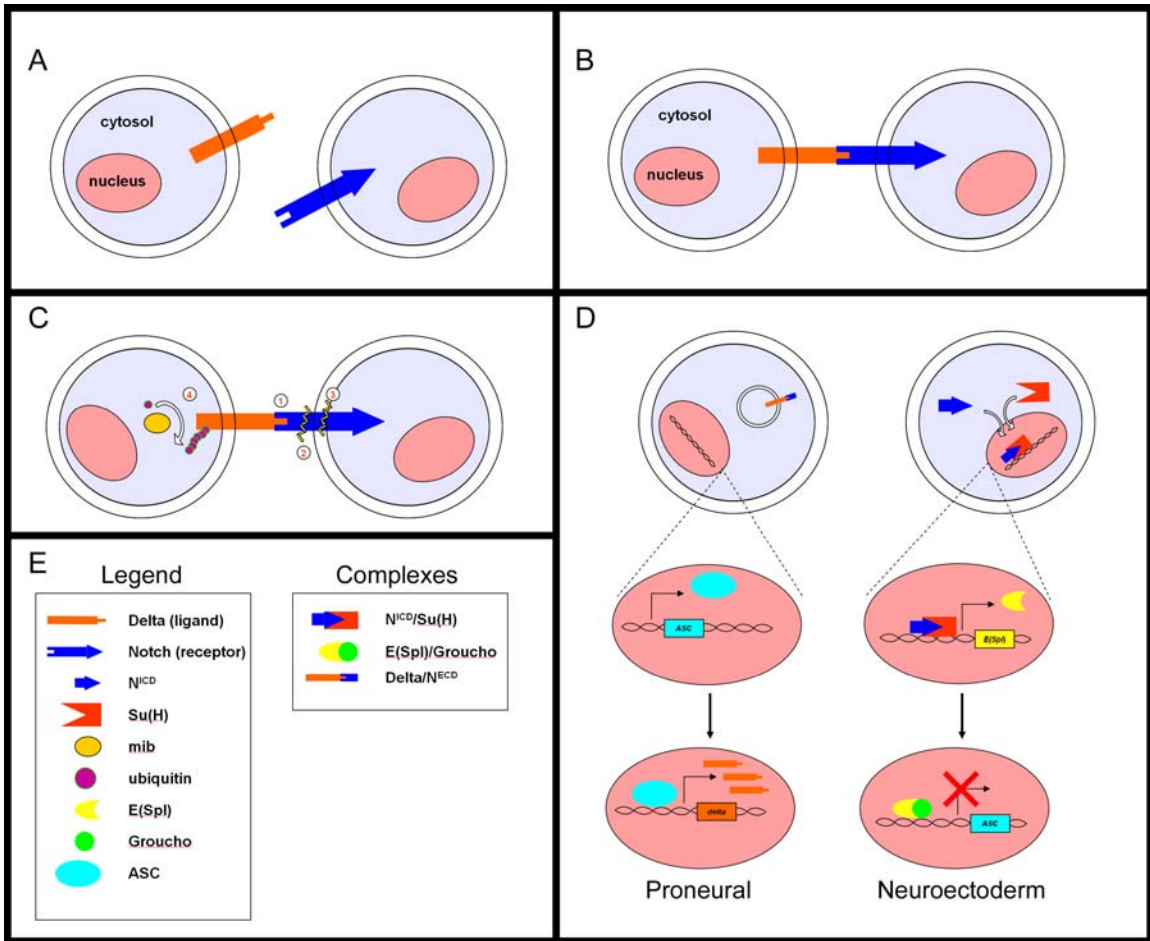
FIGURE 3. Mechanism of Notch-Delta Signaling

(A): Initially, two neighboring neuroectodermal cells produce Delta ligand (orange) and Notch receptor (dark blue arrow) signaling components. For simplicity, only Delta ligand on one cell and Notch receptor on a neighboring cell is illustrated. **(B):** Ligand-receptor interactions activate signaling from the Delta-presenting cell to the Notch-presenting cell. **(C):** Several events unfold after ligand-receptor dimerization to facilitate Notch signal transduction. First, a TACE metalloprotease cleaves full-length Notch receptor (dark blue arrow) at an extracellular domain. Second, a γ-secretase cleaves the remaining portion of the Notch receptor fragment inside the transmembrane domain. The resulting fragment, called the Notch-intracellular domain fragment (NotchICD), is free to enter the nucleus of the neuroectodermal cell on the right. In the left neuroectodermal cell, the intracellular domain of Delta ligand is ubiquitinated by the Mindbomb E3 (RING) ligase. Following ubiquitination, complexes of Delta ligand to Notch-extracellular domain fragments (NotchECD) become endocytosed. **(D):** In neuroectodermal cells with endocytosed Delta/NotchECD complexes, bHLH-class transcription factors of the Achaete-Scute-Complex (ASC) activate expression of proneural genes, including *delta*. In neuroectodermal cells in which NotchICD is produced, complexes between NotchICD and Su(H) enter the nucleus as transcriptional activators. Notch signaling activates expression of a second set of bHLH-class transcription factors of the Enhancer of Split (E(Spl)) family. E(Spl) complexes with the transcriptional corepressor, Groucho, to shut off the expression of the proneural ASC genes. Thus, cells that receive the most NotchICD fragments remain neuroectodermal while cells that produce the most Delta ligands undergo a proneural program.

Recent work has implicated ubiquitination in mediating Notch signaling (Figure 3C) (Artavanis-Tsakonas et al., 1999; Hicke, 2001; Weissman, 2001). Ubiquitin is a small peptide which covalently tags target proteins for degradation, processing, or localization (Hicke, 2001; Weissman, 2001). Ubiquitination requires three enzymes (1) E1, ubiquitin-activating enzyme, (2) E2 ubiquitin-conjugating enzyme, and (3) E3 ubiquitin ligase. Following ubiquitin activation by E1 in an ATP-dependent process, activated ubiquitin is transferred to E2, which functions as a scaffold for ubiquitin and later as an ubiquitin donor. E3 ubiquitin ligase facilitates transfer of ubiquitin from E2 to target proteins (Hicke, 2001; Weissman, 2001).

Numerous E3 ligases have been reported to regulate the Notch signaling pathway. For instance, both Sel-10/Fbw7 and Itch negatively regulate Notch signaling by promoting the *in vitro* degradation of Notch[ICD] (Qiu et al., 2000; Wu et al., 2001). In mouse *fbw7* knockouts, quantitative RT-PCR reveals up-regulation of mRNA levels for *hes1*, *herp1*, and *herp2*, indicative of elevated levels of Notch signaling (Tetzlaff et al., 2004). In contrast, LNX positively regulates Notch signaling by promoting the *in vitro* degradation of Numb, a negative regulator of the Notch signaling pathway (Nie et al., 2002). Likewise, the RING-type E3 ligase, *neuralized*, functions as a positive regulator of the Notch signaling pathway by inducing the endocytosis and degradation of Delta ligand (Deblandre et al., 2001; Lai et al., 2001; Pavlopoulos et al., 2001). Finally, in the E3 ligase *mindbomb* (*mib*) mutant, supernumerary primary neurons form in the spinal cord at the expense of later-born neurons (Itoh et al., 2003; Jiang et

al., 1996; Park and Appel, 2003; Schier et al., 1996). Further, Delta fails to internalize in cell cultures transfected with mutant *mib* (Itoh et al., 2003). Thus, *mib* E3 ligase may regulate Delta endocytosis for the activation of Notch signaling in neurogenesis (Figure 3C). **We examined the role of *mib* for neurogenesis in the zebrafish hindbrain in Chapter 3.**

1.1.5 Segmentation

Segmentation is conserved from invertebrates to higher mammals and is believed to confer a developmental foundation in which adult structures might arise. In all vertebrates, ten neuromeres, or segments, initially form along the anterior-posterior axis (Graper, 1913; Kimmel et al., 1995; Lumsden, 1990; Vaage, 1969). Of these ten, the anterior-most three neuromeres expand dramatically to become the telencephalon, the diencephalon, and the mesencephalon (midbrain). At the midbrain/hindbrain boundary, the fourth neuromere (also called rhombomere 1) becomes the cerebellum. The remaining neuromeres occupy the rhombocephalon, and therefore are called rhombomeres 2-7 (r2-r7) (Lumsden, 1990), with rhombomere 4 the earliest forming segment (Maves et al., 2002; Moens et al., 1998).

The rhombomeres are transient, lineally-restricted compartments. In chickens, clonal analysis reveals that rhombomere boundaries restrict cell mixing and have a two-segment periodicity (Fraser et al., 1990). Grafting experiments in chicken demonstrate that cells derived from even and odd rhombomeres exclude

one another (Guthrie et al., 1993) while *in vitro* cell mixing assays show that cells from even and odd rhombomeres repulse from one another compared to cells from even/even or odd/odd compartments (Wizenmann and Lumsden, 1997).

The molecular basis for rhombomere formation has been well described (Moens and Prince, 2002). Krox20, a zinc-finger transcription factor, is expressed as early as neural plate stages in presumptive r3 and r5 (Wilkinson et al., 1989). Mutations in mouse *krox20* eliminate r3 and r5 identity, misroute axonal connections, and lead to the progressive loss of the trigeminal motor neurons, a cell type born in r3 (Schneider-Maunoury et al., 1997). Mutations in zebrafish *mafB*, a bZip class transcription factor, eliminate r5 and r6 identity (Moens et al., 1996). Further, *mafB* functions cell-autonomously for r5 and r6 identity as cells lacking *mafB* become excluded from r5 and r6 of wild type embryos (Moens et al., 1998; Moens et al., 1996). Mutations in the mouse ortholog, MafB, also eliminate r5 identity (Cordes and Barsh, 1994). Thus, in vertebrates, *krox20* and *mafB* are essential for proper rhombomere specification.

The Hox gene family, orthologues to the *gap* gene family of *Drosophila*, have a critical role in establishing the vertebrate anterior-posterior pattern (Moens and Prince, 2002). Hox genes are transcription factors containing a homeodomain, or a helix-turn-helix DNA-binding motif. A most remarkable feature of Hox genes is that of colinearity, where Hox gene clusters found on the 3' ends of DNA chromosomes pattern anterior regions, while those found on 5' ends pattern posterior regions. Expression of the 3' Hox clusters, paralog groups 1-4, is found in the hindbrain (McGinnis and Krumlauf, 1992; Moens and Prince,

2002; Wilkinson et al., 1989). Hox gene regulation is under the control of MafB and also retinoic acid, which is derived from paraxial mesoderm (Moens and Prince, 2002). In mouse, MafB binding elements are found in the enhancer regions of Hoxb3 and Hoxa3 (Manzanares et al., 1997; Manzanares et al., 1999), while retinoic acid response elements (RAREs) are located in the Hoxb1 enhancer (Giguere, 1994; Marshall et al., 1994; Studer et al., 1994).

Retinoic acid signaling is necessary for posterior rhombomere formation (Moens and Prince, 2002). Pharmacological inhibition of RA signaling is sufficient to eliminate r5 identity (Begemann et al., 2004). Concurrently, vitamin-A deficient quail embryos display disrupted hindbrain segmentation, as assayed by *hox* and *krox20* expression (Gale et al., 1999; Maden et al., 1996). Further, excess RA is sufficient to expand the hindbrain as a whole in a rostral direction, at the cost of forebrain and midbrain structures (Durston et al., 1989; Gale et al., 1996; Marshall et al., 1992). Thus, RA signaling is necessary and sufficient for rhombomere patterning. Taken together, hindbrain segmentation provides a mechanism for cell restriction enabling the future development of specialized cells, including neurons.

1.2   NEURAL FATE ESTABLISHMENT

1.2.1   Neuronal Fate Induction

The notochord structure, derived from axial mesoderm, plays a critical role in ventral neural tube cell type development. Surgical deletions of the notochord in chick embryos is sufficient to eliminate ventral neural tube cell types (Hirano et al., 1991; Placzek, 1995; Placzek et al., 1990; van Straaten and Hekking, 1991; Yamada et al., 1991). Similarly, zebrafish mutations in *cyclops* (*nodal-related 2*) or *floating-head* (*flh*), in which notochord is missing, lead to severe reductions in ventral neural tube cell types (Chandrasekhar et al., 1997; Chandrasekhar et al., 1998; Halpern et al., 1995). Surgical grafts of ectopic notochords are also sufficient to induce ectopic expression of ventral neural tube markers (Placzek et al., 1990; Yamada et al., 1991). Taken together, the notochord generates a signal that is essential for floor plate and ventral neuronal cell type differentiation.

In vertebrates, Hedgehog (Hh) ligands are the signaling peptides derived from the notochord and floor plate for the specification of cell type identity in the ventral neural tube (Figure 4A) (Jessell, 2000; Roelink et al., 1994). Upon exposure to Shh, naive neural plate is transformed into either floor plate or motor neurons (Roelink et al., 1994), in a manner dependent on Shh concentration (Roelink et al., 1995). Function-blocking antibodies against Sonic Hedgehog (Shh), one of three vertebrate Hh ligands, is sufficient to block notochord-mediated induction of undifferentiated neural tube explants, demonstrating that Hh signaling from the notochord is essential for neuronal induction (Ericson et al., 1996; Marti et al., 1995). Likewise, in mice knockouts for *shh*, floor plate and

20

ventral neural cell types are eliminated in the spinal cord (Chiang et al., 1996). In

zebrafish, morpholino-mediated knockdown of both Tiggy-winkle-hedgehog and

Sonic-hedgehog protein translation is sufficient to eliminate all cranial motor

neurons (Bingham et al., 2001) while mutations in a critical component of the Hh

pathway receptor complex, *smoothened*, are sufficient to eliminate motor

neurons in the trunk (Chen et al., 2001; Varga et al., 2001). **We investigated**

the role of the *smoothened* receptor and therefore the Hh signaling

pathway for cranial motor neuron development in Chapter 4.

1.2.2   Significance of Hedgehog Signaling

Misregulation of the Hedgehog signaling pathway can give rise to a

multitude of disorders, indicative of the extensive usage of this pathway in many

biological contexts. Disorders range from carcinomas, including

medulloblastoma and basal cell carcinomas (Goodrich et al., 1997; Nilsson et al.,

2000; Oro et al., 1997) to developmental abnormalities, such as polydactyly

(Bose et al., 2002) or holoprosencephaly, where prosencephalic precursors fail to

divide, resulting in a cyclopic, fused brain structure (Belloni et al., 1996; Chiang

et al., 1996). Therefore, a fundamental understanding of the mechanism

underlying Hedgehog signal transduction would be most valuable in translating

basic research into therapy.
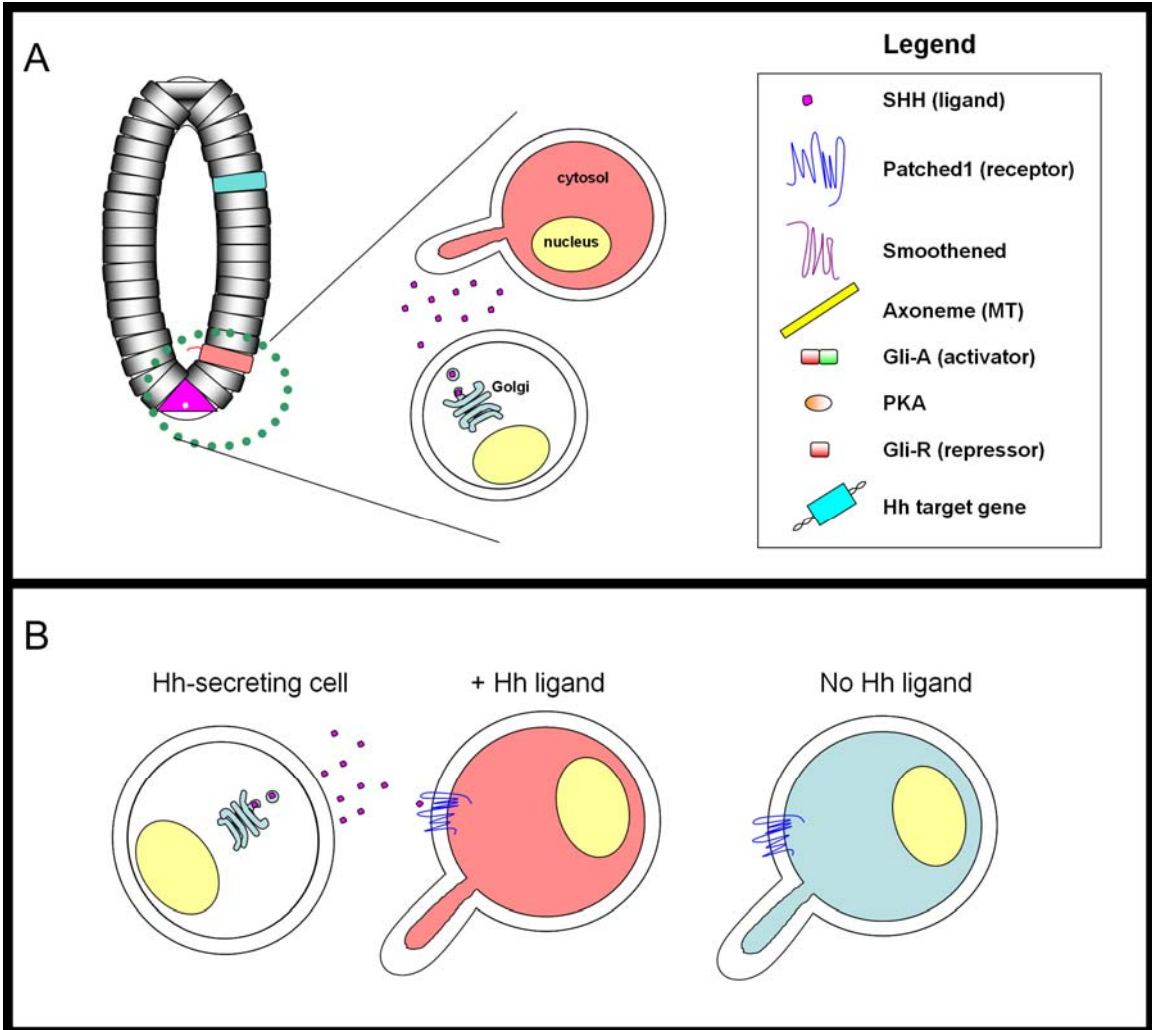
FIGURE 4. Hedgehog Signaling in the Vertebrate Neural Tube

(A): Diffusible Sonic-hedgehog (Shh) ligand, initially synthesized by the floor plate (purple

triangle) in the ventral neural tube, is perceived strongly by nearby neural progenitors (pink cells)

and weakly by dorsally-located neural progenitors (blue cells). **(B):** Shh ligand, produced in floor

plate cells for secretion by Golgi organelles, binds to the 12-pass transmembrane receptor,

Patched1 (pink cells). In cells found in the dorsal neural tube, Patched1 receptors are mostly

without Shh ligand (blue cells).

1.2.3 Hedgehog Signaling: A Fruit Fly's Story

Hedgehog (Hh) signaling was first studied in fruitflies over 20 years ago, whereby the *hh* gene was originally identified from a segment polarity screen in *Drosophila melanogaster* (Hooper and Scott, 2005; Ingham and McMahon, 2001; Nusslein-Volhard and Wieschaus, 1980). In the wild type fly larvae, hair-like structures called denticles normally form in the anterior half of each segment; posterior segments which lack denticles are called naked cuticles. In *hh* mutants, naked cuticles are eliminated as denticles form in both anterior and posterior compartments, which gives rise to a continuous sheet of denticles across the larvae proper, a phenotype resembling the bristle-toting mammal, Hedgehog (*Erinaceous albiventris*) (Nusslein-Volhard and Wieschaus, 1980). Following the cloning of the *Drosophila hh* gene (Mohler and Vani, 1992) and sequencing of the peptide (Tashiro et al., 1993), it became apparent that Hh protein functioned as a secreted protein due to the presence of a signal sequence (Tashiro et al., 1993).

Hh is synthesized only in the posterior compartments of the wing imaginal disc (Ingham, 1995). In cells that secrete Hh morphogen, Hh protein must first undergo several post-translational modifications prior to activation as a mature ligand (Hooper and Scott, 2005; Ingham and McMahon, 2001). Precursor 45 kDa Hh protein first autocatalytically cleaves into an 18 kDa N-terminal (Hh-N) fragment and a 25 kDa C-terminal fragment (Lee et al., 1994; Porter et al., 1995). Upon cleavage of the precursor protein, a cholesterol moiety becomes covalently attached to the carboxyl terminus of the Hh-N fragment, the precursor signaling

peptide (Porter et al., 1996). Cholesterol modification appears to regulate the effective range of the mature Hh morphogen as sterolation inhibition results in ectopic Hh signaling phenotypes in fly larval cuticles (Burke et al., 1999; Porter et al., 1996). Radiolabeling experiments also revealed that Hh-N is palmitoylated on the N-terminus (Pepinsky et al., 1998), a post-translational modification that confers, *in vitro*, a 30-fold increase in an alkaline phosphatase induction assay, implying that palmitoylation regulates the efficacy of Hh signaling *in vivo* (Kinto et al., 1997; Pepinsky et al., 1998). Further, in the fly *sightless* mutant, a condition resulting in non-palmitoylated Hh-N, expression of the Hh target gene, *patched*, is lost (Chamoun et al., 2001; Lee and Treisman, 2001; Micchelli et al., 2002). Thus, palmitoylation of Hh is necessary for proper signaling function.

Mature Hh signaling peptide is then exported by Dispatched, a 12-pass transmembrane protein carrying sterol-sensing domains (Burke et al., 1999). Mosaic analysis in wing imaginal discs demonstrates that Dispatched is necessary only in posterior cells for proper Hh signaling in anterior cells (Burke et al., 1999). Further, in cell culture luciferase induction assays, Dispatched is required for the proper export of Hh signaling peptide (Ma et al., 2002). Thus, Dispatched is necessary for export of a diffusible Hh protein.

Propagation of the Hh morphogen extracellularly relies heavily on heparan sulfation and glypicans (Ingham and McMahon, 2001; Lum and Beachy, 2004). Glypicans consist of a core proteoglycan protein decorated by heparan sulfate chains, which consists of alternating repeats between N-acetylglucosamine (GlcNAc) and glucoronic acid (GlcA). In flies, mutations in *dally* or *dally-like*

glypican genes result in abnormal Hh signaling in the anterior compartments of wing discs, while juxtacrine (adjacent) signaling is unaffected in the posterior compartment (Han et al., 2004). Thus, glypicans are necessary for long-range signal propagation, presumably by mediating extracellular diffusion of Hh signal peptide. Consistent with this, loss of function mutations in heparan sulfate polymerase in *tout-velu* mutants disrupts expression of Hh target genes, such as *patched*, in anterior compartments of the wing disc (Bellaiche et al., 1998). Mosaic analysis reveals that *tout-velu* mutants are only capable of disrupting Hh signaling when mutant clones are located in anterior, but not posterior, compartments (Bellaiche et al., 1998). In *sulfateless* mutants, where sulfation of glycosaminoglycans is lost due to mutations in N-deacetylase/N-sulfotransferase, naked cuticles are eliminated in the posterior compartments of each embryonic segment (Lin and Perrimon, 1999). Such segment polarity phenotypes are also seen in *slalom* mutants. *Slalom* encodes a PAPS transporter, found on Golgi membranes, which is necessary to pump PAPS (adenosine 3'-phosphate 5' phosphosulfate), a high energy sulfate donor, from the cytosol to the Golgi. PAPS are used in sulfating glycosaminoglycans, and mutations in *slalom* generate cuticle phenotypes similar to *sulfateless*. Taken together, heparan sulfation and proteoglycans mediate long-range Hh signaling from posterior to anterior compartments of the wing imaginal disc, presumably by regulating Hh diffusion, and thereby Hh morphogen gradients.

The receptor for active Hh ligand is Patched (Ptc), a 12-pass transmembrane protein with two extracellular loops and a sterol-sensing domain

(Figure 4B) (Marigo et al., 1996; Stone et al., 1996). Radiolabeling experiments

reveal that Shh-N binds to Ptc, in a 1:1 stoichiometric fashion (Fuse et al., 1999).

Deletion of the second extracellular loop results in a mutant Ptc incapable of

binding Hh ligand (Briscoe et al., 2001; Taipale et al., 2002). In the absence of

Hh ligand, Ptc negatively regulates Smoothened (Smo), a seven-pass serpentine

receptor (Hooper and Scott, 2005; Ingham and McMahon, 2001). Ptc negatively

regulates Smo by a substoichiometric mechanism, likely catalytic in nature

(Figure 5) (Taipale et al., 2002). For instance, Ptc negatively regulates Smo at a

1:50 molar ratio (Taipale et al., 2002). Genetic mosaics of the fly wing disc

reveals that, in mutant *ptc* clones, Smo protein expression is up-regulated (Denef

et al., 2000). Further, Smo and Ptc both traffic to late endosomes/lysosomes for

protein degradation in cell culture (Incardona et al., 2002). Thus, Ptc efficiently

regulates Smo protein levels by presumably shuttling Smo for lysosomal

degradation. Upon binding of Hh ligand, negative regulation upon Smo is

relieved, permitting Smo to signal intracellularly (Figure 5). Presentation of Hh

ligand in cell culture is sufficient to segregate Smo from Ptc in early endosomes;

under these conditions, Smo accumulates on the plasma membrane, while Hh-

Ptc complexes continue to late endosomes/lysosomes for degradation

(Incardona et al., 2002). In vivo, overexpression of Ptc in mutant clones lacking

Hh is sufficient to downregulate Smo protein levels (Denef et al., 2000). Thus,

Hh signaling is necessary to derepress Smo, by targeting Ptc for degradation.

Active Smo signals intracellularly, through the Costal2-Fused-SuFu

complex, to ultimately activate Cubitus interruptus (Ci), the invertebrate ortholog

27

to the Gli family of zinc-finger transcription factors (Figure 5) (Hooper and Scott, 2005; Ingham and McMahon, 2001). Ci exists in two different isoforms, a full length transcriptional activator (155 kDa) and a C-terminally truncated transcriptional repressor (75 kDa) (see also Figure 9A). Isoform production is generated by the presence or absence of Hh ligands (Ingham and McMahon, 2001). Hh signaling, through Smo, generates full length, activated forms of Ci for nuclear entry (Figure 5). In the absence of Hh signaling, Ci is sequestered in the cytosol to microtubules via association with the Costal2-Fused-SuFu signaling complex, permitting Ci repressor isoformation (Methot and Basler, 2000; Wang et al., 2000b; Wang and Holmgren, 2000). Ci sequestration occurs via Costal2, a kinesin-related protein with microtubule binding domains (Robbins et al., 1997; Sisson et al., 1997). In the presence of Hh ligand, Fused and Costal2 become phosphorylated (Nybakken et al., 2002; Stegman et al., 2000; Therond et al., 1996), and phosphorylated Costal2 and Fused have been shown to coimmunoprecipitate with the C-terminus of Smo (Jia et al., 2003). Costal2-Fused complexes then loosen from microtubules (Robbins et al., 1997; Sisson et al., 1997), permitting full length Ci isoforms to evade proteolytic processing machinery and enter the nucleus as 155 kDa transcriptional activators (Figure 5).

Motor Neuron Induction

No Motor Neuron Induction

(Modified from Huangfu and Anderson, 2006)
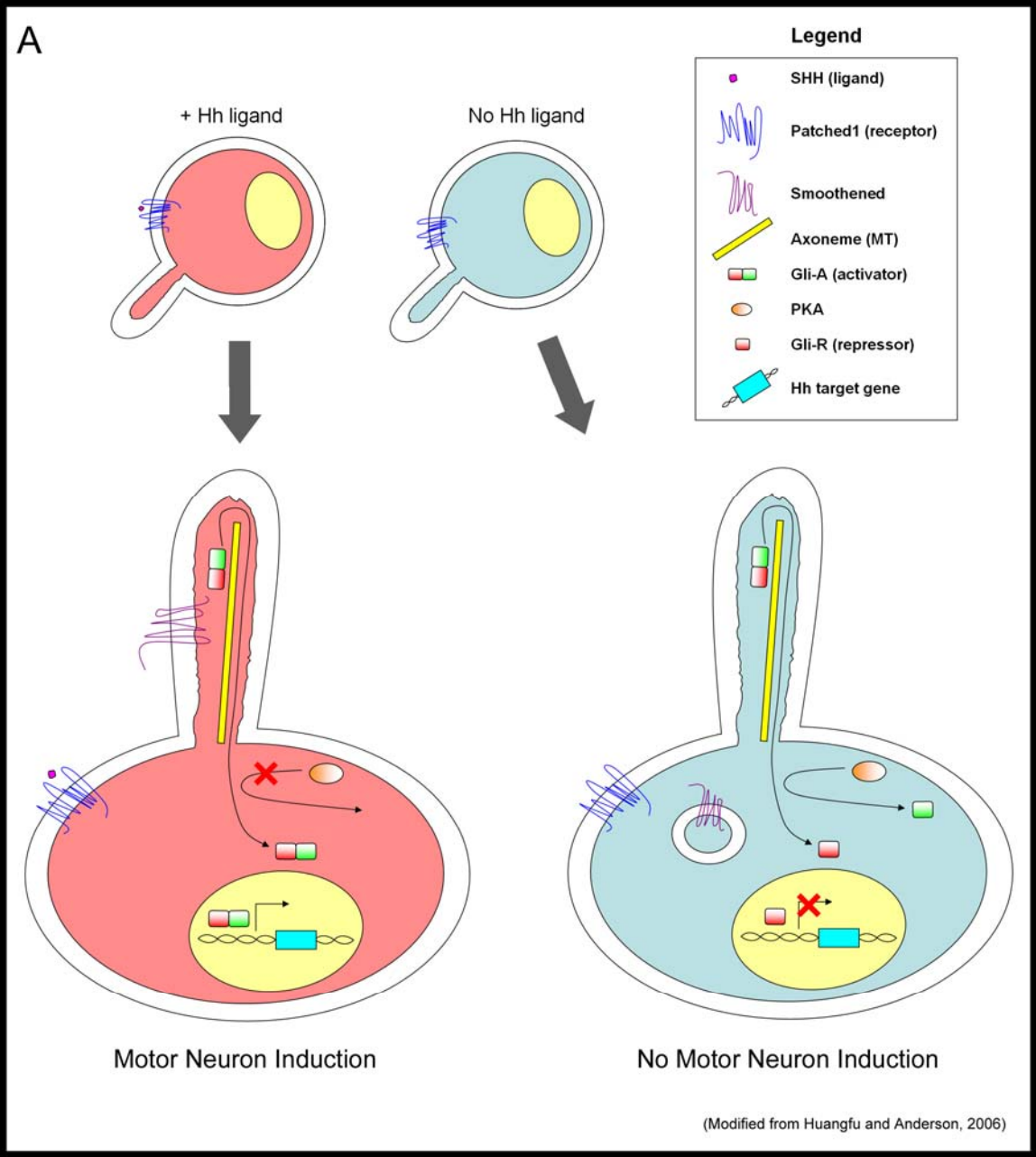
FIGURE 5. Role of Primary Cilium and Hedgehog Signaling in the

Vertebrate Neural Tube

(A): Primary cilium, found on lumenal surfaces of neural progenitors decorating the neural tube, very likely plays a role in mediating Hedgehog signaling for motor neuron development. In cells (pink) that receive Hh ligand, the 12-pass transmembrane protein, Patched1, permits accumulation of Smoothened protein in distal tips of the primary cilium. Smoothened ultimately transduces signal for the nuclear entry of full-length Gli transcriptional activators (Gli-A): to activate expression of Hh target genes, such as the motor neuron differentiation marker, *islet1*. In cells (blue) that do not receive Hh ligand, Patched1 blocks accumulation of Smoothened to the primary cilium. In these cells, full-length Gli proteins, transported along the axoneme to the cytosol, are partially proteolytically processed by PKA (and GSK3, CKI, SlimB): to generate a truncated repressor-only Gli isoform (Gli-R). Gli-R then enters the nucleus to facilitate the repression of Hh target genes. Thus, cells (blue) producing Gli-R do not become motor neurons while cells (pink) producing Gli-A initiate a motor neuron specification & differentiation program.

1.2.4   Hedgehog Signaling Components are Duplicated in

Vertebrates

In vertebrates, most components of the Hh signaling pathway have been duplicated. Mice have three Hh genes, *sonic hedgehog*, *desert hedgehog*, and *indian hedgehog* (Bitgood et al., 1996; Chiang et al., 1996; St-Jacques et al., 1999), while in zebrafish, of five Hh genes present (http://zfin.org) (Huangfu and Anderson, 2006), three Hh ligands, *sonic hedgehog* (*shh*), *tiggywinkle hedgehog* (*twhh*, named after Beatrix Potter's dashing protagonist), and *echidna hedgehog* (*ehh*) have developmental functions (Currie and Ingham, 1996; Ekker et al., 1995). In both mice and fish, *dispatched*, the 12-pass transmembrane protein required for ligand secretion, has been duplicated, as *dispatched1* and *dispatched2* (http://zfin.org) (Caspary et al., 2002; Kawakami et al., 2002; Nakano et al., 2004). Likewise, *patched*, the Hh receptor, has been duplicated as *patched1* and *patched2* in mouse and fish (Goodrich et al., 1997; Koudijs et al., 2005; Wolff et al., 2003). All signaling, however, converges upon a single vertebrate Smo, the 7-pass transmembrane protein essential for Hh signaling (Chen et al., 2001; Varga et al., 2001; Zhang et al., 2001). Signaling components downstream of Smo in vertebrates are still being unraveled, but all signaling ultimately activates the Ci orthologues, the Glioblastoma gene product (Gli) family of zinc-finger transcription factors. In mouse, fish, and frog, three *gli* genes (*gli1*, *gli2*, and *gli3*) have been described (Bai et al., 2004; Karlstrom et al., 1999; Karlstrom et al., 2003; Lei et al., 2004; Motoyama et al., 2003; Ruiz i Altaba, 1998; Tyurina et al., 2005).

1.2.5   Hh Signaling and Dorsal-ventral Patterning of the Mouse
Neural Tube

In mouse, the Hedgehog signaling pathway plays a critical role in establishing progenitor cell programs and ultimately, cell fate identity, in the ventral neural tube (Figure 6A). Patterning is setup by a concentration gradient of Sonic Hedgehog (Shh), highest in the ventral neural tube and decreasing in a dorsal vector (Figure 6B) (Gritli-Linde et al., 2001; Jessell, 2000). Different concentrations of recombinant Shh are sufficient to induce the 6 different neural cell types of the ventral neural tube *in vitro* (Figure 6A-B) (Jessell, 2000). For instance, induction of ventralmost structures, such as the V3 interneurons and the floor plate, requires the greatest amount of Shh concentration, while induction of the V0 interneurons, the dorsalmost cell type in the ventral half of the neural tube, requires the least amount of Hh signaling (Figure 6B) (Jessell, 2000). In fact, the *in vivo* dorsoventral position of a neural cell type correlates with the amount of Shh concentration required to generate that cell type *in vitro* (Jessell, 2000).

Hh signaling accomplishes this remarkable feat in a 3-step process (Jessell, 2000). Initially, the Shh concentration gradient sets up overlapping expression domains of progenitor-specific homeodomain transcription factors, by repression of Class I homeodomain proteins (Pax7, Dbx1, Dbx2, Irx3, and Pax6) and by activation of Class II homeodomain proteins (Nkx6.1 and Nkx2.2) (Figure 6C) (Briscoe et al., 2000; Jessell, 2000). Neighboring Class I and Class II homeodomain proteins further refine expression boundaries by cross-repressive

inhibition (Briscoe et al., 2000). For example, at the boundary between Pax6 (Class I) and Nkx2.2 (Class II), misexpression of Pax6 in chick neural tubes is sufficient to inhibit expression of Nkx2.2 while misexpression of Nkx2.2 is also sufficient to inhibit Pax6 expression (Briscoe et al., 2000). Further, in mouse Pax6/Sey mutants, in which all Pax6 expression is eliminated, Nkx2.2 expression expands dorsally demonstrating that Pax6 is essential to maintain the boundary between Pax6 and Nkx2.2. Likewise, at the expression boundary between Dbx2 (Class I) and Nkx6.1 (Class II), misexpression of Dbx2 is sufficient to decrease Nkx6.1 expression while Nkx6.1 is sufficient to inhibit Dbx2 expression (Briscoe et al., 2000). In Nkx6.1 mutants, Dbx2 expression expands ventrally at the expense of Nkx6.1 expression, resulting in ectopic ventrally-expanded En1-expressing interneurons at the cost of more ventral cell types, such as motor neurons (Sander et al., 2000). Taken together, at expression boundaries where Class I and Class II homeodomain transcription factors meet, cross-repressive inhibition is necessary and sufficient for boundary maintenance (Jessell, 2000).

As homeodomain proteins are expressed in overlapping domains, at each of six dorsoventral positions (Figure 6C), a unique combination of homeodomain proteins exists to carry out a progenitor program. Thus, in the mouse neural tube, progenitors to motor neurons (pMN) express the unique combination of Pax6, Nkx6.1, and Olig2 while dorsal neighbors express Pax6, Nkx6.1, and Irx3 to become progenitors to V2 interneurons (p2) (Figure 6C) (Jessell, 2000). Later in development, this unique pMN code (Pax6, Nkx6.1, Olig2) will become

33

A

Ventricular Zone	Mantle Layer
pd4	D4
pd5	D5
pv0	V0
pv1	V1
pv2	V2
pmn	MN
pv3	V3
FP	FP
Progenitor	Fate

N

B

Gli3^R Gli2^R
Gli2^A Gli1^A
SHH
Gli^R
Gli^A

Progenitor	Fate
pd4	D4
pd5	D5
pv0	V0
pv1	V1
pv2	V2
pmn	MN
pv3	V3
FP	FP

(Modified from Jacob and Briscoe, 2003)

C

Gli^R
Gli^A

Pax7, Dbx1, Dbx2, Irx3, Pax6, Nkx6.1, Olig2, Nkx2.2

	Progenitor	Fate / Differentiation Code
pd4	D4	Lhx1, Lbx1
pd5	D5	Lmx1b
pv0	V0	Evx1/2
pv1	V1	En1
pv2	V2	Chx10
pmn	MN	MNR2, Hb9, Isl1/2
pv3	V3	Sim1
FP	FP	HNF3β

Progenitor Code

(Modified from Jessell 2000)

34

FIGURE 6. Translation of Hh Gradients for Cell Fate Acquisition

(A): In the ventral half of the mouse neural tube (boxed region), six ventral cell types and two dorsal cell types are found. Cells nearest the lumen are located in the ventricular zone and function as neural subtype-specific progenitors. Cells distal to the lumen are located in the mantle layer as differentiated neurons. In vivo, numerous cells occupy stereotypic locations along the ventral-dorsal axis of the neural tube. FP, floor plate; V3-V0, ventral interneurons; MN, motor neurons; D4-D5, dorsal interneurons. **(B):** Sonic Hedgehog (Shh), synthesized by floor plate and notochord (N), forms a gradient strongest in the ventral neural tube and weakest in the dorsal neural tube locations. Formation of a Shh gradient, facilitates the formation of overlapping Gli-activator (Gli^A) and Gli-repressor (Gli^R) domains for an overall Gli activity code that specifies neuronal identity. Thus, Shh ligand gradients are translated into Gli activity gradients within neural progenitors across the neural tube. **(C):** Gradients of Shh ligand and Gli activity set up expression of unique and overlapping homeodomain transcription codes. Boundaries are established and maintained by cross-repressive interactions amongst Class I and Class II homeodomain transcription factors (see Introduction 1.2.5). To be a motor neuron progenitor (pMN), a cell would express a combination of Nkx6.1, Olig2 (a bHLH-type transcription factor), and Pax6. Unique homeodomain progenitor codes then facilitate the acquisition of a cell fate program whereby expression of a new set of differentiation-specific transcription factors is executed. For example, differentiated motor neurons would gradually down-regulate pMN programs and specifically express MNR2, Hb9, and Islet1/Islet2.

supplanted by the expression of a fate-specific motor neuron code (Mnr2, Isl1, Isl2, and Hb9) (Figure 6C) (Jessell, 2000).

In the analysis of mouse mutants of the Hh signaling pathway, it is helpful to classify patterning phenotypes into two categories: ventral-to-dorsal conversion versus dorsal-to-ventral conversion (Figure 7) (Huangfu and Anderson, 2006). For instance, in mutants that disrupt Hh signaling, ventral cell types are nearly eliminated while dorsal markers are ectopically expressed in the ventral neural tube. In such mutants, the neural tube has become **dorsalized**, at the expense of ventral cell types (Figure 7C). Conversely, in mutants that disrupt negative regulators of the Hh signaling pathway, ventral cell types are typically found ectopically in the dorsal neural tube and expression of dorsal markers is greatly reduced. Such neural tubes have become **ventralized**, at the expense of dorsal cell types (Figure 7B).

1.2.6   Zebrafish Motor Neurons of the Hindbrain

Cranial motor neurons (CMNs) are a highly organized population of cell bodies found at specific D/V and A/P locations within specific rhombomeres (Figure 8). Each rhombomere houses a unique subset of CMNs which in turn innervate a unique set of muscle targets. Cranial motor neurons (CMNs) can be subdivided into branchiomotor neurons (BMNs) and somatic motor neurons (Figure 8) (Chandrasekhar, 2004). The trigeminal motor neurons (nV), which
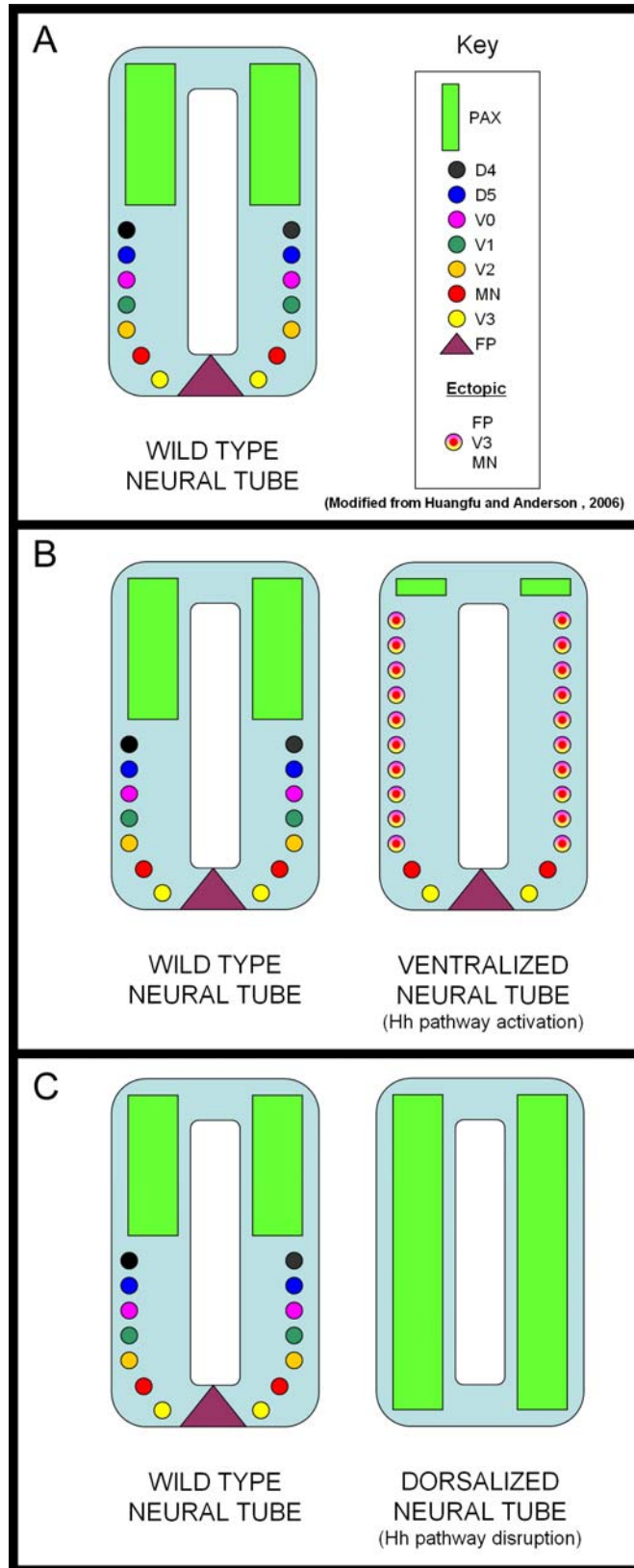
FIGURE 7. Mouse Hh Signaling Phenotypes for Motor Neuron Development

(A): Pax genes (green rectangle) are expressed normally in the dorsal neural tube while floor plate (purple triangle) and motor neurons (red) occupy the ventral neural tube. **(B):** In mouse mutants in which Hh signaling pathway becomes hyperactivated, expression of Pax is severely reduced while formation of ventral cell types such as motor neurons and floor plate is ectopically expanded into dorsal levels of the neural tube. In these mutants, the neural tube is severely **ventralized** at the expense of dorsal cell types. **(C):** Conversely, in mouse mutants in which Hh signal transduction is disrupted, all motor neurons and floor plate cell types are eliminated while Pax expression ectopically expands into the ventral neural tube. Such neural tubes are **dorsalized** at the expense of ventral neural tissue.

innervate the mandibular arch, are found in rhombomeres 2 and 3 (r2 and r3); the facial motor neurons (nVII), which innervate the hyoid arch, are found in r6 and r7; the glossopharyngeal motor neurons (nIX), which innervate gill arch 1, are found in r7; and the vagal motor neurons (nX), which innervate gill arches 2-5, are found in the caudal hindbrain (Chandrasekhar et al., 1997). Although nVII BMNs are located in r6 and r7, zebrafish nVII BMNs are first born in r4 (asterisk, Figure 8) and then migrate tangentially into r6 and r7 (Bingham et al., 2002; Jessen et al., 2002). Axonal projections of CMNs exit at even-numbered rhombomeres, a characteristic feature found in many species (Figure 8) (Carpenter et al., 1993; Lumsden and Keynes, 1989). Of the somatic motor neurons, the oculomotor (nIII) and the trochlear (nIV), which innervate eye muscles, are found in the midbrain; and the abducens (nVI), which also innervates eye muscle, are found in r5 and r6 (not shown) (Chandrasekhar, 2004; Higashijima et al., 2000; Kimmel et al., 1985; Trevarrow et al., 1990).

1.2.7   Vertebrate Hh signaling phenotypes: Hh to Smo

In the mouse *Shh* targeted knockout, a null condition generated by replacement of exon2 with a neomycin cassette (Chiang et al., 1996), all Shh protein in the neural tube and notochord is eliminated (Chen et al., 2004a). Loss of mouse *Shh* results in the elimination of nearly all ventral cell types (floor plate, V3, and MN) while expression of Class I homeodomain proteins (Dbx1, Pax7, Pax3), normally repressed by Hh signaling, are found ectopically expanded in the
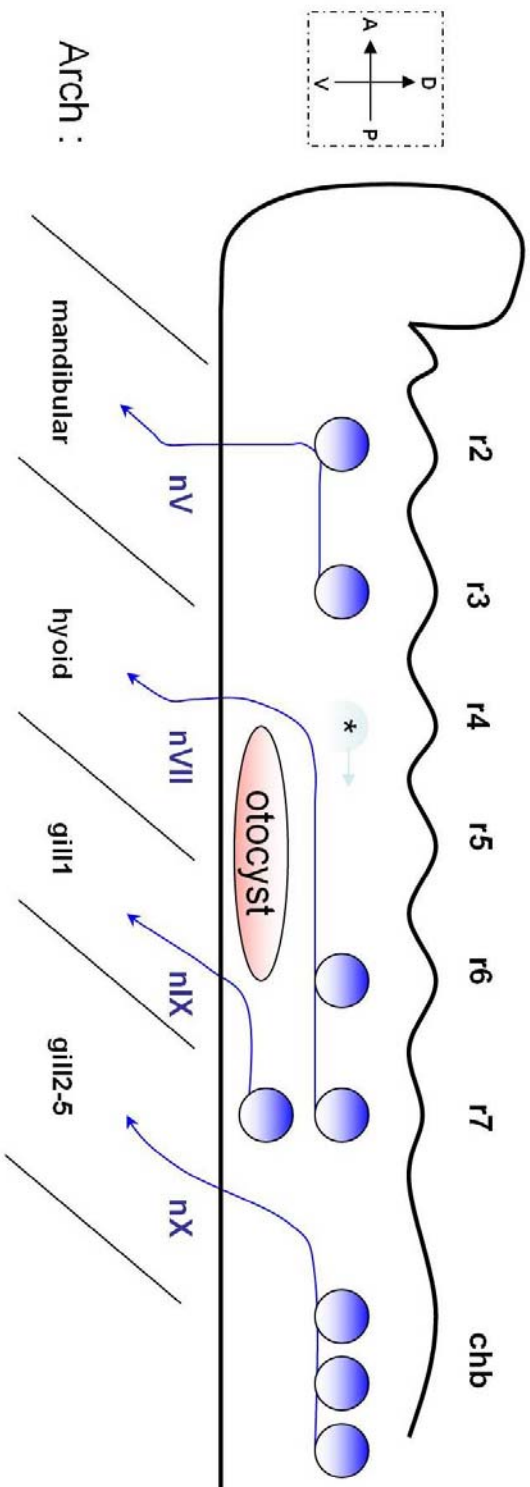
Arch :

(Modified from Chandrasekhar et al., 1997)

40

FIGURE 8. Zebrafish Branchiomotor Neurons

Cell bodies of zebrafish motor neurons occupy stereotypic locations in different compartments, or rhombomeres, of the hindbrain. As in other vertebrates, motor axon projections exit at even rhombomeres (Carpenter et al., 1993; Lumsden and Keynes, 1989) for the innervation of pharyngeal arch tissues, including the mandibular, hyoid, and gill slots 1-5 (Chandrasekhar et al., 1997). Cranial motor neurons (CMNs) can be subdivided into branchiomotor neurons (BMNs) and somatic motor neurons (Chandrasekhar, 2004). The trigeminal motor neurons (nV), which innervate the mandibular arch, are found in rhombomeres 2 and 3 (r2 and r3); the facial motor neurons (nVII), which innervate the hyoid arch, are found in r6 and r7; the glossopharyngeal motor neurons (nIX), which innervate gill arch 1, are found in r7; and the vagal motor neurons (nX), which innervate gill arches 2-5, are found in the caudal hindbrain (Chandrasekhar et al., 1997). Although nVIIs are located in r6 and r7, zebrafish nVIIs are first born in r4 (asterisk) and then migrate tangentially into r6 and r7 (Bingham et al., 2002; Jessen et al., 2002).

ventral neural tube (Bulgakov et al., 2004; Chiang et al., 1996; Wijgerde et al., 2002). Misexpression of *shh* using a dorsal neural tube-specific promoter is sufficient to induce the ectopic expression of ventral markers, such as *nkx2.2* and *pax6* in the dorsal neural tubes of transgenic mice (Rowitch et al., 1999). Thus, mouse *Shh* is both necessary for motor neuron induction, and sufficient for ventral neural tube cell type induction (Figure 7C).

Likewise, in zebrafish *shh* deficiency mutants, in which *shh* has been spontaneously deleted (Schauerte et al., 1998), motor neurons of the head (Chandrasekhar et al., 1998) and trunk (Lewis and Eisen, 2001) are severely reduced in number. In the hindbrain, morpholino-mediated knockdown of Shh and Twhh protein disrupts all cranial motor neuron induction (Bingham et al., 2001). Similarly, inhibition of Shh, Twhh, and Ehh protein translation is sufficient to disrupt the formation of all spinal motor neurons (Lewis and Eisen, 2001). Furthermore, transient misexpression of *shh* mRNA is sufficient to induce ectopic cranial motor neurons, at the expense of dorsal cell types, such as cerebellar or sensory commissural neurons (Chandrasekhar et al., 1998). Taken together, in all vertebrates, the Hh ligands are essential for motor neuron induction in the neural tube, and when misexpressed, *shh* is sufficient to partially ventralize the dorsal neural tube.

Mutations disrupting *dispatched1*, a 12-pass transmembrane protein required for the export of Hh ligand, also generate a ventral neural tube phenotype. In mouse *dispatched1* targeted knockouts, in which exon8 and all twelve transmembrane (TM) domains are deleted (Caspary et al., 2002;

Kawakami et al., 2002), all Hnf3β and Shh expression in the floor plate is lost and

Islet1-expressing motor neurons are absent. Likewise, mutations in zebrafish

dispatched1, in which Y164 is substituted by a premature stop codon resulting in

a protein truncated prior to all 12TM domains, Islet-expressing spinal motor

neurons are reduced (Nakano et al., 2004). Zebrafish *dispatched1* mutants also

exhibit loss of *fkd4*-expressing lateral floor plate and loss of all *nk2.2* expression

(Nakano et al., 2004). Thus, *dispatched1* is necessary for floor plate and motor

neuron induction (Caspary et al., 2002; Kawakami et al., 2002; Nakano et al.,

2004).

In contrast, targeted mutations to delete the ATG start codon of mouse

patched1, the Hh receptor, ventralize the neural tube (Figure 7B) (Goodrich et

al., 1997). For instance, mouse *patched1* knockouts display ectopic expression

of ventral neural tube markers, such as Nkx2.2 (vp3), Shh (FP), Hnf3β (FP), and

Islet1/2 (MN) in the dorsal aspect of the neural tube (Caspary et al., 2002;

Goodrich et al., 1997; Motoyama et al., 2003). Meanwhile, expression of dorsal

neural tube markers, such as Pax6 and Pax7, are eliminated (Figure 7B)

(Goodrich et al., 1997; Motoyama et al., 2003). In chick, misexpression of a

dominant negative Patched, in which deletion of the second extracellular loop

prevents Hh ligand binding, is sufficient to reduce Mnr2- and Hb9-expressing

motor neuron cell number (Briscoe et al., 2001). Dominant-negative Ptc is also

sufficient to induce the ventral expansion of dorsal neural tube markers (Dbx2

and Pax7) as well as En1 (V1) and Evx1/2 (V0) interneurons (Briscoe et al.,

2001). In zebrafish, morpholino-mediated knockdown of Patched1 protein results

in supernumerary muscle pioneer cell number, a cell type regulated by Hh signaling (Wolff et al., 2003). Epistasis experiments using compound double mutants between *ptc1*;*disp1* in mouse confirm that *patched1* functions downstream of *dispatched1* for Hnf3β floor plate induction (Caspary et al., 2002). Thus, in vertebrates, *patched1* is epistatic to *dispatched1* to negatively regulate Hh signaling for the induction of motor neurons and other ventral cell types.

Targeted mutations in mouse *smoothened* (*smo*), the 7-pass transmembrane protein essential for Hh signal transduction, result in the loss of all ventral neural cell types (Figure 7C) (Wijgerde et al., 2002; Zhang et al., 2001). In mouse *smo* mutants, in which the ATG start codon has been replaced by a neomycin cassette (Zhang et al., 2001), all Hb9 motor neurons are eliminated, while expression of Nkx2.2 (vp3) and Hnf3β (floor plate) is also lost (Eggenschwiler et al., 2006; Wijgerde et al., 2002). In mouse chimeric neural tubes consisting of *smo* mutant and wildtype cells, Mnr2 and Isl1/2 expressing motor neurons are reduced, while *smo* mutant cells never express motor neuron differentiation markers or motor neuron progenitor markers, such as Olig2 and Nkx6.1 (Wijgerde et al., 2002). In contrast, expression of dorsal markers, such as Dbx1, Dbx2, Irx3, Pax6, and Pax7, is expanded ventrally in chimeric neural tubes and *smo* mutant cells do express dorsal neural tube markers, such as Pax7 (Wijgerde et al., 2002). In chick embryos, pharmacological inactivation of Smo by administration of the teratogenic compound cyclopamine is also sufficient to dorsalize the neural tube (Incardona et al., 1998; Keeler, 1969; Taipale et al., 2000). For instance, in cyclopamine-treated embryos, all Shh-

44

expressing floor plate cells and Nkx2.2-expressing vp3 interneuron progenitors are eliminated (Incardona et al., 1998). Further, Islet1/2-expressing motor neurons are severely reduced while Pax6 expression is ventrally expanded following cyclopamine administration (Incardona et al., 1998). **Using cyclopamine, we investigated the temporal role of the Hh signaling pathway for branchiomotor and somatic motor neuron specification in zebrafish embryos in Chapter 5.**

In zebrafish *smo* null alleles, in which exon2 is compromised, primary and secondary spinal motor neurons are reduced in number (Chen et al., 2001; Varga et al., 2001). Further, in the chick neural tube, in ovo electroporation of a constitutively active Smo (SmoM2), a Trp535Leu in the 7th transmembrane domain (Xie et al., 1998), is sufficient to cell-autonomously induce Hb9 and Islet1/2 motor neuron cells in ectopic, dorsally-shifted locations of the neural tube (Hynes et al., 2000). Thus, in all vertebrates, *smo* is necessary and sufficient for the cell-autonomous induction of ventral neural tube cell types (Chen et al., 2001; Hynes et al., 2000; Varga et al., 2001; Wijgerde et al., 2002; Zhang et al., 2001). In the absence of *smo*, the mouse neural tube becomes dorsalized at the expense of the ventral cell types (Figure 7C). **We investigated the role of zebrafish *smoothened* for cranial motor neuron specification in Chapter 4**.

1.2.8 Role of Vertebrate Gli genes

In the mouse *gli1* knockout, in which three of five C_2H_2-type zinc fingers of the DNA binding motif are deleted, *gli1* mutants are viable and fertile, suggesting an intact motor system (Ding et al., 1998; Matise et al., 1998; Park et al., 2000). Misexpression of mouse *gli1* in the dorsal neural tubes of transgenic mice is sufficient to induce ectopic Hnf3β and Shh floor plate, but not motor neurons (Hynes et al., 1997; Park et al., 2000). In *Xenopus*, transient overexpression of *gli1* is sufficient to induce Hb9 spinal motor neurons in ectopic dorsal regions (Ruiz i Altaba, 1998). Thus, although *gli1* can activate the Hh pathway, *gli1* is not essential for spinal motor neuron induction. Consistent with this, zebrafish *gli1* mutants have normal spinal motor neurons (Chandrasekhar et al., 1999).

In targeted mouse *gli2* knockouts, in which DNA binding motifs are also partially deleted, all Shh floor plate is eliminated and Nkx2.2 vp3 cells severely reduced (Eggenschwiler et al., 2006; Matise et al., 1998). Hb9 or Isl1/2 motor neurons, however do form, but expand ventrally in regions occupied by floor plate and V3 interneurons. Like *gli1*, *Xenopus gli2* is sufficient to induce ectopic Hb9 spinal motor neurons (Ruiz i Altaba, 1998). Mouse *gli2* therefore is necessary for the induction of the ventralmost neural tube cell types, floor plate and V3 interneurons, but also appears to be dispensable for spinal motor neuron induction. **We investigated the role of zebrafish *gli2* for branchiomotor and spinal motor neuron specification in Chapter 4.**

The mouse *gli3* allele, *extra toe jam*, is caused by a genomic deletion of approximately 50 kb encompassing the *gli3* locus resulting in loss of all Gli3

protein expression (Huangfu and Anderson, 2005; Hui and Joyner, 1993; Maynard et al., 2002). In *gli3* mutants, motor neurons (Hb9, Isl1/2) and floor plate (Shh) forms normally, but the dorsally-located dl5 interneurons (Lmx1b) are severely reduced (Eggenschwiler et al., 2006; Persson et al., 2002). Upon knock-in of a repressor-only *gli3* (*gli3R*), by targeted deletion of the C-terminal activator region (Bose et al., 2002), Lmx1b-expressing dl5 interneuron specification is rescued in cell number (Persson et al., 2002). In these *gli3R* knock-in mice, motor neurons remain unaffected (Persson et al., 2002). Thus, in the mouse neural tube, single loss-of-function manipulations to the *gli* genes reveals a *gli2* requirement for V3 interneuron and floor plate induction, as well as a *gli3* repressor requirement for dl5 interneuron specification. Although *gli1* and *gli2* are sufficient for motor neuron induction, removal of single *gli* genes have very little, if any, consequence on motor neuron specification, suggesting the possibility of functional redundancy. **We examined functional redundancy amongst the zebrafish *gli* genes for spinal motor neuron specification in Chapter 4.**

Although zebrafish *gli1* mutants have normal spinal motor neurons, all branchiomotor neurons are eliminated in *gli1* mutant hindbrains (Chandrasekhar et al., 1999). The zebrafish *gli1^te370^* mutant results from a Q920Stop which prematurely truncates mutant protein prior to the C-terminal transactivator domain (see section 1.3, see also Figure 9B) (Karlstrom et al., 2003). In Mns2 cell culture, mutant *gli1^te370^* fails to induce luciferase activity in a transcriptional assay employing *gli* binding sites, suggesting that the *gli1^te370^* mutant is a null

allele (Karlstrom et al., 2003). Thus, although mouse *gli1* is dispensable for

motor neuron induction, zebrafish *gli1* is necessary for cranial, but not spinal

motor neuron specification. **We examined the role of zebrafish *gli2* and *gli3* in**

cranial motor neuron induction in Chapter 4.

1.2.9   Vertebrate Hh signaling phenotypes: Gli activator vs. Gli repressor

In double mutants in mice for *gli1*;*gli2*, all Nkx2.2 (vp3) expression is

eliminated (Matise et al., 1998; Park et al., 2000). As Nkx2.2 expression is

normal in single *gli1* mutants, and moderately reduced in *gli2* mutants, this

suggests that *gli1* acts cooperatively with *gli2* for vp3 specification. However, as

gli gene products are bipotential (full length activators vs. truncated repressors),

these experiments cannot determine the precise isoformal requirement.

Transient misexpression of *Xenopus gli1* is sufficient to induce ectopic floor plate,

but coexpression of *gli2* and *gli3* blocks *gli1*-mediated Hnf3β floor plate induction

(Ruiz i Altaba, 1998). Similarly, coexpression of *gli3* with *gli1* in *Xenopus* neural

tubes, dramatically reduces the number of *gli1*-induced Hb9 spinal motor

neurons. Thus, *gli1* appears to lack repressor activity and likely exists as a full-

length transcriptional activator of Hh signaling.

To determine whether Gli2 activator function is deficient in *gli2* knockout

mice, mouse *gli1* was knocked in place of all mouse *gli2* at the *gli2* endogenous

loci (Bai and Joyner, 2001). In *gli2* mutants, all Shh floor plate is missing while

48

Nkx2.2 expression is moderately reduced (Matise et al., 1998). However, mouse *gli1*, in place of *gli2*, is sufficient to rescue all floor plate and Nkx2.2 vp3 specification. Further, ventrally expanded Hb9 motor neurons found in *gli2* knockouts (Matise et al., 1998) are found in normal positions when *gli1* replaces *gli2* coding sequence (Bai and Joyner, 2001). Thus, these data suggest that in *gli2* knockouts, Gli2 activator function is necessary for floor plate and proper vp3 interneuron specification.

Similarly, human *GLI3*, when knocked in place of mouse *gli2*, is sufficient to rescue some Shh-expressing floor plate and some Nkx2.2 vp3 interneurons (Bai et al., 2004), demonstrating partial redundancy amongst Gli activator isoforms for ventral neural tube development. However, as floor plate, vp3 interneurons, and motor neurons are unaffected in *gli3* repressor-only knock-in mice (Persson et al., 2002), Gli3 activator isoforms are clearly not essential for ventral neural tube development (Bose et al., 2002; Persson et al., 2002). Consistent with a role for Gli2 and Gli3 activator functions, misexpression of Gli3 activator-only constructs, in which N-terminal repressor domains are deleted, are sufficient to induce ectopic Hnf3β floor plate, Nkx2.2 vp3 interneuron progenitors (Lei et al., 2004), Nkx6.1 motor neuron progenitors (Stamataki 2005), and Hb9 motor neurons (Stamataki et al., 2005) in the chick neural tube.

In compound *gli2^{zfd}*;*gli3^{xtj}* mutant mice, all *gli1* expression is eliminated and therefore all Gli activity lost in the neural tube (Bai et al., 2004; Lei et al., 2004). In this "triple" loss-of-function mutant, spinal motor neurons are reduced in number, and severely mispatterned along the dorsoventral neural tube axis

49

(Bai et al., 2004; Lei et al., 2004; Motoyama et al., 2003). Further, *gli2*;*gli3*

mutants display mixed populations of Chx10 (V2) and En1 (V1) interneurons.

Motor neuron progenitor markers are also mispatterned: Pax6 expression is

ventrally expanded, Olig2 expression is both dorsally and ventrally expanded,

and Nkx6.1 expression is expanded from the ventricular zone to the mantle layer,

a region normally occupied by differentiated motor neurons (Bai et al., 2004; Lei

et al., 2004; Motoyama et al., 2003). Thus, overall Gli activity is necessary for

the proper patterning of the mouse ventral neural tube (see also Figure 6).

Although removal of all *gli* genes results in reduction in motor neuron cell

number, it is likely that this reduction is caused by dramatic mispatterning

phenotypes. Surprisingly, motor neurons can still form in the spinal cords of mice

missing all three *gli* genes, suggesting that other genes and perhaps other

pathways might regulate motor neuron induction. For instance, retinoic acid

signaling has recently been shown to be necessary for motor neuron

development in post-mitotic neurons (Sockanathan et al., 2003). As a significant

number of motor neurons in mouse require *gli* genes for specification, **we**

therefore examined the phenotypes of zebrafish spinal motor neurons after

attenuating overall Gli activity using dominant negative approaches in

Chapter 4.

Taken together, overall Gli activator function mediates Hh signaling for

mouse ventral neural tube development, while at least Gli3 repressor activity is

necessary for the induction of some interneurons in the intermediate neural tube.

A primary function of Hh signaling in mouse ventral neural tube development is to prevent the accumulation of Gli3 repressor isoforms, and therefore permit motor neuron formation (Litingtung and Chiang, 2000; Wijgerde et al., 2002). Consistent with this, expression of C-terminally truncated human *GLI3* in MNS70 cells is sufficient to inhibit transcriptional activation of artificial Gli reporter assays (Dai et al., 1999). In mouse mutants for either *shh* or *smo*, all motor neurons, floor plate cells, and vp3 interneuron progenitors are eliminated (Figure 7C) (Chiang et al., 1996; Wijgerde et al., 2002; Zhang et al., 2001). Simultaneously, *shh* mutants lack all expression of *gli1* (Bai et al., 2002; Bulgakov et al., 2004) and *ptc1* (Bulgakov et al., 2004). Further, expression of *gli3*, which normally is found in the dorsal two-thirds of the neural tube, is found ectopically in the ventral neural tubes of *shh* mutants (Bulgakov et al., 2004). In compound mouse mutants between *shh*;*gli3* or *smo*;*gli3*, all floor plate and Nkx2.2 vp3 interneuron progenitors are still lost as in *shh* or *smo* single mutants (Chiang et al., 1996; Litingtung and Chiang, 2000; Wijgerde et al., 2002; Zhang et al., 2001). However, remarkably, in *shh*;*gli3* or *smo*;*gli3* mutant mice, motor neurons still form, albeit greatly mispatterned. Similarly, Chx10 (V2) and En1 (V1) interneurons are mispatterned, with ectopic interneurons located in the ventral neural tube (Litingtung and Chiang, 2000; Wijgerde et al., 2002). Thus, removal of *gli3*, in a background in which Hh signaling is lost, permits spinal motor neuron induction in mice. Consistent with this, misexpression of *gli3* repressor-only in the chick neural tube is sufficient to reduce expression of pMN markers (Nkx6 and Olig2) as well as inhibit Mnr2 motor neuron induction

(Persson et al., 2002). Further, in mouse *smoothened* embryo extracts, Western analysis reveals a decrease in full-length activator isoforms of Gli3 accompanied by an increase in Gli3 repressor isoforms (Huangfu and Anderson, 2005). In *shh* mutants, *gli3* mRNA, normally expressed in the dorsal neural tube, is ventrally expanded and occupies the entire neural tube (Bulgakov et al., 2004). Thus, Hh signaling in the mouse ventral neural tube functions either to repress either *gli3* expression (Bulgakov et al., 2004) or to prevent the accumulation of Gli3 repressor isoforms (Huangfu and Anderson, 2005; Wijgerde et al., 2002), thereby derepressing motor neuron formation. In the absence of Hh signaling (*smo* mutants), Gli3R accumulates and dorsalizes the ventral neural tube (Figure 7C). In contrast, in *patched* mutants in which the neural tube is ventralized (Figure 7B) (Goodrich et al., 1997; Motoyama et al., 2003), all Gli3 repressor isoforms are lost while Gli3 activator isoforms are still present (Huangfu and Anderson, 2005). As Gli3 protein is unstable in the *gli3* (*extra toe jam*) mutant allele (Huangfu and Anderson, 2005; Hui and Joyner, 1993), in *smo*;*gli3* double mutants, Gli3R fails to accumulate, permitting motor neurons and other ventral neural tube cell types to form, albeit they are severely mispatterned. Although not yet biochemically demonstrated, a similar mechanism likely explains how motor neurons are able to form in *shh*;*gli3* double mutants.

1.2.10 Vertebrate Hh signaling: Intracellular Transduction Components

Recent work in mouse and zebrafish has unraveled orthologous transduction components (e.g. Fused, Cos2, SuFu) as well as vertebrate-specific effectors functioning downstream of the Patched receptor. However, the genes for several of these components, such as cAMP-dependent protein kinase A (PKA), have been duplicated, complicating phenotypic analyses.

PKA as a holoenzyme consists of two catalytic subunits and two regulatory subunits (Amieux and McKnight, 2002; Brandon et al., 1997). The catalytic subunits contain kinase activity, while the regulatory subunits carry an allosteric cAMP binding motif (Amieux and McKnight, 2002). In mice, two catalytic genes (Prka-cα, Prka-cβ) and four regulatory subunit genes (RIα, RIβ, RIIα, RIIβ) have been described. Upon binding of cAMP to the regulatory subunits of the PKA tetrameric holoenzyme, catalytic subunits dissociate from the holoenzyme and function as active kinases (Amieux and McKnight, 2002). Targeted mouse knockouts for either *Prka-cα* and *Prka-cβ* are null alleles as proteins levels of Prka-cα or Prka-cβ, respectively, are eliminated in mutants (Qi et al., 1996; Skalhegg et al., 2002). Homozygous mouse knockouts for either *Prka-cα* or *Prka-cβ* have no neural tube defects. However, in double mutants in which three of four alleles are knocked out (*Prka-c$\alpha^{/-}$;Prka-c$\beta^{/+}$* or *Prka-c$\alpha^{-/+}$;Prka-c$\beta^{/-}$*), a condition referred to as PKA deficiency, the neural tube becomes ventralized, at the expense of the dorsal neural tube markers (Figure 7B) (Huang et al., 2002). For instance, in PKA deficient embryos, Hnf3β-expressing floor

plate and Nkx2.2-expressing vp3 interneuron progenitors become dorsally expanded. Likewise, PKA deficient neural tubes exhibit dorsally expanded Islet-expressing motor neurons, while expression of dorsal markers, such as Pax6, is greatly reduced (Figure 7B) (Huang et al., 2002). Similarly, in zebrafish, misexpression of a dominant-negative regulatory subunit (dnPKA), in which mutations in cAMP binding sites prevent allosteric-mediated activation of catalytic subunits (Hammerschmidt et al., 1996; Ungar and Moon, 1996), is sufficient for branchiomotor neuron induction (Chandrasekhar et al., 1999), a Hh pathway gain-of-function phenotype similar to misexpression of *shh* ligand alone (Chandrasekhar et al., 1998). Transient misexpression experiments in zebrafish reveals that PKA functions downstream of *smoothened* (Chen et al., 2001; Varga et al., 2001), and upstream of *gli1* (Chandrasekhar et al., 1999) for motor neuron induction. Taken together, in vertebrates, PKA function is a necessary and sufficient negative regulator of the Hh signaling pathway for motor neuron induction. **While characterizing zebrafish *gli2* mutant alleles, we examined epistasis between *PKA* and *gli2* for cranial motor neuron induction and other Hh-regulated events in Chapter 4.**

In zebrafish, a novel Hh transduction component, *β-arrestin 2* (*βarr2*) has recently been implicated in muscle development. β-arrestins are scaffold proteins utilized by heptahelical transmembrane receptors (7TM) for signal transduction (Wilbanks et al., 2004). Morpholino-mediated inhibition of β-arrestin 2 protein translation results in the elimination of muscle pioneer cells and reduced slow muscle fiber formation, a phenotype shared by *smo* null mutants

(Barresi et al., 2000; Chen et al., 2001). Transient misexpression of dnPKA

mRNA, but not *shh* mRNA, in *β-arrestin 2* zebrafish morphants (animals exposed

to morpholinos) restores slow muscle fiber number to wild type levels, indicating

that β-arrestin 2 functions downstream of Shh and upstream of PKA (Wilbanks et

al., 2004). In mammalian cell culture, β-arrestin 2 colocalizes and

coimmunoprecipitates with activated, phosphorylated Smoothened protein (Chen

et al., 2004b). Further, pharmacological activation of the Hh signaling pathway

via administration of Smo agonist (SAG) to HEK293 cells is sufficient to

internalize Smo protein in a β-arrestin 2-dependent manner (Chen et al., 2004b).

Taken together, β-arrestin 2 is a necessary component of the Hh signaling

pathway at least for muscle development, and may function *in vivo* by regulating

the internalization of activated Smoothened proteins.

As in flies, mutations in vertebrate orthologs to SuFu, Cos2, and Fused

generate Hh signaling phenotypes. For instance, in targeted mouse *SuFu*

mutants, in which deletion in exon 7 results in loss of SuFu protein (Cooper et al.,

2005), ventral neural tube cell types, such as Hnf3β-expressing floor plate and

Nkx2.2-expressing vp3 interneuron progenitors, are located in ectopic dorsal

regions of the neural tube. Further, mouse *SuFu* mutants lack expression of

Pax6 and Pax7, markers normally expressed in the dorsal neural tube. Although

motor neurons have not been examined yet, *SuFu* mutants likely exhibit deficits,

as *SuFu* neural tubes are ventralized at the expense of dorsal cell types. In

zebrafish, morpholino-mediated knockdown of both SuFu and Cos2 translation

results in a dramatic ectopic increase in muscle pioneer cell number (Tay et al.,

2005). Induction of muscle pioneers and slow-muscle fiber formation requires

Hedgehog signaling as *smoothened* mutants are missing all muscle pioneers

(Barresi et al., 2000; Chen et al., 2001). In *smoothened* mutants injected with

SuFu morpholino, formation of slow-muscle fibers is restored to wild type levels

(Wilbanks et al., 2004), demonstrating that SuFu acts downstream of Smo to

negatively regulate Hh signaling. In contrast, morpholino-mediated inhibition of

the serine-threonine kinase Fused translation results in the elimination of all

muscle pioneer cells, demonstrating that Fused is essential for muscle pioneer

induction (Wolff et al., 2003). Thus, in vertebrates, SuFu and Cos2 function as

negative regulators of Hh signaling, while Fused functions as a positive regulator

of Hh signaling.

   fkbp8, an immunophilin gene, has also been implicated in Hedgehog

signaling in vertebrates. Immunophilins, named after the type of

immunosuppressive drug they bind to, exhibit peptidyl-prolyl-cis/trans isomerase

(PPIase) activity, an important but slow step in protein folding (Edlich and

Fischer, 2006; Hamilton and Steiner, 1998). The *fkbp8* gene encodes the

Fkbp38 protein, an integral membrane protein which binds the

immunosuppressive macrolide FK506 (Bulgakov et al., 2004). In targeted mouse

fkbp8 mutants, in which all Fkp38 protein is lost due to replacement of exons 4-6

with a neo cassette, ventral neural tube cell types are dorsally expanded (Figure

7B) (Bulgakov et al., 2004). For instance, Nkx2.2-expressing vp3 interneuron

progenitors and Hnf3β-expressing floor plate are dorsally expanded and

ectopically located in the intermediate neural tube. Islet1/2-expressing motor

neurons are also ectopically induced in the dorsal aspect of the neural tube, while expression of the dorsal marker Pax6 is severely reduced (Bulgakov et al., 2004). In *fkbp8* mutants, expression of *gli3* in the dorsal neural tube is severely reduced while ectopic expression of ventral markers, *gli1* and *ptc1*, is found in the dorsal neural tube. Thus, *fkpb8* is necessary to limit Hh signaling to the ventral neural tube and therefore functions as a negative regulator of the Hh signaling pathway. Double mutant analysis between *shh;fkbp8* reveals that *fkbp8* functions downstream of *shh* for ventral neural tube induction and patterning (Bulgakov et al., 2004). For example, while motor neurons and other ventral cell types are lost in *shh* single mutants (Chiang et al., 1996; Wijgerde et al., 2002), in *shh;fkbp8* mutant neural tubes, Islet1/2-expressing motor neurons are present, resembling *fkbp8* mutant phenotypes (Figure 7B). Further, Hnf3β-expressing floor plate and Nkx2.2-expressing vp3 interneuron progenitors are also found in *shh;fkbp8* mutants, two cell types lost in *shh* mutants (Bulgakov et al., 2004; Chiang et al., 1996; Wijgerde et al., 2002). Expression of *gli3* is also restored to normal levels in *shh;fkbp8* double mutants (Bulgakov et al., 2004). Thus, *fkbp8* functions downstream of *shh* to prevent ectopic Hh signaling in the dorsal neural tube through regulation of *gli1* and *gli3* expression domains. In the absence of *fkbp8*, ventral neural tube cell types are induced in the dorsal neural tube at the expense of dorsal cell types while simultaneously, expression of *gli1*, normally in the ventral one-third of the neural tube, is found ectopically in the dorsal neural tube, at the expense of *gli3* expression, which normally is expressed in the dorsal two-thirds of the neural tube (Bulgakov et al., 2004).

Rab genes are GTPases involved in vesicular trafficking and have been shown to be involved in various signal transduction pathways. For instance, in the wing imaginal disc, *rab5* is necessary for propagating Dpp signaling (the fly ortholog to TGFβ), via a dynamin-dependent internalization event in the Dpp-receiving cells (Entchev et al., 2000). In flies misexpressing a dominant negative *rab5*, in which GDP is constitutively bound (OFF state), expression of *spalt* (*sal*), a Dpp-regulated gene, is eliminated wherever dominant-negative *rab5* is expressed (Entchev et al., 2000; Stenmark et al., 1994). In flies overexpressing *rab5*, ectopic *sal* expression domains are found in the wing discs (Entchev et al., 2000). In addition to a role in the Dpp signaling pathway, *rab5* is necessary for EGFR internalization in cell culture (Lanzetti et al., 2000). Thus, *rab5* is necessary and sufficient in regulating Dpp signaling *in vivo*, and EGF signaling in mammalian cell culture.

Rab23 has been implicated in motor neuron development in mice. In the mouse *rab23opb2* allele, an Enu-induced stop codon prematurely truncates mutant Rab23 protein, resulting in loss of C-terminally located GTP-binding domains and the Rab effector binding domains (Eggenschwiler et al., 2001). As both of these domain types are necessary for vesicular trafficking, the mouse *rab23opb2* mutant is likely a null allele (Eggenschwiler et al., 2001). In *rab23opb2* mutants, ectopic motor neurons expressing Hb9, Isl1/2, and Mnr2 form in the dorsal neural tube (Figure 7B) (Eggenschwiler and Anderson, 2000; Eggenschwiler et al., 2001). Expression of dorsal markers such as Pax6 is decreased in *rab23opb2* mutant neural tubes (Eggenschwiler and Anderson, 2000). Western analysis of whole

embryo extracts reveals that levels of Gli3 repressor isoforms (Gli3R) are severely down-regulated in *rab23* mutants (Eggenschwiler et al., 2006). Epistasis experiments reveal that *rab23* functions downstream of *smoothened* but upstream of *gli2* (Eggenschwiler et al., 2006). For instance, while all motor neurons are missing in *smoothened* mutants (Wijgerde et al., 2002; Zhang et al., 2001), in *rab23;smo* double mutants, Hb9-expressing motor neurons are present and in ectopic locations, as in single *rab23* mutants (Eggenschwiler et al., 2006). However, in double *rab23;gli2* mutants, all ectopic Hb9-expresssing motor neurons in the dorsal neural tube are lost but Hb9-expressing motor neurons at normal DV levels are unaffected, a phenotype strongly resembling the *gli2* single mutant phenotype (Eggenschwiler et al., 2006; Matise et al., 1998). Taken together, *rab23* functions downstream of *smoothened* but upstream of *gli2*, to regulate processing of Gli3 and therefore Hh signaling. In mouse *rab23* mutants, the neural tube becomes ventralized as Gli3 repressor isoforms fail to form in the dorsal neural tube. Loss of *rab23* function also permits activation of *gli2*-mediated Hh signaling in the dorsal neural tube for at least motor neuron induction. Thus, *rab23* likely promotes the *in vivo* formation of Gli3 repressor isoforms to inhibit Hh signaling transduction in the dorsal neural tube (Eggenschwiler et al., 2006).

DAZ-interacting protein (Dzip1) has also been implicated in Hh signaling. Dzip1 is a novel protein containing an NLS, a putative NES, and several protein-protein interaction domains (PEST, coiled-coil, zinc-finger) (Sekimizu et al., 2004; Wolff et al., 2004). In zebrafish *dzip1/iguana* mutants, expression of ventral

neural tube markers such as *nkx2.2* is severely reduced both in the hindbrain and in the spinal cord (Sekimizu et al., 2004). Epistatic analysis reveals that zebrafish *dzip1* functions downstream of PKA and upstream of *gli* genes (Sekimizu et al., 2004). For instance, cyclopamine-mediated disruption of the Hh signaling pathway results in loss of *nk2.2* expression at all axial levels (Keeler, 1969; Sbrogna et al., 2003). However, expression of *nk2.2* in *dzip1/iguana* mutants is unaffected by cyclopamine treatment, suggesting that *dzip1* functions downstream of cyclopamine's pharmacological target, Smoothened (Keeler, 1969; Sekimizu et al., 2004; Taipale et al., 2000). Likewise, misexpression of dominant-negative PKA (Ungar and Moon, 1996) fails to induce ectopic *nk2.2* expression in *dzip1/iguana* mutants. Forskolin treatment pharmacologically activates adenylyl cyclase, which results in increased cAMP levels; as a consequence, increased allosteric binding of cAMP to regulatory subunits of the PKA holoenzyme releases active, catalytic PKA subunits. In this way, pharmacological activation of PKA activity via forskolin administration to *iguana* mutant embryos also fails to induce ectopic *nk2.2* expression in the neural tube (Sekimizu et al., 2004). However, in double mutants between *dzip1/iguana*;*gli1* or *dzip1/iguana*;*gli2*, expression of *nk2.2* in the neural tube is severely reduced (Sekimizu et al., 2004). Thus, zebrafish *dzip1* functions downstream of *smo* and *pka* but upstream of *gli* genes for progenitor specification in the ventral neural tube (Sekimizu et al., 2004).

1.2.11 Intraflagellar Transport (IFT) Proteins and Hedgehog Signaling

Recent work in vertebrates has also demonstrated that primary cilia have a role in regulating Hh signal transduction (Figure 4 and 5) (Huangfu and Anderson, 2006). Nearly every vertebrate cell when not in mitosis carries primary cilia (Scholey, 2003; http://members.global2000.net/bowser/cilialist.html). Primary cilia are cytoplasmic hair-like protrusions, likened to cellular antennae (Scholey, 2003). Like other cilium, a cross section of primary cilia reveals an axoneme, consisting of nine outer doublet microtubules plus two inner microtubules. Non-motile primary cilia have a 9+0 arrangement. The primary cilium's axoneme serves a scaffold for motor proteins. As primary cilium lack ribosomes and the axoneme's microtubules are in dynamic equilibrium, intraflagellar transport (IFT) is necessary to maintain the integrity of the primary cilium. Kinesin-II (anterograde) motor proteins load cargo and other IFT proteins, also called IFT particles, at the basal body, the centriole, and deliver IFT cargo along the microtubules to the distal tip of the primary cilium (Scholey, 2003). Dynein (retrograde) motor proteins then recycle Kinesin-II motors and other IFT particles from the tip back to the basal body (Scholey, 2003). The formation of the primary cilium, and hence the process of intraflagellar transport, requires the function of IFT motors (Kinesin-II or Dynein) and IFT particles (Huangfu and Anderson, 2006; Scholey, 2003).

Primary cilia have been shown to be involved in numerous signaling pathways (Scholey, 2003). For instance, in cell culture, expression of the IFT

particle, *ngd5*, is down-regulated by opioid signaling (Wick et al., 1995). In

mouse fibroblast cells, the IFT particle, Ift88/Polaris, is necessary for the up-

regulation of platelet-derived growth factor receptor-α, (PDGFRα) at the primary

cilium membrane. In Ift88/Polaris mutant fibroblasts, phosphorylation and hence

activation of the PDGFRα effectors, Mapk and Erk1/2, is disrupted presumably

due to a requirement for PDGFRα localization to the primary cilia (Schneider et

al., 2005). IFT proteins are not only necessary for the construction of primary

cilia, but also for mediating signal transduction from within primary cilia (Wang et

al., 2006). For example, in the green algae, *Chlamydomonas*, zygote formation

requires both the agglutinin signaling pathway and flagellar adhesion between

algal gametes. In such ciliated algal gametes, temperature-sensitive mutants in

kinesin-II grown under restrictive conditions fail to activate effectors of the

agglutinin transduction cascade, including the phosphorylation of a tyrosine

kinase and a cGMP-dependent protein kinase (PKG) (Wang et al., 2006). Thus,

primary cilia appear to be necessary as scaffolds for receptor localization (PDGF

signaling) as well as signaling organelles (agglutinin signaling) for proper effector

activation (Schneider et al., 2005; Wang et al., 2006).

In the mouse ventral node, posteriorly-oriented primary cilia have been

implicated in the establishment of left-right asymmetry (Hirokawa et al., 2006;

Nonaka et al., 1998). The primary cilia of ventral nodal cells are motile and beat

in a clockwise fashion to generate a net leftward fluid flow, also known as nodal

flow (Hirokawa et al., 2006). In mouse IFT motor mutants either for *kinesin*

(Nonaka et al., 1998) or *dynein* (Supp et al., 1999; Supp et al., 1997), both nodal

flow and specification of left-right asymmetry is eliminated. Forced, artificial

nodal flow in a rightward vector across the mouse ventral node in wild type

embryos is sufficient to eliminate left-right asymmetry (Nonaka et al., 2002).

However, artificial nodal flow in a leftward vector in the mouse ventral node of

dynein mutant embryos is sufficient to re-establish left-right asymmetry (Nonaka

et al., 2002). Thus, the biophysics behind primary cilium rotation appears to

drive left-right asymmetry establishment. Alternatively, *in vivo* imaging and TEM

analysis has revealed vesicular budding from the membranes of primary cilium

(Haycraft et al., 2005; Tanaka et al., 2005). Pharmacological inhibition of FGF

signaling results in loss of vesicular buds, the nodal vesicular parcels (NVPs)

(Tanaka et al., 2005). NVPs contain Shh ligand, and misexpression of Shh in

mouse embryos pharmacologically treated with FGF signaling blockers is

sufficient to rescue NVP secretion (Tanaka et al., 2005). Thus, in the mouse

ventral node, vesicular buds released from primary cilium appear to be a source

of Hh ligand.

In addition to the Hh ligand, localization of Hh signaling components to the

primary cilium has also been described. In cell cultures of the mouse limb bud,

the Hh pathway effectors, Gli1, Gli2, Gli3, and SuFu are localized to the distal

tips of primary cilium (Figure 5) (Haycraft et al., 2005). Interestingly, Gli3-

repressor isoforms fail to localize to primary cilia (Haycraft et al., 2005). In the

ventral node of mouse embryos, Smoothened localizes to primary cilia (Corbit et

al., 2005). In Madin–Darby canine kidney (MDCK) cells, Hh signaling is

necessary and sufficient for Smo localization to the primary cilia (Corbit et al.,

2005). In MDCK cells, transfection of a mutant Smo (Smo-CLD), carrying a two

residue substitution in a ciliary localization signal that is conserved across

multiple serpentine receptors, results in failure to localize mutant Smo protein to

primary cilia (Corbit et al., 2005). In vivo, morpholino-mediated knockdown of

Smoothened protein in zebrafish embryos results in the elimination all muscle

pioneer cells, a phenotype rescued by the co-injection of wild type *smo* mRNA

(Corbit et al., 2005). However, no rescue of muscle pioneers is observed in *smo*

morphants injected with *smo*-CLD mRNA. Taken together, Smo localization to

the primary cilium is very likely an essential event in Hh signal transduction at

least for muscle development. As primary cilia have also been reported

decorating the apical/lumenal surfaces of cells occupying the ventricular zone of

the mouse neural tube (Huangfu and Anderson, 2005), it is highly probable that

Hh pathway effectors localize to primary cilia for neural tube patterning and motor

neuron specification.

In mouse, neural tube patterning phenotypes arise in mutants of either IFT

motor proteins or IFT particles. For instance, mutations in either the Kinesin-II

anterograde subunit *kif3a* or in the Dynein retrograde motor *dnch2* are sufficient

to dorsalize the neural tube (Figure 7C) (Huangfu and Anderson, 2005).

Targeted mouse *kif3a* mutants result in a null condition because a floxed exon2

deleted by Cre recombinase activity creates a frameshift, with the concomitant

loss of Kif3a expression (Marszalek et al., 1999). In *kif3a* mutants, all Shh-

expressing floor plate and Nkx2.2-expressing vp3 interneuron progenitors are

eliminated, while expression of dorsal markers such as Pax6 is ventrally

64

expanded (Huangfu et al., 2003). Although not yet assayed, it is likely that motor neurons are also eliminated as *kif3a* mutant neural tubes resemble dorsalized mutants, similar to *smoothened* knockouts (Figure 7C) (Huangfu et al., 2003; Wijgerde et al., 2002; Zhang et al., 2001). Primary cilia are also lost in mouse ventral nodes of *kif3a* mutants (Marszalek et al., 1999). Epistatic analysis reveals that *kif3a* functions downstream of the *patched1* (*ptch1*) receptor (Huangfu et al., 2003). In the mouse *ptch1* knockout, expression of Hh-regulated genes, including a *lacZ* reporter under *ptch1* control, is severely up-regulated and found in ectopic locations including the dorsal neural tube (Goodrich et al., 1997; Huangfu et al., 2003). However, in *kif3a*;*ptch1* double mutants, expression of Hh-regulated genes such as *ptch1* is severely reduced, a phenotype closely resembling single *kif3a* mutants (Huangfu et al., 2003). Taken together, *kif3a* functions downstream of *ptch1*, for the specification of ventral neural tube cell types, presumably through a requirement for anterograde motors and primary cilia formation in mediating Hh signaling.

Similarly, mouse *dnchc2* mutants also exhibit dorsalized neural tube phenotypes (Huangfu and Anderson, 2005). In *dnchc2* mutants, all Shh-expressing floor plate and Nkx2.2-expressing vp3 interneuron progenitors are eliminated. Interestingly, all Hb9-expressing motor neurons are normal in the caudal spinal cord but are lost in the rostral segments of *dnchc2* mutants (Huangfu and Anderson, 2005). The *dnchc2* mutant phenotype results from an Enu-induced substitution of F3890S, occurring within the sixth AAA (ATPase associated with cellular activities) motif, likely representing a hypomorph (Garcia-

Garcia et al., 2005; Huangfu and Anderson, 2005). In double mutant neural

tubes between *dnchc2*;*ptch1*, expression of Hh-regulated genes is also severely

reduced. Thus, mouse Dnchc2, an IFT dynein motor, acts downstream of *ptch1*

to mediate Hh signaling for induction of motor neurons and other ventral neural

tube cell types (Huangfu and Anderson, 2005).

       Loss of function in the machinery of other IFT components, such as IFT

particles, is also sufficient to generate ventral neural tube defects. In the

targeted mouse *Ift88/polaris* mutant, in which replacement of exons two and

three with a LacZ cassette results in loss of transcript (Murcia et al., 2000), all

Shh-expressing floor plate is eliminated while expression of dorsal neural tube

markers such as Pax6 is ventrally expanded (Huangfu et al., 2003). Further, in

Ift88/polaris mutants, Lhx3-expressing motor neurons are severely reduced and

mispatterned (Liu et al., 2005), while Hb9-expressing motor neurons are

completely eliminated (Huangfu et al., 2003). *Ift88/polaris* mutants also lack

primary cilia in the mouse ventral node structure (Huangfu et al., 2003). Double

mutant analysis reveals that *Ift88/polaris* is epistatic to *patched1* but upstream of

gli genes (Huangfu and Anderson, 2006). For instance, although all motor

neurons are lost in *shh* mutants (Bulgakov et al., 2004; Chiang et al., 1996),

Lhx3-expressing motor neurons still form in *Ift88/polaris*;*shh* mutants, indicating

that *Ift88/polaris* functions downstream of *shh* (Liu et al., 2005). Likewise, the

ectopic expression of *patched1* in *ptc1* mutants is eliminated in *Ift88/polaris*;*ptch1*

mutant neural tubes (Huangfu et al., 2003). Interestingly, while *rab23* mutants

exhibit ectopic Hb9-expressing motor neurons in the dorsal neural tube

(Eggenschwiler 2000), all motor neurons are severely reduced in

Ift88/polaris;rab23 double mutants (Huangfu et al., 2003). Thus, a likely

endocytic event mediated by *rab23* is required upstream of a requirement for

Ift88/polaris in Hh signaling and motor neuron specification. Further, in

Ift88/polaris;gli3 double mutants, all Shh-expressing floor plate is eliminated while

Hb9-expressing motor neurons are present, albeit greatly reduced (Huangfu et

al., 2003). As motor neurons are lost in *Ift88/polaris* mutants, but form normally

in *gli3* mutants, *Ift88/polaris* therefore acts epistatic to *gli3* for motor neuron

specification. However, as floor plate forms normally in *gli3* mutants

(Eggenschwiler et al., 2006; Hui and Joyner, 1993) but not *Ift88/polaris* mutants

(Huangfu et al., 2003), *Ift88/polaris* acts epistatic to *gli3* for floor plate induction.

Taken together, *Ift88/polaris* functions upstream of *gli3* but downstream of *ptch1*,

to mediate Hh signaling and motor neuron specification.

Similarly, mutations in another IFT particle, *Ift172/wimple*, result in a

dorsalized neural tube (Figure 7C) (Huangfu and Anderson, 2006). In

Ift172/wimple mutants, in which an Enu-induced mutation results in a Leu564Pro

substitution, all primary cilia fail to form in the mouse ventral node (Huangfu et

al., 2003). In *Ift172/wimple* mutant neural tubes, all Shh-expressing floor plate

cells and Hb9-expressing motor neurons are eliminated, while expression of

Pax6 is ventrally expanded (Huangfu et al., 2003). Epistatic analysis reveals that

Ift172/wimple, like *Ift88/polaris*, functions between *ptch1* and *gli3*. In

Ift172/wimple;ptch1 double mutants, expression of Hh-regulated genes is

severely reduced, resembling single *Ift172/wimple* mutant phenotypes (Huangfu

et al., 2003). In *Ift172/wimple*;*smoothened* double mutants, Lhx3-expressing motor neurons and Chx10-expressing V2 interneurons form, albeit mispatterned (Huangfu and Anderson, 2005). As all motor neurons and Chx10-expressing V2 interneurons are missing in *smoothened* mutants (Wijgerde et al., 2002; Zhang et al., 2001), *Ift172/wimple* must therefore be epistatic to *smoothened* for motor neuron development and ventral neural tube patterning (Huangfu and Anderson, 2005). While ectopic motor neurons are found in single *rab23* mutants (Eggenschwiler and Anderson, 2000), Hb9-expressing motor neurons are severely reduced in *Ift172/wimple*;*rab23* mutants (Huangfu et al., 2003). Thus, *Ift172/wimple*;*rab23* neural tubes are dorsalized and resemble that of single *Ift172/wimple* mutants (Figure 7C), indicating that *Ift172/wimple* acts epistatic to *rab23* for motor neuron specification (Huangfu et al., 2003). However, motor neurons, but not floor plate, forms in *Ift172/wimple*;*gli3* mutants, indicating that *gli3* is epistatic to *Ift172/wimple* for motor neuron induction (Huangfu et al., 2003). Thus, *Ift172/wimple* functions downstream of *smoothened* but upstream of *gli3* for ventral neural tube patterning and motor neuron development.

In all IFT mutants, Gli3R isoforms are severely reduced in whole embryo extracts, biochemically demonstrating that IFT-mediated Hh signaling is necessary for Gli3 processing *in vivo*. However, genetic removal of *gli3* in IFT mutants, such as *Ift172/wimple* or *Ift88/polaris*, restores induction of most ventral neural tube cell types, including motor neurons (Huangfu et al., 2003). Such rescue of motor neuron specification strongly resembles *smo*;*gli3* or *shh*;*gli3* mutant phenotypes, with a notable exception (Litingtung and Chiang, 2000;

Wijgerde et al., 2002). In *smo*, and perhaps *shh* mutants, all motor neurons are

lost while formation of Gli3-repressor (Gli3R) is up-regulated at the expense of

Gli3-activator (Gli3A) isoforms (Chiang et al., 1996; Huangfu and Anderson,

2005; Litingtung and Chiang, 2000; Wijgerde et al., 2002; Zhang et al., 2001).

Thus, the loss of motor neurons in *smo* mutants correlates with the accumulation

of Gli3R isoforms, and genetic removal of *gli3* in a *smo* mutant background

permits motor neuron formation, presumably due to the absence of Gli3R

isoforms (Huangfu and Anderson, 2005; Wijgerde et al., 2002; Zhang et al.,

2001). A similar mechanism likely explains how motor neurons are rescued in

double mutants between *gli3* and either *Ift172/wimple* or *Ift88/polaris*. Although

IFT machinery is necessary biochemically for Gli3 processing and hence, Gli3R

accumulation, low levels of Gli3R isoforms might still accumulate in single IFT

mutants. Genetic removal of *gli3* would then eliminate all Gli3 isoforms,

permitting motor neuron specification akin to *smo*;*gli3* or *shh*;*gli3* mutant neural

tubes (Huangfu and Anderson, 2005; Huangfu and Anderson, 2006). Finally,

motor neurons specified in this fashion (by genetic removal of *gli3*) no longer

require *shh*, *smo*, or *Ift* components, implicating IFT machinery in preventing *gli3*

repressor function.

1.3   REGULATION OF GLI TRANSCRIPTION FACTOR

FUNCTION

1.3.1   Biochemical Nature of Gli Proteins

The ultimate effectors of the vertebrate Hh pathway are the Gli family of zinc-finger transcription factors. In *Drosophila*, only one *gli* homolog, the segment polarity gene *cubitus interruptus* (*ci*), mediates all Hh signaling while vertebrates, in contrast, express three *gli* genes (Hui et al., 1994; Karlstrom et al., 1999; Karlstrom et al., 2003; Lee et al., 1997; Nusslein-Volhard and Wieschaus, 1980; Stone et al., 1996). All *gli* genes encode a highly conserved 5-zinc-finger DNA binding domain near the N-termini, of which, the last four of five fingers have been shown to make direct contacts to Gli DNA binding sites (Figure 9A) (Pavletich and Pabo, 1993). As *gli* genes are bipotential, a cleavage site carrying PKA phosphodegron targets is located roughly in the middle of the protein, downstream of the DNA binding domains (Figure 9A) (Aza-Blanc et al., 1997). A nuclear localization signal is found near the 5th zinc finger DNA binding domain but upstream of the cleavage site (Wang and Holmgren, 1999). Two nuclear export sequences are located about 100 residues downstream of the cleavage site (Figure 9A) (Chen et al., 1999). Ci also carries two Cos2 binding domains in the N- and C-terminus and one SuFu binding site in the N-terminus (Figure 9A) (Wang et al., 2000b; Wang and Jiang, 2004). In the N-terminus, SuFu and Cos2 binding appears to be mutually exclusive (Wang and Jiang, 2004). Ci, Gli2, and Gli3 also contain an N-terminal repressor domain upstream of the zinc finger domain (Aza-Blanc et al., 1997; Dai et al., 1999; Ruiz i Altaba, 1999; Sasaki et

70

al., 1999), while Gli1 lacks repressor function (Dai et al., 1999; Karlstrom et al., 2003). A VP16-like transactivator domain, capable of recruiting general transcription factors such as $TAF_{II}31$, is found in the C-termini of Gli proteins (Yoon et al., 1998). Also in the C-termini, Gli proteins contain a binding domain for the transcriptional co-activator, cAMP-response-element-binding-protein (CBP, Figure 9A) (Dai et al., 1999). The CBP binding domain is essential for transactivator function *in vivo* (Chen et al., 2000).

1.3.2 Layers of Hh Regulation on Ci/Gli Proteins

Hh signaling regulates Gli proteins at transcriptional, post-translational, and subcellular localization levels (Ingham and McMahon, 2001). In mouse, *gli1* is expressed in the ventral half of the neural tube, while *gli2* and *gli3* are expressed in the dorsal two-thirds (Lee et al., 1997; Ruiz i Altaba, 1998). As a general rule, expression of *gli1* is dorsally expanded in mouse mutants in which Hh signaling is activated. Conversely, *gli3* expression becomes ventrally expanded in mutants that disrupt Hh signaling. For instance, in mouse *shh* mutants, with a loss of Hh signaling, *gli1* expression is severely reduced while *gli3* expression is ventrally expanded (Bai et al., 2002; Bulgakov et al., 2004; Chiang et al., 1996). Conversely, in mouse *ptch1* mutants, in which the Hh pathway is activated due to loss of a negative regulator, ectopic *gli1* expression is found in the dorsal neural tube (Goodrich et al., 1997). Meanwhile,

(Modified from Lum and Beachy, 2004)
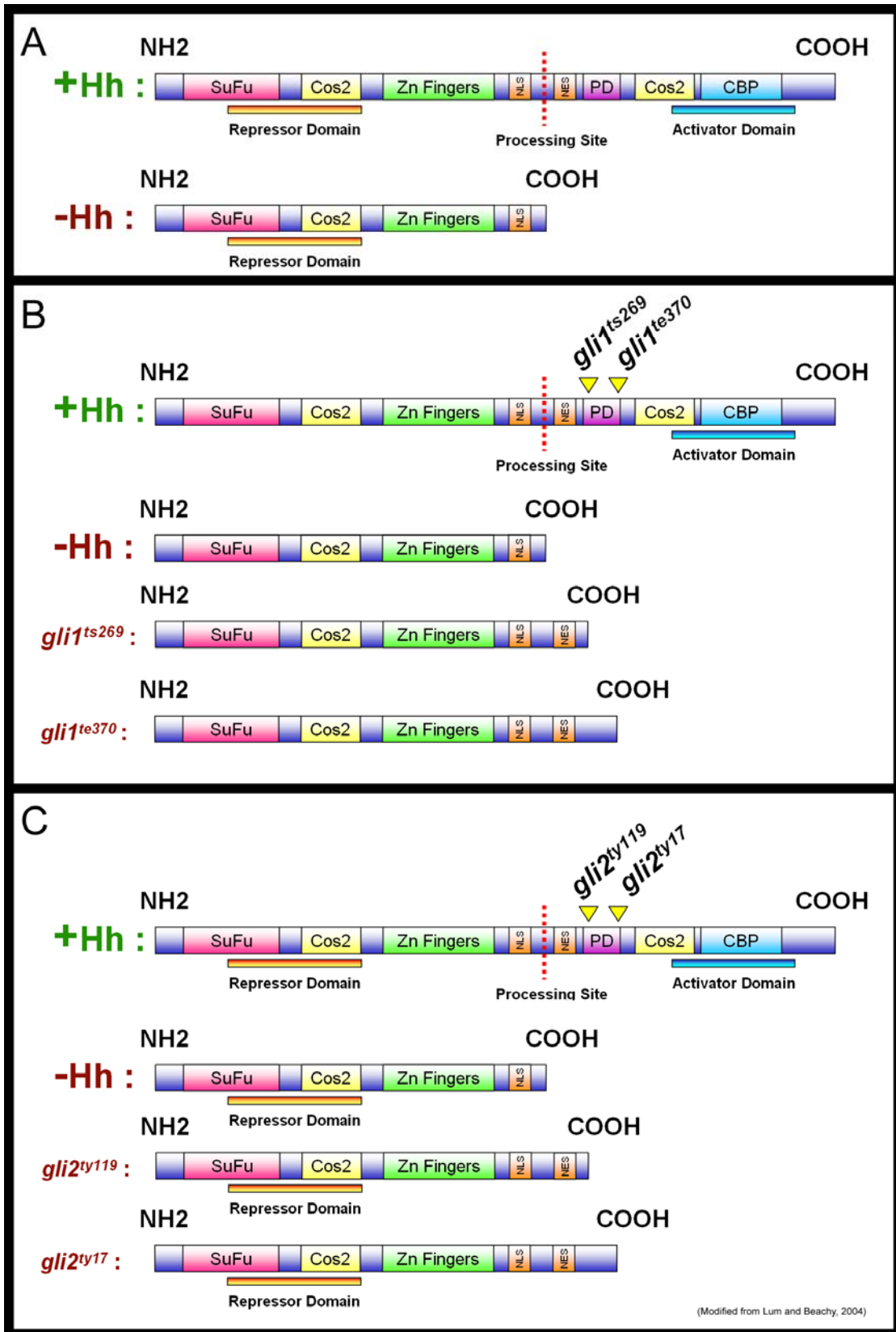
FIGURE 9. Gli Protein Structure

(A): Vertebrate Gli proteins exist as full-length transcriptional activators or truncated transcriptional repressors depending on the presence or absence of Hh ligand, respectively. Gli proteins carry an N-terminally located repressor domain upstream of the 5-zinc-fingered DNA binding domain. Protein interaction domains to SuFu and Cos2 are also found in the N-terminus, while the C-terminus contains both a Cos2 and CBP (Creb-Binding-Protein) interaction domain. In the C-terminus, a transcriptional activator is also found downstream of a Hh-regulated processing site. In the absence of Hh signaling, full-length Gli proteins are cleaved via a PKA/GSK3/CKI phosphodegron (PD) site near the processing site. Truncated Gli proteins enter the nucleus as transcriptional repressors of Hh target genes. **(B):** In zebrafish *gli1* mutant alleles, premature stop codons are found near the phosphodegron sites, upstream of the transcriptional activator domains. As zebrafish wild type Gli protein lacks N-terminal repressor function, mutant Gli1 proteins therefore lack both repressor and activator functions, resulting in a null condition (Karlstrom et al., 2003). **(C):** Like *gli1* mutants, zebrafish *gli2* mutant alleles are also generated by premature termination codons near the phosphodegron site. However, wild type zebrafish Gli2 does carry transcriptional repressor activity. Zebrafish *gli2* mutant alleles are therefore antimorphic in nature, with the ability to dominantly-negate Hh signal transduction (see Chapter 4) (Karlstrom et al., 1999; Karlstrom et al., 2003).

misexpression of *gli1* in the dorsal neural tubes of transgenic mice is sufficient to induce expression of several Hh-regulated genes at the expense of *gli3* expression (Hynes et al., 1997). Like the mouse, expression of zebrafish *gli1* and *gli2* in the neural tube is located in the ventral half and dorsal two-thirds, respectively. In zebrafish *smo* mutants, *gli1* expression is severely reduced (Chen et al., 2001; Karlstrom et al., 2003; Varga et al., 2001). Cyclopamine-mediated disruption of Hh signaling also severely reduces zebrafish *gli1* expression, phenocopying the *smo* mutant phenotype (Karlstrom et al., 2003). Thus, a basal level of *gli1* expression appears independent of Hh signaling at early embryonic stages. Misexpression of *shh* in the dorsal neural tube is also sufficient to induce ectopic *gli1* expression in mouse transgenic embryos (Rowitch et al., 1999). Therefore, Hh signaling is necessary and sufficient to regulate expression of *gli1* positively and *gli3* negatively, both in mouse and zebrafish. Mutations in Gli effectors also reveal feedback functions. For instance, *gli1* expression is severely reduced in mouse *gli2* knockouts, while all *gli1* expression is lost in *gli2;gli3* double mutants (Bai et al., 2004; Ding et al., 1998; Lei et al., 2004). Consistent with this, in cell culture, mouse Gli3 binds directly to the *gli1* promoter to induce *gli1* expression in the presence of Hh signaling (Dai et al., 1999). Thus, *gli*-mediated Hh signaling is necessary for the expression of at least *gli1* in mice. **We examined the role of the zebrafish *gli* genes for *gli1* expression in the hindbrain in Chapter 4.**

At the post-translational level, Hh signaling inhibits proteolytic processing of Ci, the *Drosophila* Gli homolog. In the absence of Hh signaling, full-length 155

kDa Ci is C-terminally truncated to a 75 kDa isoform that represses Hh signaling (Figure 5 and 9A) (Aza-Blanc et al., 1997; Robbins et al., 1997). C-terminally truncated isoforms lack CBP and VP16-like domains (Figure 9A) (Dai et al., 1999; Karlstrom et al., 1999). In the absence of Hh signaling, full-length Ci is sequentially phosphorylated by three protein kinases, PKA, GSK3, and CKI, generating a phosphodegron target recognized by the SCF[Slimb] complex, an E3 Ub ligase (Chen et al., 1998; Deshaies, 1999; Jia et al., 2002; Jiang, 2002; Price and Kalderon, 1999; Price and Kalderon, 2002; Wang et al., 1999). SCF[Slimb] facilitates neddylation of Ci which then targets full-length Ci for partial proteasome processing into the 75 kDa isoform (Jiang, 2002; Ou et al., 2002). Of the three vertebrate Glis, only Gli2 and Gli3 have been shown to be proteolytically processed in the absence of Hh signaling (Aza-Blanc et al., 2000; Dai et al., 1999; Wang et al., 2000a). In vivo, Hh signaling in mouse is necessary to prevent the accumulation of Gli3 repressor isoforms (Goodrich et al., 1997; Huangfu and Anderson, 2005; Wijgerde et al., 2002). However, loss of mouse IFT machinery, a condition in which Hh signaling is disrupted, also results in reduction of Gli3 repressor isoforms (Huangfu and Anderson, 2005; Liu et al., 2005), as primary cilia are believed to be locations for Gli3 processing (Haycraft et al., 2005; Huangfu and Anderson, 2006). In summary, Gli proteins are bipotential: C-terminally truncated isoforms act as repressors while full-length isoforms function as activators of Hh signaling (Figure 9A) (Koebernick and Pieler, 2002).

At the subcellular localization level, accumulating evidence in *Drosophila* suggests that, in the absence of Hh signaling, Ci is sequestered by the Hh Signaling Complex (HSC) to microtubules (Nybakken et al., 2002; Robbins et al., 1997; Sisson et al., 1997; Stegman et al., 2000). The Hedgehog Signaling Complex is made up of the serine/threonine kinase Fused, kinesin-like Costal2, and SuFu (Preat et al., 1990; Stegman et al., 2000). Microtubule association occurs via Costal2 (Wang et al., 2000b; Wang and Jiang, 2004). In this HSC-sequestered state, full-length Ci is processed to truncated Ci via PKA and Slimb (Jiang, 2002; Wang et al., 2000b). Upon Hh signaling, Fused and Costal2 become phosphorylated (Nybakken et al., 2002; Stegman et al., 2000). Costal2 then is recruited to the cytoplasmic tail of Smoothened, and the HSC loosens from its microtubule association, permitting Ci to evade processing for nuclear entry. In vertebrates, nuclear entry appears to be mediated by dZip1 (Sekimizu et al., 2004; Wolff et al., 2004).

Thus, Hh signaling prevents processing of Ci, permitting full-length Ci isoforms access to the nucleus, away from microtubule sequestration in the cytosol (Figure 5) (Chen et al., 1998; Ingham and McMahon, 2001; Jiang and Struhl, 1995; Wang et al., 2000b). In vertebrate limb bud cells, all three full-length Gli proteins localize to the distal tips of primary cilia (Haycraft et al., 2005). Interestingly, SuFu also localizes to primary cilia tips, while Gli3-repressor only isoforms fail to localize to primary cilia (Haycraft et al., 2005). Thus, primary cilia might serve as scaffolds for the processing of Gli proteins, although more evidence is needed to support this hypothesis (Figure 5).

CHAPTER 2

PROTOCOLS & TECHNIQUES

2.1   FISH MAINTENANCE

Zebrafish stock lines were maintained on a constant day/night cycle as previously described (Westerfield, 1995). Embryos were generated by pairwise crossings between heterozygous carriers, collected, and grown under standard 28.5°C incubation in embryonic medium (E3) until desired developmental endpoints. Throughout the text, the developmental age of the embryo refers to the hours elapsed since fertilization (hours post-fertilization, hpf). To maintain transparent embryos, the pharmacological pigmentation blocker, phenylthiourea (PTU, Sigma) is added between 18 hpf to 22 hpf. At appropriate ages depending on the experiment, embryos were fixed overnight in 4% paraformaldehyde in phosphobuffered saline (PBS).

2.1.1   Genotyping Adult Fin Clips

Working anesthetic (tricaine, Finquel MS222) is made by adding 10 ml of stock tricaine to 240 ml of fish water and brought to pH 7.0 using sodium

bicarbonate. Fish are briefly anesthetized in a small plastic container for up to

two minutes, and then placed on the index finger using a plastic spoon (with

holes to help drain liquid). Fin clips are made halfway between the tip of the fin

to a point at which fish scales end. Fish returned to holding cages revive rapidly

(within several minutes) and will regenerate clipped fins within two weeks.

To extract genomic DNA, 0.5 ml of lysis buffer is added per fin clip (15ml Lysis

Buffer: 12.3 ml ddH20, 1.5 ml 1M Tris, pH8-8.5, 750 µl 4M NaCl, 150 µl EDTA,

150 µl 20% SDS, 150 µl ProteinaseK @ 12 mg/ml). Fin clips are digested by

rocking overnight at 55°C incubation. The following day, undigested material is

pelleted by centrifugating for 20 minutes at room temperature. Clear supernatant

(containing genomic DNA) is transferred to fresh tubes containing 0.5 ml 100%

ethanol and rocked at room temperature for several hours (3-4 hrs). The

viscosity of the solution will gradually disappear and white/yellow strands will

precipitate, indicating completion. Genomic DNA can be harvested by a 20

minute centrifugation at 4°C followed by an ethanol series precipitation wash

(100% to 70%), and resuspended in 10-30 µl Tris-EDTA (TE). The DNA is then

stored at 4°C.

2.1.2 Genotyping Embryonic Trunks

Instruments (scissors and deyolking needle) are sterilized between each

trunk clip using ethanol. The water bath is preset to 50° C (48.4 setting).

Embryos are selected for genotyping, and in 70% glycerol, the trunks of three

embryos are arranged in a triangle and carefully clipped. The head and trunk

fragments are then placed in pre-labeled 1.7 ml microfuge tubes. Cuts are

repeated three at a time for remaining embryos, which helps process samples

expediently. Head fragments are then stored 4°C for potential slide mount

preparation.

For each trunk, to avoid cross-contamination, a separate pipette tip is

used to remove as much 70% glycerol as possible. 50 µl of extraction buffer is

then added per trunk per tube (10 ml Extraction Buffer: 8.25 ml ddH20; 1 ml 1M

Tris-HCl, pH 8.0; 500 µl 4M NaCl; 100 µl 0.5 M EDTA; 100 µl 20% SDS; 52.2 µl

of 23 mg/ml ProteinaseK). Using a different pipette per tube, both the 70%

glycerol and extraction buffer is gently mixed. Samples are then digested at

50°C for 2 hours, with gentle vortexing every 30 minutes. By the 2nd or 3rd

vortex, trunks should not be visible, indicating that the ProK reaction is working.

At this step, fiber optics (Fiberlite MI-150) or any acute source of bright, overhead

illumination is shone upon the samples to examine the extent of the ProK

digestion. Completed reactions will typically lack all tissue material except for

two black dots, representing the pigmented eyeballs. (Hints: Spin down any

condensation under tube caps as necessary. Push tubes completely in water

bath racks to minimize condensation formation underneath cap). After digestion

is complete, 1ul of 20mg/ml glycogen is added to each tube to aid in precipitation

followed by a very gentle vortex. For precipitation, 100 µl of 100% ice-cold

ethanol is then added to each tube, and each tube is gently vortexed again.

Genomic DNA is precipitated for 1-2 nights to increase yield by storing samples

at -20° C. After precipitation, DNA is harvested by microcentrifugation at 13,000 G for 30 min. A visible white pellet should form, representing the glycogen carrier and genomic DNA. Pellets are washed with 100 µl ice-cold 70% ethanol and dry very briefly. It is important to not let the pellet dehydrate at this point. Pellets are then resuspended in 10 µl ddH20 and 2 µl of this resuspension is used per PCR reaction.

2.2   MUTANT LINES

2.2.1 *slow-muscle omitted* (*smu*)

The *smu^{b641}* mutant allele studied herein was generated via ENU-mediated mutagenesis (van Eeden et al., 1996) resulting in a G242R substitution within the second of seven transmembrane domains of the Smoothened protein (Varga et al., 2001). *smu^{b641}* mutant embryos were phenotypically sorted and identified on the basis of trunk morphology and somite curvature at 21 hpf (Barresi et al., 2000; van Eeden et al., 1996; Varga et al., 2001). At ages earlier than 21 hpf, *smu^{b641}* mutants were identified by analyzing Hh target gene expression by in situ hybridization across entire embryo clutches, for comparison to theoretical, predicted Mendelian ratios. In mouse and zebrafish, loss of Smoothened function results in loss of all motor neurons (see Chapter 4) (Chen et al., 2001; Varga et al., 2001; Wijgerde et al., 2002).

2.2.2 *detour* (*dtr*)

dtr^te370 and *dtr^ts269* mutant alleles were generated by large scale chemical mutagenesis (van Eeden et al., 1996). *dtr* mutations are in the *gli1* gene, a member of the Gli family of zinc-finger transcription factors (Karlstrom et al., 2003) (see also Figure 9B). Both alleles are null conditions resulting from ENU-induced premature termination codons (*dtr^te370* = Q920Stop; *dtr^ts269* = Q881Stop) (Karlstrom et al., 2003). Both *dtr* alleles exhibit similar losses in cranial motor neuron cell number (Chandrasekhar et al., 1999).

The *dtr^ts269* mutation generates a restriction enzyme site for HpyCH4III (NEB, catalog number R0618S). To genotype *dtr^ts269* mutants, PCR primers were designed to amplify a 600 bp sequence flanking HpyCH4III (Forward Primer: 5'_CACCTGGCAACAACACAAGA_3', Reverse Primer: 5'_CATTCCTGCACCCTGGTATT_3'). The RFLP is resolved by HpyCH4III digestion (30 µl reaction: 6.5 µl ddH20, 3 µl 10X NEB 4 restriction buffer, 0.3 µl 100X bovine serum albumin, 0.2 µl HpyCH4III at 5 units/µl, 20 µl PCR product). HpyCH4III cuts only once in mutant *dtr^ts269* embryos, resulting in two bands: 247 bp and 346 bp. HpyCH4III does not cut PCR products amplified from wild type genomic DNA. The two bands are best resolved on 2% agarose gels.

2.2.3   *you-too* (*yot*)

yot^ty17 and *yot^ty119* mutants were also isolated from an ENU mutagenesis

screen (van Eeden et al., 1996). Like *smu* mutants, *yot* alleles were

phenotypically identified on the basis of somite morphology and tail curvature at

21 hpf (Karlstrom et al., 1999). Both *yot* alleles carry mutations in the Gli2

transcription factor (Karlstrom et al., 1999; see also Figure 9C) and are

antimorphic, functioning as dominant-negative repressors of Hh signaling (see

Chapter 4) (Karlstrom et al., 2003).

Genotyping of *yot^ty17* mutants was performed as previously described

(Karlstrom et al., 2003). Briefly, the *yot^ty17* mutation disrupts an NlaIV site (NEB,

catalog number R0126S). PCR amplification using forward

(5'_CCACCTAGCATATCAGAGAAC_3') and reverse

(5'_CTTGCTCACCGATATTCTGAC_3') primers amplifies a 589 bp overlapping

the *yot^ty17* mutant loci. NlaIV digestion of wild type PCR product results in two

cuts producing 227 bp, 253 bp, and 109 bp bands while digestion of *yot^ty17*

mutant PCR product results in one cut producing a 227 bp and a 362 bp band,

best resolved on 2.5% agarose gels (30 µl reaction: 5.7 µl ddH20, 3 µl 10X NEB

4 restriction buffer, 0.3 µl 100X bovine serum albumin, 1 µl NlaIV at 1 unit/µl, 20

µl PCR product).

As the *yot^ty17* allele is not a complete antimorph like the *yot^ty119* mutant

(see Chapter 4) (Karlstrom et al., 1999; Karlstrom et al., 2003), we developed a

genotyping method for the *yot^ty119* allele. The *yot^ty119* mutation (Karlstrom et al.,

1999) creates an NlaIII site (NEB, catalog number R0125S), thus serving as an

RFLP. PCR primers designed to silence nearby NlaIII sites amplify a 137 bp

product (Forward: 5'_ ATGATGCCTCGAAGTTCC_3'; Reverse:

5'_GGCAGACGTGATAGGTGT_3'). NlaIII digestion fails to cut wild type PCR

product (137 bp) while *yot*^{ty119} mutant PCR product is cut once (102 bp, 35 bp),

an RFLP best resolved on a 3% agarose gel (30 μl reaction: 6.5 μl ddH20, 3 μl

10X NEB 4 restriction buffer, 0.3 μl 100X bovine serum albumin, 0.2 μl NlaIII at

10 units/μl, 20 μl PCR product).

2.2.4 *mind bomb* (*mib*)

mib mutant alleles were also generated from an ENU-induced

mutagenesis screen. The *mib*^{ta52b} mutant allele carries a M1013R residue

substitution in the RING domain of an E3 ubiquitin ligase of the Notch-Delta

signaling pathway. *mib*^{ta52b} mutants appear to result in null conditions (Itoh et al.,

2003).

2.2.5 *islet1*-GFP transgenic line

Islet1 is a LIM/homeobox gene expressed in postmitotic neurons at or

near the verge of cell cycle exit (Appel et al., 1995; Ericson et al., 1992;

Hutchinson and Eisen, 2006; Korzh et al., 1993; Osumi et al., 1997). Expression

in branchiomotor neurons (nV, nVII, nX) by the *islet1*-GFP reporter line faithfully

recapitulates islet immunohistochemical labeling except in the nIX subpopulation

(Chandrasekhar et al., 1997; Higashijima et al., 2000). The *islet1*-GFP transgene
was bred into carriers of the above mutant alleles for the *in vivo* monitoring of
cranial motor neuron development.

2.2.6   *olig2*-GFP transgenic line

Expression of *olig2*-GFP is most prominent at 48 hpf, at which time
somatic motor neurons of the head and tail become labeled (see Chapter 5)
(Park et al., 2004). The *olig2*-GFP was bred into wild type lines for
pharmacological experiments involving cyclopamine.

2.3   <u>CELL BIOLOGY</u>

2.3.1   BrdU (5-bromo-2-deoxyuridine) Birthdating

As a base analog of thymidine, BrdU (Roche, catalog number 280879)
can become incorporated by DNA replication during S-phase of the cell cycle.
To incorporate BrdU, at 2 hpf of development, Pronase-E dechorionated *islet1*-
GFP transgenic embryos were transferred to 1.2% agar coated Petri dishes and
grown at 28.5°C. At desired developmental ages (9hpf to 27 hpf), embryos were
transferred to glass cavity blocks containing 4 ml of 10 mM BrdU / 15% DMSO in
embryonic medium (E3) without methylene blue (50 mM stock solution: 153.5 mg
BrdU dissolved into 10 ml of ddH20). BrdU treatment lasted for 30 minutes on

ice and embryos were subsequently returned to E3 and grown until 36 hpf and then fixed. Fixed embryos were then shifted to methanol for 2 days at -20°C.

For detection of BrdU-incorporation, fluorescent immunolabeling was performed. Briefly, embryos were rehydrated with PBTx (1X phosphobuffered saline + 3% Triton-X), washed twice for 5 minutes in PBTx, rinsed in 2N HCl in PBTx twice for 5 minutes each, incubated in 2N HCl in PBTx for 30 minutes, and rinsed in PBTx twice for 5 minutes each. Embryos were then blocked for 5-7 hours in PBTxB (PBTx + 0.25% BSA). For simultaneous incubation with mouse anti-BrdU antibody (1:50) and rabbit anti-GFP IgG (1:1000), embryos were rocked gently overnight at 4°C. Embryos were then washed 8 times with PBTx for 30 minutes each, blocked in PBTxB for 30 minutes, and simultaneously incubated with goat anti-mouse AlexaFluor 568 (1:500) and goat anti-rabbit AlexaFluor 488 (1:500), overnight on a 4°C rocker in the dark. Embryos were then washed three times in 1X PBS, fixed in 4% paraformaldehyde for 45 minutes, and washed three times again in 1X PBS. Imaging of BrdU-treated samples was performed on an Olympus IX70 microscope equipped with a BioRad Radiance 2000 confocal laser system, using the following settings: Z-step of 2.5 microns, 20X Uplanar objective, 512 x 512 resolution, 500 lps scan speed, and a Kahlman averaging value of two. Two permit cell counts, individual optical Z-sections were preserved for both BrdU (RITC) and *islet1*-GFP (FITC) channels.

For quantification of confocal images, individual Z-planes (2.5 microns deep) from samples double stained with anti-BrdU and anti-GFP antibodies (for

vendor and concentration info, see Table 1) were scored for both the total number of BMNs expressing the *islet1*-GFP transgene (GFP$_{total}$) and also the total number of *islet*-GFP expressing BMNs which incorporated BrdU (GFP$_{BrdU}$). For each transgenic embryo exposed to BrdU, ratios between GFP$_{BrdU}$:GFP$_{total}$ were calculated per optical Z-section per BMN subpopulation. BMN-specific ratios were then averaged and standard deviations generated using Graphpad InStat software for all embryos exposed to a given BrdU timepoint, with sample sizes of at least five embryos per timepoint.

2.3.2   Acridine Orange Labeling

Acridine orange (3,6-dimethylaminoacridine) is a cell-permeable nucleic acid binding dye used to visualize the extent of cellular degeneration. Acridine orange fluoresces green (FITC channel) when bound to double-stranded DNA and red (rhodamine/RITC channel) for single-stranded DNA (a marker for cellular degeneration). To detect degenerating cells, live dechorionated embryos were placed into glass petri dishes and incubated for 1 hour in PBS, pH 7.1 with 2 mg/ml of acridine orange (Sigma). Embyros were then embedded in methyl cellulose or viewed under a depression slide using an Olympus BX-60 equipped with RITC/FITC filter sets.

2.4   PHARMACOLOGY

2.4.1   PTU Treatments

To block pigmentation and preserve specimen transparency, stock 40 mM (200X) phenylthiourea (PTU) was administered to embryos in embryonic medium (E3) at a working concentration of 0.2 mM from 18 hpf to 22 hpf.

2.4.2   Cyclopamine Treatments

Embryos were treated with the Hh pathway inhibitor, cyclopamine (Toronto Research Chemicals, catalog number C988400) (Taipale et al., 2000) as described previously (Karlstrom et al., 2003), with the following modifications. Cyclopamine stock (10 mM in 95% ethanol) was administered at a high (100 µM) or low (25 µM) concentration in E3 medium containing 0.5% DMSO. For controls, embryos were exposed to a high (1%) or low (0.25%) ethanol concentration. Embryos were exposed as early as 3 hpf and as late as 48 hpf, depending on the experiment.

2.5   TRANSIENT mRNA MISEXPRESSION

At 1-cell to 8-cell stages, zebrafish cells are syncytial and mRNA or morpholino can be delivered for transient misexpression throughout the embryo. Briefly, embryos are lined up on glass slide trays, composed of two glass slides

87

glued together, with the top slide cut in half. Embryos are orientated with animal layers pointing towards the glass tray, furthest from the injection side. Pre-pulled microcapillary needles are loaded with either mRNA or morpholino depending on the experiment and then installed into a micro-manipulator. The micro-manipulator is connected to a gas-pressure pulse regulator that permits controlled pressure injections (~3-4 nl per embryos). Microcapillary needles must first be gently broken by bumping into the edge of the glass slide tray. Activated needles penetrate through the yolk for delivery of mRNA or morpholino either to the blastomere or the boundary between blastomere and yolk.

2.6   RNA PRODUCTION

2.6.1   mRNA Synthesis

Antisense (control) or sense mRNA is synthesized using an appropriate Ambion Message Machine Kit (T7 or Sp6) per manufacturer's recommendations. Briefly, 1.2 ug of linearized DNA template (at 1 ug / µl) is incubated at 37°C with 4.8 µl RNAse-free water, 10 µl of 2X ribonucleotide mix, 2 µl of 10X transcription buffer, and 2 µl of 10X RNA polymerase mix (T7 or Sp6), generating a final reaction volume of 20 µl. After 2 hours (3 hours for Sp6 RNA polymerase) at 37°C, each tube receives 30 µl of nuclease-free ddH20 and 25 µl of Lithium Chloride. To precipitate messages, samples are stored overnight at -20°C. The next day, samples are microcentrifuged for 20 minutes at 4°C, washed with 70%

ethanol, and resuspended in 25 μl of nuclease-free ddH20. Messages are stored

at -20°C. Yields and quality are determined by RNA gel electrophoresis and U.V.

spectroscopy.

2.6.2   Probe RNA Synthesis

Antisense probes are prepared from appropriately linearized DNA

templates using kit components (Roche) for visualization of endogenous

transcripts. Briefly, 1.2 ug of linearized DNA (at 1 ug/μl) is mixed with 5 μl of 10X

transcription buffer, 5 μl of 10X hapten (digoxygenin or fluorescein) NTP mix, 2 μl

of 25X RNasin, and 5 μl of 10X RNA Polymerase Mix (T3, T7, or Sp6), and

brought to a final volume of 50 μl. Hapten NTP mixes can be either digoxigenin-

or fluorescein-conjugated to uracil nucleotides. Reactions are incubated in a

37°C water bath for 2 hours. Probe RNA is then precipitated by adding 1 μl of 20

ug/μl glycogen, 5 μl of 0.2 M EDTA, 6.3 μl of 4M LiCl, and 190 μl of 100%

ethanol, followed by overnight storage at -20°C. The next day, samples are

microcentrifuged at 4°C for 20-30 minutes, and after washing with 70% ethanol,

resuspended in 30 μl of nuclease-free ddH20. Probes are stored at -20°C.

Probes are run on an RNA agarose gel to assess quality of *in vitro* transcription.

2.6.3   RNA Gel Electrophoresis

To enforce single-strandedness, formaldehyde agarose gels are prepared for visualizing quality of RNA syntheses as described (Davis et al., 1986). Briefly, in a 500 ml Erlenmeyer flask, 1 gram of agarose is melted in 84.8 ml of ddH20. Under a fume hood, 5.2 ml of room-temperature 37% formaldehyde is then added and gently swirled to prevent solidification. Next, 10 ml of 10X MOPS (0.2 M MOPS, 0.05 M sodium acetate, 0.01 M EDTA, pH 7.0, store at 4˚C) is added and gently swirled before casting the RNA gel. Once solid, the gel is flooded with 1X MOPS as running buffer. Each lane is loaded with 2-3 µl of RNA sample, 1 µl of ethidium bromide (1 mg/ml), and 16 µl of 1.25X RNA loading buffer (720 µl deionized formamide, 160 µl 10X MOPS buffer, 260 µl of 37% formaldehyde, 240 µl ddH20, 80 µl glycerol, 20 µl bromophenol blue, and 20 µl xylene cyanol) . Smeared bands indicate a low quality synthesis, while discrete bands typically indicate a successful transcription reaction.

2.7   EXPRESSION ANALYSIS

2.7.1   In Situ Hybridization

Due to the small size of the zebrafish embryo, whole-mount in situ hybridization is routinely performed to detect endogenous mRNA expression patterns. An in situ hybridization experiment takes three days, with probe hydbridization on day one, hapten recognition on day two, and chromogenic

90

substrate conversion on day three. Embryos must first be fixed in 4%

paraformaldehyde for at least twelve hours, followed by a methanol dehydration

series. Embryos are stored in methanol -20°C to clear background. Optimal

staining is achieved when using recently fixed (within 2 weeks) embryos and

prolonging methanol dehydration (3-5 days). All steps are performed at room-

temperature unless indicated otherwise. Embryos are rehydrated from methanol

through a series of methanol/PBST washes as follows: 1X5 min. 50% MeOH /

50% PBST, 1X5 min. 30% MeOH / 70% PBST, and then 2X5 min. PBST. To

better control staining variability, mutant and wild type sibling specimens are

combined into the same tube, after carefully clipping mutant trunks (somite

morphologies become difficult to distinguish rapidly after an in situ hybridization).

Samples are then fixed for 1 hour with 4% paraformaldehyde. Next, embryos are

permeabilized to increase probe penetration chances with: 3X5 min. PBST, 1X

ProteinaseK in PBST, and 2X5 min. PBST. ProteinaseK treatment times vary

according to age of embryo (hpf): 20 hpf, 5' ; 24 hpf, 7' ; 30 hpf, 10' ;36 hpf, 14' ;

48 hpf, 20'. Samples are then fixed for 1 hour to kill residual ProteinaseK

function. Next, embryos are washed 3X5 min. in PBST, followed by 1X10 min. in

50% PBST / 50% hybridization buffer. The Hybridization (Hyb) buffer contains

excess yeast transfer RNA (Roche, catalog number 109223) and thus functions

as a non-specific RNA blocker. Samples are placed into Hybridization buffer and

rocked gently at 70°C for at least two hours (I recommend five hours). Following

this blocking step, pre-warmed antisense probe RNA is added at a dilution of

1:100 in Hyb (some probes require 1:12.5, see Table 1), and samples hybridize

under gentle rocking for 12-16 hours at 70°C. Probe RNA can be either tagged with digoxigenin or fluorescein haptens.

After hybridization, samples are prepared for detection of the appropriate hapten (digoxygenin or fluorescein). First, hybridization buffer is pre-warmed to 70°C for at least 20 minutes. Next, probe is recovered and saved for reuse (good for 3-4 experiments). Samples are subsequently washed: 1X60 min. Hyb, 2X30 min. wash A (2X SSC, 50% formamide, 0.1% tween-20), 1X30 min. wash B (2X SSC, 0.1% tween-20), 2X30 min. wash C (20% wash B, 0.1% tween-20), all at 70°C. Next, specimens are washed at room temperature 1X10 min. in 50% wash C / 50% maleic acid-tween-20, followed by 2X10 min. maleic acid-tween-20. Tween-20 helps to permeablize cells as well as to prevent embryonic surfaces from sticking to (and tearing across) microcentrifuge tubes. Embryos are then first washed 1X10 min. in Blocking Solution, and then rocked in Blocking Solution for 3-5 hours. Blocking Solution contains excess casein proteins to increase signal to background ratios by sequestering non-specific protein binding partners. Next, an appropriate antibody directed against either digoxigenin or fluorescein is added and rocked at room temperature overnight (recommended 12-16 hours if possible). Both antibodies raised against either digoxygenin or fluorescein haptens are conjugated to alkaline phosphatase units.

The next day, embryos are washed 8X15 minutes in maleic acid-tween-20 in preparation for color development. For dark blue color reactions involving the alkaline phosphatase substrates NBT (Nitroblue tetrazolium chloride, Roche catalog number 1383213) and BCIP (5-Bromo-4-chloro-3-indolyl-phosphate, 4-

toluidine salt, Roche, catalog number 1383221), embryos are washed 3X10 min. in TMNT (100 mM Tris-HCl, pH 9.5; 50 mM MgCl$_2$; 100 mM NaCl; 0.1% tween-20; 1 mM levamisole), and then incubated at 37°C with TMNT + 0.45% NBT + 0.35% BCIP substrates. Alkaline phosphatase reactions dramatically accelerate at 37°C and NBT/BCIP product is thermostable. NBT/BCIP reactions typically take no longer than 4 hours. For Fast Red (Sigma) color reactions, embryos are washed 3X10 min. in 1M Tris-HCl, pH 8.2-Tween-20, and then mixed with 0.1M Tris-HCl, pH 8.2 + 1 mg / ml Fast Red + 0.4 mg / ml Napthol (Sigma F-4648). Fast Red substrate is toxic, extremely volatile, thermolabile, and light-sensitive. Fast Red reactions can only be developed at room temperature and require fresh substrate exchange every hour. Typically, an experiment requires five maximum substrate exchanges and the reaction can continue for 2-3 days if necessary. Finally, Fast Red is quite versatile: visible under standard light microscopy and excitable by rhodamine/RITC filter sets for fluorescent imaging.

After either blue or red color development, 3X5 min PBS washes are performed to remove NBT/BCIP carcinogens and samples are fixed overnight in 4% paraformaldehyde in PBS at 4°C. I've found that fixing for greater than one night reduces cellular quality. The next day, samples are washed through a glycerol series: 2X5 min. PBS, 1X10 min. 25% glycerol, 1X10 min. 50% glycerol, 1X10 min. 70% glycerol. Embryos are then deyolked in 70% glycerol or stored at 4°C.

2.7.2   Double In Situ Hybridization

Two-color labeling of mRNA transcripts in whole mount in situ preparations differs from single probe hybridizations in a few minor steps. First, a probe cocktail, consisting of digoxigenin-conjugated probe A mixed with fluorescein-conjugated probe B, is used overnight for day one hybridization. On day 2, only one of two alkaline phosphatase-conjugated antibodies (either anti-dig-AP or anti-flu-AP) is added after the blocking step. The antibody chosen is that which would produce the NBT/BCIP blue color reaction. On the third day, blue color is developed as in a single in situ hybridization, with the following exception. After color development, embryos are washed 3X5 min. in ddH20-Tween-20, and then 2X30 min. in 0.1M glycine-HCl, pH2.2 to deactivate all alkaline phosphatase activity. Samples are then washed 3X5 min in ddH20-Tween-20, 2X10 min. in maleic acid-Tween-20, and blocked anew as in the second day. After the blocking step, samples are treated with the second hapten-conjugated antibody for 12-16 hours. The next day, a Fast Red reaction is performed as described above for a single in situ hybridization. As NBT/BCIP is a chromogenic substrate and Fast Red is mostly fluorogenic, it is most helpful to develop NBT/BCIP prior to Fast Red development, as Fast Red color product rapidly disappears if developed prior to NBT/BCIP (blue) and subjected to 37°C during the second color reaction.

2.7.3   Chromogenic Immunohistochemistry

Antibody labeling procedures to visualize endogenous protein expression patterns also last for three days. On day one, samples are washed 4X45 min. in incubation buffer (IB: 1X PBS, 10 mg/ml bovine serum albumin, 0.5% triton-x100, 1% DMSO), 1X60 min. in IB + 1% horse serum (HS) (Sigma), and then exposed for 12-16 hours to diluted primary antibody in IB + 1% HS. Incubation buffer contains excess protein (bovine serum albumin, 10 mg / ml, Sigma) for blocking and TritonX100 (0.5%) and DMSO (1%) as permeants. Primary antibody dilutions used in this study are listed in a table below (see Table 1). Starting the first day of an immunohistochemistry on the second day of an in situ hybridization is most feasible, as such experiments become efficiently tiered. After overnight incubation with the desired primary antibody, embryos are then washed 2X30 min. in IB, 1X30 min. in IB + 1% HS (horse serum), and then exposed to a biotinylated secondary antibody (1:250 in IB+HS, Vectastain) directed against the F_{AB} fragments of the primary antibody. Biotinylated secondary antibody exposure lasts 6-8 hours and is followed by 3X30 min. washes in IB to clear unincorporated complexes. Next, specimens are washed in 3X30 min. in IB again and then treated 12-16 hours with avidin and biotinylated horse-radish peroxidase (HRP) to amplify signal (0.01% reagent A, 0.01% reagent B in IB, Vectastain). On day three, all unincorporated complexes are washed 6X15 min. in PBS +1% DMSO. Next, samples are incubated with 0.5 mg / ml 3,3'-diaminobenzidine (DAB, the HRP substrate) in PBS + 1% DMSO for 15 minutes. DAB color development is initiated by addition of 0.03% hydrogen peroxide, and

stopped after about 4-7 minutes with cold PBS + 0.1% sodium azide (an HRP blocker). Samples are washed 3X7 min. in PBS before the addition of 4% paraformaldehyde to kill residual HRP activity. After storage at 4°C in fix overnight, all samples are shifted to 70% glycerol as described for single in situ hybridizations.

2.7.4 Flurophoric Immunohistochemistry

Fluorescent antibody labeling procedures do not utilize HRP and instead use direct detection. On day one, like chromogenic immunohistochemical procedures, embryos are exposed to appropriate primary antibodies directed against endogenous epitopes. On day two, samples are then washed 7X30 min. in IB, followed by 2X30 min. IB + 1% HS. Embryos are then covered in foil and exposed to FITC- or RITC-conjugated secondary antibodies (Molecular Probes) at 4°C on a rocker for 12-16 hours. At this step, all manipulations are done in the dark or in foil to maximize stability of the flurophores. The next day, unincorporated complexes are washed away in 3X5 min. PBS, followed by 4% paraformaldehyde fixation for 1 hour. Samples are then washed 3X5 min. in PBS in the dark. As glycerol affects fluorophore stability, only a few embryos are shifted to 70% glycerol for immediate imaging while the rest are stored at 4°C in PBS. Images are then captured on an Olympus IX70 microscope equipped with a BioRad Radiance 2000 confocal laser system.

TABLE 1. Antibody and In Situ Probe Concentrations.

Reagent Concentrations (AB or IS)

Reagent	Concentration	Vendor	Catalog Number	Method	2° Concentration	Vendor	Catalog Number
mus-α-Zn5	1:10	DSHB	zn-12	goat-α-mus,RITC	1:500	MP/Invitrogen	A-11-004
mus-α-BrdU	1:50	DSHB	G3G4	goat-α-mus,RITC	1:500	MP/Invitrogen	A-11-004
rab-α-GFP	1:1000	Invitrogen	A-11-122	goat-α-rab,FITC	1:500	MP/Invitrogen	A-11-008
rab-α-pH3	1:750	Upstate	06-570	goat-α-rab,RITC	1:500	MP/Invitrogen	A-11-011
mus-α-GFP	1:750	Chemicon	MAB3580	goat-α-mus,FITC	1:500	MP/Invitrogen	A-11-001
mus-α-Islet	1:200	DSHB	39.4D	DAB			
mus-α-3A10	1:500	DSHB	3A10	DAB			
mus-α-A-tub	1:500	Sigma	T-6793	DAB			
rab-α-GFP	1:4000	Invitrogen	A-11-122	DAB			
α-myc	see 4/5/5			DAB			
mus-α-His	not tested yet	Novagen	70796-4				
all IS probes	1:100			N/B or Fred			
glf1 IS probe	1:12.5			F.Red			
nk2.2 IS probe	1:75			N/B			
fkd4 IS probe	1:12.5			N/B			

DSHB	Developmental Studies Hybridoma Bank
GFP	Green Fluorescent Protein
RITC	Rhodamine (Red) emission
FITC	Fluorescein (Green) emission
DAB	horse-radish peroxidase substrate
N/B	NBT/BCIP, an alkaline phosphatase substrate

TABLE 1. Antibody and In Situ Probe Concentrations.

For in situ hybridization, all probes were used at 1:100 dilution in hybridization buffer, except for

gli1 (1:12.5), *fkd4* (1:12.5), *phox2b* (1:12.5), and *nk2.2* (1:75). For primary antibodies (left

column), listed dilutions were used for whole-mount immunohistochemistry. Secondary

antibodies were used for flourescent antibody labeling (right column) at indicated dilutions.

Vendors and catalog numbers are also listed. Abbreviations: A-tub, aceytylated tubulin; BrdU, 5-

bromo-2-deoxyuridine; DAB, 3,3'-diaminobenzidine, a horse-radish peroxidase substrate; DSHB,

Developmental Studies Hybridoma Bank; GFP, Green Fluorescent Protein; F.Red, Fast Red;

FITC, fluorescein (green); mus, mouse; N/B, NBT/BCIP, an alkaline phosphatase substrate; pH3,

phosphohistone3; rab, rabbit; RITC, rhodamine (red).

2.8　　PROBE & ANTIBODY CONCENTRATIONS

All probes used in this study are diluted 1:100 in hybridization buffer, except for *gli1* (1:12.5), *fkd4* (1:12.5), *phox2b* (1:12.5), and *nk2.2* (1:75). Primary and secondary antibody concentrations (and vendor catalog numbers) for whole mount immunohistochemistry are listed in Table 1. Of note, when using rabbit anti-GFP (Invitrogen A-11-122) for chromogenic immunohistochemistry with DAB, use only 1:4000. For fluorophoric immunohistochemistry, rabbit anti-GFP at a 1:1000 dilution yields excellent results.

2.9　　QUANTIFICATION OF NEURONAL POPULATIONS

Quantification of islet-expressing motor neurons in the hindbrain and spinal cord was performed as previously described (Chandrasekhar et al., 1999). Briefly, immunostained embryos were carefully deyolked in 70% glycerol and slide mounts of head and trunk fragments made under an Olympus dissecting scope. Under differential interference contrast (DIC) imaging conditions on an Olympus BX60 slide microscope, dorsal preparations were counted for cranial motor neurons and lateral mounts for spinal motor neurons. In the hindbrain, cranial motor neuron cell bodies occupy stereotypic locations (see Figure 8) (Chandrasekhar et al., 1997). Cranial motor neuron cell bodies were scored for each rhombomeric compartment by counting nuclei using islet antibody. In the

spinal cord, motor neuron nuclei of a three hemisegments were counted at the level of the caudal yolk tube.

2.10   SOLUTION RECIPES

2.10.1 Common Use Solutions

<u>Embryo medium E3, (1L)</u>   <u>Final Concentration</u>

0.3 g NaCl   5 mM

13 mg KCl   0.17 mM

0.49 g $CaCl_2$ •$2H_2O$ 0.33 mM

80 mg $MgSO_4$ •$7H_2O$ 0.33 mM

Bring to final volume with ddH_2O

<u>0.1 M Phosphate Buffer (640 ml)</u>   <u>Final Concentration</u>

512 ml 0.1 M Na_2HPO_4 (13.7 g Na_2HPO_4 / 512 ml ddH_2O)   0.08 M

128 ml 0.1 M NaH_2PO_4 (1.76 g NaH_2PO_4 / 128 ml ddH_2O)   0.02 M

pH to 7.4 with 1 N NaOH   -

Use immediately for making 2X PBS

2X PBS (1.6 L)	Final Concentration
25.6 g NaCl	270 mM
0.64 g KCl	5 mM
640 ml 0.1 M Phosphate Buffer, pH 7.4	40 mM
Bring up to 1.6 L with ddH$_2$0	-
Aliquot into 4 X 500 ml bottles and autoclave	

1X PBS (400 ml)	Final Concentration
200 ml 2X PBS	-
200 ml ddH$_2$0	-
Autoclave in a 500 ml bottle	

4% Paraformaldehyde (500 ml)	Final Concentration
20 g paraformaldehyde (Acros 41678-500)	4%
250 ml ddH$_2$0	-

In hood, cover flask with parafilm and heat (medium, 2.5 setting) while stirring for

20 minutes to an hour, to dissolve granular paraformaldehyde.

Add 3-4 drops of 10 N NaOH to clear solution.

Filter solution using a funnel fitted with filter paper.

Bring up to 500 ml with 2X PBS.

Return filtered solution to flask.

Stir for 5 minutes, then check the pH using pH indicator paper (EM Reagents, catalog number 9590).

Adjust pH to 7.4 using 1 N NaOH.

Store in 40 ml aliquots at -20°C.

10X TBE Buffer (1 L)	Final Concentration
108 g Tris•base	0.88 M
55 g boric acid	0.88 M
40 ml 0.5 M EDTA, pH 8.0	0.2 M
Bring up to 1 L final volume with ddH$_2$0	-
No need to autoclave	

TE Buffer, pH 8.0 (100 ml)	Final Concentration
1 ml 1M Tris•HCl, pH 8.0	10 mM
0.2 ml 0.5 M EDTA, pH 8.0	1 mM

10X MOPS Buffer (1L)	Final Concentration
46.3 g MOPS	0.2 M
6.8 g Sodium Acetate	0.05 M
3.72 g EDTA	0.01 M

Adjust to pH 7.0. -

Bring to final volume with ddH$_2$0. -

Sterilize by autoclaving for 20 minutes.

1.25X RNA Loading Buffer (1.5 ml)	Final Concentration
720 µl deionized 100% formamide	48%
160 µl 10X MOPS buffer	1.1X
260 µl 37% formaldehyde	6.4%
240 µl ddH$_2$0	-
80 µl 100% glycerol	5.3%
20 µl 100% bromophenol blue	1.3%
20 µl 100% xylene cyanol	1.3%
6.8 g Sodium Acetate	0.17 mM

200X 1-Phenyl-2-thiourea, PTU (100 ml)	Final Concentration
6.1 g 1-Phenyl-2-thiourea (Sigma, P-7629)	40 mM
100 ml Dimethyl Sulfoxide, DMSO (Fisher, BP231-1)	-

Measure granular PTU in hood, with fan off, and a protective mask on.

To block zebrafish pigmentation, add 50 µl of 40 mM PTU per 10 ml of E3 between 18-22 hpf.

1X Danieau Buffer, pH 7.6 (500 ml)	Final Concentration
29 ml 1M NaCl	58 mM
0.7 ml 0.5 M KCl	0.7 mM
0.4 ml 0.5 M $MgSO_4$	0.4 mM
0.6 ml 0.5 M $Ca(NO_3)_2$	0.6 mM
2.5 ml 1M Hepes	5 mM
Bring to final volume with ddH_2O	-

Adjust pH to 7.6 using 1 N NaOH.

Do not autoclave. Filter sterlize each component.

2.10.2 Genomic DNA Isolation

Adult Fin Clip Lysis Buffer (10 ml)	Final Concentration
8.25 ml ddH20	-
1ml 1M Tris-HCl, pH 8.0	100 mM
0.5 ml 4M NaCl	200 mM
0.1 ml 0.5 M EDTA	5 mM
0.1 ml 20% SDS	0.2%
52.2 µl 23 mg/ml ProK	0.12 mg/ml

Embryonic Trunk Lysis Buffer (1 ml)	Final Concentration
886.3 μl ddH20	-
10 μl 1M Tris-HCl, pH 8.0	100 mM
50 μl 4M NaCl	200 mM
20 μl 0.5 M EDTA	10 mM
25 μl 20% SDS	0.5%
8.7 μl 23 mg/ml ProK	0.2 mg/ml

2.10.3 In Situ Hybridization

Use Diethyl pyrocarbonate (DEPC)-treated stock reagents to minimize RNAse contamination. Add 0.1% (v/v) DEPC (Sigma, D-5758) to autoclaved stock reagents, let sit in fume hood overnight after vigorous mixing, and autoclave for 20 minutes the following day.

PBST (40 ml)	Final Concentration
20 ml DEPC-treated ddH$_2$0	-
20 ml DEPC-treated 2X PBS	1X
40 μl Tween-20 (Sigma, P9416)	0.1%

Do not autoclave, make fresh and use immediately.

20X SSC (1L)	Final Concentration
175.3 g NaCl	2.99 M
88.2 g Sodium Citrate	0.29 M
800 ml ddH$_2$0	-
Adjust pH to 7.0 with 10N NaOH.	-
Bring to final volume with ddH$_2$0.	-
Sterlize by autoclaving for 20 minutes.	

Hybridization Buffer (30 ml)	Final Concentration
15 ml formamide (Fisher)	50%
7.5 ml 20X SSC	5X
30 µl 50 mg/ml heparin (Fisher)	50 µg/ml
1.5 ml 10 mg/ml yeast tRNA (Roche)	500 µg/ml
30 µl 100% Tween-20 (Sigma)	0.1%
276 µl 1M citric acid, pH 6.0 (LabChem, LC131180-1)	9.2 mM
5.664 ml DEPC-treated ddH$_2$0	-
Vortex at highest setting after adding each component.	-
Store at -20°C.	

Wash A (10 ml)	Final Concentration
1 ml 20X SSC	2X
5 ml formamide	50%
10 µl 100% Tween-20	0.1%
4 ml ddH$_2$0	-

Wash B (10 ml)	Final Concentration
1 ml 20X SSC	2X
10 µl 100% Tween-20	0.1%
9 ml ddH$_2$0	-

Wash C (10 ml)	Final Concentration
1 ml 100% Wash B	10% (0.2X SSC)
9 µl 100% Tween-20	0.09%
9 ml ddH$_2$0	-

Maleic Acid Buffer (1.6L)	Final Concentration
18.58 g Maleic Acid (Fisher)	100 mM
14.03 g NaCl	150 mM
9.6 g NaOH	150 mM

Adjust pH to 7.5 with 10N NaOH.   -

Bring to final volume with ddH$_2$0.   -

Sterilize by autoclaving for 20 minutes.

10% Stock Blocking Reagent (100 ml)	Final Concentration
10 g Blocking Reagent (Roche, 1096176)	10%
100 ml Maleic Acid Buffer	-
Dissolve granular blocking reagent in a microwave.	-
Avoid boiling over by microwaving at 30% power setting.	-
Sterilize by autoclaving for 15 minutes.	

2% Blocking Solution (10 ml)	Final Concentration
2 ml 10% Stock Blocking Reagent	2%
8 ml Maleic Acid Buffer	-
10 µl 100% Tween-20	0.1%

TMNT Buffer (10 ml)	Final Concentration
8.23 ml ddH$_2$0	-
1 ml 1M Tris•HCl, pH 9.5	100 mM
500 µl 1M MgCl$_2$	50 mM

250 μl 4M NaCl	100 mM
10 μl 100% Tween-20	0.1%
10 μl 1M Levamisole	1 mM

Do not autoclave. Use immediately.

NBT-BCIP Substrate Solution (10 ml)	Final Concentration
10 ml TMNT Buffer	-
45 μl 100 mg/ml Nitroblue tetrazolium chloride (Roche 1383213)	0.45 mg/ml
35 μl 50 mg/ml BCIP (Roche 1383221)	0.17 mg/ml

Note: BCIP's full name is 5-Bromo-4-chloro-3-indolyl-phosphate, 4-toluidine salt

Use immediately under dimly lit conditions.

Fast Red Substrate Solution (1 ml)	Final Concentration
Fast Red TR	1 mg/ml
Napthol AS-MX	0.4 mg/ml
Levamisole	0.15 mg/ml
Tris Buffer	0.1 M

Fast Red Substrate Solution (Sigma, F-4648) was prepared per manufacturer's directions. Briefly, one tablet of Fast Red TR/Napthol AS-MX and one tablet Tris Buffer/Levamisole is dissolved in 1 ml of ddH$_2$0 to generate working Fast Red Substrate Solution.

0.1 M glycine•HCl, pH 2.2 (200 ml)	Final Concentration
1.5 g glycine	100 mM
Adjust pH to 2.2 with 12 N HCl.	-
Bring to final volume using ddH$_2$0.	-
Filter sterilize into pre-autoclaved bottles.	

2.10.4 Immunohistochemistry

Incubation Buffer, IB (40 ml)	Final Concentration
20 ml 2X PBS (non-DEPC-treated)	1X
400 mg bovine serum albumin, fraction IV (Sigma, A7906)	10 mg/ml
200 µl 100% TritonX100 (Fisher, BP151)	0.5%
400 µl 100% Dimethyl Sulfoxide, DMSO (Fisher, BP231-1)	1%
19.4 ml ddH$_2$0	-

Use immediately or store at 4°C for next day use.

Incubation Buffer + Horse Serum (10 ml)	Final Concentration
10 ml Incubation Buffer	-
100 µl 100% Normal Horse Serum (Vectorlabs, S-2000)	1%

Make fresh, and use immediately.

Avidin-Biotin (AB) Solution (1 ml)   Final Concentration

1 ml Incubation Buffer   -

10 µl 1% Reagent A (Vectorlabs, PK6102 kit)   0.01%

10 µl 1% Reagent B (Vectorlabs, PK6102 kit)   0.01%

Make fresh, and use immediately.

PBS + DMSO (PD) solution (40 ml)   Final Concentration

40 ml 1X PBS (non-DEPC-treated)   -

400 µl 100% Dimethyl Sulfoxide, DMSO (Fisher, BP231-1)   1%

Make fresh and use immediately.

Diaminobenzidine (DAB) Stock Solution (66 ml)   Final Concentration

100 mg DAB (isopac, Sigma, D-9015)   1.5 mg/ml

66 ml ddH$_2$0   -

Extremely toxic, light sensitive   -

Under dim light conditions, remove aluminum seal on isopac.   -

Puncture rubber stopper with a syringe needle to remove pressure.   -

Do not remove rubber stopper as DAB exposure is very toxic.   -

Using a second syringe, inject 66 ml of ddH20 into isopac bottle.   -

Keep on ice and shake periodically until dissolved.   -

Store at -20°C in 1 ml aliquots.

Working DAB Substrate Solution (20 ml)	Final Concentration
13 ml PD solution	66% (0.66% DMSO)
6.67 ml 1.5mg/ml (3X) DAB stock solution	1X: 0.5 mg/ml

Working 0.03% Peroxide Substrate Solution (1 ml)	Final Concentration
1 μl 30% Hydrogen Peroxide (Fisher, H325-100)	0.03%
1 ml ddH$_2$0	-

To initiate horse-radish peroxidase reaction for immunohistochemistry, add 100 μl of 0.03% H$_2$0$_2$ substrate solution per well containing 1 ml of working DAB substrate solution.

Color reaction will complete within 4-14 minutes.

HRP reaction blocker (20 ml)	Final Concentration
200 μl 100X sodium azide	1X
20 ml 1X PBS	-

To kill horse-radish peroxidase activity, expose samples to pre-chilled HRP reaction blocker.

2.10.5 Pharmacology

Cyclopamine Stock Solution (243 ul)	Final Concentration
1 mg Cyclopamine (Toronto Research Chemicals, C988400)	10 mM
243 µl 100% ethanol	~95%
Vortex well and store at -20°C.	-

100 µM Cyclopamine Working Solution (1 ml)	Final Concentration
10 µl of 10 mM Cyclopamine Stock Solution	100 µM
5 µl 100% Dimethyl Sulfoxide, DMSO	0.5%
1 ml embryonic medium (E3)	-

Make working cyclopamine solution in individual microcentrifuge tubes.

Vortex well before exposing animals to cyclopamine.

Caution: Cyclopamine is a potent teratogen.

2.10.6 BrdU (5-bromo-2-deoxyuridine) solutions

Stock BrdU (5-bromo-2-deoxyuridine) solution (10 ml)	Final Concentration
153.5 mg BrdU (Roche 280879)	50 mM
10 ml ddH$_2$0	-

Working BrdU solution (10 ml)	Final Concentration
2 ml 50 mM stock BrdU solution	10 mM
1.5 ml 100% Dimethyl Sulfoxide, DMSO	15%
6.5 ml embryonic medium (E3) without methylene blue	-

CHAPTER 3

THE NEUROGENIC PHENOTYPE OF MIND BOMB MUTANTS LEADS TO SEVERE PATTERNING DEFECTS IN THE ZEBRAFISH HINDBRAIN

Note: My contribution to this publication includes the analysis of the *mib* mutant hindbrain for precocious neuronal differentiation as well as ventral neural tube defects (see Figures 10, 13, and 14; see also Table 4).

3.1   INTRODUCTION

In the vertebrate neural tube, specific types of neurons and non-neuronal cells are generated from neuroepithelial cells in well-defined spatial and temporal patterns to permit normal growth, patterning, and function of the nervous system. The mechanisms that underlie the choice between specific neuronal and non-neuronal fates have been intensively studied in vertebrates and invertebrates. The highly conserved Notch-Delta signaling pathway has been demonstrated to

play a central role in regulating production of different types of cells in both the nervous system and other tissues (Artavanis-Tsakonas et al., 1999). During vertebrate neural development, proneural gene expression defines domains in the neuroectoderm where cells have the potential to become neurons. Proneural genes drive expression of the Notch ligand, Delta. Delta activates Notch in neighboring cells and inhibits proneural gene function (and neuronal fate) in these cells in a process called lateral inhibition. In the absence of Notch-mediated lateral inhibition, too many cells in the proneural domains differentiate into neurons, generating a neurogenic phenotype (Chitnis et al., 1995; de la Pompa et al., 1997).

Mutagenesis screens in zebrafish have identified several genetic loci that encode components of the Notch signaling pathway (Jiang et al., 1996; Schier et al., 1996). Mutations in *deltaD* (*after eight*) and *notch1* (*deadly seven*) result in weak neurogenic phenotypes (Gray et al., 2001; Holley et al., 2000; Holley et al., 2002; van Eeden et al., 1996), suggestive of partially redundant functions shared with other *notch* and *delta* genes. A dominant negative mutation in *deltaA* generates a strong neurogenic phenotype (Appel et al., 1999; Riley et al., 1999). Loss-of-function mutations in *mind bomb* (*mib*) (Jiang et al., 1996; Schier et al., 1996), which encodes an E3 ubiquitin ligase required for effective Delta function (Itoh et al., 2003), result in a strong neurogenic phenotype (Haddon et al., 1998a; Jiang et al., 1996; Riley et al., 1999; Schier et al., 1996; van Eeden et al., 1996). In *mib* mutants, there is excess production of neurons born early in development (i.e., primary neurons), and a concomitant reduction in the number of later-born

(secondary) neurons (Itoh et al., 2003; Jiang et al., 1996; Park and Appel, 2003; Schier et al., 1996). In a 24-hr mutant embryo, the developing spinal cord is nearly filled with cells expressing *huC* (Itoh et al., 2003; Park and Appel, 2003), an early neuronal differentiation marker (Kim et al., 1996; Lyons et al., 2003).

Analysis of zebrafish Notch signaling mutants, including *mib*, showed that this pathway regulates cell fate decisions in trunk midline tissues (Appel et al., 1999). Other studies of *mib* mutants have demonstrated the significance of Notch signaling in preventing precocious generation of primary neurons so that sufficient undifferentiated cells are retained to acquire alternate fates such as secondary neurons, glial cells, and neural crest-derived cell types (Haddon et al., 1998a; Itoh et al., 2003; Jiang et al., 1996; Park and Appel, 2003; Riley et al., 1999). However, little is known about other consequences of premature neuronal differentiation in *mib* mutants. For example, it is not clear whether excessive neurogenesis in *mib* mutants can lead to the loss of signaling tissues that regulate later development or interferes with processes that maintain segmental identity. In this report, we have examined the differentiation and organization of various hindbrain cell types such as branchiomotor neurons, interneurons, and ventral midline cells to understand the consequences of the *mib* neurogenic phenotype for hindbrain segmentation and ventral midline signaling. We found that severe defects in segmental patterning and midline signaling seen after 21 hr in the mutant hindbrain correlate with the premature and extensive formation of neuronal cells. We suggest that these deficits are due to the loss of neuroepithelial cells that are normally prevented from

117

becoming neurons by Notch signaling, thus allowing them to serve essential roles in segmental patterning and midline signaling.

3.2   MATERIALS AND METHODS

3.2.1   Animals

Zebrafish were reared and maintained as described (Westerfield, 1995). Embryos were collected from pairwise matings, and developed at 28.5°C in E3 embryo medium (Bingham et al., 2002). Throughout the text, the developmental age of the embryos corresponds to the hours elapsed since fertilization (hours postfertilization, hpf). Embryos were transferred to E3 medium containing phenylthiourea between 18 and 22 hpf to prevent pigmentation. The *mind bomb* mutants (mib^{ta52b}) were identified on the basis of the morphology of the tectum and hindbrain at 24 hpf (Jiang et al., 1996). For analysis of branchiomotor neuron development, the motor neuron-expressed *GFP* transgene (Higashijima et al., 2000) was crossed into the *mib* mutant background.

3.2.2   Immunohistochemistry and In Situ Hybridization

Whole-mount immunohistochemistry was performed with various antibodies as described previously (Bingham et al., 2002; Chandrasekhar et al., 1997). Synthesis of digoxigenin- and fluorescein-labeled probes, whole-mount in

situ hybridization, and two-color development were carried out as described previously (Bingham et al., 2002; Chandrasekhar et al., 1997; Prince et al., 1998). Embryos were deyolked, mounted in glycerol, and examined with an Olympus BX60 microscope. In all comparisons, at least 10 wild type and 10 mutant embryos were examined. For sectioning, embryos were gently deyolked in glycerol, transferred to PBS (Westerfield, 1995) and embedded in 7% agarose (Ultra Low Melting Point Agarose, Fisher). Sections (50 μm) were made by using a Vibratome 1000 Plus system and were mounted in glycerol.

3.2.3 Confocal Microscopy

Confocal imaging was carried out on live or fixed embryos embedded in a dorsal orientation in 1.2% agarose. Images were captured on an Olympus IX70 microscope equipped with a Bio-Rad Radiance 2000 confocal laser system. For obtaining virtual cross-sections, the *GFP*-expressing cell bodies at a given axial level were identified and boxed. Metamorph software rotated the Z-stacks within the boxed area 90 degrees to provide a cross-sectional view.

For quantifying cellular morphologies, 30-40 Z-sections (×40 magnification) of 2 μm thickness were obtained at the level of the otic vesicle in the ventral neural tube, where the rhodamine-dextran labeled donor-derived cells were located. Four consecutive sections were stacked, and the resulting nonoverlapping Z-stacks were scored for cellular morphologies, taking care not to count the same cell twice. Cells were classified as neuroepithelial if they

exhibited columnar morphology (Figure 15E) and as neuronal if they were round and possessed at least one dendritic process (Figure 15F).

3.2.4   RNA Injections

Synthesis of full-length *shh* RNA was carried out as described previously (Chandrasekhar et al., 1998). RNA (~1 ng/embryo) was injected into one- to eight-cell stage embryos as described previously (Chandrasekhar et al., 1998).

3.2.5   Quantification of Neuronal Populations

Islet antibody-labeled nuclei of hindbrain neurons, ventral spinal cord neurons, and Rohon-Beard sensory neurons of the dorsal neural tube were counted in strongly labeled, preparations of 36 hpf embryos. Counts were performed under ×40 magnification.

3.2.6   Mosaic Analysis

Gastrula stage transplants and analysis of motor neuron development were performed essentially as described previously (Jessen et al., 2002; Moens and Fritz, 1999).

3.3 RESULTS

3.3.1 Premature Neuronal Differentiation in the *mind bomb* Mutant Hindbrain

To better understand the role of *mib* in hindbrain development, we monitored the expression of the pan-neuronal marker *huC* (Kim et al., 1996; Lyons et al., 2003) from early somitogenesis in embryos obtained from *mib +/-* crosses. In wild type embryos, *huC*-expressing cells were restricted to the lateral margins of the hindbrain at all axial levels (Figure 10A, 11C) at 17 hr postfertilization (hpf) and 24 hpf. In contrast, *mib* mutants contained large numbers of *huC*-expressing cells throughout the hindbrain (Figure 10B, 11D). In addition, expression of a neurogenesis marker *deltaD* (Haddon et al., 1998b) was mostly absent in the mutant hindbrain at 24 hpf (Figure 10E, 11F). These results indicate that a majority of cells at all axial levels in the mutant hindbrain initiate neuronal differentiation prematurely, with a concomitant loss of neuronal progenitor cells beyond 24 hpf.

To determine whether premature *huC* expression in the *mib* mutant hindbrain affected the development of later-born neurons, we examined the expression of a zebrafish *even-skipped* homolog *evx1*, which identifies *Dm-Grasp*-expressing (zn5/8 antibody-labeled) hindbrain commissural neurons and other interneurons (Fashena and Westerfield, 1999; Kanki et al., 1994; Thaeron et al., 2000; Trevarrow et al., 1990). In wild type embryos, *evx1* was expressed in medial and lateral domains in the hindbrain from 24 hpf (Figure 10G and data

121

WT | mib^{ta52b}

A — *huC* — tg, pg — 17 h
B — *huC* — tg, ag, pg
C — *huC* — tg, pg — 24 h
D — *huC* — tg, ag, pg
E — *deltaD* — tec, eye — 24 h
F — *deltaD* — tec, eye
G — *evx1* — cb — 36 h
H — *evx1* — cb
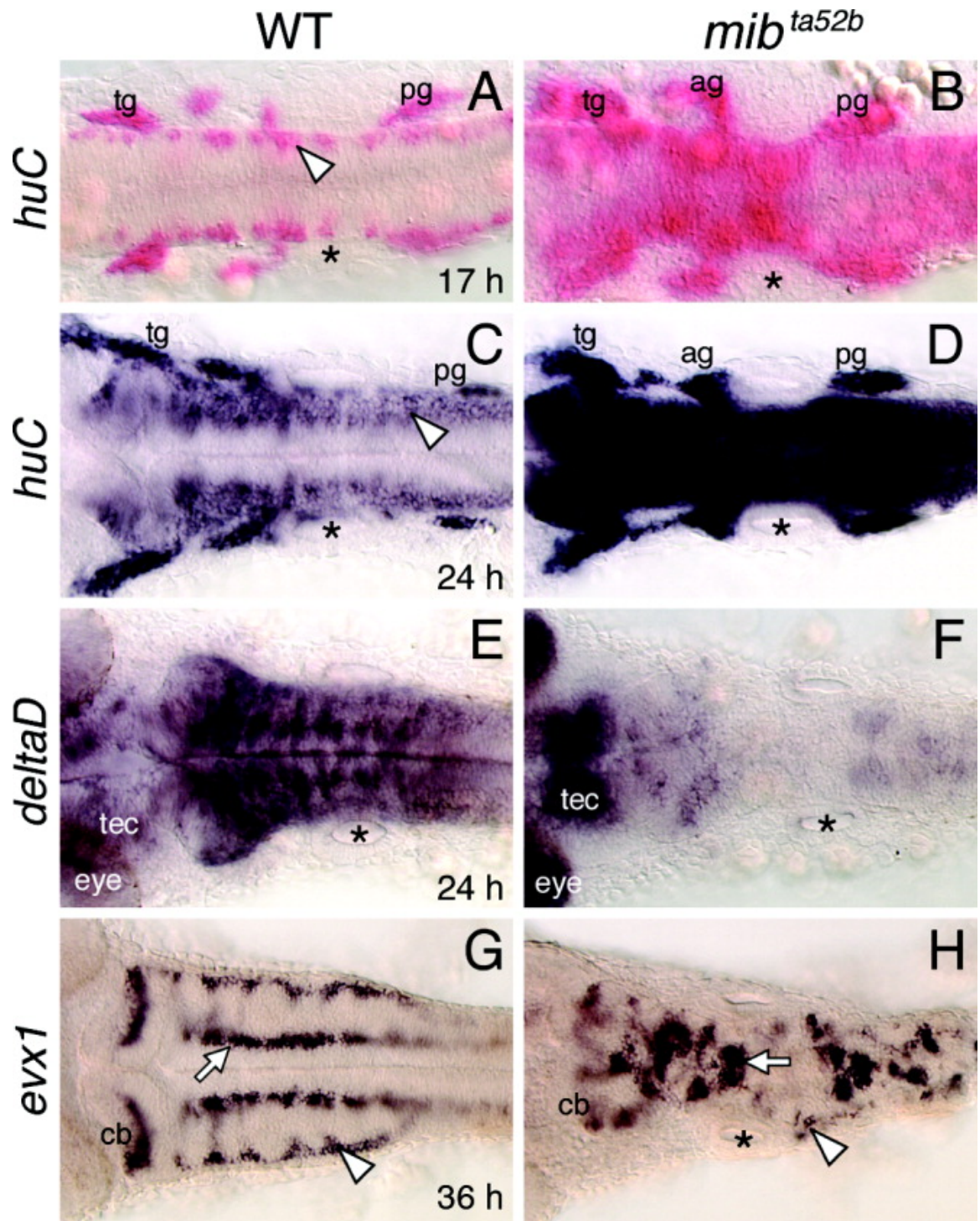
FIGURE 10. Defective neurogenesis in the *mind bomb* mutant hindbrain.

All panels show dorsal views of the hindbrain with anterior to the left. The asterisks in all panels indicate the location of the otocyst. **(A,B):** In a 17 hours postfertilization (hpf) wild type embryo (WT; A), *huC* is expressed in small clusters of cells (arrowhead) located at the lateral margins of the hindbrain. In a *mib* mutant (B), *huC*-expressing cells are found throughout the hindbrain, with higher densities at some axial levels. **(C,D):** In a 24 hpf wild type embryo (C), the *huC* expression domain has expanded medially, and expressing cells are found at all axial levels, including the caudal hindbrain (arrowhead). In a *mib* mutant (D), the hindbrain at all axial levels is filled with *huC*-expressing cells. **(E,F):** In a 24 hpf wild type embryo (E), *deltaD* is expressed extensively, with higher expression in segmentally reiterated cell clusters. In the *mib* mutant (F), *deltaD* expression is greatly reduced or absent in the hindbrain and sharply higher in the tectum (tec) and eye. **(G,H):** In a 36 hpf wild type embryo (G), *evx1* is expressed in commissural neurons (arrowhead), cerebellar neurons (cb), and putative interneurons (arrow). In a *mib* mutant (H), the *evx1*-expressing commissural neurons are greatly reduced (arrowhead), while the cerebellar neurons and interneurons (arrow) are disorganized and fused, and reduced in number. ag, acoustic ganglion; cb, cerebellum; tec, tectum; tg, trigeminal ganglion; pg, posterior lateral line ganglion.

not shown) (Thaeron et al., 2000). In *mib* mutants, *evx1*-expressing cells were reduced in number and disorganized (Figure 10H). The loss of *evx1*-expressing commissural neurons between 24 and 36 hpf anticipates the observed loss of zn5/8 antibody-labeled commissural neurons in the mutant hindbrain at 36 hpf (Jiang et al., 1996). Thus, the premature widespread appearance of *huC*-expressing cells in the mutant hindbrain between 17 and 24 hpf correlates with the loss and disorganization of a hindbrain neuron type that begins to differentiate at 24 hpf.

3.3.2   Development of Hindbrain Motor Neurons Is Disrupted in *mind bomb* Mutants

Three major subtypes of hindbrain branchiomotor neurons (BMNs) in zebrafish are the nV, nVII, and nX neurons, which arise at different axial levels, with nV being the most rostral and nX the most caudal (Chandrasekhar, 2004; Chandrasekhar et al., 1997; Higashijima et al., 2000). Expression of the motor neuron marker *islet1* (Appel et al., 1995) appears first in nVII neurons at ~15 hpf, in nV neurons at ~18 hpf, and in nX neurons at ~24 hpf (Chandrasekhar et al., 1997; Higashijima et al., 2000). In wild type embryos harboring the *islet1-GFP* transgene (Higashijima et al., 2000), the various BMN populations were found in normal numbers and locations, as previously described (Figure 11A) (Chandrasekhar et al., 1997; Higashijima et al., 2000). In *mib* mutants, the BMN
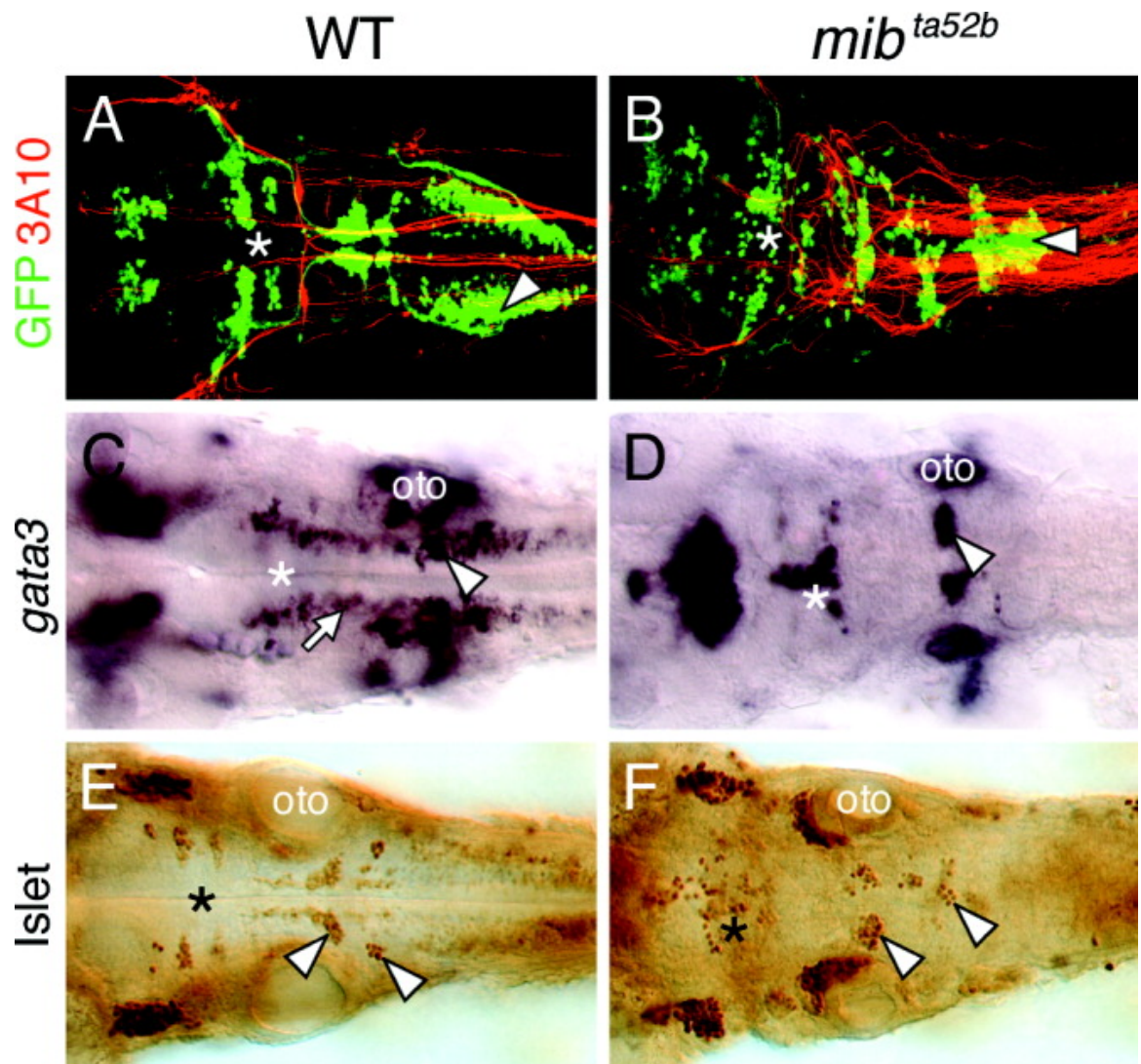
FIGURE 11. Branchiomotor neuron (BMN) development is severely disrupted in the mind bomb mutant hindbrain.

All panels show dorsal views of the hindbrain with anterior to the left. A and B are composite confocal images and identify *GFP*-expressing motor neurons in the fluorescein channel and 3A10-labeled Mauthner (M) reticulospinal neurons and axons in the rhodamine channel. The asterisks in all panels indicate the location of the trigeminal motor neurons in rhombomeres 2 and 3. **(A,B):** In a 36 hpf wild type embryo (WT; A), the BMN clusters are found in their characteristic locations and numbers. The 3A10 antibody-labeled Mauthner cell axons decussate and descend contralaterally into the spinal cord. In a *mib* mutant (B), the BMNs clusters are disorganized and are variably fused. The supernumerary M cell axons cross the midline and descend contralaterally in a normal manner, whereas the nX motor neurons (arrowhead) in the same region exhibit extensive fusion across the midline. **(C,D):** In a 36 hpf wild type embryo (C), *gata3* is expressed by putative interneurons (arrow) and the nVII (arrowhead) and nV motor neurons (asterisk). In a *mib* mutant (D), *gata3*-expressing motor neurons (arrowhead, asterisk) are disorganized and the putative interneurons are absent. **(E,F):** In a 36 hpf *mib* mutant (F), islet antibody-labeled BMNs (asterisk, arrowheads) are disorganized and variably fused and are reduced in number compared with wild type siblings (E). oto, otocyst.

clusters were smaller. Furthermore, the clusters were variably fused across the

midline (Figure 11B). Similarly, expression analysis of the zinc finger

transcription factor *gata3* (Bingham et al., 2002) revealed that nV and nVII motor

neurons were frequently reduced and fused across the midline in *mib* mutants,

while other *gata3*-expressing hindbrain cells were absent (Figure 11D, 11D). We

quantified specific neuronal populations in the hindbrain and spinal cord by using

an anti-islet monoclonal antibody (Korzh et al., 1993) (Figure 11E, 11F). As

reported previously (Appel et al., 1999), the number of early differentiating

Rohon-Beard neurons was substantially increased in the *mib* mutant spinal cord,

with a concomitant decrease in the number of late-differentiating secondary

motor neurons and interneurons (Table 2). In the *mib* hindbrain, the total number

of BMNs spanning rhombomeres 2 through 7 was decreased by 46% compared

with wild type siblings (Table 2) (Figure 11E, 11F). Of interest, nV motor

neurons, which begin to differentiate at 18 hpf, were less affected (27% loss)

than nVII neurons (56% loss), which begin to differentiate at 15 hpf (Table 2). In

addition, nX motor neurons, which begin to differentiate at 24 hpf in the caudal

hindbrain were reduced but not absent in *mib* mutants (Figure 11A, 11B). These

data show that there is no correlation between the time of onset of differentiation

and change in BMN numbers at all axial levels in the *mib* mutant hindbrain.

However, the identities of other neurons generated from the same local precursor

populations as specific BMN subtypes, and their fate in *mib* mutants, are not

known (see Discussion section 3.4).

TABLE 2. Branchiomotor Neurons Are Reduced in Number in *mind bomb* Mutants

Islet antibody-labeled cell type	WT[a]	*mib*[ta52b]	Ratio (mutant/WT)
Total number of labeled cells in hindbrain[b] (r2-r7)	205.9 ± 10.4 (11)	111.1 ± 15.5 (14)	0.54
Total number of labeled cells in r2 and r3 (nV neurons: Differentiate ≈ 18 hpf)	70.8 ± 7.8 (11)	51.5 ± 5.3 (14)	0.73
Total number of labeled cells in r4 to r7 (nVII neurons: Differentiate ≈15 hpf)	135.1 ± 8.6 (11)	59.1 ± 13.5 (14)	0.44
Number of labeled cells in ventral spinal cord[c] (Differentiate ≈24 hpf)	24.1 ± 1.6 (6)	12.9 ± 1.5 (6)	0.54
Number of Rohon-Beard cells[d] (Differentiate ≈10 hpf)	4.7 ± 0.4 (6)	9.8 ± 0.9 (6)	2.1

TABLE 2. Branchiomotor Neurons Are Reduced in Number in *mind bomb* Mutants

[a] Embryos were scored at 36 hours postfertilization (hpf). Numbers in parentheses represent number of embryos.

[b] The number corresponds to the total number of labeled cells (nV, nVII) in rhombomeres 2-7.

[c] Labeled cells (motor neurons and interneurons) were counted on one side in the ventral spinal cord in three contiguous segments at the level of the tip of the yolk tube. The number shown corresponds to the number of cells per hemisegment.

[d] Rohon-Beard cells, which are very darkly labeled cells in the dorsal-most neural tube, were counted on one side of the spinal cord in three contiguous segments at the level of the tip of the yolk tube. The number shown corresponds to the number of cells per hemisegment.

We tested whether the loss of BMNs in *mib* mutants reflects the loss of precursor cells that generate motor neurons in response to hedgehog signals by examining the effects of *shh* overexpression on BMN number in *mib* mutants (Figure 12). *Shh* was overexpressed in *mib* mutants by injecting full-length *shh* RNA into embryos obtained from *mib* +/-; *islet1-GFP* +/- parents. In wild type siblings, *shh* overexpression led to sharp increases in BMN number, especially in rhombomere 2 (r2) and r4 (Figure 12A, 13C). Cell counts in islet antibody-labeled embryos revealed a 48% average increase over control wild type siblings (Table 3), which is similar to previous results (Chandrasekhar et al., 1998). Importantly, *shh* overexpression also led to an increase in *GFP*-expressing cells in the *mib* mutant hindbrain (Figure 12B, 13D), with a 42% average increase compared with control mutant embryos (Table 3). While many of the excess *GFP*-expressing cells were located in the dorsal neural tube, as described previously (Chandrasekhar et al., 1998), many cells were also found in the ventral neural tube where the putative motor neuron precursor pools would be located (Figure 12E-H). These data indicate that cells in the ventral neural tube of *mib* mutants can differentiate into the motor neurons in response to Shh, suggesting that precursor cells are still present in the mutant hindbrain. Furthermore, while the absolute number of BMNs is substantially lower in *mib* mutants, *shh* overexpression increases BMN number by roughly the same extent in wild type (48%) and mutant (42%) embryos, suggesting that the motor neuron precursor pool is smaller in mutants.
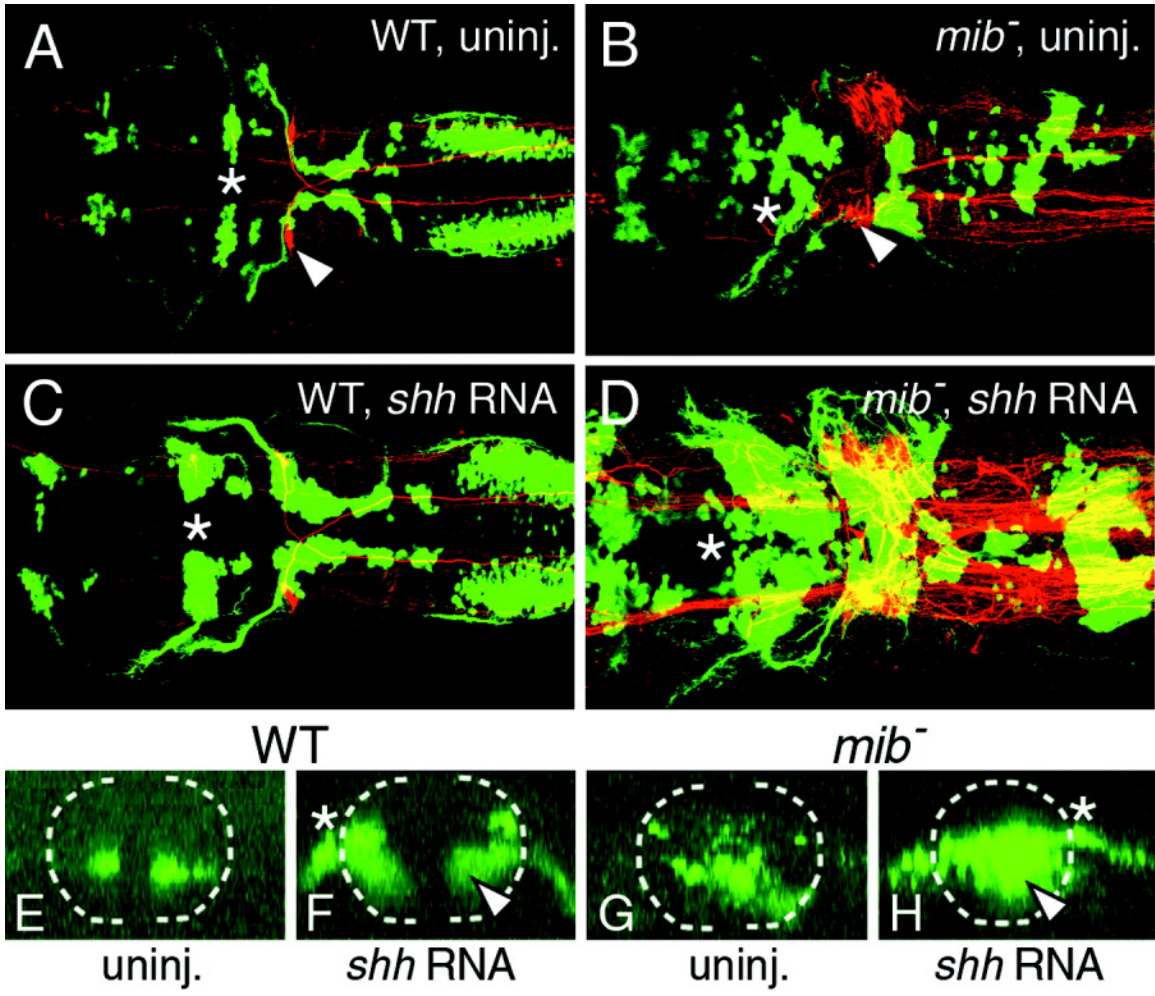
FIGURE 12. *Shh* overexpression induces branchiomotor neurons (BMNs) in the *mind bomb* mutant hindbrain.

A-D show dorsal views of the hindbrain with anterior to the left and are composite confocal images, identifying *GFP*-expressing motor neurons in the fluorescein channel and 3A10-labeled Mauthner reticulospinal neurons and axons in the rhodamine channel. Asterisks in A-D indicate the location of the trigeminal (nV) motor neurons in rhombomere 2 (r2). E-H show confocal projections (virtual cross-sections) of *GFP*-expressing cells at the level of r4 and r5, and illustrate the effects of *shh* overexpression on nVII motor neurons. The broken line marks the outline of the neural tube, with dorsal to the top. The asterisks in F and H indicate the exit point of nVII axons from the neural tube. **(A):** In a control wild type embryo (WT), one Mauthner (M) neuron (arrowhead) is found on each side in r4 and BMNs are found in characteristic locations and numbers. **(E):** In addition, the nVII motor neuron cell bodies are found in the ventral neural tube. **(C):** In a *shh* RNA-injected wild type embryo, the various *GFP*-expressing BMN clusters contain significantly larger numbers of cells, while M cell number is not affected. **(F):** While most of the ectopic nVII motor neurons are found in the dorsal neural tube, a significant number (arrowhead) is also found in ventral locations. **(B):** In a control *mib* mutant, there are excess M cells (arrowhead) and the BMNs exhibit the *mib* mutant phenotype. **(G):** The nVII neurons are distributed randomly in the ventral half of the neural tube. **(D):** Upon *shh* RNA injection, there is a sharp increase in the various BMN populations, while M cell number is not affected. **(H):** Significantly, many of the ectopic nVII motor neurons (arrowhead) in the mutant are found in the ventral neural tube. The mutant embryo shown in D had an unusually large increase in motor neuron number at all axial levels.

TABLE 3. Shh Overexpression Induces Ectopic Motor Neurons in *mind bomb* Mutants

	Injected RNA	No. of embryos[a]	Wild-type[b]	*mind bomb*[b]
Embryos with ectopic *GFP*-expressing cells in hindbrain[c]	None	197 (3)	0% (146)	0% (51)
	shh	231 (3)	94% (159)	100% (72)
Number of islet antibody-labeled cells in hindbrain[d]	None	5 (1)	188 ± 16.6	104.7 ± 9
	shh	5 (1)	277.4 ± 11.4	148.8 ± 23
	Ratio (*shh* / control)		1.48	1.42

TABLE 3. *Shh* Overexpression Induces Ectopic Motor Neurons in *mind bomb* Mutants

[a] Numbers in parentheses represent number of experiments.

[b] Numbers in parentheses represent number of embryos. Embryos were scored as mutant if the branchiomotor neurons exhibited fusion across the midline (Figure 12B and 12D). The mutant embryo in Figure 12D exhibited an unusually large increase in motor neuron number.

[c] Embryos (36 hours postfertilization) were considered to have ectopic expression if the number of *GFP*-expressing branchiomotor neurons were increased relative to uninjected controls. The ectopic neurons were especially evident in rhombomeres 2 and 4 (Compare Figure 12A and 12C), where ectopic neurons were located dorsally along the lateral margin of the neural tube, and in the caudal hindbrain.

[d] The number corresponds to the total number of labeled cells (nV, nVII) in rhombomeres 2-7.

While BMNs were frequently fused across the midline in *mib* mutants, the nV and nVII motor axons extended normally out of the hindbrain into the pharyngeal arches (Figure 11B; Figure 12B). To test whether fusion of motor neuron clusters correlated with the absence of midline cues, we examined the development of the Mauthner reticulospinal neurons and their decussating axons in 36 hpf embryos by using the 3A10 antibody (Hatta, 1992). As demonstrated previously, the number of Mauthner neurons was greatly increased in *mib* mutants (Figure 11B) (Jiang et al., 1996). However, the Mauthner axons never aberrantly re-crossed the midline in mutant embryos, even in regions with extensive fusion of putative nX motor neurons (Figure 11B), indicating that midline cues (and ventral midline cells) required for Mauthner axon pathfinding (Hatta, 1992) were unaffected in the *mib* mutant hindbrain at the time when these early differentiating neurons extended axons.

3.3.3 Development of Ventral Tissues Is Defective in the *mind bomb* Mutant Hindbrain

Although Mauthner axon pathfinding is normal, the fusion of BMN clusters in *mib* mutants suggests that some aspects of midline tissue development may be affected in the mutant hindbrain. Indeed, specification of trunk midline cell fates is altered in *mib* mutants such that excess notochord cells are generated, with a concomitant loss of floor plate and hypochord cells (Appel et al., 1999). Therefore, we monitored floor plate development in the mutant hindbrain using

shh expression as a marker (Krauss et al., 1993). Embryos were processed for *huC* and *shh* double in situ hybridizations to identify mutant embryos at younger ages (Figure 13A-D). At 16.5 hpf and 21 hpf, *shh*-expressing floor plate cells were found throughout the hindbrain, without any gaps, in wild type and mutant embryos (compare Figure 13A,C with Figure 13B,D). Although no obvious decrease in the number of floor plate cells was evident in *mib* mutants, it is possible that there is a small but significant reduction, similar to the spinal cord (Appel et al., 1999). In contrast, by 25 hpf, *shh* expression in *mib* mutants was displaced dorsally in some rhombomeres and missing in other regions, with a nonexpressing patch frequently coinciding with r4 (Figure 13F) (Table 4). Expression of another floor plate marker *axial* (Strahle et al., 1993) was similarly affected in 24 hpf *mib* mutants (data not shown). Expression of the Shh target gene *nk2.2* in the ventral neural tube (Barth and Wilson, 1995) was also patchy in the mutant hindbrain with a nonexpressing patch frequently coinciding with r4 (Figure 13G,H) (Table 4). Expression of the Shh-regulated axon guidance gene *net1b* in the ventral neural tube (Strahle et al., 1997) was maintained throughout the mutant hindbrain, but in a smaller number of cells than normal, with a distinctive gap frequently coinciding with r4 (Figure 13I,J) (Table 4). These results suggest that ventral tissues, including the midline, are significantly reduced, especially in r4, in *mib* mutant embryos.

If BMN fusion (Figure 11B) were a consequence of defects in ventral midline signaling, it should be less evident before 21 hpf, when midline signaling appears normal in *mib* mutants. However, the nV and nVII neuron clusters were

TABLE 4. Defects in Ventral Neural Tube Gene Expression in the *mind bomb* Mutant Hindbrain[a]

Gene	Genotype	Defect in Expression Pattern		
		No Defects	Gap in r2/r3	Gap in r4
shh (25 hpf)	Wild-type (20)	20/20	0/20	0/20
	Mutant (14)	6/14	2/14	6/14
nk2.2 (24 hpf)	Wild-type (20)	20/20	0/20	0/20
	Mutant (24)	6/24	1/24	17/24
net1b (30 hpf)	Wild-type (20)	20/20	0/20	0/20
	Mutant (52)	16/52	0/52	36/52

TABLE 4. Defects in Ventral Neural Tube Gene Expression in the *mind bomb* Mutant Hindbrain[a]

[a] Number of embryos are shown in parentheses. Gaps in rhombomeres 2, 3, and 4 (r2, r3, r4) were scored, while gaps in the caudal hindbrain, which were infrequent, and other defects in expression pattern were excluded from analysis. The position of the gap in expression was determined relative to the outlines of the otic vesicle, which spans rhombomeres 4-6 at the developmental stages examined. hpf, hours postfertilization.

	WT			_mib_ _ta52b_
A	B	C	D	
shh	16.5 h	WT	21 h	_mib_ _ta52b_
huC		_shh_		
		huC		
E	F	G	H	
shh _hoxb1a_	25 h	_hoxb1a_ _nk2.2_	24 h	
r4	r4	r4	r4	
I	J	K	L	
net1b	30 h	GFP	18 h	

139
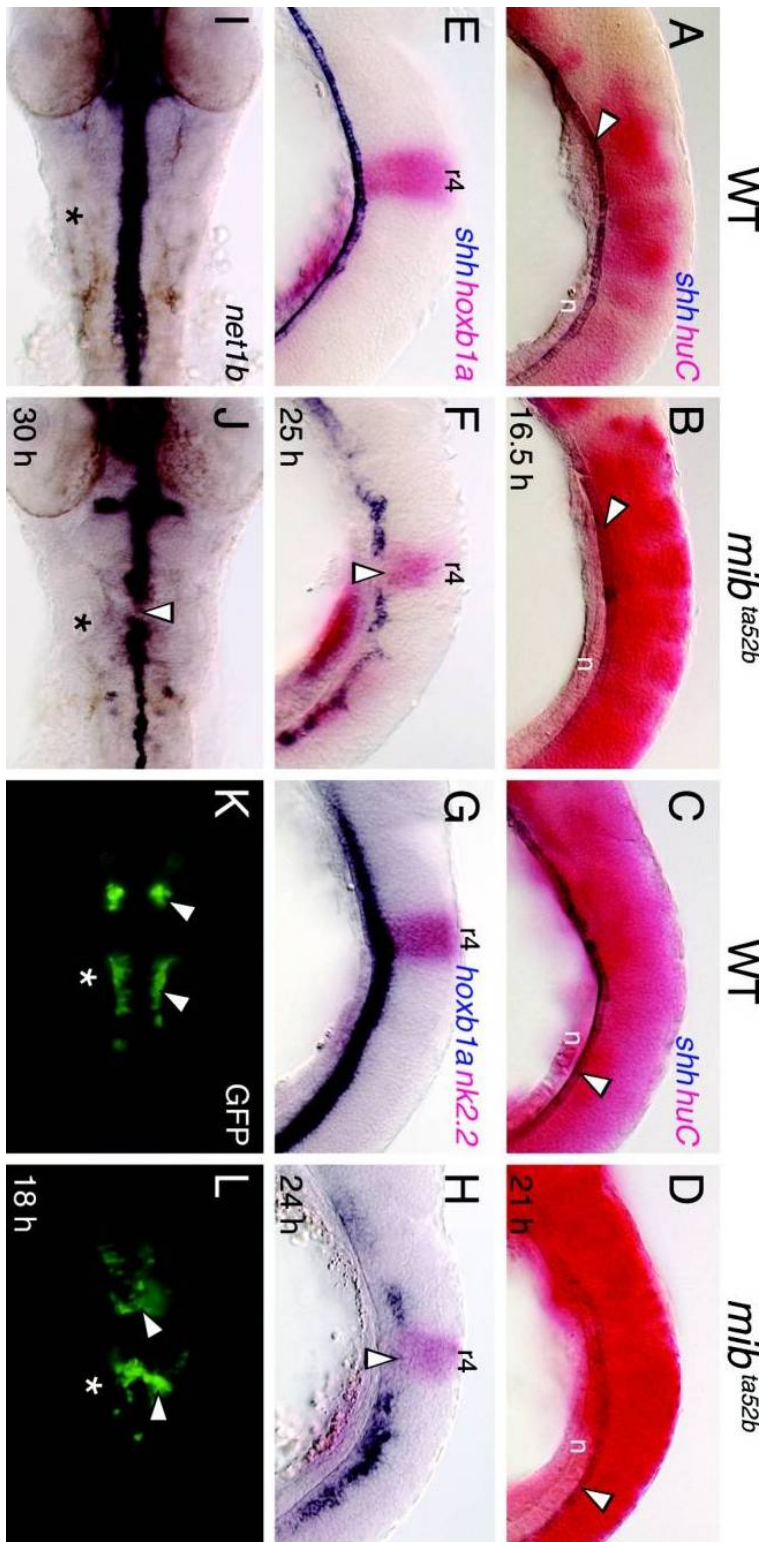
FIGURE 13. Development of ventral neural tube tissue is defective in the

***mind bomb* hindbrain.**

A-H show lateral views and I-L show dorsal views of the hindbrain, with anterior to the left. Asterisks (I-L) indicate the location of the otocyst. **(A, D):** At 16.5 hours postfertilization (hpf; A,B) and 21 hpf (C,D), *shh*-expressing floor plate cells (arrowheads) are found in a continuous row in wild type (WT) and *mib* mutant embryos, even though *huC*-expressing cells are greatly increased in the mutant (B, D). **(E,F):** In a 24 hpf *mib* mutant (F), *shh*-expressing floor plate cells are disorganized and slightly reduced in number compared with a wild type sibling (E), with an absence of expressing cells in rhombomere 4 (r4, arrowhead), which is identified by *hoxb1a* expression. **(G, H):** In a 24 hpf *mib* mutant (H), expression of *nk2.2* in the ventral neural tube is greatly reduced compared with a wild type embryo (G), with an absence of expression in r4 (arrowhead). **(I, J):** In a 30 hpf *mib* mutant (J), *net1b* expression is reduced at all axial levels compared with wild type (I), with a gap of nonexpression in r4 (arrowhead). **(K, L):** In an 18 hpf wild type embryo (K), *GFP*-expressing nV and nVII motor neurons (arrowheads) are found bilaterally in r2 (nV neurons) and in a longitudinal column spanning r4 and r5 (nVII neurons). In a *mib* mutant (L), the motor neuron clusters (arrowheads) are disorganized, with considerable fusion across the midline. n, notochord.

disorganized and variably fused in 18 hpf mutant embryos (Figure 13K,L),

indicating that these BMN defects arise before any obvious defects in *shh*

expression at the ventral midline.

3.3.4   Relationship Between the *mind bomb* Ventral Midline and Neurogenic Phenotypes

Since gaps appear in the floor plate only after 21 hpf (Figure 13F), we

wondered whether the patchy loss of ventral midline tissue in *mib* mutants was

linked to the extensive generation of *huC*-expressing cells in the mutant

hindbrain (Figure 10A-D). This issue was addressed by examining the

arrangement of *huC*- and *shh*-expressing cells in the ventral hindbrain at different

axial levels. Cross-sections of the hindbrain were prepared from wild type and

mutant embryos processed for *huC* or *huC*; *shh* in situ hybridizations. In 24 hpf

wild type hindbrains, *huC*-expressing cells were restricted to the lateral margins

of the neural tube and excluded from the floor plate (Figure 14A). In *mib*

mutants, *huC*-expressing cells filled the hindbrain but were frequently excluded

from the ventral midline, likely the floor plate cells (Figure 14B). We confirmed

this in two-color in situ hybridizations, which showed that the patch of non-*huC*-

expressing cells at the ventral midline in mutants expressed *shh* (Figure 14C,D).

However, in mutant embryos, many ventral midline cells appeared to coexpress

shh and *huC* (Figure 14F). Furthermore, in hindbrain regions containing no *shh*-

expressing cells, *huC*-expressing cells were often, but not always, located at the

ventral midline, immediately dorsal to the notochord (Figure 14E). These results
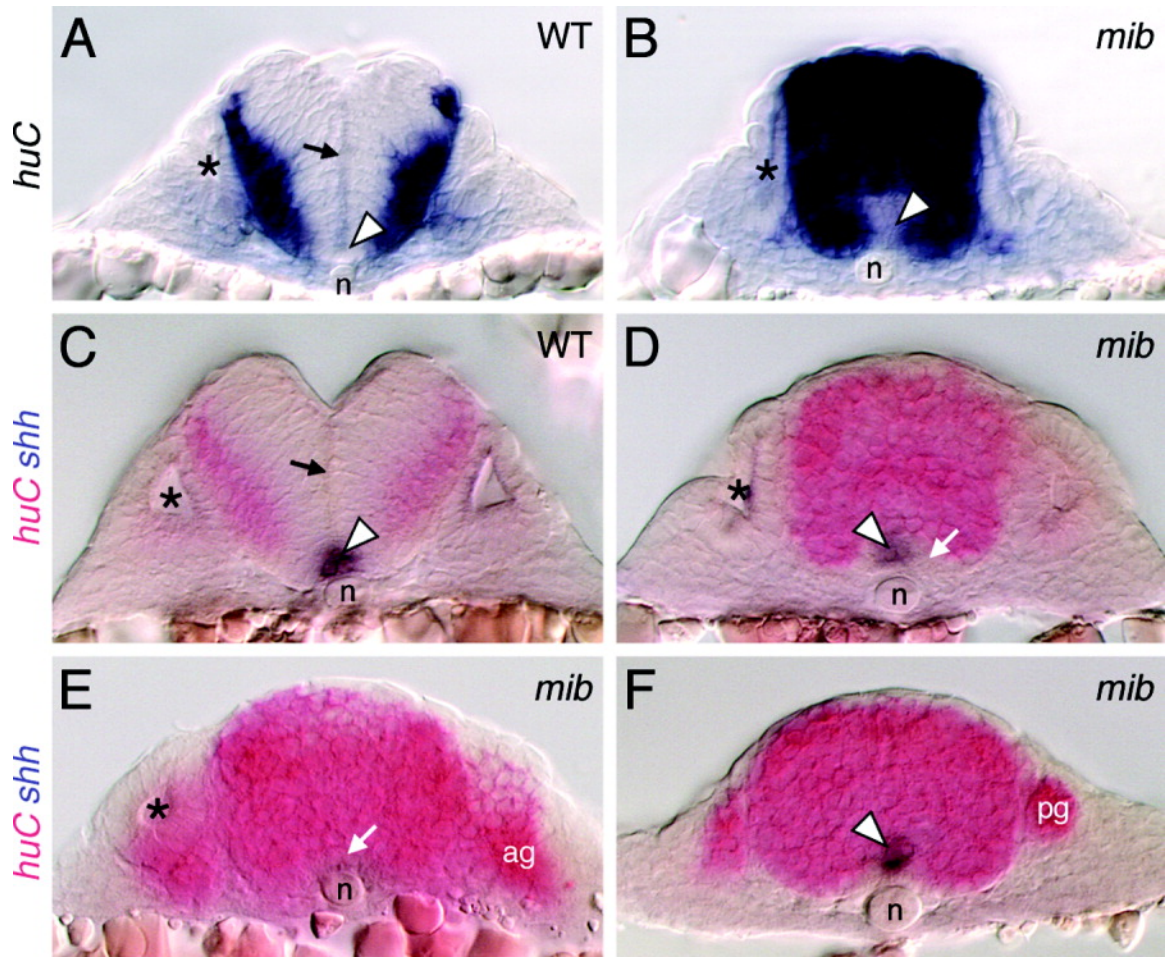
FIGURE 14. Distribution of neural cells in the *mind bomb* mutant hindbrain.

All panels show cross-sections of the hindbrain in 24 hours postfertilization embryos at the level of rhombomere 5 (A-D), rhombomere 4 (E), and the caudal hindbrain (F). Asterisks in A-E identify the otocyst. **(A, C):** In wild type (WT) embryos, the *huC*-expressing cells are found at the lateral margins of the neural tube, outside the ventricular zone along the middle of the neural tube (arrows). The ventral midline contains floor plate cells (arrowheads) that express *shh* (C). (**B, D):** In *mib* mutants, the entire neural tube is filled with *huC*-expressing cells, except at the ventral midline (arrowhead in B), which contains *shh*-expressing cells (arrowhead in D) and other cells that express neither *shh* nor *huC* (arrow in D). The ventricular zone is absent in mutant embryos. **(E):** In this mutant, *huC*-expressing cells (arrow) occupy the ventral midline immediately dorsal to the notochord, and no *shh*-expressing cells are found. **(F):** In this mutant, the ventral midline cells coexpress *shh* and *huC* (arrowhead). ag, acoustic ganglion; n, notochord; pg, posterior lateral line ganglion.

suggest that the patchy loss of *shh* expression after 21 hpf in the *mib* hindbrain may result in part from the differentiation of *shh*-expressing floor plate cells into *huC*-expressing neural cells.

3.3.5 Defects in BMN Patterning in *mind bomb* Mutants Are Generated Non-Cell Autonomously

Previous studies have suggested that *mib* is required nonautonomously for effective Notch signaling (Itoh et al., 2003). Therefore, we tested whether the aberrant patterning and midline fusion phenotypes of BMNs of *mib* mutants also reflect a non-cell autonomous requirement for *mib* in the hindbrain.

Heterochronic transplants were performed using sphere stage (4 hpf) donor embryos transgenic for *islet1-GFP* and labeled with rhodamine dextran and nontransgenic, unlabeled, shield stage (6 hpf) host embryos (Figure 15A). In control experiments, donor-derived wild type cells that differentiated into *GFP*-expressing BMNs in wild type host embryos formed clusters in the appropriate locations and did not fuse across the midline (Figure 15B; 88 neurons, 2 embryos). In contrast, donor-derived wild type motor neurons were positioned randomly within the *mib* mutant hindbrain. Wild-type cell bodies and axons frequently straddled the midline, reflecting the fusion phenotype, and indicating that the mutant environment drives wild type BMN patterning (Figure 15C; 42 neurons, 3 embryos). Conversely, donor-derived *mib* mutant motor neurons were patterned normally in wild type host hindbrains and never exhibited any

A. Sphere stage *islet1-GFP* donor → Shield stage Non-GFP host

Examine distribution of *GFP*-expressing cells (donor-derived motor neurons) in host embryos

B. Wt ^{gfp} --> Wt

C. Wt ^{gfp} --> *mib*

D. *mib* ^{gfp} --> Wt

E. Wt --> Wt

F. Wt --> *mib*
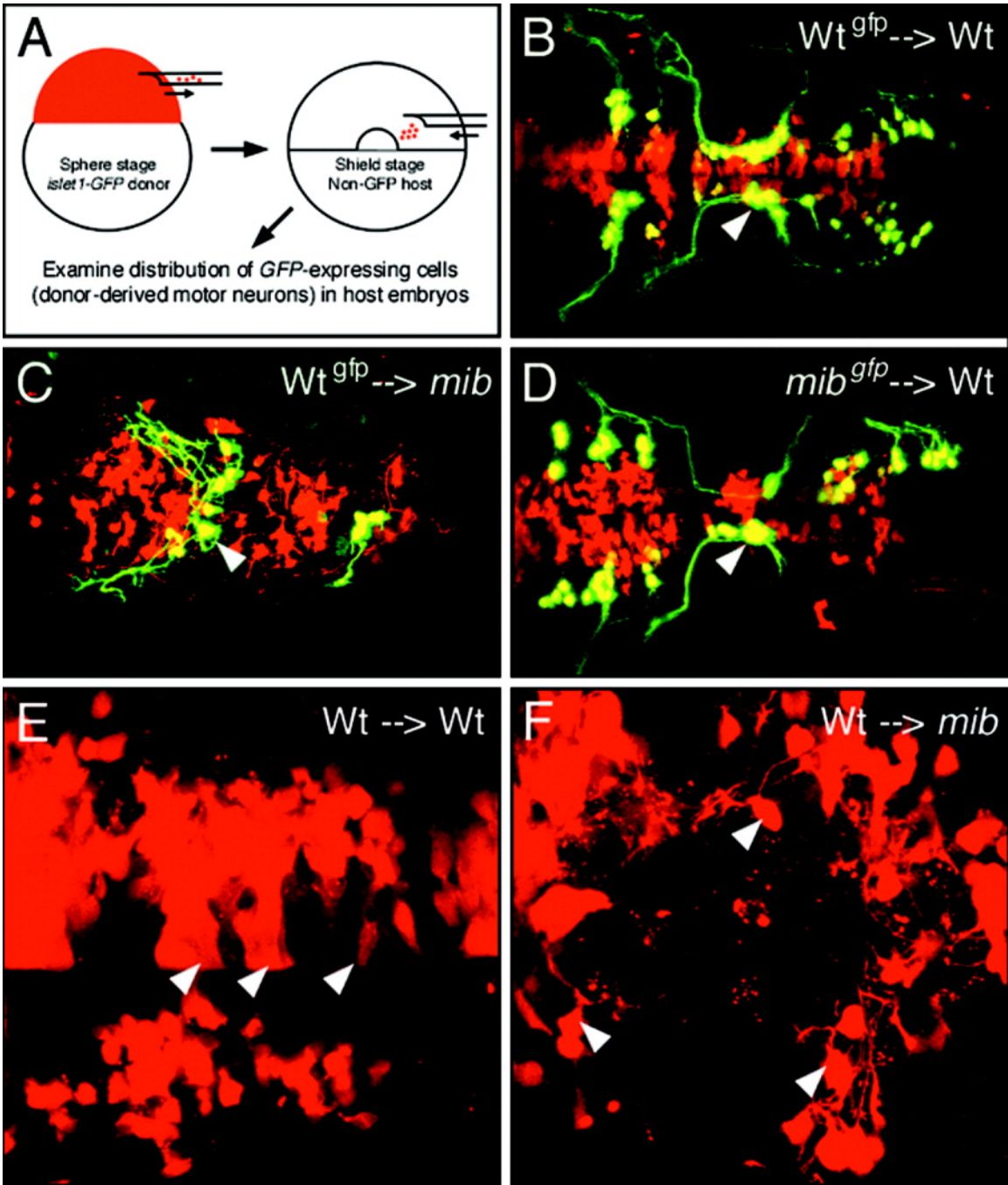
FIGURE 15. The *mind bomb* branchiomotor neuron (BMN) phenotype arises non-cell autonomously.

B-F show dorsal views of the hindbrain with anterior to the left. In B-F, donor-derived cells are labeled red with rhodamine-dextran. In B-D, donor-derived BMNs are labeled yellow due to colocalization of *GFP* expression and rhodamine-dextran. **(A):** The transplantation procedure. **(B):** In a control experiment, wild type (Wt) cells that differentiate into motor neurons (arrowhead) in a wild type host are correctly organized into characteristic clusters. **(C):** When donor-derived wild type cells differentiate into motor neurons in a *mib* mutant host, the wild type neurons (arrowhead) and their axons are loosely organized and straddle the midline, the characteristic mutant phenotype. **(D):** When donor-derived *mib* mutant cells differentiate into motor neurons in a wild type host, the mutant neurons (arrowhead) and their axons exhibit wild type organization. **(E):** In a wild type host, many donor-derived cells exhibit a columnar morphology (arrowheads), suggestive of neuroepithelial cells. **(F):** In a *mib* host, most donor-derived cells are round with short processes (arrowheads), suggestive of neurons.

midline fusion (Figure 15D; 142 neurons, 4 embryos). These results demonstrate a nonautonomous requirement for *mib* in neural patterning, analogous to its previously defined role in Notch signaling (Itoh et al., 2003). The nonautonomous BMN patterning phenotype may result from defects in ventral midline signaling (Figure 13) and rhombomere patterning (Figure 16; see below) in *mib* mutants.

While performing the mosaic analysis, we noticed that wild type cells transplanted into mutant embryos (Figure 15C) seldom exhibited the columnar morphologies suggestive of neuroepithelial cells (compare with Figure 15B,D). Therefore, we examined the morphologies of rhodamine-dextran labeled donor cells at higher magnification in 36 hpf wild type and mutant hosts, and classified them as being neuroepithelial (columnar morphology) and neuronal (round cells with at least one short process; (Figure 15E,F; see Materials and Methods section 3.2). Approximately 30% of labeled cells in each host background could not be scored for either morphology and were excluded from analysis. Approximately 98% of scored wild type cells in *mib* mutants had neuronal morphology (Figure 15F; 218/222 cells, 6 embryos). In sharp contrast, only 68% of scored donor cells (wild type or mutant) in wild type hosts exhibited neuronal morphology (Figure 15E; 98/144 cells, 8 embryos), and approximately 30% of the cells exhibited neuroepithelial morphologies. These observations suggest that the *mib* mutant environment is unable to either prevent transplanted wild type cells from becoming neurons or preserve them as neuroepithelial cells.

3.3.6 Late, but not Early, Rhombomere Patterning Is Defective in *mind bomb* Mutants

Since neuroepithelial cells are essential for morphogenesis and patterning of the neural tube, including the hindbrain (Geldmacher-Voss et al., 2003; Moens and Prince, 2002), we monitored rhombomere patterning in *mib* mutants from 16.5 to 24 hpf, when the neurogenic phenotype becomes progressively severe (Figure 16). Embryos from *mib* +/- crosses were processed for two-color in situ hybridizations with *huC* and *krox20* to monitor rhombomere organization in young embryos. *Krox20* (Oxtoby and Jowett, 1993) was expressed normally in rhombomeres 3 and 5 in 16.5 and 20 hpf *mib* mutants, even though excessive neurogenesis was evident in the mutant hindbrain (Figure 16A-D). Furthermore, no defects in the expression of *hoxb1a* in r4 (Prince et al., 1998), and *valentino* in r5 and r6 (Moens et al., 1998) were observed in 18 hpf embryo clutches obtained from *mib* +/- crosses (data not shown). These data demonstrate that rhombomeres are formed and boundaries are established normally in mutant embryos. However, by 24 hpf, *krox20* expression in r3 and r5 (Figure 16E) was severely reduced or absent in *mib* mutants (Figure 16F). In addition, *hoxb1a* expression in r4 was greatly reduced in *mib* mutants, and the boundaries with adjacent compartments were poorly defined (Figure 16E,F; see also Figure 13E-H). We performed acridine orange staining on live embryos to monitor cell death patterns in the hindbrain (Brand et al., 1996a). There were no differences in the distribution of dying cells between wild type and mutant embryos at 24 and 36
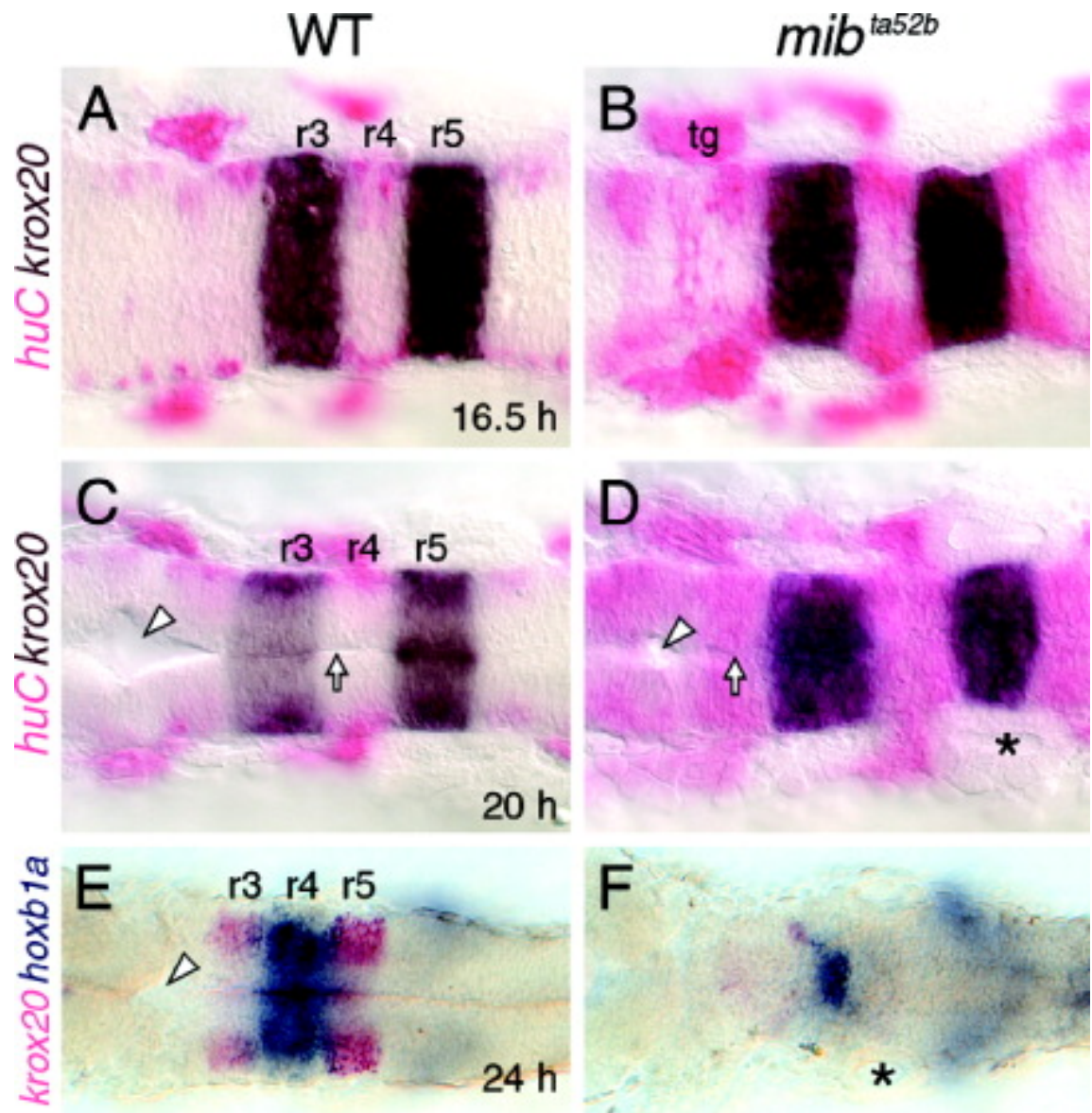
FIGURE 16. Rhombomere patterning is established but not maintained in

***mind bomb* mutants.**

All panels show dorsal views with anterior to the left. Asterisks identify the otocyst. (**A-D):** At

16.5 hours postfertilization (hpf; A,B) and 20 hpf (C,D), *krox20* is expressed normally in

rhombomeres 3 and 5 (r3 and r5) in wild type (WT) and mutant embryos, even though *huC*-

expressing cells are greatly increased in the mutant hindbrains (B,D). By 20 hpf, the ventricular

surface (arrow) and lumen (arrowhead) are well developed in the wild type embryo (C) but are

poorly developed in the mutant (D). **(E,F):** In a *mib* mutant (F), *krox20* expression in r3 and r5 is

absent, while *hoxb1a* expression in r4 is maintained but greatly reduced, compared with a wild

type sibling (E). In addition, the ventricle (arrowhead) seen in the wild type embryo is missing in

the mutant. tg, trigeminal ganglion.

hpf (data not shown), indicating that loss of rhombomere boundaries in mutants was not due to increased cell death. These results suggest strongly that the excessive differentiation of neurons between 16.5 and 24 hpf in *mib* mutants occurs at the expense of neuroepithelial cells that may be required for maintaining rhombomere identities and boundaries beyond 24 hpf.

3.4 <u>DISCUSSION</u>

Previous studies have shown that excess primary neurons are generated in *mib* mutants while secondary neurons are reduced (Itoh et al., 2003; Jiang et al., 1996; Park and Appel, 2003; Schier et al., 1996). In addition, neurogenesis genes such as *ngn1*, *zash1a*, *zash1b*, and *deltaD* are expressed ectopically and at high levels during early somitogenesis (10-18 hpf), but greatly reduced at subsequent stages (Itoh et al., 2003; Jiang et al., 1996). The production of neurons at a higher density within proneural domains at 12-13 hpf characterizes the initial neurogenic phenotype in *mib* mutants (Itoh et al., 2003; Jiang et al., 1996). However, between 17 and 24 hpf, the neurogenic phenotype becomes more expansive with most cells of the neural tube expressing the neuronal marker *huC* by 24 hpf (Figure 10) (Itoh et al., 2003; Park and Appel, 2003). These striking changes in the patterns of neurogenesis suggest that the failure of lateral inhibition in *mib* mutants permits too many neuronal precursors to differentiate early and assume the fate of early born neurons, depleting the

neural tube of neuroepithelial cells that would otherwise have adopted alternate

fates and contributed to the formation of later-born neurons. Our detailed

analysis of cell differentiation and patterning in the hindbrain is consistent with

this view. In addition, our studies suggest strongly that the extensive loss of

neuroepithelial cells in *mib* mutants leads to severe secondary defects in

patterning.

3.4.1 Potential Mechanisms Underlying BMN Loss in *mind bomb* Mutants

In the *mib* hindbrain, *huC*-expressing cells are sharply increased in

number between 17 and 24 hpf, compared with wild type, such that *evx1*-

expressing neurons that normally appear at 24 hpf are reduced in mutants

(Figure 10). Therefore, we expected that early differentiating BMNs, such as the

nVII neurons in rhombomere 4 (r4-r7), and the nV neurons in r2 and r3, which

begin to differentiate at 15 hpf (nVII) and 18 hpf (nV), would be generated in

excess in *mib* mutants and that the nX BMNs, which begin to differentiate at 24

hpf in the caudal hindbrain, would be greatly reduced or missing. However, both

the nV and nVII motor neurons are reduced in *mib* mutants, and significant

numbers of nX neurons are induced (Figure 11). There are several possible

explanations. First, because nV and nVII neurons are born continuously over an

extended time period beginning at 18 and 15 hpf, respectively, it is possible that

nV and nVII neurons born early are indeed generated in excess in mutants, while

the later-differentiating nV and nVII neurons are completely lost, leading to a variable net reduction in BMNs. Alternatively, although some BMN subtypes are born earlier than others, BMNs, as a whole, may represent a cell type that differentiates relatively late compared with other types of neurons generated from the same local precursor pools. Consequently, the reduction in BMNs in *mib* mutants may be the result of excessive formation of other earlier-born neurons, and the variable reduction in BMN subtypes may reflect the degree to which the early neurogenic phenotype depletes local precursor pools in different rhombomeres. However, in the absence of specific markers to distinguish between early- and late-born nV and nVII neurons or information about other neurons that might be generated earlier from the common precursor pools that generate BMNs, these models cannot be tested.

The *shh* overexpression experiments (Figure 12) were originally performed to determine whether the loss of BMNs in *mib* mutants was due to a loss of precursor cells capable of responding to Shh or was due to a loss/reduction of Shh signal from the ventral midline. The results do not clearly distinguish between these possibilities. As shown previously in wild type embryos (Chandrasekhar et al., 1998), *shh* overexpression induces ectopic BMNs in *mib* mutants in domains that include the ventral neural tube, indicating that Shh-responsive precursor pools are not completely depleted in mutants. In addition, while BMN number is increased by roughly similar extents (~45%) in wild type and *mib* mutants after *shh* overexpression, the absolute number of neurons induced is lower in mutants (Table 3), consistent with the idea that Shh-

responsive precursor pools are smaller in *mib* mutants. However, we cannot rule

out that the patchy loss of *shh* expression at the ventral midline also contributes

to the BMN deficit in *mib* mutants. Hence, although the precise mechanism that

leads to the reduction in BMN number in *mib* mutants remains unclear, the

observed deficits are likely to be, in part, secondary consequences of an early

neurogenic phenotype.

3.4.2   Ventral Midline Defects in the *mind bomb* Mutant

Hindbrain

Midline defects have been described previously in the trunk region of *mib*

mutants (Appel et al., 1999), where there is a small (25%) but significant

decrease in the number of floor plate and hypochord cells, and a corresponding

increase in notochord cells. These and other data suggested that Notch-Delta

signaling mediates cell fate decisions at the trunk midline (Appel et al., 1999).

Because components of the Notch-Delta signaling pathway are expressed in the

gastrula and tail bud organizer regions (Appel et al., 1999; Holley et al., 2002;

Itoh et al., 2003), it is likely that Notch signaling also mediates midline cell fate

decisions of the hindbrain region during gastrulation. There are two aspects to

the ventral midline defects that we have described (Figure 13,15), one of which is

consistent with a role for Notch signaling in determining floor plate fate in the

ventral midline (Appel et al., 1999), whereas the other appears to be related to

the role of the Notch pathway in regulating neurogenesis in the neural tube.

In the *mib* hindbrain, floor plate cells expressing *shh* are found in a continuous row (no gaps) between 15 and 21 hpf (Figure 13B,D; data not shown). Furthermore, Mauthner axons, which extend through the hindbrain between 17 and 21 hpf (Hatta, 1992; Mendelson, 1986), pathfind normally in mutants (Figure 11B), indicating that ventral midline cues necessary for Mauthner axon pathfinding (Hatta, 1992) are expressed normally in *mib* mutants. However, even though no obvious defect in floor plate development is evident in the 15-21 hpf mutant hindbrain, a small but significant reduction in the number of floor plate cells may have been missed. This putative, early reduction in cell number could result directly from defective midline cell fate specification in the *mib* hindbrain during gastrulation (Appel et al., 1999). However, the second aspect of *mib* ventral midline defects is the appearance of gaps in *shh* and *axial* (and Shh-regulated *nk2.2* and *net1b*) expression after 21 hpf (Figure 13E-J; data not shown). The gaps in *shh* expression can arise in at least two ways. First, an existing floor plate cell may down-regulate *shh* expression, perhaps due to trans-differentiation into another cell type. Alternatively, some daughter cells of mitoses in the floor plate may fail to differentiate into floor plate cells. Our results (Figure 14) are consistent with both possibilities. In the *mib* hindbrain, while the domains of expression of the neural and floor plate markers (*huC* and *shh*, respectively) are mostly exclusive (Figure 14A-D), there are numerous instances when the two genes appeared to be coexpressed at the ventral midline (Figure 14F). In addition, wherever *shh*-expressing cells are missing (i.e., gaps in expression), *huC*-expressing cells are frequently found at the ventral midline,

immediately dorsal to the notochord (Figure 14E). Therefore, the patchy

expression of *shh* at 24 hpf is likely not due to defective midline specification

during gastrulation, but may result from the conversion of ventral midline cells

into neuronal cells. This mechanism may also explain the consistent, but not

absolute, loss (gap) of expression of *shh* and Shh-regulated target genes (*nk2.2*,

net1b) in r4 in *mib* mutants (Figure 13) (Table 4). Premature and excessive

neurogenesis, as evidenced by increased *zash1a* and *zash1b* expression, occurs

first in r3/r4 at 16 hpf in mutants (Jiang et al., 1996), suggesting that the ventral

midline cells in this hindbrain region may be especially susceptible to neuronal

differentiation.

3.4.3   Genesis of Patterning Defects in *mind bomb* Mutants

In addition to a marked decrease in BMN number, the rhombomere-

specific clustering of BMNs is lost in *mib* mutants. This defect may result directly

from the dramatic loss of rhombomere-specific gene expression by 24 hpf. Of

interest, rhombomere-specific gene expression in *mib* mutants is initiated

correctly and maintained until approximately 21 hpf, by which time virtually the

entire mutant hindbrain undergoes neuronal differentiation (Figure 16).

Rhombomere boundaries may be lost rapidly between 21 and 24 hpf due to the

cumulative loss of cells that express molecules mediating repulsive cell-cell

interactions (Cooke et al., 2001; Xu et al., 1999). In addition, the absence of

zrf1-positive radial glial cells (Lyons et al., 2003), which are found at rhombomere

boundaries (Trevarrow et al., 1990), in *mib* mutants (Jiang et al., 1996) may also play a role in the loss of rhombomere boundaries. Of interest, the radial glial cells in the zebrafish hindbrain are found in the ventricular zone, are mitotically active, and may give rise to neurons (Lyons et al., 2003). Therefore, the absence of these cells in *mib* mutants could have independent effects on rhombomere patterning and neurogenesis.

Although rhombomere boundaries and rhombomere-specific BMN organization are severely compromised in *mib* mutants, BMNs extend axons in a manner consistent with their anteroposterior location (Figure 11B; data not shown). BMNs in the vicinity of r2 and r3 extend axons into the first branchial arch (nV neurons), whereas those in the vicinity of r4, r5, and r6 extend axons into the second branchial arch (nVII neurons). This observation suggests that the establishment and transient stability of rhombomere identity and boundaries up to ~21 hpf may be sufficient to impart region-specific identities to nV and nVII motor neurons. Our results are consistent with previous studies, which showed that failure to initiate and establish rhombomere-specific gene expression can lead to a complete loss of hindbrain compartment and BMN identities (Waskiewicz et al., 2002).

3.4.4 Role of Neuroepithelial Cell Loss in Generating the *mind bomb* Hindbrain Phenotype

The zebrafish neural tube forms by cavitation of the neural rod/keel, which is generated by an inward, convergent movement and a thickening of the neural plate, rather than by invagination, as in other vertebrates (Kimmel et al., 1995). Consequently, at the neural keel stage, proliferation of neuroepithelial cells leads to bilaterally positioned daughter cells because their movement is not restricted by a central lumen (Geldmacher-Voss et al., 2003; Kimmel et al., 1994). Furthermore, the proliferative zone containing neuroepithelial cells is restricted to a well-defined layer immediately adjacent to the hindbrain ventricle (Lyons et al., 2003). Our observations suggest strongly that neuroepithelial cells are greatly reduced in number in *mib* mutants, especially after 21 hpf. First, quantification of cells with specific morphologies in wild type and mutant hindbrains suggests that neuroepithelial cells are extremely rare in *mib* mutants at 36 hpf (Figure 15), and this effect may be evident earlier. Second, while the ventricular zone of neuroepithelial cells is clearly defined in 24 hpf wild type embryos, it is absent in *mib* mutants, because no ventricle is evident in cross-sections, and *huC*-expressing cells densely populate the entire neural tube in mutant embryos (Figure 14). This phenotype is also obvious in cross-sections of *GFP*-expressing mutant embryos, where the various BMN subtypes, especially the nX neurons, are extensively clumped across the putative midline or ventricle (data not shown). Finally, at 16.5 hpf (neural keel stage), the rudiment of a central lumen,

bordered by neuroepithelial cells, is visible in wild type hindbrains and to a lesser degree in *mib* mutants (Figure 16; data not shown). We propose that loss of neuroepithelial cells, especially after 21 hpf, leads to the patterning defects evident in *mib* mutants after 21 hpf. However, staining of live embryos with Bodipy ceramide to outline cell shapes (Cooper et al., 1999) has thus far not revealed any obvious differences in the number of neuroepithelial cells between wild type and mutant hindbrains at 18 or 24 hpf (data not shown).

In conclusion, neural defects characterized in the *mib* mutant have thus far focused on the neurogenic phenotype of early born neurons, occurring at the cost of later-born neurons. Our data on BMN induction are consistent with this scenario. Moreover, the loss of BMN organization and rhombomere boundaries by 24 hpf in *mib* mutants underscores the importance of non-neuronal cells in maintaining patterning mechanisms. Our observations suggest strongly that premature neurogenesis in *mib* mutants leads to the extensive loss of neuroepithelial cells that have important roles in rhombomere boundary formation and midline signaling in the hindbrain. The potential roles of neuroepithelial cells in hindbrain patterning and ventral midline signaling processes can be studied in embryos where genetic or biochemical perturbation leads to severe disruption of neuroepithelial cell polarity and organization (Geldmacher-Voss et al., 2003; Jiang et al., 1996; Masai et al., 2003; Pujic and Malicki, 2001).

3.5   ACKNOWLEDGEMENTS

CHAPTER 4

GLI FUNCTION IS ESSENTIAL FOR MOTOR NEURON

INDUCTION IN ZEBRAFISH

4.1   INTRODUCTION

The signaling pathway initiated by the hedgehog (Hh) family of secreted proteins plays an essential role in the induction and patterning of numerous cell types during invertebrate and vertebrate development (Ingham, 2001). Furthermore, defective Hh signaling has been implicated in tumorigenesis in humans (Wechsler-Reya and Scott, 2001), leading to extensive interest in elucidating the molecular mechanisms underlying Hh-mediated signal transduction. The Hh protein binds to a twelve-pass transmembrane protein Patched, relieving inhibition of a seven-pass transmembrane protein Smoothened and resulting in signaling into the cell. The ultimate transcriptional effectors of Hh signaling within the responding cell are the Gli family of zinc finger transcription factors (Lum and Beachy, 2004), although Gli-independent mechanisms have also been described (Krishnan et al., 1997). Glis generally contain an N-terminal repressor domain, a zinc finger DNA-binding domain, and

a C-terminal activator domain. The Drosophila *gli* homolog, *cubitus interruptus* (*ci*), is the best-understood member of this family. In the absence of an Hh signal, Ci is proteolytically cleaved between the zinc finger and the activator domains to generate a repressor that blocks expression of Hh target genes. Upon Hh binding, proteolysis of Ci is inhibited, and the full-length protein functions as a transcriptional activator of Hh target genes (Aza-Blanc et al., 1997; Lum and Beachy, 2004). The situation in vertebrates is considerably more complex because the function of *ci* has been expanded and distributed between at least three *Gli* genes. In the mouse spinal cord, the cellular response to Hh signaling is mediated primarily by the activator function of Gli2 and the repressor function of Gli3, while the activator forms of Gli1 and Gli3 also play smaller but significant roles (Bai et al., 2004; Lei et al., 2004; Motoyama et al., 2003). Glis similarly mediate Hh signaling in the zebrafish neural tube, but Gli1 is the primary activator of Hh signaling, with Gli2 and Gli3 playing minor activator and repressor roles (Karlstrom et al., 1999; Karlstrom et al., 2003; Tyurina et al., 2005).

Despite this general picture of Gli function in neural patterning, the roles of the various vertebrate *Gli* genes in the formation of particular cell types such as motor neurons have not been fully resolved. In frog, misexpression of *Gli1* or *Gli2* but not *Gli3* can induce ectopic motor neurons, supporting a role for *Gli1/2* in motor neuron formation (Ruiz i Altaba, 1998). In the chick spinal cord, inhibition of all *Gli* activator function blocks motor neuron induction (Persson et al., 2002), and ectopic expression of Gli2 activator can induce ventral neural tube markers (Lei et al., 2004), suggesting that Gli1 and/or Gli2 activator function is necessary

and sufficient for motor neuron formation. In contrast, mouse *Gli* single and

double knockouts exhibit no defects in motor neuron induction. Motor neurons

are induced normally in the spinal cords of *Gli1*, *Gli2*, and *Gli3* single mutants, as

well as in *Gli1*;*gli2*, and *Gli1*;*gli3* double mutants (Ding et al., 1998; Matise et al.,

1998; Park et al., 2000). Importantly, in *Gli2*;*gli3* double mutants, which are

essentially *Gli1*;*gli2*;*gli3* knockouts since *Gli1* expression is lost in these mutants,

a small but significant number of spinal motor neurons differentiate although their

migration and patterning are affected (Bai et al., 2004; Lei et al., 2004). In

Smo;*gli3* double mutants, which completely lack an Hh response, relatively

normal numbers of motor neurons are induced at the forelimb level, while no

motor neurons differentiate more posteriorly (Wijgerde et al., 2002). These

results collectively indicate that while the induction of a majority of spinal motor

neurons in mouse requires Gli-dependent Hh signaling, a small number of motor

neurons can also be induced by Hh- and Gli-independent processes.

　　　　We therefore tested whether Gli function is absolutely necessary for motor

neuron induction in zebrafish. We have been investigating the roles of Hh

pathway components in motor neuron induction in zebrafish embryos using gain-

and loss-of-function approaches (Bingham et al., 2001; Chandrasekhar et al.,

1999; Chandrasekhar et al., 1998). In *detour* (*dtr*) null mutant alleles (Brand et

al., 1996b; Karlstrom et al., 1996), induction of midbrain and hindbrain motor

neurons (branchiomotor and somatomotor neurons) is completely blocked, while

spinal motor neurons are induced normally (Chandrasekhar et al., 1999). Since

dtr encodes the zebrafish *gli1* homolog (Karlstrom et al., 2003), these results

indicate that zebrafish *gli1* plays different roles in motor neuron induction in the hindbrain and spinal cord. Therefore, we were particularly interested in examining the roles of zebrafish *gli2* and *gli3* in motor neuron development. We show here that *you-too* (*yot*) mutants (Brand et al., 1996b; van Eeden et al., 1996), which encode dominant repressor (DR) forms of Gli2 (Karlstrom et al., 1999; Karlstrom et al., 2003), exhibit severe loss of motor neurons in the hindbrain and spinal cord. However, the motor neuron phenotype appears to be an indirect effect of mutant Gli2^{DR} protein on Gli activator functions in the neural tube, since we show that wild type *gli2* plays only a minor role in motor neuron induction within the spinal cord, and no discernable role in the hindbrain. In contrast, *gli3* plays a more prominent role in motor neuron induction in the hindbrain and spinal cord. By combining different *gli* mutants with *gli* antisense morpholinos to inhibit the function of multiple *gli* genes, we demonstrate that, unlike in mouse, Gli activator function (encoded by *gli1*, *gli2*, and *gli3*) is absolutely required for motor neuron induction at all axial levels in the zebrafish neural tube.

4.2   MATERIALS AND METHODS

4.2.1   Animals

Maintenance of zebrafish stocks and collection and development of embryos in E3 embryo medium were carried out as described previously (Bingham et al., 2002; Chandrasekhar et al., 1997; Chandrasekhar et al., 1999;

Westerfield, 1995). Throughout the text, the developmental age of the embryos corresponds to the hours elapsed since fertilization (hours post-fertilization, hpf, at 28.5°C).

You-too (yot^{ty17} and yot^{ty119}) and slow muscle omitted (smu^{b641}) mutants were generated by crossing heterozygous parents and mutants were then identified on the basis of the morphology of the somites at 21 hpf (Barresi et al., 2000; van Eeden et al., 1996; Varga et al., 2001). Detour mutants (dtr^{te370}) were also generated by crossing heterozygous parents and then identified on the basis of defects in motor neuron development or Hh target gene expression in the hindbrain following immunohistochemistry or in situ hybridization (Chandrasekhar et al., 1999). For analysis of branchiomotor neuron development, the motor neuron-expressed islet1-GFP transgene (Higashijima et al., 2000) was crossed into these mutant backgrounds. Since the islet1-GFP reporter is not suitable for counting neuronal cell bodies, islet antibody labeling was used for quantifying motor neuron populations (see below).

4.2.2 Immunohistochemistry, in situ hybridization, and imaging

Whole-mount immunohistochemistry was performed with the various antibodies as described previously (Bingham et al., 2002; Chandrasekhar et al., 1997). The following antibodies, with dilutions indicated, were used: zn5/8, 1:10 (Trevarrow et al., 1990); islet (39.4D5), 1:200 (Korzh et al., 1993); 3A10, 1:500

(Hatta, 1992). For fluorescent immunolabeling (zn5 and 3A10), RITC-conjugated secondary antibody (Jackson Immunochemicals) was used.

Synthesis of the digoxygenin- and fluorescein-labeled probes and whole-mount in situ hybridization were carried out as described previously (Bingham et al., 2003; Chandrasekhar et al., 1997; Prince et al., 1998). Two-color in situ hybridizations were performed essentially as described (Prince et al., 1998) with the following modifications. After deactivating the first in situ reaction with 0.1M glycine, embryos were washed several times in 0.1M glycine before the blocking and antibody incubation steps for the second in situ probe. Fast Red substrate (Sigma) was used for the second reaction, and the substrate was replaced every 45 min until the desired color intensity was reached (usually after 5–6 hours). The following in situ probes were used: *fgf3* (Maves et al., 2002); *gli1* (Karlstrom et al., 2003); *gli2* (Karlstrom et al., 1999); *krox20* (Oxtoby and Jowett, 1993); *net1a* (Lauderdale et al., 1997); *nk2.2* (Barth and Wilson, 1995); and *ptc1* (Concordet et al., 1996).

Embryos were de-yolked, mounted in glycerol, and examined with an Olympus BX60 microscope. In all comparisons, at least ten wild type and ten mutant embryos were examined. Confocal imaging was carried out on fixed embryos mounted in 70% glycerol. Images were captured on an Olympus IX70 microscope equipped with a BioRad Radiance 2000 confocal laser system.

4.2.3 Vibratome sectioning

Embryos processed for in situs were removed from 70% glycerol, rehydrated in PBS, and embedded in 7% low melting point agarose. Embryos were oriented to obtain transverse sections in the hindbrain. This process was facilitated in 15 hpf embryos (Figure 26) by processing them for two-color in situs with *fgf3* (and *gli2*) to label the midbrain–hindbrain boundary. Since *fgf3* is also expressed in rhombomere 4 (Maves et al., 2002), the *fgf3* staining was developed very weakly to avoid interference with visualization of the *gli2* signal in the hindbrain. 50-µm-thick slices were generated using the Vibratome Plus 1000 system. The appearance of the notochord (in caudal r4) and the otic vesicle (spanning r4–r6) was monitored in successive sections and used to assign rhombomere identities to particular sections.

4.2.4 mRNA and antisense morpholino oligonucleotide injections

Synthesis of capped, full-length *dnPKA* mRNA (Ungar and Moon, 1996) was carried out as described previously (Chandrasekhar et al., 1998). Synthetic mRNAs were checked for purity and size by gel electrophoresis, estimated by u.v. spectrophotometry, and diluted to 400 ng/µl. mRNA (~1–2 ng/embryo) was injected into 1–8 cell stage embryos as described previously (Chandrasekhar et al., 1999; Chandrasekhar et al., 1998).

Antisense morpholino oligonucleotides (MOs) against *gli1*, *gli2*, and *gli3* mRNA sequences were described previously (Karlstrom et al., 2003; Tyurina et al., 2005). Working dilutions of *gli1* MO (1.8 ng/nl), *gli2* MO (3 ng/nl), and *gli3* MO (10 ng/nl) were prepared in Danieau buffer (for recipe, see Materials and Methods section 2.10.1), and morpholinos (5–30 ng/embryo) were injected into 1–4 cell stage embryos. The effective concentration for each morpholino was determined through dose–response experiments (see footnotes of Table 7 and Table 8 for more details). Since injection of control (5 base mismatch) morpholinos had no effects on motor neuron development or Hh-regulated gene expression (Figure 17), uninjected embryos served as controls in all experiments described here.

4.2.5 Genotyping of embryos

The tails of fixed embryos were clipped and stored in 70% glycerol. DNA was extracted for genotyping as described previously (Westerfield, 1995) with the following modifications: tail fragments were washed five times in 1 M Tris–HCl, pH 8.2 prior to digestion, and 20 µg of glycogen (Roche) was added to each sample prior to ethanol precipitation for 48 h at −20°C.

A restriction site (*Nla*III) disrupted by the *yot*^{ty119} point mutation (Karlstrom et al., 1999) served as an RFLP marker. PCR primers were designed (Fwd: 5′ ATG ATG CCT CAC GAA GTT CC 3′; Rev: 5′ GGC AGA CGT GAT AGG TTC GT 3′) to introduce mutations to silence nearby, endogenous *Nla*III sites

unaffected by the *yot^ty119* mutation. Undigested PCR products from wild type and

yot^ty119 mutant alleles were 137 base pairs (bp) in length. *Nla*III treatment

digested the PCR product from the *yot^ty119* allele into 102 bp and 35 bp

fragments, and the larger fragment could be distinguished from the uncut wild

type product on a 3% agarose gel.

4.2.6   Cyclopamine treatment

Embryos were treated with cyclopamine (Taipale et al., 2000) as

described previously (Karlstrom et al., 2003) with the following modifications.

Embryos were staged and synchronized at 5.25 hpf by discarding any embryos

not at 50% epiboly. Cyclopamine stock (10 mM in 95% ethanol) was diluted to a

working concentration of 100 µM in E3 medium containing 0.5% DMSO, and

treated embryos were incubated in 12-well tissue culture plates.
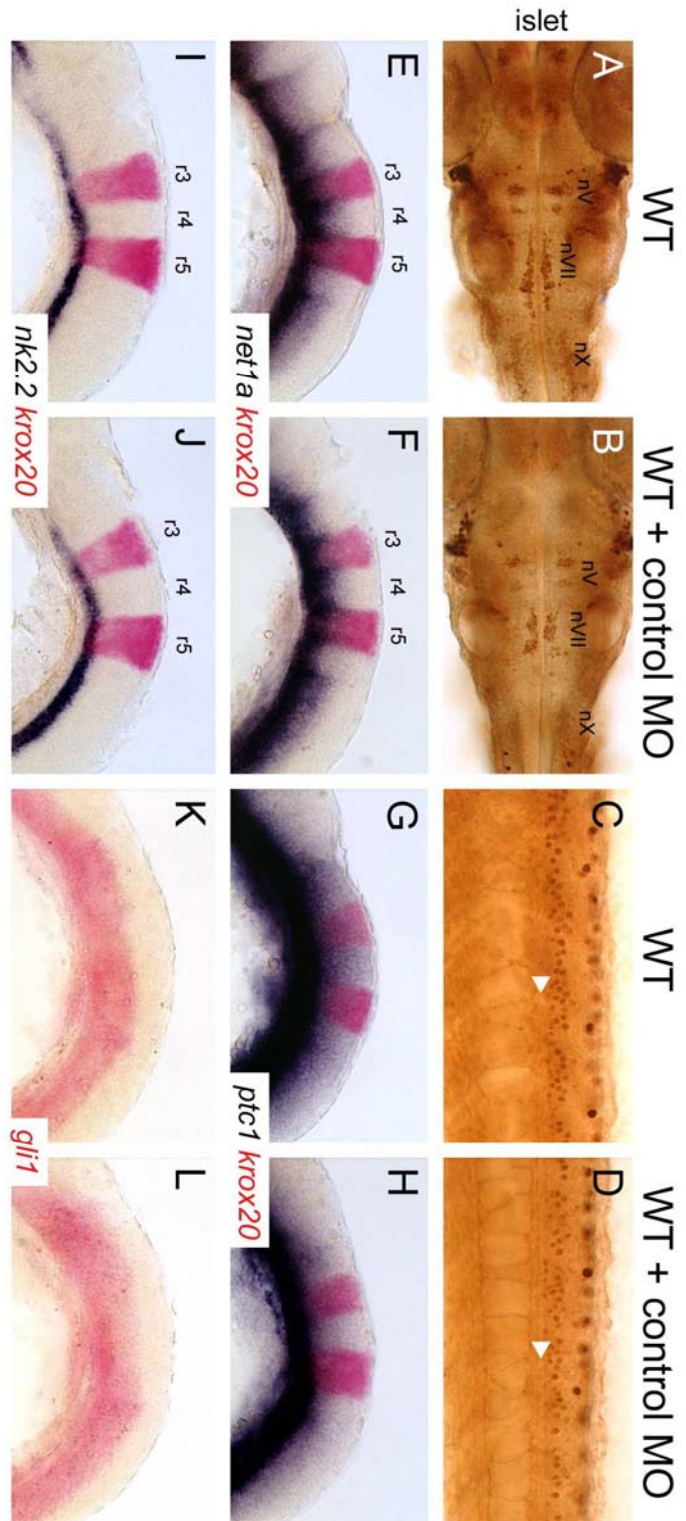
FIGURE 17. Control *gli1* mismatch morpholinos have no effect on motor neuron development and expression of Hedgehog-regulated genes.

Panels A, B, and C–L show dorsal and lateral views, respectively, with anterior to the left. **(A and B):** In a 36-hpf wild type embryo, either uninjected (A) or control-morpholino injected (B), the islet antibody-labeled nV, nVII, and nX motor neurons are found in their characteristic positions in the hindbrain. The nX neurons are out of focus in both panels. **(C and D):** In a 36-hpf wild type background, islet antibody-labeled spinal motor neurons (arrowheads) are found in similar numbers in both uninjected (C) and control morpholino-injected (D) embryos. **(E–L):** In uninjected 22 hpf wild type embryos, Hedgehog-regulated genes such as *net1a* (E), *ptc1* (G), *nk2.2* (I), and *gli1* (K) are expressed in characteristic patterns in the ventral hindbrain. In wild type embryos injected with control morpholino, the expression patterns of *net1a* (F), *ptc1* (H), *nk2.2* (J), and *gli1* (L) are not affected. Expression of *krox20* in rhombomeres 3 and 5 was essentially the same in uninjected embryos (E, G, I) and control morpholino-injected embryos (F, H, J).

4.2.7 Quantification of neuronal populations

Islet antibody-labeled nuclei of hindbrain motor neurons and neurons in the ventral spinal cord were counted in strongly labeled preparations. Counts were performed under 40 × magnification. Spinal motor neurons were counted on one side in three contiguous segments at the level of the tip of the yolk tube. To determine whether observed differences were statistically significant, we performed one-way, parametric ANOVA analyses (with Bonferroni post-tests) using Graphpad Instat version 3 software (GraphPad Software, Inc.).

4.3 RESULTS

4.3.1 Induction of cranial and spinal motor neurons is affected in *you-too* (*gli2*) mutants

In zebrafish *detour* (*dtr* (*gli1*⁻)) mutants (Brand et al., 1996b; Karlstrom et al., 1996; Karlstrom et al., 2003), cranial (midbrain and hindbrain) motor neurons are not induced, while spinal motor neurons are induced normally (Chandrasekhar et al., 1999), indicating that *gli1* is necessary for cranial motor neuron induction, and suggesting that other *gli* genes may function redundantly in spinal motor neuron induction. To test this hypothesis, we examined motor neuron development and Hh-regulated gene expression in *you-too* (*yot*) mutants (Brand et al., 1996b; Karlstrom et al., 1996), which encode dominant repressor forms of Gli2 (Gli2^{DR}) that block Gli1-mediated Hh signaling in reporter assays

(Karlstrom et al., 1999; Karlstrom et al., 2003). The characteristic organization in

a wild type embryo of the motor neurons in the midbrain (nIII, nIV) and the

branchiomotor neurons in the hindbrain (nV, nVII, nX) has been described

previously (Figure 18A and D) (Chandrasekhar et al., 1997; Higashijima et al.,

2000). In yot^{ty17} mutants, midbrain motor neurons (nIII, nIV) were mostly missing,

and branchiomotor neurons in the hindbrain were significantly reduced (Figure

18B and E), consistent with the idea that Gli2^{DR} proteins block Gli1-mediated

motor neuron induction. In yot^{ty119} mutants, branchiomotor neuron induction was

even more severely affected, with the nV neurons in rhombomeres 2 and 3 (r2

and r3), and the nX neurons in the caudal hindbrain almost completely missing

(Figure 18C and F). Similarly, the zn5 antibody-labeled nVI motor neurons in r5

and r6 (Figure 18G) (Chandrasekhar et al., 1997; Trevarrow et al., 1990) were

reduced in number in yot^{ty17} mutants (Figure 18H), and completely lost in yot^{ty119}

mutants (Figure 18I). There were no observable differences in the patterns of

neurogenesis (*ngn1*, *ash1a*, *ash1b*, *deltaD* expression) or cell death (acridine

orange labeling) in the hindbrain between wild type and *yot* mutant embryos

(data not shown), suggesting that motor neuron induction, and not neurogenesis

or cell death, is specifically affected in these mutants.

In contrast to *dtr* (*gli1*⁻) mutants, *yot* (*gli2*^{DR}) mutants had reduced

numbers of islet-expressing primary and secondary motor neurons in the spinal

cord (Figure 18K and L; data not shown), confirming that Gli function plays a role

in spinal motor neuron induction. We quantified motor neuron loss in yot^{ty17} and

yot^{ty119} mutants (36 hpf) labeled with the islet antibody and showed that these
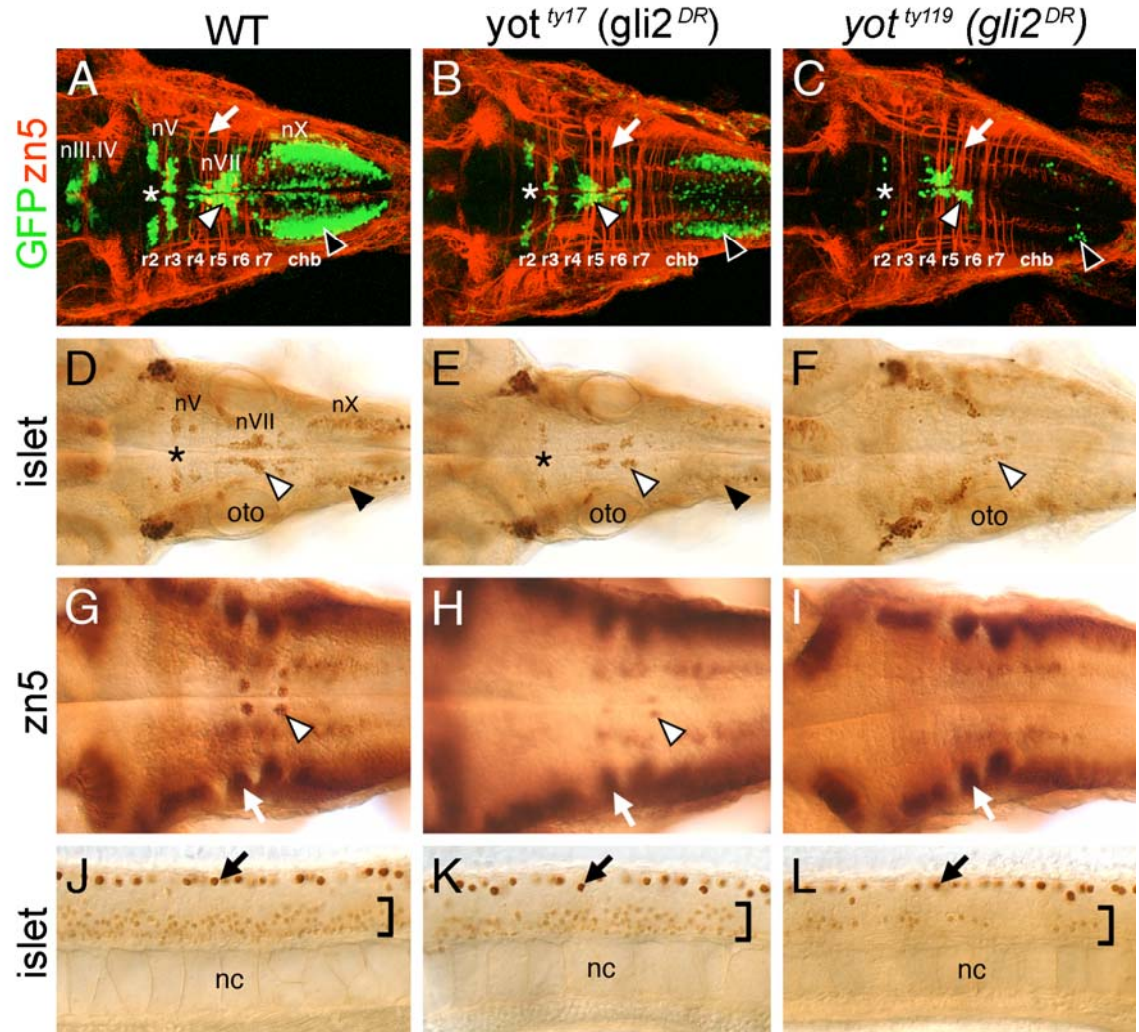
FIGURE 18. Cranial and spinal motor neuron development is affected in

***you-too* (*yot*) mutants.**

Panels A–I show dorsal views of the hindbrain, and panels J–L show lateral views of the trunk,

with anterior to the left. Asterisks in A–E indicate the location of nV motor neurons in

rhombomere 2. Panels A–C are composite confocal images of embryos and identify *GFP*-

expressing cranial motor neurons in the fluorescein channel, and zn5 antibody-labeled

commissural neurons and axons at rhombomere boundaries (arrows) in the rhodamine channel.

(A–C): Cranial motor neurons expressing the *islet1*-GFP transgene occupy stereotypic locations

across different rhombomeres of the hindbrain. In a 48-h post-fertilization (hpf) wild type embryo

(A), the nIII and nIV somatic motor neurons are located in the midbrain, the trigeminal motor

neurons (nV; asterisk) in r2 and r3, the facial motor neurons (nVII; white arrowhead) in r5, r6, and

r7, and the vagal motor neurons (nX; black arrowhead) in the caudal hindbrain (chb). The nV

neurons are reduced in number in *yot*^{ty17} mutants (B), and almost absent in *yot*^{ty119} mutants (C),

and, similarly, the nX neurons (black arrowheads) exhibit progressively severe losses in *yot*^{ty17}

and *yot*^{ty119} mutants. While nVII neurons (white arrowheads) are also reduced in number in both

mutant alleles, the reduction is less severe than those for nV and nX neurons. **(D–F):** At 36 hpf,

the islet antibody labels hindbrain motor neurons in characteristic locations (arrowheads, asterisk;

see panel A for details) in wild type embryos (D), and these neurons are found in progressively

reduced numbers in *yot*^{ty17} (E) and *yot*^{ty119} (F) embryos. **(G):** In a 48-hpf wild type embryo, the

zn5 antibody labels axons and cell bodies of the nVI abducens motor neurons in rhombomeres 5

and 6 (arrowhead), and the commissural neurons at rhombomere boundaries (arrow). **(H and I):**

In both *yot* mutants, the commissural neurons (arrows) develop normally, while the nVI neurons

are reduced in number in *yot*^{ty17} mutants (H), and absent in *yot*^{ty119} mutants (I). **(J–L):** At 36 hpf,

the islet antibody labels motor neurons in the ventral spinal cord (bracket) in wild type embryos

(J), and these neurons are found in progressively reduced numbers in *yot*^{ty17} (K) and *yot*^{ty119} (L)

embryos. The strongly labeled cells in the dorsal spinal cord (arrows) are Rohon-Beard sensory

neurons. oto, otocyst; nc, notochord.

TABLE 5. Motor neuron induction is reduced in the hindbrain and spinal cord of *you-too* mutants

Phenotype*	Number of islet antibody-labeled cells		
	Hindbrain (nV, nVI, nVII neurons)#	Hindbrain (nVI, nVII neurons)§	Ventral spinal cord (motor neurons)@
WT (ty17)	201.2 ± 26.4	137.8 ± 18.5	21.8 ± 1.3
you-too^{ty17}	96.5 ± 14.9	72.3 ± 11.4	12.7 ± 4.0
Ratio (mut/WT)	0.48	0.53	0.58
Wt (ty119)	190.3 ± 24.9	132.3 ± 16.9	23.1 ± 1.4
you-too^{ty119}	45.3 ± 6.5	42.8 ± 7.2	4.8 ± 0.8
Ratio (mut/WT)	0.24	0.32	0.21

TABLE 5. Motor neuron induction is reduced in the hindbrain and spinal cord of *you-too* mutants

* Six embryos were scored for each phenotype.

\# Total number of labeled cells in rhombomeres 2–7.

§ Total number of labeled cells in r4–r7 (nVI and nVII neurons in WT, nVII neurons in mutants).

@ Number of labeled cells per hemisegment.

two alleles affect motor neuron induction to different degrees (Table 5). While

motor neuron number was reduced ~40–50% in the hindbrain and spinal cord of

yot^{ty17} mutants, there was a ~75% loss in yot^{ty119} mutants, suggesting that the

yot^{ty119} allele encodes a more potent repressor of motor neuron induction than

does the yot^{ty17} allele (Table 5). This is consistent with molecular identification of

these alleles showing that both alleles encode truncated Gli2 proteins, with the

mutant Gli2^{ty119} protein missing more of its putative transcriptional activator

domain (Karlstrom et al., 1999) (see also Figure 9C). Interestingly, the number

of motor neurons in r4–r7 (corresponding to nVI and nVII neurons in the wild type

embryo) was less reduced in yot^{ty119} mutants (only nVII neurons present) than

were other branchiomotor neuron populations (nV, nX) (Table 5) (Figure 18A and

C). Given that nVII neurons are born in r4 and undergo tangential migration

through r5 into r6 and r7 (Bingham et al., 2002), these data suggest that motor

neuron induction in r4 is less severely affected than in other rhombomeres in

yot^{ty119} mutants.

4.3.2 Hh signaling in r4 is largely unaffected in yot mutants

To determine the extent to which Hh signaling occurs normally in r4 of *yot*

mutants, we examined the expression of several Hh target genes in the ventral

hindbrain. While *nk2.2* (Barth and Wilson, 1995) was expressed without gaps

along the anteroposterior (AP) axis in wild type siblings at 21 hpf (Figure 19A and

C), its expression was almost completely eliminated in yot^{ty119} mutants except in

WT, *net1a*

nk2.2 krox20

WT, EtOH

ptc1

nk2.2 krox20

P — EtOH@6 hpf

M — r3 r4 r5

I — rhombomere 4

E — r3 r4 r5

A — WT — r3 r4 r5

Q — CyA@6 hpf

N — *yot*, EtOH

J

F

B — *yot^ty119*

R — CyA@18 hpf

O — WT or *yot*, cyclopamine

K — rhombomere 6

G — r3 r4 r5 — *net1a krox20*

C — WT — r3 r4 r5

S — CyA@24 hpf

L

H — *net1a krox20*

D — *yot^ty119*
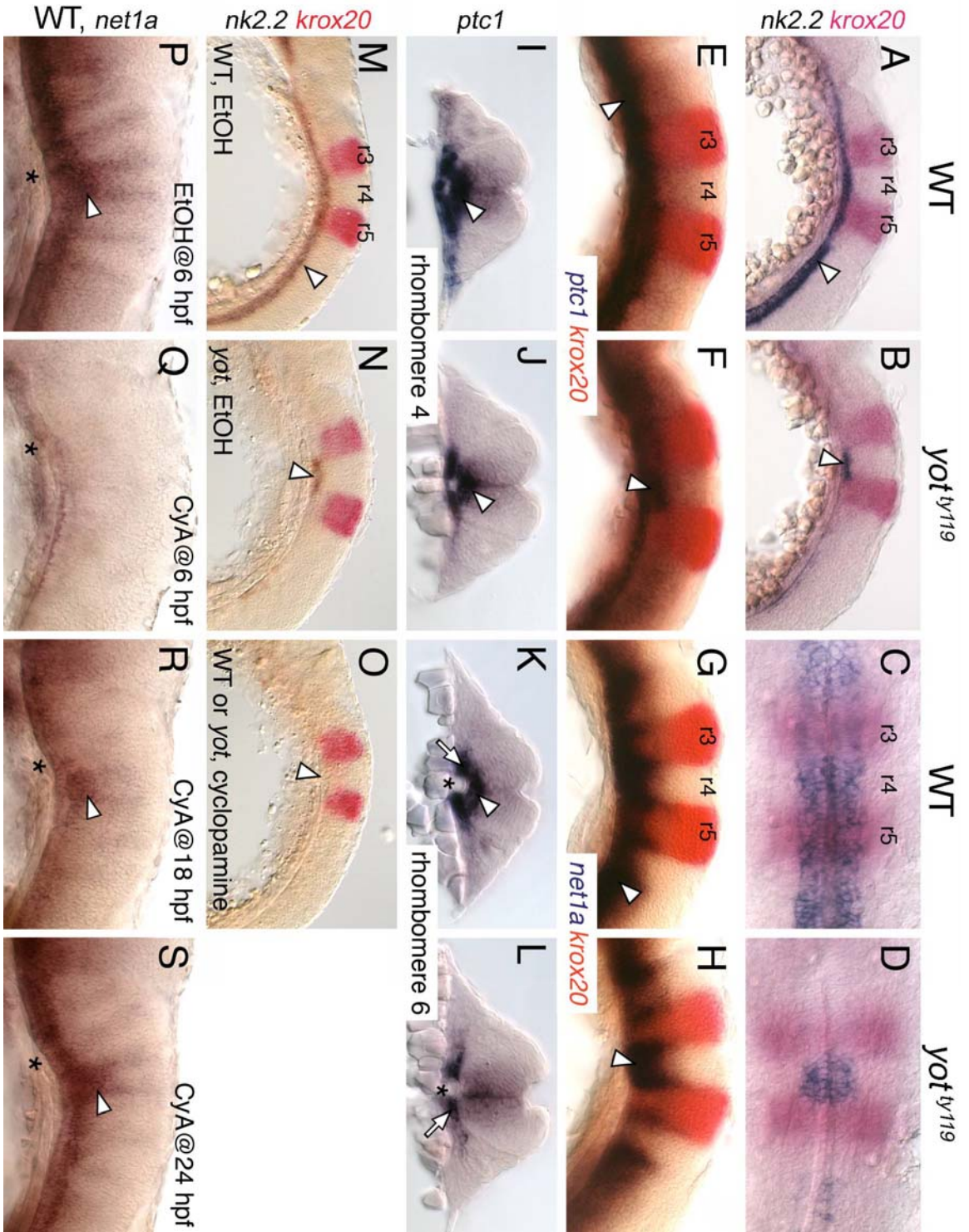
FIGURE 19. Hh signaling is significantly normal in rhombomere 4 of *yot* mutants.

Panels A, B, E–H, and M–S show lateral views of hindbrain, with anterior to the left. Panels C and D show dorsal views with anterior to the left. Panels I–L show cross sections of the hindbrain (top is dorsal) at the indicated rhombomere levels. **(A–D):** In 21 hpf wild type embryos (A and C), *nk2.2* is expressed (arrowhead) in the ventral neural tube at all axial levels. In *yot^{ty119}* mutants (B and D), *nk2.2* expression (arrowhead) is virtually absent at all axial levels, except in rhombomere 4 (r4), delineated by the expression of *krox20* in r3 and r5. Within r4 (D), the *nk2.2* expression domain is slightly reduced compared to wild type. **(E–H):** In 21 hpf wild type embryos, *ptc1* (E) and *net1a* (G) are expressed (arrowheads) at all axial levels in the ventral neural tube. In *yot^{ty119}* mutants, *ptc1* expression (F) is greatly reduced, with significant expression retained in r4 (arrowhead). Similarly, while *net1a* expression is substantially reduced in the *yot^{ty119}* mutant hindbrain (H), it is significantly normal in r4 (arrowhead). **(I–L):** In rhombomere 4 (r4), *ptc1* expression (arrowheads) in the ventral neural tube is comparable between wild type (I) and *yot* mutants (J). In contrast, *ptc1* expression in r6 (K) (arrowhead) is greatly reduced in *yot* mutants (L), while its expression in paraxial mesoderm (arrows) appears normal. Asterisk, notochord. **(M–O):** While *nk2.2* is specifically expressed in r4 of mutants (N, arrowhead), *nk2.2* expression in all rhombomeres, including r4 (arrowhead), is completely absent in wild type and mutant embryos treated with cyclopamine (O). **(P):** In a control 30 hpf wild type embryo treated with EtOH from 6 hpf, *net1a* expression is normal, with elevated expression in r4 (arrowhead). **(Q):** In a wild type embryo treated with cyclopamine (CyA) from 6 hpf, *net1a* expression is completely absent at all axial levels. **(R):** In an embryo treated from 18 hpf, *net1a* is mostly expressed in r4 (arrowhead). **(S):** In an embryo treated from 24 hpf, *net1a* expression is mostly normal, with prominent expression in r4 (arrowhead). Asterisks in P–S mark the anterior end of the notochord in r4.

r4 (Figure 19B and D). There was a slight decrease in the number of *nk2.2*-expressing cells in r4 of mutants (Figure 19D), but the boundaries of expression coincided precisely and reproducibly with r4 (*n* = 30 embryos). Similarly, the expression of *patched1* (*ptc1*) (Concordet et al., 1996) was severely reduced throughout the mutant hindbrain except in r4 (Figure 19E and F). Another Hh target, *netrin1a* (*net1a*) (Lauderdale et al., 1997), is normally expressed throughout the ventral neural tube, with marked upregulation at rhombomere boundaries (Figure 19G). In *yot^{ty119}* mutants, however, *net1a* expression was reduced in many rhombomeres (especially evident in r5 and r6) with the exception of r4 and adjacent boundaries (Figure 19H). In cross-sections, *ptc1* was expressed ventrally in r4 in mutants, albeit in a smaller number of cells (Figure 19I and J), while expression was completely missing in adjacent rhombomeres including r6 (Figure 19K and L), thus highlighting the rhombomere-specific nature of this expression pattern in *yot* mutants.

We next tested whether residual *nk2.2* and *net1a* expression in r4 of *yot^{ty119}* mutants required Hh signaling using the alkaloid cyclopamine (CyA) to block Hh signaling at the level of the Smoothened receptor (Barresi et al., 2000). In ethanol-treated control embryos, the wild type (*n* = 15) and mutant (*n* = 4) expression patterns were unaffected (Figure 19M and N). Following CyA treatment beginning at 3 hpf, *nk2.2* expression was completely lost along the AP axis, including r4, in wild type and mutant embryos (Figure 19O; *n* = 44), demonstrating that Hh signaling is required for the r4-specific expression of ventral neural tube markers in *yot^{ty119}* mutants. Interestingly, blocking Hh

signaling at different times had differential effects on the pattern of *net1a* expression, assayed at 30 hpf. While an early block (CyA treatment beginning at 15 hpf or earlier) blocked *net1a* expression throughout the hindbrain (Figure 19; data not shown; *n* = 12), CyA treatment from 18 hpf blocked *net1a* expression in all rhombomeres except in r4 (Figure 19R; *n* = 3), while CyA treatment from 24 hpf or later had no significant effect on *net1a* expression (Figure 19S; *n* = 6). These observations indicate that *net1a* expression in r4 has different temporal requirements for Hh signaling and suggest that retention of Hh target gene expression in r4 of *yot* mutants may reflect the inability of the mutant Gli2 protein to block early Hh signaling in this rhombomere.

4.3.3   Activation of Hh signaling can alleviate defective motor neuron induction and Hh target gene expression in yot mutants

Since the *yot* alleles encode dominant repressors of Hh signaling (Karlstrom et al., 2003), we wondered whether ectopic activation of Hh signaling upstream of the Gli transcription factors by overexpression of dominant-negative protein kinase A (dnPKA) (Ungar and Moon, 1996) could overcome the repressive effects of these mutations on Hh target gene (*nk2.2*, *net1a*) expression and motor neuron induction. When *dnPKA* RNA was injected into embryos from *yot^ty119^+/−;islet1-GFP* crosses, there was a dramatic increase in the number of *GFP*-expressing branchiomotor neurons in all rhombomeres, and

in ectopic, dorsal locations along the dorsoventral axis, in ~80% of wild type

siblings (Figure 20A and B; Table 6). Consistent with this, *nk2.2* expression was

upregulated in the ventral neural tube and at ectopic locations throughout the

hindbrain in ~88% of *dnPKA*-injected wild type embryos (Figure 20E and F). In

marked contrast, no ectopic, dorsally-located *GFP*-expressing cells were seen in

dnPKA-injected *yot^{ty119}* mutants, but there was a small, reproducible increase in

the number of nVII neurons, and less frequently nX neurons (Figure 20C and D;

Table 6). Furthermore, while *nk2.2* was not expressed in the ventral hindbrain or

in ectopic dorsal locations in *dnPKA*-injected *yot^{ty119}* mutants, its expression in

ventral r4 was slightly but reproducibly upregulated (Figure 20G and H).

Interestingly, when *dnPKA* RNA was injected into embryos from *yot^{ty17}*+/−;*islet1-*

GFP crosses, *net1a* was expressed ectopically in the dorsal neural tube at all

axial levels in wild type and *yot^{ty17}* mutants, but more weakly in mutants (Figure

20I–L; Table 6). Similarly, ectopic *GFP*-expressing motor neurons and *nk2.2*-

expressing cells were found in r2 and r4 of *dnPKA*-injected *yot^{ty17}* mutants (data

not shown). These results suggest that while both *yot* alleles encode dominant

repressors, their inhibitory activities can be overcome to different extents by

hyperactivation of Hh signaling, with the *ty119* allele being most resistant to this

treatment. These observations are consistent with our earlier results that the *yot*

alleles represent a phenotypic series, with the *ty119* allele encoding a stronger

repressor of motor neuron induction (Table 5), in accordance with reporter

assays (Karlstrom et al., 2003).

GFP 3A10   *nk2.2 krox20*   *net1a krox20*

WT, control

WT, *dnPKA*

yot^DR, control

yot^DR, *dnPKA*

A   r2 r3 r4 r5 r6 r7 chb

B

C   r2 r3 r4 r5 r6 r7 chb

D

E   r3   r4   r5

F

G

H

I   r3   r4   r5

J

K

L

yot^ty119 allele   *yot^ty17* allele
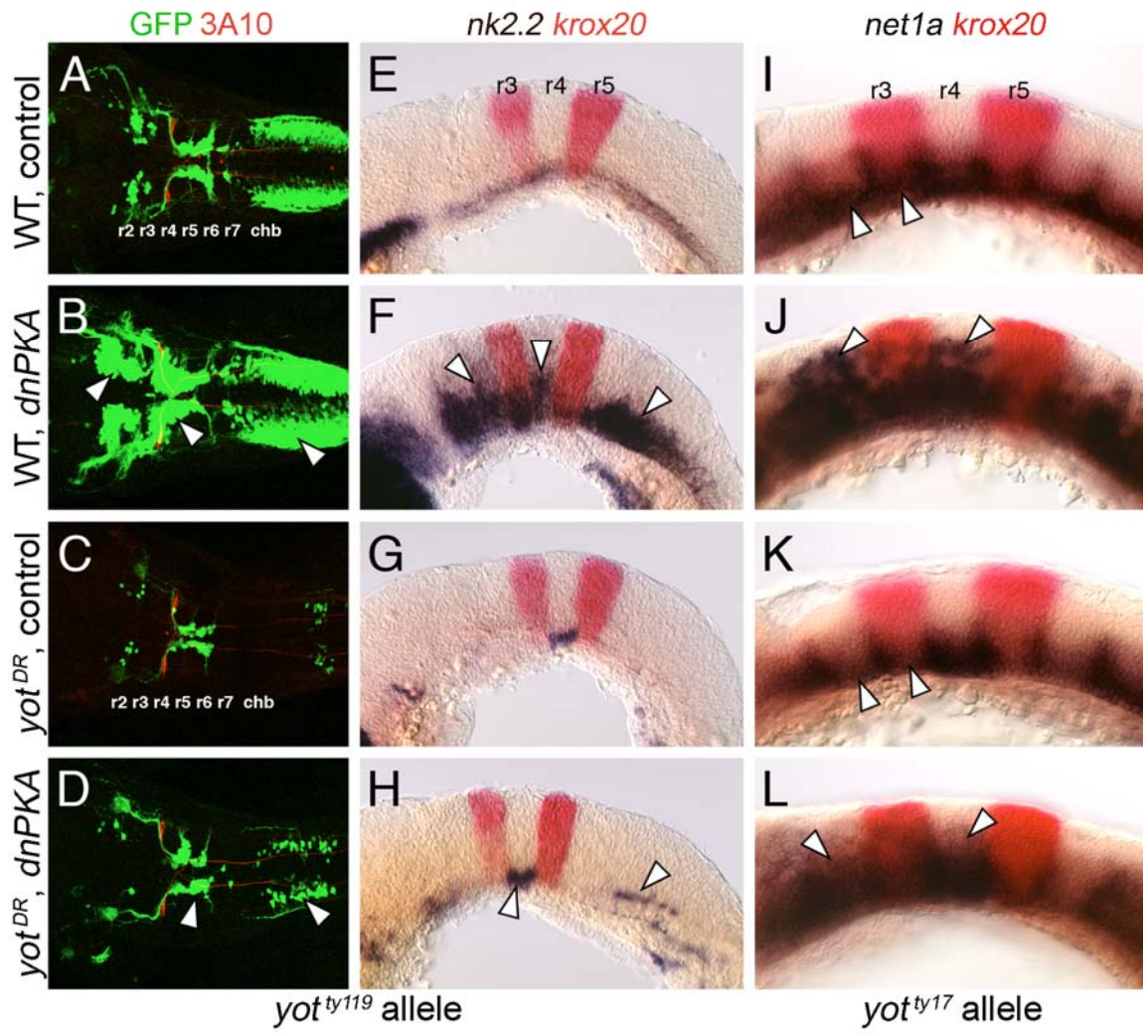
FIGURE 20. Hh-regulated events in *yot^{ty119}* mutants are resistant to ectopic Hh pathway activation.

Anterior is to left in all panels. Panels A–D show dorsal views, and panels E–L show lateral views. A–D are composite confocal images of embryos, and identify *GFP*-expressing branchiomotor neurons (green), and 3A10 antibody-labeled Mauthner neurons and axons in rhombomere 4 (red). **(A and E):** In control wild type embryos, *nk2.2* is expressed ventrally at all axial levels at 21 hpf (E), and branchiomotor neurons are found at their characteristic locations at 36 hpf (A). **(B and F):** In *dnPKA* RNA-injected wild type embryos, *nk2.2* is expressed at high levels, and at ectopic locations (arrowheads) in all rhombomeres (F). Branchiomotor neurons are also greatly increased in number (arrowheads), and found at ectopic locations at all axial levels (B). **(C and G):** In control *yot^{ty119}* mutants, *nk2.2* expression is missing throughout the hindbrain, except within r4 (G), and, concomitantly, there is a severe loss of branchiomotor neurons at all axial levels, except nVII neurons, which originate in r4 (C). **(D and H):** In *dnPKA* RNA-injected *yot^{ty119}* mutants, *nk2.2* expression is increased within its normal ventral domain in r4, and slightly within the caudal hindbrain (H, arrowheads). There is a corresponding increase in the number of branchiomotor neurons originating in r4 and the caudal hindbrain (arrowheads), but there is no effect on motor neurons in other rhombomeres (D). **(I–L):** In a control 21 hpf wild type embryo (I), *net1a* is expressed ventrally at all axial levels (arrowheads), with dorsal expansion at rhombomere boundaries. In a *dnPKA* RNA-injected wild type embryo (J), *net1a* expression is expanded dorsally (arrowheads) at all axial levels. In a control *yot^{ty17}* mutant (K), *net1a* expression is reduced in all rhombomeres except r4 (arrowheads; compare to I). In a *dnPKA* RNA-injected *yot^{ty17}* mutant (L), *net1a* expression is expanded dorsally in all rhombomeres including r2 and r4 (arrowheads).

TABLE 6. Effects of ectopic Hh pathway activation on hindbrain gene

expression in *yot* mutants

yot allele (marker gene)	Injected RNA	Number of embryos	Fraction of embryos with ectopic marker expression	
			Wild-type (+/+ and +/−)[#]	Mutant (−/−)[#]
you-too[ty17](*netrin1a* expression at 21 hpf)	none	137	0% (0/97)	0% (0/40)
	dnPKA*	128	91% (84/92)	81% (29/36)
you-too[ty119](*nk2.2* expression at 21 hpf)	none	32	0% (20/20)	0% (12/12)
	dnPKA*	60	88% (38/43)	0% (0/17)[@]
you-too[ty119](*islet1-GFP* expression at 36 hpf)	none	27	0% (20/20)	0% (7/7)
	dnPKA*	52	79% (30/38)	0% (0/14)[@]

TABLE 6. Effects of ectopic Hh pathway activation on hindbrain gene expression in *yot* mutants

[#] While *dnPKA*- injected *yot* mutants could be readily identified after in situ hybridization, roughly half of the embryos in each experiment were genotyped by PCR. Since there was perfect correlation between PCR genotyping and morphological identification, the data from embryos scored by the two methods were pooled.

[*] Approximately 1 ng of *dnPKA* RNA (see Materials and methods) was injected per embryo, generating the Hh overexpression phenotype in 80-90% of injected wild type embryos (Chandrasekhar *et al*., 1999).

[@] Although no *nk2.2*-or *GFP*- expressing cells were found at ectopic locations in the *yot*[ty119] mutant hindbrain following *dnPKA* overexpression, expressing cells were found in the caudal hindbrain of several embryos, where nX neurons are normally found (see Figures 20D, 20H). In addition, the number of *GFP*-expressing nVII neurons was markedly increased, and *nk2.2* expression in ventral r4 was consistently upregulated in many of these embryos.

4.3.4   Hh signaling is essential for branchiomotor neuron induction

Given that the *yot* (*gli2^{DR}*) mutations affect branchiomotor neuron number, and that Hh signaling may regulate Gli2 activator and repressor functions (Stamataki et al., 2005), we determined the overall requirement for Hh signaling in motor neuron induction, and compared it to the requirement for Gli1, which possesses only activator function (Karlstrom et al., 2003; Tyurina et al., 2005). To do this, we examined branchiomotor neuron induction and Hh-regulated gene expression in *slow muscle omitted* (*smu^{b641}*) mutants where Hh signaling is blocked due to a loss-of-function mutation in *smoothened* (*smo*) (Barresi et al., 2000; Chen et al., 2001; Varga et al., 2001), and in *detour* (*dtr^{te370}*) mutants, which carry a loss-of-function mutation in *gli1* (Karlstrom et al., 2003).

In *smu* (*smo$^-$*) and *dtr* (*gli1$^-$*) mutants, the motor neurons in the midbrain (nIII, nIV) and the branchiomotor neurons in the hindbrain (nV, nVII, nX) were almost completely missing (Figure 21B and C; compare to Figure 21A), demonstrating that the functions of the Smo receptor and Gli1 transcription factor are essential for their induction (Chandrasekhar et al., 1999). Consistent with this, the expression of several Hh-regulated genes in the hindbrain (Figure 21D, G, J, M) was greatly reduced or completely lost in *smu* mutants (Figure 21E, H, K, N) (Chen et al., 2001; residual *net1a* and *gli1* expression likely due to maternally supplied Smo function). While *nk2.2* expression was similarly absent in *dtr* mutants (Figure 21F), significant levels of *ptc1* and *net1a* expression were retained (Figure 21I and L), indicating that some aspects of their expression do
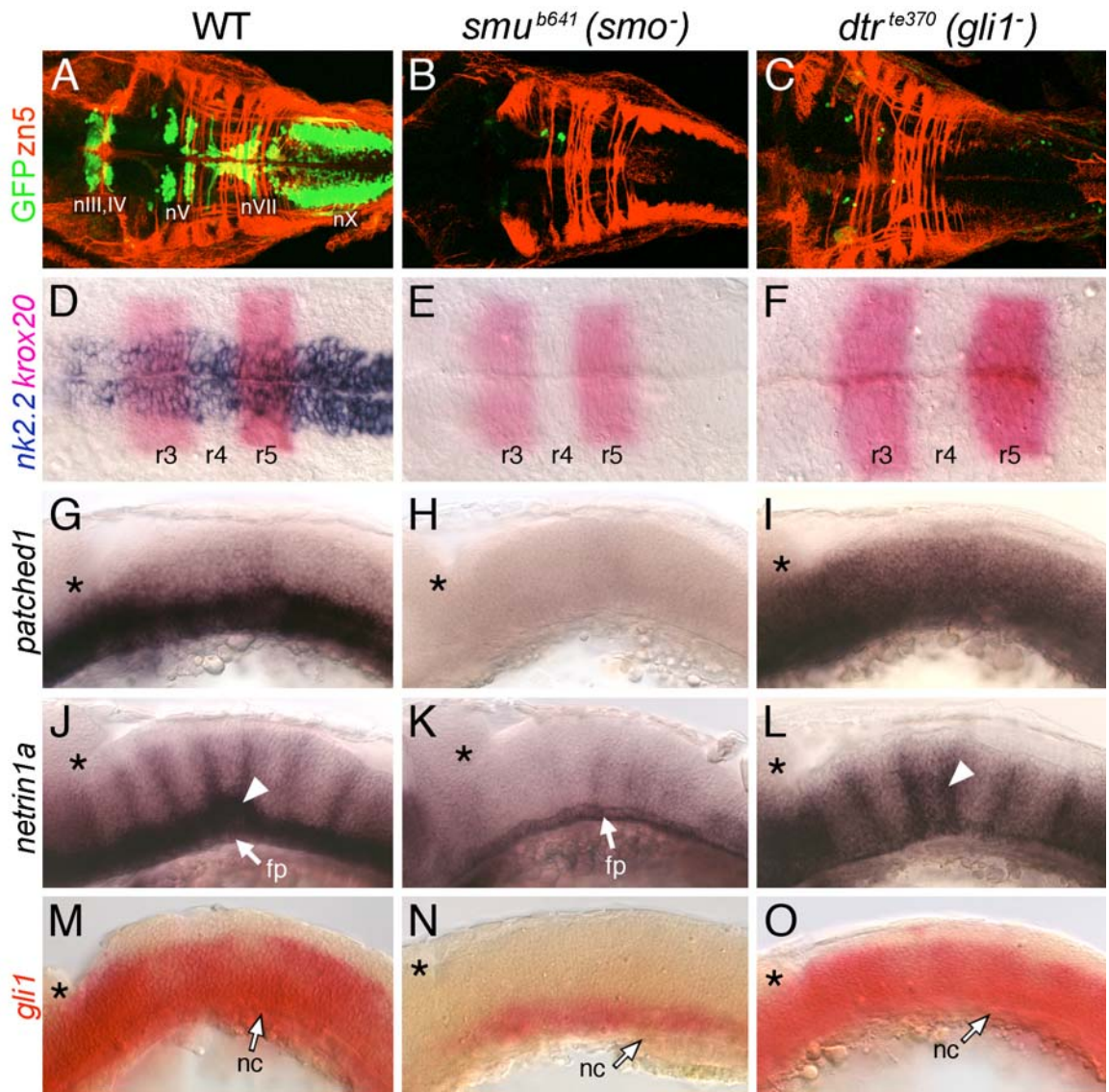
FIGURE 21. Hh signaling and Gli1 function are essential for branchiomotor neuron development.

Panels A–F and G–O show dorsal and lateral views, respectively, of the hindbrain with anterior to the left. Asterisks in G–O mark the cerebellum. **(A):** In a 48-hpf wild type embryo, the nIII, nIV, nV, nVII, and nX motor neurons are found in their characteristic positions. **(B–C):** In *slow muscle-omitted* (*smu*; B) and *detour* (*dtr*; C) mutants, *GFP*-expressing cranial motor neurons are almost completely missing, while the zn5-labeled axons at rhombomere boundaries are unaffected. **(D):** In a 21-hpf wild type embryo, *nk2.2* is expressed throughout the ventral neural tube at all axial levels. **(E–F):** In *smu* (E) and *dtr* (F) mutants, *nk2.2* expression is lost, while *krox20* expression in r3 and r5 is unaffected. **(G–I):** In a 24-hpf wild type embryo (G), *ptc1* is expressed in the ventral hindbrain, while it is expressed diffusely at a reduced level in *dtr* mutants (I), and not expressed at all in *smu* mutants (H). **(J):** In a 30-hpf wild type embryo, *net1a* is expressed in the ventral hindbrain and at rhombomere boundaries (arrowhead). **(K):** In *smu* mutants, *net1a* expression is mostly lost, with residual expression in the floor plate (fp). **(L):** In *dtr* mutants, *net1a* expression in the ventral hindbrain is greatly reduced, but expression at rhombomere boundaries (arrowhead) is unaffected. **(M–O):** In a 21-hpf wild type embryo (M), *gli1* is expressed in the ventral two-thirds of the neural tube, while its expression is greatly reduced in *smu* mutants (N), and is unaffected in *dtr* mutants (O). The anterior tip of the notochord (nc) is at the level of r4, and is indicated by arrows.

not require *gli1* function. Furthermore, *gli1* expression, which is greatly reduced

in *smu* mutants, was essentially unaffected in *dtr* mutants (Figure 21O),

indicating that *gli1* expression depends on Hh signaling but does not require Gli1

function. These results demonstrate that some Hh-regulated events in the

hindbrain (motor neuron induction, and expression of ventral neural tube (*nk2.2*)

and motor neuron (*isl1*, *tag1*) markers (data not shown) require *gli1* function,

while others (expression of *ptc1*, *net1a*, *gli1*) do not, suggesting that other Glis

(encoded by *gli2* and/or *gli3*) may activate some Hh target genes in the hindbrain

(Figure 28) (Tyurina et al., 2005). Strikingly, most Hh-regulated events including

motor neuron induction occur normally in the *dtr* mutant spinal cord

(Chandrasekhar et al., 1999; Karlstrom et al., 2003) (data not shown; see also

Table 7), suggesting that Glis may function in a redundant fashion in the spinal

cord (Figure 28) (Tyurina et al., 2005).

4.3.5   Gli2 plays a minor role in spinal motor neuron induction

Given that Gli2 contributes to the Hh response in the zebrafish midbrain

(Karlstrom et al., 2003), we tested whether *gli2* plays any role in motor neuron

development. To knock down *gli2* function, we injected *gli2* antisense

morpholinos (MOs) into embryos obtained from crossing heterozygous *yot*[ty119]

parents carrying the *islet1*-GFP transgene. In such crosses, *yot* clutches

typically consist of an average of 25% homozygous mutant *yot* embryos. There

was no difference in the number or distribution of *GFP*-expressing motor neurons

in the midbrain or hindbrain between control (16/16 embryos) and *gli2* MO-injected (57/57 embryos) wild type siblings at 48 hpf (Figure 22A and B; see Table 7 for quantification using islet antibody). Similarly, there were no effects on *nk2.2* expression in the ventral neural tube of 21 hpf control (43/43 embryos) and *gli2* MO-injected (25/25 embryos) wild type siblings (Figure 22E and F). These results demonstrate that *gli2* plays little or no role in branchiomotor neuron development.

Strikingly, loss of *GFP*-expressing motor neurons in *yot^{ty119}* (*gli2^{DR}*) mutants was largely rescued upon injection of *gli2* MO (Figure 22D; 19/20 embryos; compare to control: Figure 22C; 8/8 embryos), and motor neurons were found in all rhombomeres at their characteristic locations. This result confirms that the *gli2* MOs effectively block translation of *gli2* mRNA. Furthermore, since no full-length Gli2 protein is present in *yot* mutants, the rescue of the *yot* mutant phenotype convincingly demonstrates that branchiomotor neurons can be specified in the absence of full length, presumably activator forms of Gli2, as suggested by the normal induction of these neurons in *gli2* MO-injected wild type embryos (Figure 22B). Although the *yot* mutant phenotype is rescued, motor neuron numbers, especially evident for nX neurons, were still lower than in wild type siblings. Furthermore, the nIII and nIV motor neurons in the midbrain never reappeared in *gli2* MO-injected mutants. Consistent with these results, *nk2.2* expression was restored in large regions of the ventral hindbrain, but never in the midbrain, of *gli2* MO-injected *yot* mutants (Figure 22H; 8/8 embryos; control, Figure 22G: 11/11 embryos). Therefore, the incomplete rescue of the mutant

GFP zn5   nk2.2 krox20

A — WT, control — nV nVII nX — r2 r3 r4 r5 r6 r7 chb

B — r3 r4 r5

C — WT, gli2 MO — r2 r3 r4 r5 r6 r7 chb

D

E — yot^ty119, control — r2 r3 r4 r5 r6 r7 chb

F — r3 r4 r5

G — yot^ty119, gli2 MO — r2 r3 r4 r5 r6 r7 chb

H

I — dtr^te370 — control

J — gli2 MO

net1a

K — dtr^te370 — control

L — gli2 MO

islet
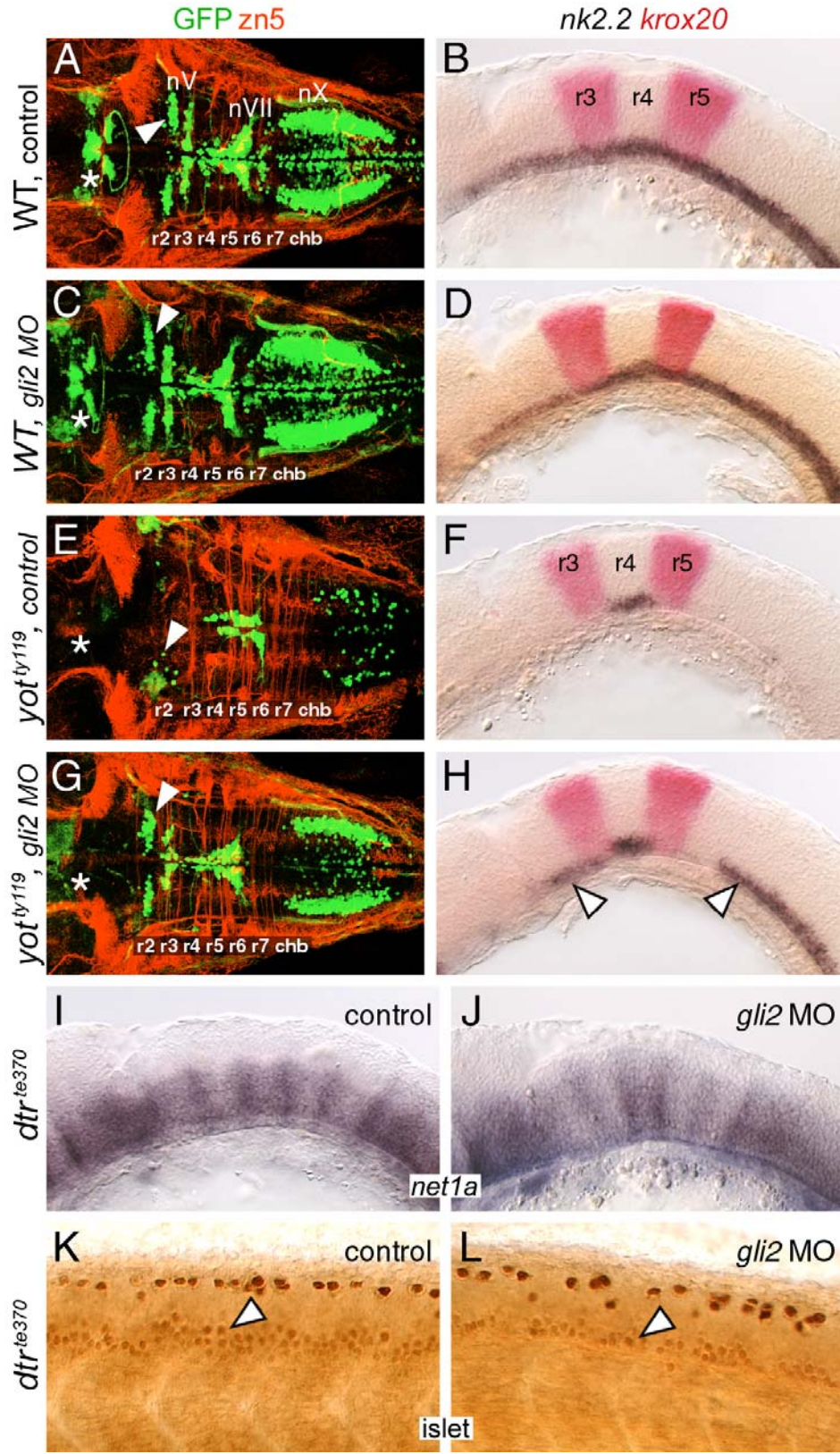
FIGURE 22. *Gli2* contributes to spinal motor neuron induction.

Panels A–D show dorsal views, and panels E–L show lateral views of the hindbrain (E–J) and

spinal cord (K and L), with anterior to the left. Asterisks in A–D indicate the position of the nIII

and nIV motor neurons in the midbrain (A and B), and their absence (C and D). Arrowheads in

A–D indicate the nV neurons in r2. **(A and E):** In control wild type embryos, *nk2.2* expression (E)

and organization of cranial motor neurons (A) are identical to those described previously. **(B and**

F): In *gli2* MO-injected wild type embryos, expression of *nk2.2* (F) and development of cranial

motor neurons (B) are identical to control embryos. **(C and G):** In control *yot*^{ty119} mutants, the

patterns of loss of *nk2.2* expression (G) and cranial motor neurons (C) are similar to those

described previously. **(D and H):** In *gli2* MO-injected *yot*^{ty119} mutants, *nk2.2* expression is

significantly restored in anterior rhombomeres and the caudal hindbrain (H, arrowheads).

Concomitantly, the number of nV neurons (arrowhead) and nX neurons is significantly increased

(D), and the pattern looks similar to that in control wild type embryos. **(I and K):** In control *dtr*^{te370}

mutants, *net1a* is expressed at low levels in the ventral hindbrain, and at higher levels at

rhombomere boundaries (I). In the mutant spinal cord (K), islet antibody-labeled motor neurons

(arrowhead) are found in similar numbers to wild type embryos. **(J and L):** In *gli2* MO-injected

dtr^{te370} mutants, *net1a* expression in the hindbrain (J) shows no significant change (loss). In

contrast, the number of motor neurons in the ventral spinal cord (arrowhead) is slightly but

reproducibly reduced in MO-injected mutants (L).

TABLE 7. Gli2 and Gli3 contribute to spinal motor neuron induction.

Morpholino	Number of islet-labeled cells in the hindbrain		Number of islet-labeled cells in ventral spinal cord[#]	
	Wild-type (*gli1+*)[*]	***dtr* mutant (*gli1−/−*)**[*]	**Wild-type (*gli1+*)**[*]	***dtr* mutant (*gli1−/−*)**[*]
none	294.8 ± 14.6 (6)	16.7 ± 10 (6)	22.3 ± 2.3 (6)	20.4 ± 0.6 (6)
gli2 MO[§]	294 ± 25.4 (6)	5.2 ± 2.8 (6)	22.7 ± 2.1 (6)	15.6 ± 1.2 (6)
	$P > 0.05$ (NS)	$P > 0.05$ (NS)	$P > 0.05$ (NS)	$P < 0.001$
none	287.5 ± 22 (4)	12 ± 4.5 (4)	35.2 ± 3.4 (4)	38.9 ± 4.5 (4)
gli3 MO[£]	214.5 ± 5.3 (4)	14.8 ± 3.3 (4)	16.2 ± 2.6 (4)	13.6 ± 2.9 (4)
	$P < 0.001$	$P > 0.05$ (NS)	$P < 0.001$	$P < 0.001$

TABLE 7. Gli2 and Gli3 contribute to spinal motor neuron induction[@]

[@] While the numbers of control and MO-injected embryos were much higher (>40 for each treatment), we counted motor neuron cell bodies in 4-6 representative embryos for each condition. Mutant embryos were identified by the severe loss of hindbrain motor neurons.

[#] Number of labeled cells per hemisegment.

[*] Number of embryos scored in parenthesis.

[§] Approximately 10 ng of *gli2* MO (see Materials and methods) was injected per embryo based upon previous studies (Karlstrom et al., 2003).

[£] Approximately 30 ng of *gli3* MO was injected per embryo. In our hands, this high dose was needed to generate the ectopic *fkd4* expression phenotype described for *gli3* morphants (Tyurina et al., 2005). No non-specific effects were seen, and >90% of injected embryos survived and were healthy when fixed at 36 hpf.

phenotype in the midbrain and hindbrain of *gli2* MO-injected *yot* mutants may reflect substantial, but not complete, knockdown of $Gli2^{DR}$ synthesis.

If Hh-regulated events could be mediated redundantly by activator functions of Gli1, Gli2, and Gli3 (see model in Figure 28), the lack of a phenotype in *gli2* MO-injected wild type embryos may merely reflect the relative contributions of the various Glis in mediating specific events. In this case, we would predict that minor roles for the Gli2 activator would be discernable in the absence of functional Gli1. We therefore examined Hh-regulated events in the hindbrain and spinal cord of *detour* (*gli1⁻*) mutants following *gli2* MO injection. The number of islet antibody-labeled motor neurons in the spinal cord was reproducibly and significantly reduced by ∼25% in *gli2* MO-injected *dtr* mutants (Figure 22L; Table 7) compared to those in uninjected and *gli2* MO-injected wild type embryos, and uninjected *dtr* mutants (Figure 22K; Table 7). Furthermore, the residual, but substantial, expression of *net1a* in the *dtr* mutant hindbrain (Figure 21 and Figure 22; *n* = 15 embryos) was either slightly reduced or unaffected following *gli2* MO injection (compare Figure 22I to 22J; 21/21 embryos), and *net1a* expression was unaffected in wild type siblings injected with *gli2* MO (*n* = 40; data not shown) as seen for *nk2.2* (Figure 22E and F). These observations suggest strongly that although *gli2* appears to play no role in motor neuron induction or Hh target gene activation in the hindbrain, Gli2 activator function is needed for inducing some spinal motor neurons.

4.3.6 Dominant repressor Gli2 blocks motor neuron induction by interfering with Gli1 function

If motor neuron loss in *yot* mutants were a consequence of Gli2^{DR}-mediated interference with Gli1 activator function in hindbrain, and with Gli1 and other Gli activator functions in the spinal cord (see Figure 28), one would predict that the *yot* (*gli2^{DR}*) mutant motor neuron phenotype would be exacerbated upon reduction of Gli1 activator function. We tested this by injecting *gli1* MO into embryos obtained from *yot^{ty119}*+/− crosses, and examining motor neuron development with islet antibody labeling (Figure 23; Table 8). In wild type (*gli2+/+*) embryos, injection of a sub-optimal amount of *gli1* MO (Karlstrom et al., 2003) did not result in a discernable loss of motor neurons in the hindbrain or spinal cord, and the embryos looked identical to control *gli2+/+* embryos (data not shown). In contrast, *gli1* MO injection into *gli2* heterozygotes (*gli2+/DR*) led to a substantial loss of hindbrain motor neurons (Figure 23B), with the pattern of loss greatly resembling that found in control *yot* (*gli2* DR/DR) mutants (Figure 23C). However, differing from the hindbrain, spinal motor neuron loss was less severe in *gli1* MO-injected *gli2* heterozygotes (Figure 23J) compared to *yot* mutants (Figure 23K; Table 8). Finally, as predicted, *gli1* MO injection into *yot* mutants led to the complete loss of motor neurons in the hindbrain and spinal cord (Figure 23D and L; Table 8), similar to the phenotype of *smu* mutants and cyclopamine-treated embryos (data not shown). These results suggest strongly that the Gli2^{DR} protein affects motor neuron development by interfering with the activator functions of Gli1, Gli2, and possibly other Glis (Figure 28).

198

islet   *net1a krox20*   islet

gli2 +/+; control

gli2 +/DR; gli1 MO

gli2 DR/DR; control

gli2 DR/DR; gli1 MO

199
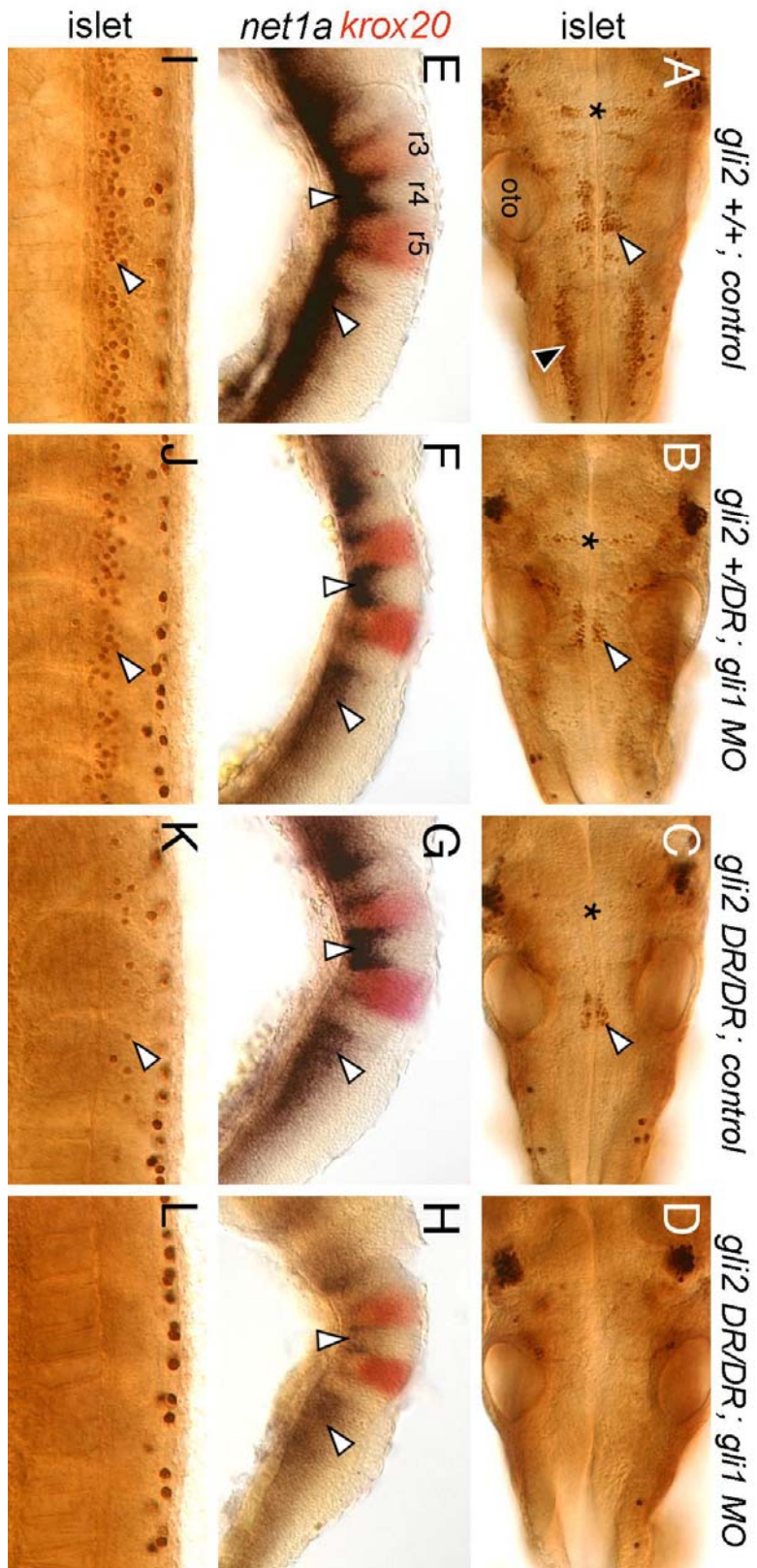
FIGURE 23. *Gli1* contributes to spinal motor neuron induction.

Panels A–D show dorsal views, and panels E–L show lateral views, with anterior to the left. **(A, E, and I):** In an uninjected 36 hpf wild type (*gli2$^{+/+}$* or *gli2$^{+/DR}$*) embryo, islet antibody labeling (A) reveals the characteristic organization of the nV neurons in r2 (asterisk), the nVII neurons (white arrowhead), the nX neurons (black arrowhead), and the patterned expression of *net1a* (E) in the ventral hindbrain and at rhombomere boundaries (arrowheads). Spinal motor neurons (arrowhead, I) are found in characteristic numbers. **(B, F, and J):** In a *gli2$^{+/DR}$* (*yot$^{+/ty119}$*) heterozygote injected with *gli1* MO, nV and nVII neurons are reduced in number (asterisk, arrowhead in B), nX neurons are absent, and *net1a* expression is significantly reduced in the hindbrain (arrowheads, F). Spinal motor neurons are slightly reduced in number (arrowhead, J). **(C, G, and K):** In an uninjected *gli2^{DR}* (*yot^{ty119}*) mutant, nV (asterisk, C), nX, and spinal motor neurons (arrowhead, K) are greatly reduced in number, while the nVII neurons (arrowhead, C) show a moderate reduction. *Net1a* expression is significantly reduced in the hindbrain (arrowheads, G). **(D, H, and L):** In a *gli2^{DR}* (*yot^{ty119}*) mutant injected with *gli1* MO, branchiomotor (D) and spinal motor neurons (L) are completely absent. *Net1a* expression (arrowheads, H) is also severely reduced in the hindbrain. The strongly labeled cells in the dorsal spinal cord (I–L) are Rohon-Beard sensory neurons, which are unaffected by these treatments.

TABLE 8. Gli2^{DR} interferes with Gli1 and Gli3 activator functions$^{@}$

Morpholino	Number of islet-labeled cells in the hindbrain		Number of islet-labeled cells in ventral spinal cord$^{\#}$	
	WT heterozygotes (*gli2*+/DR)*	*yot* mutant (*gli2* DR/DR)*	WT heterozygotes (*gli2*+/DR)*	*yot* mutant (*gli2* DR/DR)*
none§	223 ± 5 (4)	56.5 ± 4.4 (4)	34 ± 2.9 (4)	4.2 ± 1.4 (4)
gli1 MO$^{£}$	93.8 ± 8.2 (4)	2.3 ± 2.1 (4)	25.9 ± 5.8 (4)	0.5 ± 0.1 (4)
	$P ± < ± 0.001$	$P < 0.001$	$P < 0.01$	$P < 0.05$
none§	304.8 ± 23.6 (5)	84.6 ± 22.9 (5)	33.6 ± 2.2 (5)	19.4 ± 0.7 (5)
gli3 MO†	233 ± 33.2 (5)	118.8 ± 32.1 (5)	16.4 ± 2.1 (5)	3.1 ± 1.7 (5)
	$P < 0.01$	$P > 0.05$ (NS)	$P < 0.001$	$P < 0.001$

TABLE 8. Gli2^{DR} interferes with Gli1 and Gli3 activator functions[@]

[@] While the numbers of control and MO-injected embryos were much higher (>(40 for each treatment), we counted motor neuron cell bodies in 4-5 representative embryos for each condition. Embryos were genotyped by PCR.

[#] Number of labeled cells per hemisegment.

[*] Number of embryos scored in parenthesis.

[£] Approximately 5 ng of *gli1* morpholino (see Materials and methods) was injected per embryo. In our hands, this amount did not result in an observable loss of *nk2.2* expression in wild type embryos as described previously (Karlstrom et al., 2003), suggesting that it is a suboptimal dose. Injection of larger doses generated deformed embryos, and was not pursued further.

[§] The numbers of hindbrain and spinal motor neurons in control wild type and mutant embryos in the two experiments (performed about one year apart) are substantially different. We attribute these differences to variations in age of embryos, islet antibody staining intensity, and genetic background. Importantly however, the responses to *gli1* and *gli3* MO injections are very similar between the two experiments.

[†] Approximately 30 ng of *gli3* MO was injected per embryo. See Table 7 for details.

Our earlier observations that significant levels of *net1a* and *ptc1* expression are retained in *yot* and *dtr* mutants (Figure 19 and Figure 21; Figure 23G) and in *gli2* MO-injected *dtr* mutants (Figure 22J) suggested that Gli activator-independent mechanisms may be involved in regulating their expression. However, step-wise reduction of Gli activator function by *gli1* MO injection into *gli2* heterozygotes (*gli2*+/DR; 15/25 embryos) and *yot* mutants (*gli2* DR/DR; 9/13 embryos) led to additive losses in *net1a* expression (Figure 23F and H), suggesting strongly that Gli activator function is necessary for regulating all aspects of *net1a* (Figure 23) and *ptc1* (see Figure 27) expression.

4.3.7   Gli3 plays a role in branchiomotor and spinal motor neuron induction

Given the redundant functions of *gli1* and *gli2* in spinal motor neuron induction, we tested whether zebrafish *gli3* (Tyurina et al., 2005) also contributed to motor neuron induction. Since the roles of *gli1* and *gli2* in spinal motor neuron induction were revealed only in Gli-deficient backgrounds (Figure 22 and Figure 23), we examined the effects of knocking down *gli3* function using *dtr* (*gli1⁻*) and *yot* (*gli2^{DR}*) mutants. We first verified that *gli3* MO injection indeed knocked down *gli3* function by showing that ~36% of wild type embryos injected with 30 ng *gli3* MO exhibited ectopic expression of the floor plate marker *fkd4* in the dorsal hindbrain, as described previously (data not shown; 24/66 embryos) (Tyurina et al., 2005). Interestingly, injection of *gli3* MO into wild type siblings of *dtr* or *yot*

mutants led to significant reductions in both branchiomotor (Figure 24B and J;

compare to Figure 24A and I) and spinal motor neurons (Figure 24F and N;

compare to Figure 24E and M) (Table 7 and Table 8), suggesting that *gli3* plays

a more prominent role than *gli2* in motor neuron induction. In *dtr* (*gli1⁻*) mutants

injected with *gli3* MO, while the severe loss of branchiomotor neurons seen in

control embryos was maintained (Figure 24C and D; Table 7), spinal motor

neurons were greatly reduced compared to control mutant embryos (Figure 24G

and H; Table 7). This result suggests an activator role for Gli3 in spinal motor

neuron induction. In *yot* (*gli2^{DR}*) mutants injected with *gli3* MO, there was a small

decrease in branchiomotor neuron number compared to control embryos (Figure

24K and L; Table 8), but a dramatic reduction in spinal motor neuron number

over control mutant embryos (Figure 24O and P; Table 8). This result again

suggests an activator function for Gli3 in spinal motor neuron induction, and that

this function may be subject to interference from Gli2^{DR} protein. In addition, Gli3

may regulate motor neuron induction indirectly by activating *gli1* expression (see

Figure 27 and Figure 28, and Discussion section 4.4). These results also

suggest that Gli3 does not function as a repressor of motor neuron fate in the

dorsal neural tube. But we cannot rule out other roles for *gli3* in hindbrain

development because the fourth ventricle (above the hindbrain) was variably

reduced in *gli3* MO-injected embryos, and the hindbrain had a mottled

appearance suggestive of increased cell death (data not shown). Expression of

ptc1 and *krox20* (Figure 27K) however was unaffected in these embryos.
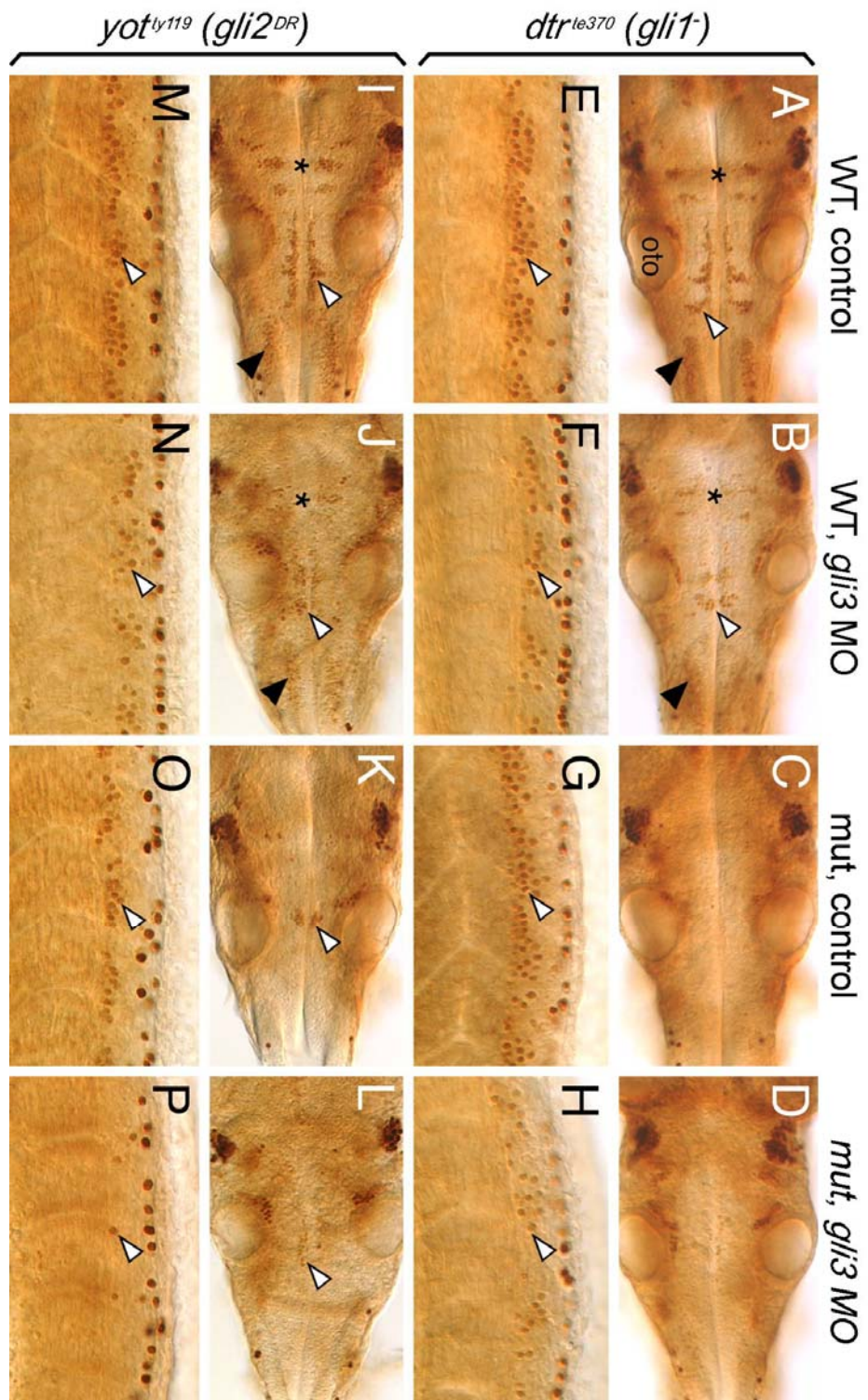
FIGURE 24. *Gli3* **plays a role in branchiomotor and spinal motor neuron induction.**

Panels A–D and I–L show dorsal views of the hindbrain, and panels E–H and M–P show lateral views of the spinal cord, with anterior to the left. **(A and E):** In an uninjected 36 hpf wild type (*dtr+/+ or +/−*) embryo, islet antibody labeling reveals the characteristic organization of the nV neurons in r2 (asterisk), the nVII neurons (white arrowhead), and the nX neurons (black arrowhead) in the hindbrain (A), and the characteristic distribution of motor neurons (arrowhead, E) in the ventral spinal cord. **(B and F):** In a wild type sibling injected with *gli3* MO, the nV (asterisk), nVII (white arrowhead), and nX (black arrowhead) neurons in the hindbrain (B), and spinal motor neurons (arrowhead, F) are reduced in number. **(C, D, G, and H):** In an uninjected *dtr* mutant (C), branchiomotor neurons are essentially absent, and this phenotype is maintained in a *gli3* MO-injected *dtr* mutant (D). In contrast, spinal motor neurons are moderately reduced in number in a *gli3* MO-injected *dtr* mutant (arrowhead, H) compared to an uninjected *dtr* mutant (arrowhead, G). **(I, J, M, and N):** In an uninjected wild type (*yot+/+ or +/−*) embryo, branchiomotor neurons are found in characteristic numbers (I; see A for details), and their numbers are moderately reduced in a *gli3* MO-injected wild type sibling (J). Similarly, spinal motor neurons are reduced in number in a *gli3* MO-injected wild type embryo (arrowhead, N) compared to an uninjected wild type sibling (arrowhead, M). **(K, L, O, P):** In an uninjected *yot* mutant (K), most branchiomotor neurons, except nVII neurons (arrowhead), are greatly reduced in number or absent, and the number of nVII neurons is slightly decreased in a *gli3* MO-injected *yot* mutant (L). In contrast, spinal motor neurons are greatly reduced in number in a *gli3* MO-injected *yot* mutant (arrowhead, P) compared to an uninjected *yot* mutant (arrowhead, O). oto, otocyst.

4.3.8 Endogenous Gli2 repressor function does not regulate branchiomotor neuron induction

While wild type *gli2* appears to play no role in branchiomotor neuron induction (Figure 22; Table 7), the Gli2 dominant repressors encoded by the *yot* alleles interfere with branchiomotor neuron induction (Figure 18 and Figure 23; Table 5 and Table 8). Therefore, we wondered whether endogenous Gli2 repressor activity normally plays any role in branchiomotor neuron development, analogous to the role of Gli3 repressor function in ventral neural tube patterning in mouse (Litingtung and Chiang, 2000; Wijgerde et al., 2002). In a 21 hpf wild type hindbrain, the *islet1* expression domain (presumptive motor neurons) in rhombomere 4 (r4) and the *nk2.2* expression domain (containing presumptive motor neurons) in r5 are located in the ventral-most neural tube, outside the *gli2* expression domain (Figure 25A and E). This dorsal pattern of *gli2* expression is evident from 16.5 hpf until 36 hpf (data not shown) (Karlstrom et al., 1999), the time period when most of the branchiomotor neurons differentiate (Chandrasekhar et al., 1997; Higashijima et al., 2000). This absence of expression in differentiating motor neurons suggests that *gli2* does not directly influence motor neuron induction at these time points. However, since motor neurons are clearly affected in *smu*, *dtr*, and *yot* mutants, this suggests either that (1) *gli2* (and therefore Gli2 or Gli2^{DR} proteins) is aberrantly expressed in the ventral hindbrain (in motor neuron progenitors) in these mutants, (2) *gli2* indirectly affects motor neuron induction, or (3) Gli-mediated motor neuron

r4   A   WT   B   *yot*^{ty119} (*gli2*^{DR})   C   *dtr*^{te370} (*gli1*−)   D   *smu*^{b641} (*smo*−)

r5   E   F

forebrain   G   H   I   J

islet1 gli2   *nk2.2 gli2*   *islet1 gli2*

208
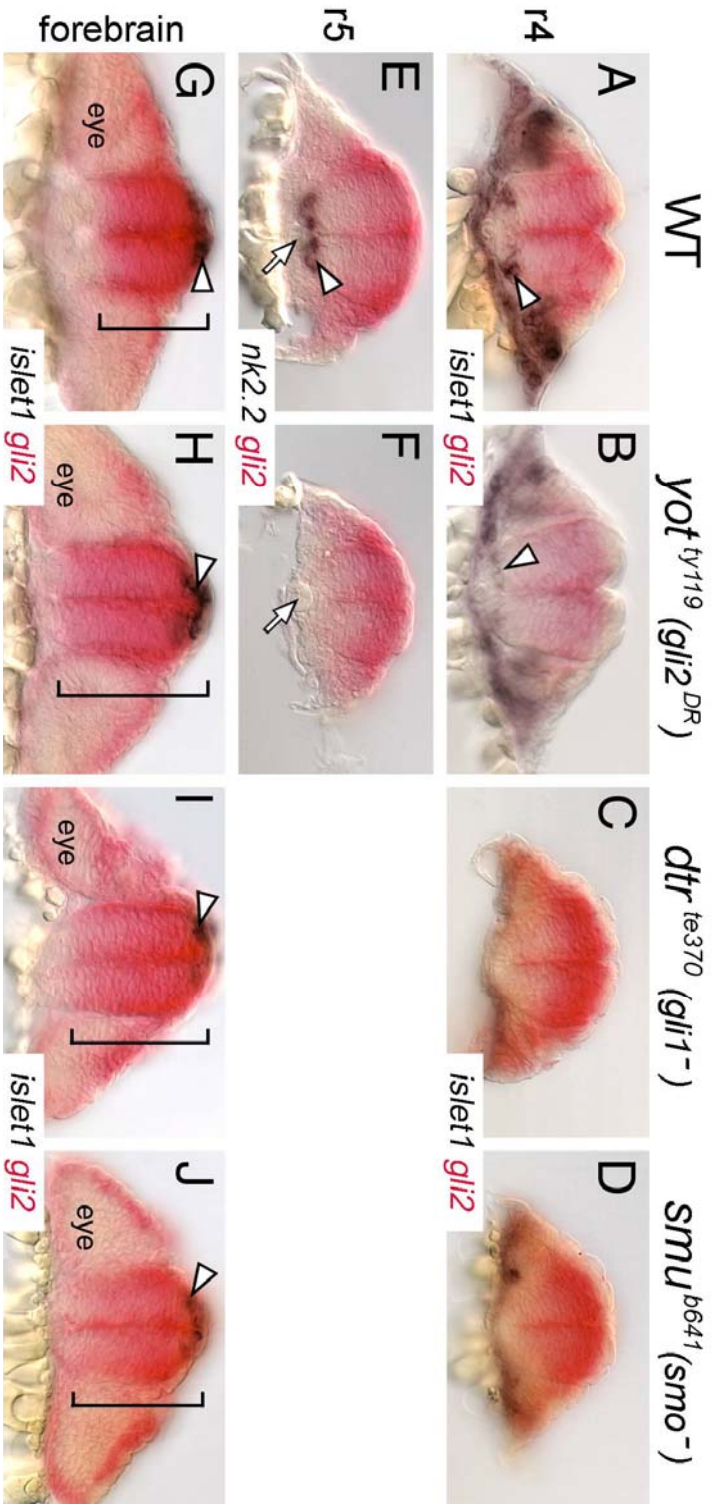
FIGURE 25. *Gli2* **expression is affected in the forebrain, but not in the**

hindbrain, of Hh pathway mutants.

All panels show cross sections of the neural tube at the indicated axial levels, with dorsal at the

top. Embryos were processed for *islet1* (purple); *gli2* (red) (A–D, G–J) or *nk2.2* (purple); *gli2* (red)

(E, F) two-color in situs. **(A–D):** In r4 of a wild type embryo (A), *islet1*-expressing motor neurons

(arrowhead) are located just ventral to the *gli2* expression domain. Similarly, the few *islet1*-

expressing neurons in *yot* mutants (arrowhead) are located ventral to the *gli2* expression domain

(B), and *gli2* expression does not extend into the ventral-most neural tube in *dtr* (C) and *smu* (D)

mutants. **(E and F):** In r5, while *nk2.2*-expressing cells (arrowhead) are found immediately

adjacent to the floor plate and notochord (arrow) in a wild type embryo (E), *nk2.2* expression is

absent in *yot* mutants (F), but the *gli2* expression domain does not expand ventrally. **(G–J):** At

the forebrain level, the *islet1*-expressing epiphysial neurons (arrowhead) are located at the roof of

the neural tube. In a 21-hpf wild type embryo (G), *gli2* expression is limited to the dorsal two-

thirds of the neural tube (bracket). In contrast, in *yot*^{ty119} (H), *dtr*^{te370} (I), and *smu*^{b641} (J) mutants,

the *gli2* expression domain is expanded ventrally to different extents (brackets).

TABLE 9. Ventral expansion of *gli2* expression domain in the forebrain of Hh pathway mutants.

Gene	Ventral margin of *gli2* expression domain[#]		P
	Wild-type[*] (+/+ and +/-)	Mutant[*]	
smu[b641]	63 ± 8% (5s, 5e)	92 ± 8% (2s, 2e)	< 0.02
dtr[te370]	63 ± 9% (4s, 4e)	74 ± 1% (7s, 5e)	< 0.005
yot[ty119]	68 ± 5% (6s, 5e)	83 ± 5% (5s, 5e)	< 0.001

TABLE 9. Ventral expansion of *gli2* expression domain in the forebrain of Hh pathway mutants.

[#] Forebrain sections were scored at the level of the epiphysis, which was identified by the presence of *islet1*-expressing cells (Figs. 25G-J). The dorsoventral height of the neural tube was measured, and the length of the *gli2* expression domain (measured from the dorsal surface) was expressed as a fraction (%) of the height of the neural tube.

[*] The first number in the parenthesis indicates the total number of sections scored, while the second number indicates the number of embryos these sections came from. Wild type (WT) embryos represent homozygous (+/+) and heterozygous (+/-) genetic conditions.

differentiation occurs prior to 16.5 hpf at a time when *gli2* is expressed in motor

neuron progenitors.

To distinguish between these possibilities, we first tested whether

branchiomotor neuron loss in *smu*, *dtr*, and *yot* mutants might result from the

ventral expansion of *gli2* expression into regions containing motor neuron

progenitors. We examined the expression domains of *gli2* at various levels along

the AP axis in 21 hpf mutant embryos processed for *gli2*;*islet1* double in situ

hybridization. There was no significant or reproducible ventral expansion of *gli2*

expression in the neural tube at hindbrain levels in any rhombomere in any of the

three mutant backgrounds (4–6 embryos examined per mutant, 5–6 sections in

the hindbrain per embryo). In the various mutants containing few (Figure 25B) or

no *islet1*-expressing cells (Figure 25C and D), or no *nk2.2*-expressing cells

(Figure 25F), *gli2* expression was clearly excluded from the ventral neural tube

containing the motor neuron progenitor domain. There was no ventral expansion

of *gli2* expression in the hindbrains of *smu* (21 and 26 hpf), *dtr* (18 and 21 hpf),

and *yot* mutants (16.5, 18, 21, and 26 hpf) (data not shown). Together, these

data suggest strongly that the loss of branchiomotor neurons in these Hh

pathway mutants is not due to the suppression of motor neuron fate by Gli2

repressor function but may simply be due to loss of Gli1 activator function (Figure

21M–O; see Figure 28 for model). Interestingly, *gli2* expression expands

ventrally in the forebrain of Hh pathway mutants. In cross sections of the

forebrain at the level of the epiphysis, *gli2* was expressed in the dorsal ~65% of

the neural tube in wild type embryos (Figure 25G; Table 9). In all mutants

examined, the *gli2* expression domain at the forebrain level was expanded

ventrally (and reproducibly) to 75–90% of the extent of the neural tube (Figure

25H–J; Table 9), demonstrating a significant effect on dorsoventral patterning

when Hh signaling is reduced or absent. Therefore, the reduction or loss of Hh

target gene expression in the forebrain in Hh pathway mutants may result from

Gli2-mediated repression.

To test the possibility that Gli2 repressor function in the dorsal neural tube

has an indirect effect on Hh-mediated events in the ventral neural tube, we asked

whether knockdown of *gli2* function could rescue any aspect of Hh signaling,

including branchiomotor neuron induction, in *smu* mutants, in a manner similar to

the rescue of motor neurons in *Shh*;*gli3* and *Smo*;*gli3* mutant mice (Litingtung

and Chiang, 2000; Wijgerde et al., 2002). When *gli2* MO was injected into

embryos from a *smu+/−*;*islet1-GFP* incross, branchiomotor neurons did not

reappear in *smu* mutants, and there was no rescue of *nk2.2* or *net1a* expression

in the mutant hindbrain (data not shown), consistent with the idea that Gli2

repressor function in the dorsal hindbrain does not influence Hh-mediated events

in the ventral hindbrain.

Finally, we tested the possibility that the loss of motor neurons in *yot*

mutants could result from the ventral expression of *gli2* (and Gli2^{DR}) in motor

neuron progenitors before 16.5 hpf. *Gli2* was expressed extensively in the neural

plate and the developing neural tube at 9 and 12 hpf (data not shown), and

continued to be expressed in the ventral neural tube at 15 hpf throughout the

hindbrain (Figure 26A–C). These results indicate that aberrant Gli2^{DR} activity in

motor neuron progenitors prior to 15 hpf can account for reduced motor neuron induction in *yot* mutants and suggest that branchiomotor neurons are specified before 15 hpf, which is several hours earlier than suggested by observations of motor neuron differentiation (Chandrasekhar et al., 1997; Higashijima et al., 2000).

4.3.9 Hh signaling is primarily required before 18 hpf to induce branchiomotor neurons

Given that Gli2^{DR} proteins block motor neuron induction in *yot* mutants by interfering with Gli1 and Gli3 function, and that *gli1* and *gli2* are co-expressed in motor neuron progenitors only before 16.5 hpf, we re-examined the idea that the branchiomotor neurons are specified continuously between 15 and 40 hpf (Chandrasekhar, 2004). To directly determine the critical period for motor neuron induction, we asked when different subsets of branchiomotor neurons were specified using the alkaloid cyclopamine (CyA) to block Hh signaling. Wild-type *islet1-GFP* transgenic embryos were treated with CyA beginning at 3, 6, 9, 12, 15, 18, 21, and 24 hpf. Control (EtOH-treated) and CyA-treated embryos were scored for motor neuron phenotypes at 48 hpf by examining *GFP* expression (Figure 26D and E), fixed and processed for islet immunohistochemistry (Figure 26F–I), and motor neurons in various rhombomeres (corresponding to specific types of branchiomotor neurons) were counted. CyA treatment at 9 hpf or earlier led to the complete loss of all branchiomotor neurons (Figure 26D–G). However,
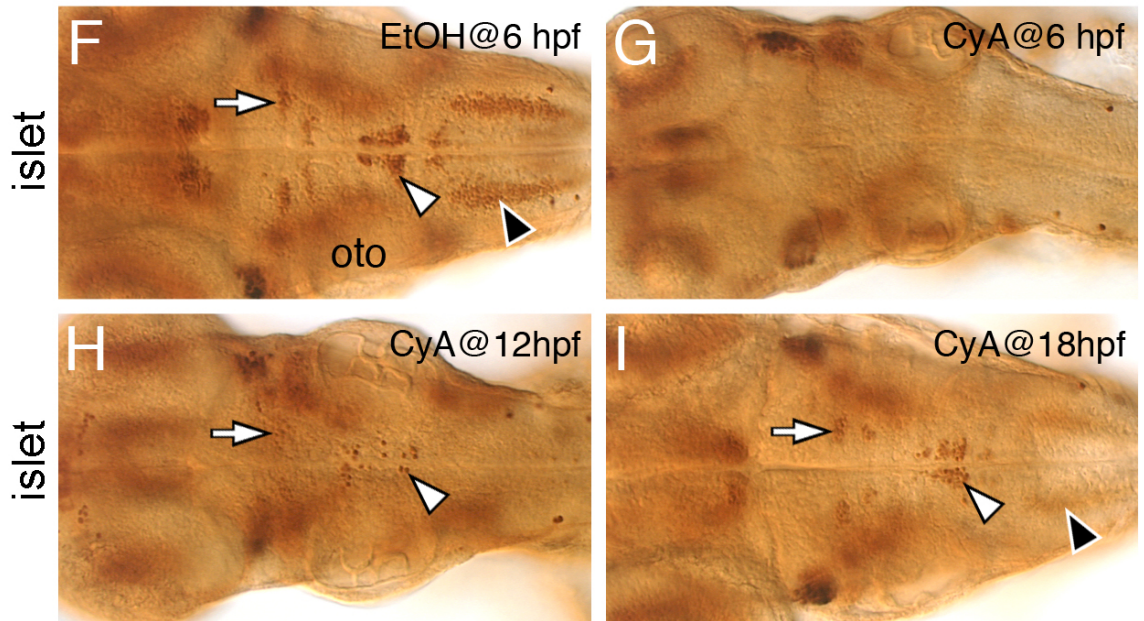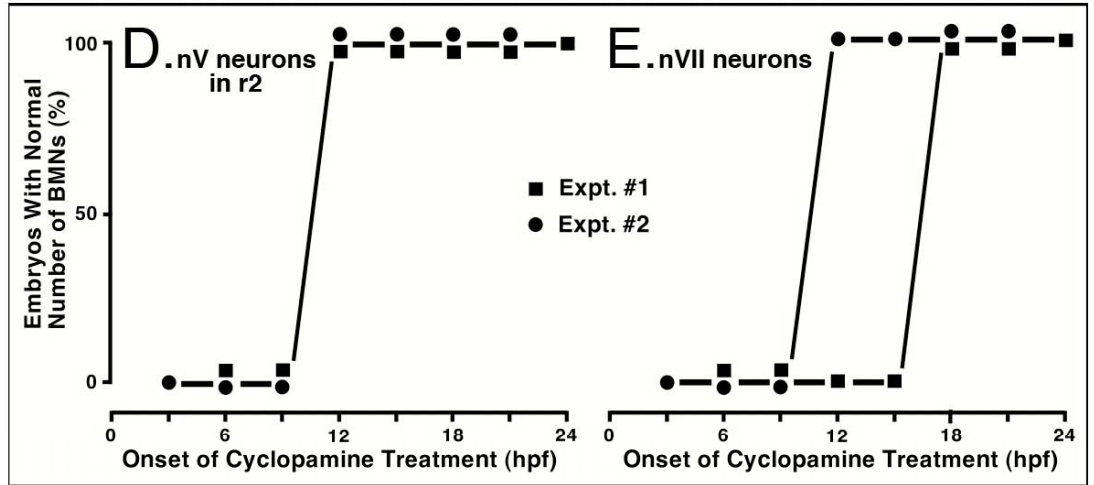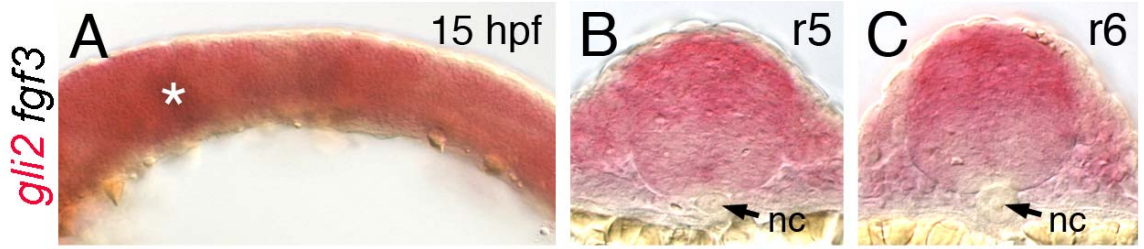
FIGURE 26. Hh signaling is required before 18 hpf for the induction of branchiomotor neurons.

Panel A shows a lateral view, and panels F–I show dorsal views of the hindbrain, with anterior to the left. **(A):** In a 15 hpf wild type embryo, *gli2* is expressed at all axial levels throughout the dorsoventral extent of the hindbrain. The asterisk marks low level of *fgf3* expression at the mid-hindbrain boundary, which was used to orient embryos for sectioning (see Materials and methods 4.2 for details). **(B and C):** Cross-sections (dorsal is up) showing that *gli2* is expressed in the ventral aspects of the neural tube in rhombomeres 5 and 6, but at lower levels than in the dorsal neural tube. nc, notochord. **(D and E):** Quantification of embryos with normal numbers of *GFP*-expressing nV motor neurons in r2 (D) and nVII neurons in r4–r7 (E) following cyclopamine (CyA) treatment beginning at the times indicated (hpf). There is no effect on nV neuron number in r2 when CyA treatment is initiated at 12 hpf or later (2 experiments; 20 embryos per experiment). There is no effect on nVII neuron number when CyA treatment is initiated at 18 hpf or later (2 experiments). **(F):** In a 48-hpf wild type embryo treated with ethanol (EtOH) from 6 hpf, islet antibody labeling reveals that the number and organization of branchiomotor neurons, including nV (arrow), nVII (white arrowhead) and nX (black arrowhead), are unaffected. **(G):** In an embryo treated with CyA from 6 hpf, islet-labeled branchiomotor neurons are absent. **(H):** In an embryo treated with CyA from 12 hpf, nV neurons in r2 are mostly present (arrow; light staining), nVII neurons are greatly reduced in number (arrowhead), and nX neurons are absent. **(I):** In an embryo treated with CyA from 18 hpf, the nV (arrow), nVII (white arrowhead), and nX neurons (black arrowhead; out of focus) are mostly unaffected. oto, otocyst.

a few nV neurons (in r2 and r3), and nVII neurons (in r4–r7) were generated

between 9 and 12 hpf (Figure 26H). Indeed, normal numbers of nV neurons

were generated in r2 even when Hh signaling was blocked from 18 hpf (Figure

26D and I). Similarly, a majority of nVII neurons were generated in 18 hpf-

treated embryos (Figure 26E and I), and essentially normal numbers of nV

neurons (r2 and r3) and nVII neurons (r4–r7) are generated in 24 hpf-treated

embryos (data not shown). These results demonstrate that Hh signaling is

required before 24 hpf for generating all branchiomotor neurons, and that a

majority of branchiomotor neurons are specified before 18 hpf, consistent with an

early inhibitory role for mutant Gli2^{DR} proteins within motor neuron progenitors in

yot mutants.

4.3.10 Gli3, but not Gli1 or Gli2, activator function is required for inducing gli1 expression

We showed earlier that while *gli1* expression is completely normal in

detour (*gli1^{-}*) null mutant alleles, it is severely reduced in *smu* (*smo^{-}*) mutants,

demonstrating that *gli1* expression is regulated by Hh signaling but does not

require Gli1 activator function (Figure 21). Similarly, while Northern blot analysis

reveals that *Gli1* expression is unaffected in *Gli1* knockout mouse embryos (Park

et al., 2000), it is completely lost in *Gli2*;*Gli3* double knockout embryos (Bai et al.,

2004). To test the potential role of Gli activator function in regulating *gli1*

expression in zebrafish, we examined *ptc1* and *gli1* expression in conditions

where overall Gli activator function was greatly attenuated (Figure 27). In the

first set of experiments, embryos from dtr^{te370}+/− crosses were injected with gli2

MO that leads to a reduction of motor neurons in the spinal cord (see Figure 22).

In uninjected (21/21 embryos) and gli2 MO-injected (36/36 embryos) wild type

siblings, ptc1 expression in the ventral hindbrain was unaffected (Figure 27A),

indicating that the reduction in Gli activator function was not sufficient to reduce

ptc1 expression. In contrast, ptc1 expression was reduced in uninjected dtr

mutants (Figure 27B; 5/5 embryos; see also Figure 21I), and severely reduced in

gli2 MO-injected dtr mutants (Figure 27C; 14/14 embryos), indicating that the Gli

activator functions encoded by gli1 and gli2 are necessary for inducing ptc1

expression. As expected, there was no effect on gli1 expression in gli2 MO-

injected wild type embryos (Figure 27D). Surprisingly, gli1 expression was

completely normal in gli2 MO-injected dtr mutants (Figure 27E), indicating that a

severe reduction in Gli1 and Gli2 activator function could not alter gli1

expression. In a second set of experiments, embryos from yot^{ty119}+/− ($gli2^{+/DR}$)

crosses were injected with gli1 MO that leads to a severe loss of motor neurons

in the hindbrain and spinal cord (see Figure 23). While ptc1 expression was

normal in control (17/17 embryos) and gli1 MO-injected wild type (Figure 27F;

20/20 embryos), the lower level of ptc1 expression seen in uninjected yot

mutants (Figure 27G; 5/5 embryos) was almost eliminated in gli1 MO-injected yot

($gli2^{DR}$) mutants (Figure 27H; 3/3 embryos). Most importantly, gli1 expression

was not affected in gli1 MO-injected yot ($gli2^{DR}$) mutants (compare Figure 27I and

J). These results again indicate that conditions that lead to severe attenuation of
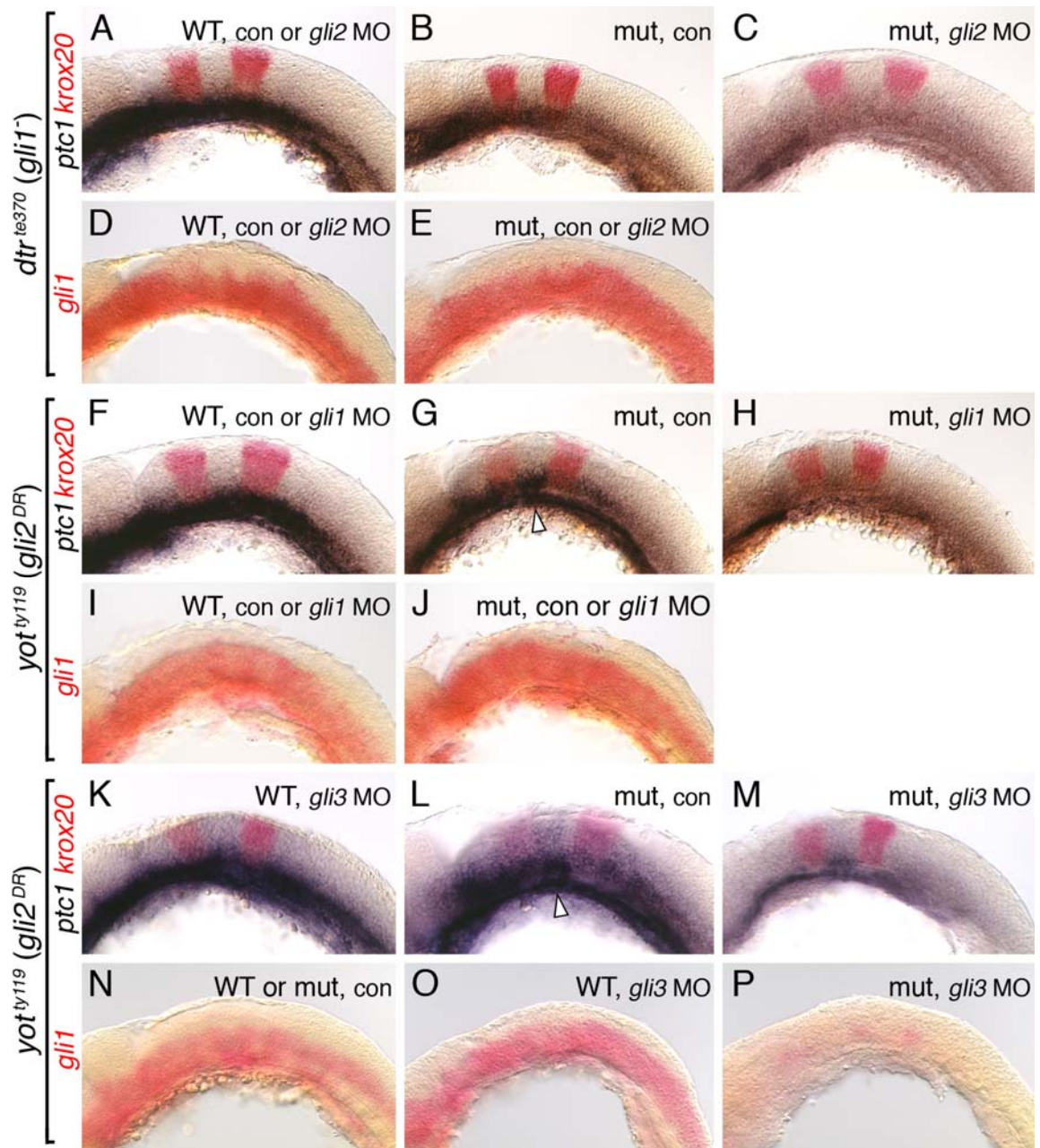
FIGURE 27. Regulation of *gli1* expression requires Gli3, but not Gli1 or Gli2, function.

All panels show lateral views of the hindbrain with anterior to the left. Embryos in A–E were obtained from crosses between dtr^{te370}+/− ($gli1^{+/-}$) heterozygotes, while those in F–P were obtained from crosses between yot^{ty119}+/− ($gli1^{+/DR}$) heterozygotes. *Krox20* expression (red) in *ptc1;krox20* double in situ panels identifies rhombomeres 3 and 5. **(A):** In 21 hpf uninjected or *gli2* MO-injected wild type embryos, *ptc1* is expressed at all axial levels in the ventral hindbrain. **(B):** In an uninjected *dtr* (*gli1*) mutant, *ptc1* expression is significantly reduced. **(C):** In a *gli2* MO-injected *dtr* (*gli1*) mutant, *ptc1* expression is completely lost in the hindbrain. **(D):** In a 21-hpf uninjected or *gli2* MO-injected wild type embryo, *gli1* is expressed at all axial levels in the ventral half/two-thirds of the hindbrain. **(E):** *Gli1* expression is unaffected in control or *gli2* MO-injected *dtr* (*gli1*) mutants. **(F–H):** *Ptc1* expression is normal in uninjected or *gli1* MO-injected wild type embryos (F), is reduced significantly in an uninjected *yot* ($gli2^{DR}$) mutant (G), and is completely lost from the hindbrain in a *gli1* MO-injected *yot* ($gli2^{DR}$) mutant (H). In *yot* ($gli2^{DR}$) mutants, *ptc1* expression is not as reduced in r4 as in other compartments (G, arrowhead). **(I and J):** *Gli1* is expressed normally in the ventral hindbrain in uninjected or *gli1* MO-injected wild type (I) or *yot* ($gli2^{DR}$) mutants (J). **(K–M):** *Ptc1* expression is slightly reduced in a *gli3* MO-injected 22 hpf wild type embryo (K), is reduced significantly in an uninjected 24 hpf *yot* ($gli2^{DR}$) mutant (L), and is almost completely lost in a *gli3* MO-injected 22 hpf *yot* ($gli2^{DR}$) mutant (M). In *yot* ($gli2^{DR}$) mutants, *ptc1* expression is not as reduced in r4 as in other compartments (L, arrowhead). **(N–P):** *Gli1* is expressed normally in the ventral hindbrain in uninjected wild type or *yot* ($gli2^{DR}$) mutant embryos (N), and in a *gli3* MO-injected wild type embryo (O). In a *gli3* MO-injected *yot* ($gli2^{DR}$) mutant, *gli1* (*gli1*) expression is greatly reduced (P).

overall Gli activator function, such that the expression of Hh target genes *net1a* (Figure 22J, 23H) and *ptc1* (Figure 27C, 27H, 27M) is severely reduced, are still unable to alter *gli1* expression.

Since we have defined an activator function for Gli3 in motor neuron induction (Figure 24), we next tested whether Gli3 may regulate *gli1* expression by injecting *gli3* MO into embryos from dtr^{te370}+/− ($gli1^{te370}$) crosses and yot^{ty119}+/− ($gli2^{+/DR}$) crosses. *Gli1* was expressed normally in all wild type and *dtr* ($gli1^{te370}$) mutant embryos injected with *gli3* MO, and the expression patterns were indistinguishable from those in control embryos (69/69 control and 49/49 *gli3* MO-treated embryos; data not shown; see Figure 27D and E for *gli1* expression patterns). These data indicate that a dose of *gli3* MO that knocks down *gli3* expression (function) substantially enough to reduce motor neuron induction (Figure 24B) is not able to affect *gli1* expression. Similarly, *gli1* expression appeared normal in *gli3* MO-injected wild type siblings obtained from yot^{ty119}+/− ($gli2^{+/DR}$) crosses (Figure 27; 124/124 embryos). Significantly, *gli1* expression was greatly reduced throughout the ventral neural tube in *yot* ($gli2^{DR}$) mutants injected with *gli3* MO (Figure 27P; 37/37 embryos). Since loss of Gli1 and Gli2 activator function alone and in combination had no effect on *gli1* expression, these data suggest that the combined effect on Gli3 function produced by Gli2^{DR}-mediated interference and *gli3* MO knockdown is responsible for the observed reduction in *gli1* expression. While *ptc1* expression was slightly reduced in some *gli3* MO-injected wild type siblings (Figure 27K; 13/36 embryos) compared to control wild type siblings (data not shown; 28/28 embryos; see

221

Figure 27F), its expression was almost eliminated in *gli3* MO-injected *yot* (*gli2^{DR}*)

mutants (Figure 27M; 13/15 embryos) compared to control mutant embryos

(Figure 27L; 9/9 embryos). Collectively, these results suggest strongly that Gli

activator functions encoded by *gli1*, *gli2*, and *gli3* are all equally capable of

inducing *ptc1* expression, whereas Gli3 activator function is specifically required

for inducing *gli1* expression (Figure 28).

4.4   DISCUSSION

4.4.1   Role of Glis in motor neuron development

In mouse and zebrafish, loss of Smoothened-mediated Hh signaling

results in the failure of motor neuron induction (this study) (Chen et al., 2001;

Varga et al., 2001; Wijgerde et al., 2002). Nevertheless, a small number of motor

neurons differentiate but are patterned abnormally in mice lacking all Gli activator

function (Bai et al., 2004; Lei et al., 2004). Moreover, while mouse *Gli1* function

is not required for motor neuron induction (Park et al., 2000), zebrafish *gli1* is

essential for motor neuron induction in the hindbrain (Chandrasekhar et al.,

1999). Given these differing roles for *gli1* in Hh-mediated motor neuron induction

in zebrafish and mouse, we tested in this study whether other zebrafish *glis* such

as *gli2* and *gli3* played any role in this process, and particularly whether Gli

activator function is essential for motor neuron induction in zebrafish. We have

addressed these questions by examining the motor neuron phenotypes of *you-

too* (*gli2^{DR}*) mutants, which carry mutations in *gli2* (Karlstrom et al., 1999;

Karlstrom et al., 2003), and of embryos treated with antisense morpholinos to knockdown specific *gli* function. Our results demonstrate that, unlike mouse, Gli activator function is absolutely required for motor neuron induction at all axial levels in zebrafish.

4.4.2   The *you-too* (*yot*, *gli2^{DR}*) motor neuron phenotype

The *yot* (*gli2^{DR}*) mutants were originally identified on the basis of defects in somite patterning, midline defects in the spinal cord, and defective retinotectal projections (Brand et al., 1996b; Karlstrom et al., 1996; van Eeden et al., 1996). The *yot* (*gli2^{DR}*) locus encodes Gli2, which contains both C-terminal activator and N-terminal repressor domains (Karlstrom et al., 1999). The *yot^{ty119}* (*gli2^{DR}*) and *yot^{ty17}* (*gli2*) alleles encode C-terminally truncated proteins that appear to function as dominant repressors (DR) of Hh signaling (Karlstrom et al., 1999; Karlstrom et al., 2003). In contrast, Gli1, encoded by the *detour* (*dtr*) locus, appears to lack the N-terminal repressor domain, and functions only as a transcriptional activator (Karlstrom et al., 2003). Consistent with this, extant *gli1* mutant alleles encode C-terminally truncated proteins missing the activator domains and exhibit no biological activity in reporter assays (Karlstrom et al., 2003).

In both *yot* (*gli2^{DR}*) alleles, there is a reduction in motor neuron number in the hindbrain and spinal cord, with the *yot^{ty119}* (*gli2^{DR}*) allele exhibiting a more severe phenotype (Figure 18; Table 5), consistent with the stronger dominant suppressor function of this allele in the transcriptional reporter assay (Karlstrom

et al., 2003). The yot^{ty119} ($gli2^{DR}$) mutants also exhibit more severe defects than

yot^{ty17} ($gli2$) mutants in the expression of Hh-regulated genes (Figure 19; data not

shown). Nevertheless, motor neuron number and Hh-regulated gene expression

are not noticeably reduced in embryos heterozygous for either allele, except for a

slight but consistent defect in $nk2.2$ expression in the yot^{ty119}+/− ($gli2^{+/DR}$)

hindbrain (data not shown). These results suggest that the mutant $Gli2^{DR}$

proteins cannot significantly affect Gli1 and Gli2 activator function when multiple

copies of the wild type genes ($gli1$ and $gli2$) are present. Consistent with this

idea, hyperactivation of Hh signaling by misexpression of dominant-negative

protein kinase A (dnPKA) leads to a substantial recovery of motor neuron

number and Hh target gene expression in the hindbrain of yot^{ty17} ($gli2$), and to a

lesser extent yot^{ty119} ($gli2^{DR}$), mutants (Figure 20; Table 6), presumably by

upregulating the level of Gli1 activator.

Strikingly, expression of many Hh target genes is greatly reduced

throughout the yot^{ty119} ($gli2^{DR}$) mutant hindbrain, except in rhombomere 4 (Figure

19). Residual gene expression in r4 is still Hh-dependent since cyclopamine-

mediated disruption of the Hh signaling pathway completely blocks $nk2.2$

expression in yot^{ty119} ($gli2^{DR}$) mutant embryos (Figure 19O). The cyclopamine

inhibitor experiments also reveal that r4-specific expression of Hh target genes

(the $gli2^{DR}$ phenotype) can be phenocopied by administration of cyclopamine to

wild type embryos beginning as early as 18 hpf (Figure 26E; data not shown),

suggesting that the yot^{ty119} ($gli2^{DR}$) mutant phenotype may reflect the failure of Hh

signaling at different times in different rhombomeres. Furthermore, ectopic Hh

pathway activation through *dnPKA* overexpression in *yot*^{ty119} (*gli2*^{DR}) mutants leads to a consistent upregulation of *nk2.2* expression within the normal ventral domain, but not at ectopic locations in r4 (Figure 20). These observations collectively suggest that the Hh signaling environment in r4 is different from that in adjacent rhombomeres, which is not surprising given that r4 develops earlier than adjacent rhombomeres, and functions as an organizer to signal to and regulate the patterning of these compartments (Maves et al., 2002).

4.4.3 Gli1, Gli2, and Gli3 activators contribute to the induction of spinal motor neurons

The normal induction of spinal motor neurons in *dtr* (*gli1*⁻) mutants (Chandrasekhar et al., 1999) suggests that Gli activator function provided by Gli1, Gli2, and Gli3 can function in a redundant fashion in the spinal cord. We tested this idea by knocking down *gli1* or *gli3* function in *yot* (*gli2*^{DR}) mutants, which led to the complete loss of motor neurons in the spinal cord (Figure 23 and Figure 24), indicating that Gli1 and Gli3 activators can contribute to spinal motor neuron induction (Figure 28).

Since knockdown of *gli2* function in wild type embryos did not reveal any defects in motor neuron development, we sought potential roles for *gli2* in sensitized conditions where the total level of Gli activator was reduced. Therefore, we examined the consequences of *gli2* knockdown in *dtr* (*gli1*⁻) mutants. While normal numbers of spinal motor neurons develop in *dtr* (*gli1*⁻)
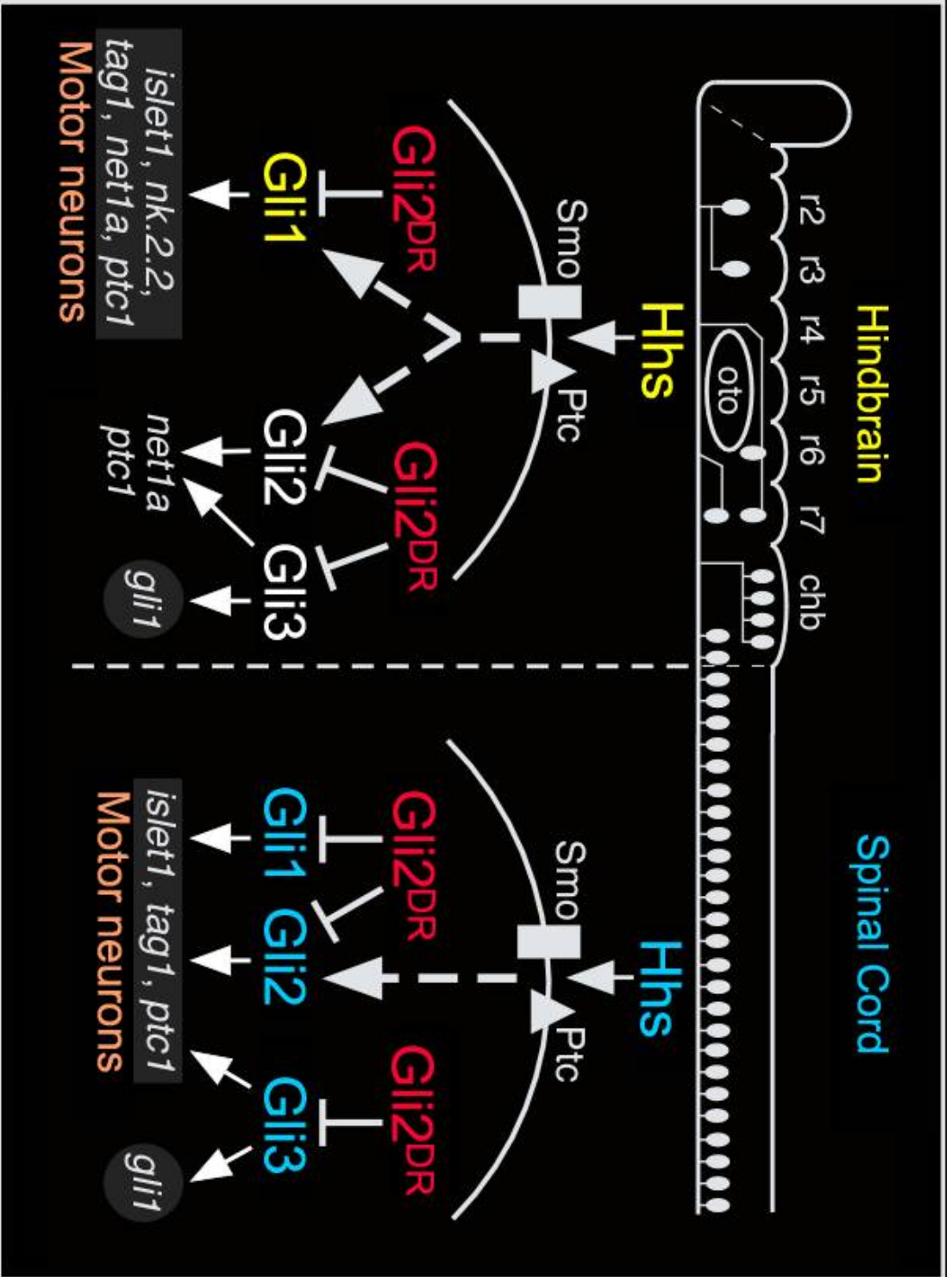
FIGURE 28. Model to explain motor neuron phenotypes of *dtr* (*gli1⁻*) and *yot* (*gli2^DR^*) mutants, and of *gli1*, *gli2*, and *gli3* morpholino injection experiments.

The hindbrain and spinal cord are shown schematically in lateral view (anterior is to left), with the branchiomotor and spinal motor neurons depicted as black ovals. Rhombomeres 2–7 (r2–r7) and the caudal hindbrain (chb) are indicated. The pathways depict signaling within ventral neural tube cells upon transduction of Hh signal through the Smoothened (Smo, black rectangle)-Patched (Ptc, black triangle) receptor system. In the hindbrain, Hh-mediated induction of motor neurons (and motor neuron markers like *nk2.2*, *islet1*, and *tag1*) is completely dependent on *gli1* function. Branchiomotor neuron loss in *yot* (*gli2^DR^*) mutants appears to result from the action of mutant Gli2 (Gli2^DR^) on Gli1 activator function. Complete activation of *net1a* and *ptc1* expression requires activator function of Gli1, Gli2, and Gli3. In the spinal cord, Gli1, Gli2, and Gli3 activator functions contribute to spinal motor neuron induction (and *islet1* and *tag1* marker gene expression). The significant loss of spinal motor neurons in *yot* mutants appears to result from the dominant repressor effect of Gli2^DR^ on all Gli activators. *Gli1* expression in the hindbrain and spinal cord appears to specifically require Gli3 activator function. Abbreviations: chb, caudal hindbrain; Gli2^DR^, mutant dominant repressor form of Gli2; Hh, Hedgehog signal peptide; *net1a*, *netrin1a*; Ptc, Patched Receptor; *ptc1*, *patched1*; oto, otocyst; r2-r7, rhombomeres 2-7; Smo, Smoothened "coreceptor".

mutants (Chandrasekhar et al., 1999) (Figure 22; Table 7), there is a small (~

25%) but significant reduction in motor neuron number following *gli2* MO

injection, demonstrating that Gli2 contributes to spinal motor neuron induction.

Since hindbrain motor neurons are essentially absent in *dtr* (*gli1⁻*) mutants

(Chandrasekhar et al., 1999), it is unlikely that *gli2* plays any role in their

formation. In contrast to *gli2*, knockdown of *gli3* led to loss of both branchiomotor

(hindbrain) and spinal motor neurons in wild type embryos, and in the *dtr* (*gli1⁻*)

and *yot* (*gli2^{DR}*) mutant spinal cords (Figure 24), indicating that Gli3 activator

function plays a more prominent role than Gli2 in motor neuron induction.

Moreover, *gli2* knockdown in *dtr* (*gli1⁻*) mutants or *gli3* knockdown in *dtr* (*gli1⁻*) or

yot (*gli2^{DR}*) mutants led to the loss of residual *ptc1* expression in the hindbrain

(Figure 27), consistent with the minor activator roles for both Gli2 and Gli3 in Hh

signaling shown previously (Karlstrom et al., 2003; Tyurina et al., 2005). Thus

the residual expression of *net1a* (Figure 22) and *ptc1* seen in *dtr* (*gli1⁻*) mutants

appears to result from the activator functions of Gli2 and Gli3 (Figure 28).

Importantly, our data now show that, in the spinal cord, Gli3 activator function is

also critical for the induction of a distinct ventral cell type, namely motor neurons.

Knockdown of *gli2* function alone had no effect on the induction of

hindbrain and spinal motor neurons (Figure 22; Table 7). Since motor neuron

number is a measure of floor plate- and notochord-derived Hh activities

228

(Chandrasekhar et al., 1998), this suggests that the development of the floor plate and other ventral cell types does not require Gli2 activity. Consistently, *nk2.2*-expressing medial and lateral floor plate cells are unaffected in *gli2* MO-injected wild type embryos (Karlstrom et al., 2003). In contrast, mouse *gli2* is essential for development of the floor plate and adjacent cells (Ding et al., 1998; Matise et al., 1998), reflective of the functional divergence in Gli2 reported earlier (Karlstrom et al., 2003). Although spinal motor neurons develop normally in mouse *Gli2* mutants due to notochord-derived Hh signals (Ding et al., 1998; Matise et al., 1998), it is not known whether mouse *Gli2* is required for motor axon outgrowth, in a similar fashion to zebrafish *gli2* (Brand et al., 1996b; Zeller et al., 2002).

In this report, we have tested whether *gli2* and *gli3* are required for motor neuron induction. Our data suggest important roles for the activator forms of both Gli2 and Gli3 in this process. In mouse, a *Gli1* knock-in (encoding only Gli activator function) can rescue *Gli2* mutant phenotypes, indicating that loss of Gli2 activator function is responsible for the phenotypes seen in *Gli2* mutants (Bai et al., 2002; Bai and Joyner, 2001). Consistent with this, knockdown of zebrafish *gli2* function in *smu* (*smo⁻*) mutants does not abrogate defective Hh-regulated events, including motor neuron induction, suggesting that the repressor function of zebrafish Gli2 does not play a significant role in Hh-regulated patterning in the hindbrain. Nevertheless, we cannot rule out that some of the effects on zebrafish spinal motor neuron development following *gli2* knockdown are indirect effects of the repressor function of Gli2. Similarly, while our data suggest strongly that Gli3

activator function contributes to branchiomotor and spinal motor neuron induction (Figure 24), it is formally possible that Gli3 repressor function may influence motor neuron fate in the hindbrain. These ideas will be tested in the future through *gli* gain-of-function and *gli2*;*gli3* double knockdown experiments.

4.4.4 Differential requirements for Gli activator function in mouse and zebrafish

While Gli2 repressor function appears to be dispensable for neural tube patterning in both mouse and zebrafish, it appears that Gli activator functions have profoundly different roles during motor neuron development in the two species. We have shown here that zebrafish *gli1*, *gli2*, and *gli3* can contribute to spinal motor neuron induction. Furthermore, we showed previously that zebrafish *gli1* is essential for the development of all motor neurons in the midbrain and hindbrain (Chandrasekhar et al., 1999) (A.C., unpublished data), and we show here that *gli3* also plays a role in hindbrain motor neuron induction. In sharp contrast, analysis of specific *Gli* single and double knockouts suggested that Gli activator function is not required for the induction of motor neurons in the mouse spinal cord (Ding et al., 1998; Matise et al., 1998; Park et al., 2000). In mouse *Gli2*;*gli3* double knockouts (which are essentially *Gli1*;*gli2*;*gli3* triple knockouts, since *Gli1* is not expressed in the double mutant), motor neuron progenitors are found in normal numbers, while the number of differentiated motor neurons is much smaller, and they exhibit patterning and migration defects

(Bai et al., 2004; Lei et al., 2004). These and other results from *Shh*;*gli3*

(Litingtung and Chiang, 2000) and *Smo*;*gli3* (Wijgerde et al., 2002) knockout

mice suggest that spinal motor neurons can be induced in small numbers by

stochastic, Gli/Hh-independent mechanisms, likely through retinoid signaling

(Novitch et al., 2003). It should also be noted that since motor neuron

development at more rostral levels (in the brainstem) was not examined in any of

these compound mutants, Gli activators may yet be found to play a role in motor

neuron induction in the mouse head, similar to zebrafish.

Why do *Gli* knockout mice and *gli* knockdown or mutant zebrafish exhibit

significantly different motor neuron phenotypes? Specifically, mouse *Gli1*

knockout mice develop motor neurons normally (at all axial levels) and are viable

(Park et al., 2000), while zebrafish *detour* (*gli1⁻*) mutants specifically fail to

generate cranial motor neurons (Chandrasekhar et al., 1999) and die as embryos

(Karlstrom et al., 1996). In *Gli1* mutant mice, *Gli2* and *Gli3* are expressed

ventrally, and their activator functions compensate for the loss of Gli1 activity (Bai

et al., 2004; Lei et al., 2004). In contrast, while zebrafish *gli2* and *gli3* are

transiently expressed in the ventral neural tube within the normal *gli1* expression

domain in *dtr* (*gli1⁻*) mutants (this study) (Karlstrom et al., 1999; Karlstrom et al.,

2003; Tyurina et al., 2005), the absence of hindbrain motor neurons in this

mutant suggests that Gli2 and Gli3 activator functions cannot compensate for the

loss of Gli1 activator function. This hypothesis can be tested through gain-of-

function experiments (see below). Interestingly, *gli3* knockdown results in

decreased numbers of hindbrain motor neurons, suggesting a role for Gli3

activator in their induction (Figure 24). However, given the *dtr* (*gli1⁻*) motor neuron phenotype, the role for zebrafish *gli3* in branchiomotor neuron induction is likely to be indirect, since *gli3* function is needed for inducing *gli1* expression (Figure 27).

Unlike the dramatic difference in cranial motor neuron phenotypes between mouse and fish *Gli1* mutants, there is a significant but subtler difference in spinal motor neuron phenotypes between the mouse *Gli* "triple" knockout (*Gli2;Gli3*) and the zebrafish *gli2$^{DR/DR}$;gli1* MO and *gli2$^{DR/DR}$;gli3* MO embryos. Differentiated, Islet⁺ motor neurons in the spinal cord are greatly reduced in number, but not completely missing in the *Gli2*;*gli3* mutant mice (Lei et al., 2004), whereas they are essentially lost in the zebrafish *gli2$^{DR/DR}$;gli1* MO and *gli2$^{DR/DR}$;gli3* MO embryos (Figure 23 and Figure 24). While the number of Olig2⁺ spinal motor neuron progenitors in the mutant mice is unaffected, mouse Gli activator function seems to be especially important for the differentiation of these progenitors and patterning of motor neurons (Bai et al., 2004; Lei et al., 2004). Since retinoic acid (RA) signaling can independently generate progenitor domains in the mouse ventral spinal cord (Novitch et al., 2003), it is possible that the small number of motor neurons differentiating in the mutant mice also result from RA-dependent mechanisms. We have not tested whether *olig2*-expressing spinal motor neuron progenitors (Park et al., 2002; Park et al., 2004) form normally in zebrafish *gli2$^{DR/DR}$;gli1* MO and *gli2$^{DR/DR}$;gli3* MO embryos, as in the mutant mice. However, it is clear that even if the progenitors are formed, they

are unable to differentiate into motor neurons in the absence of Gli1, Gli2, and Gli3 activator function.

While our studies address whether zebrafish *gli1*, *gli2*, and *gli3* are necessary for motor neuron induction, they provide no insight into whether zebrafish *glis* have different abilities to induce motor neurons, or whether *gli1-*, *gli2-*, and *gli3*-encoded activator functions are equivalent. Activator forms of mouse Gli2 and Gli3 have distinct abilities to induce ventral cell fates when expressed ectopically in the chick neural tube, with Gli2 generating a broader range of cell types (Lei et al., 2004). In addition, mouse *Gli3* expressed from the *Gli2* promoter cannot fully rescue the *Gli2* knockout phenotype (Bai et al., 2004). In contrast, mouse *Gli1* expressed from the *Gli2* promoter can fully rescue the *Gli2* knockout phenotype (Bai and Joyner, 2001). These results indicate that mouse Glis have varying degrees of overlapping activator functions. It will be of interest to test whether zebrafish Glis similarly share some functionality. Furthermore, given that zebrafish Gli1 is essential for motor neuron induction while mouse Gli1 is not, it would be instructive to test whether mouse Gli1 can participate in motor neuron formation in zebrafish. These experiments will reveal whether the different abilities of the Gli1 orthologs to induce motor neurons reflect differences in activity levels as proposed (Stamataki et al., 2005), or more fundamental differences in their abilities to induce the motor neuron fate.

4.4.5 Early role for Hh signaling in branchiomotor neuron induction

In seeking to explain the loss of branchiomotor neurons in *yot* (*gli2^{DR}*) mutants, we discovered that these neurons are specified very early during embryogenesis. In zebrafish, the reticulospinal interneurons and a few, large spinal motor neurons are specified by the end of gastrulation and represent the earliest-born (primary) neurons (Eisen, 1991; Mendelson, 1986). By contrast, smaller and more numerous spinal motor neurons are specified in a secondary wave of neurogenesis during somitogenesis and later stages (Kimmel and Westerfield, 1990). The branchiomotor neurons have been generally regarded as later-born secondary neurons since the earliest differentiated neurons appear around 15 hpf, and their numbers increase continuously until 36–40 hpf (Chandrasekhar et al., 1997; Higashijima et al., 2000; Linville et al., 2004). Therefore, we were surprised when the cyclopamine experiments (Figure 25) revealed that Hh signaling specifies virtually all branchiomotor neurons prior to 15 hpf. A significant number of nV and nVII neurons are specified between 6 and 12 hpf, spanning gastrulation. Blocking Hh signaling after 18 hpf has no effect on the induction of any branchiomotor neuron subtype including the nX neurons, most of which appear between 30 and 40 hpf. Interestingly, BrdU labeling reveals that many nV and nVII neuronal progenitors remain in S-phase at 18 and 21 hpf (A.C., unpublished), several hours after Hh signaling has specified their

formation. The temporal lag between the critical period of Hh sensitivity and the appearance of differentiated neurons likely reflects the time needed for motor neuron progenitors to undergo an orderly process of specification, cell-cycle exit, and differentiation involving the expression of numerous regional (e.g., *pax6*) and cell-type specific (e.g., *nk2.2*, *olig2*) transcription factors, in a manner similar to that described for spinal motor neurons in chick and mouse (Shirasaki and Pfaff, 2002). In addition to Hh-mediated signaling, retinoic acid (RA) also appears to play a role in inducing branchiomotor neurons, especially the nX motor neurons (Begemann et al., 2004; Linville et al., 2004), mirroring the parallel roles of Hh and RA signaling in the formation of motor neuron progenitor domains in the mouse spinal cord (Novitch et al., 2003). However, our results suggest that RA signaling cannot induce any branchiomotor neurons in the absence of Gli-mediated Hh signaling. It will be of interest to determine the relationship between these signaling pathways during motor neuron induction in zebrafish.

In summary, while a small number of motor neurons can be induced by Hh- and Gli-independent processes in mouse, our data demonstrate an absolute requirement for Gli activator function in the formation of motor neurons at all axial levels in zebrafish. Furthermore, our data have identified separable roles for Gli1, Gli2, and Gli3 activator functions in motor neuron induction. Thus, while the overall requirement for Gli function in motor neuron induction is largely conserved between zebrafish and mouse, the roles of particular Gli family members in this process appear to have diverged. Whether this functional divergence reflects

changes in gene expression patterns, changes in level of protein activity, and/or

changes in protein function remains to be determined.

4.5 ACKNOWLEDGEMENTS

CHAPTER 5

DIFFERENT TEMPORAL REQUIREMENTS FOR HEDGEHOG SIGNALING DURING MOTOR NEURON SPECIFICATION

Unpublished: Vanderlaan, G., Dorsky R., Chandrasekhar, A. (2006). (Manuscript in preparation).

INTRODUCTION

Specification of neuronal subtypes involves a tightly orchestrated convergence of numerous signaling pathways throughout development for the generation of molecular determinants. Although less understood, timing of such signaling pathways represents a key component for motoneuronal programs (Ericson et al., 1996; Incardona et al., 1998; Park et al., 2004). For motor neurons, integration of signaling pathways for neurogenesis and specification is critical for proper development (Dubreuil et al., 2002; Dubreuil et al., 2000). In all neurons, Notch signaling regulates the timing of neurogenesis, in a mechanism dependent on the function of *mind bomb* (*mib*), an E3 ligase (Itoh et al., 2003; Jiang et al., 1996) (see also Chapter 3). In all vertebrates, Hh signaling is

essential for the formation of motor neurons at all axial levels (Bingham et al., 2001; Chandrasekhar et al., 1997; Chandrasekhar et al., 1999; Chen et al., 2001; Chiang et al., 1996; Varga et al., 2001; Wijgerde et al., 2002) (see also Chapter 4, Figures 21, 23, and 24). Conditional blockade of the Hedgehog signaling pathway at the level of the Smoothened protein is made possible by application of the teratogen, cyclopamine (Cooper et al., 1998; Incardona et al., 1998). In this study, we employed cyclopamine to conditionally block Hh signaling for motor neuron specification. We show that different motor neuron subtypes (branchial vs. somatic) require Hh signaling at different times in both the head and trunk of the developing zebrafish embryo. Further, at ages much earlier than expected, Hh signaling is required for the specification of BMN subpopulations in the hindbrain. We also show that at these ages, *phox2a* expression appears in putative BMN progenitors in at least rhombomere 2 (r2). Finally, we show a correlation between timing of cell cycle exit and independence from Hh signal transduction. Overall, our results examine carefully with fine temporal resolution, the function of the Hh signaling pathway for motor neuron specification in the head and the trunk.

5.2   MATERIALS AND METHODS

5.2.1   Animals

Maintenance of zebrafish stocks and development of embryos in E3 embryonic medium was performed as described previously (Bingham et al.,

2002; Chandrasekhar et al., 1997; Chandrasekhar et al., 1999; Chandrasekhar et al., 1998; Westerfield, 1995). Throughout the text, the developmental age of the embryos corresponds to the hours elapsed since fertilization (hour-post-fertilization, hpf, at 28.5°C). *Slow muscle omitted* (*smu*[b641]) mutants were identified on the basis of somite morphology at 21 hpf (Barresi et al., 2000; Chen et al., 2001; van Eeden et al., 1996; Varga et al., 2001). *Mind bomb* (*mib*[ta52b]) mutants (Jiang et al., 1996) were generated from breeding heteryozygous parents and subsequently identified on the basis of predicted Mendelian ratios from embryos processed for an in situ hybridization. The following transgenic lines were used in this study: *islet1-GFP* (Higashijima et al., 2000), *olig2-GFP* (Park et al., 2004), and *gata2-GFP* (gift from Michael Granato).

5.2.2 Cyclopamine treatment

Embryos were treated with cyclopamine (Toronto Research Chemicals, catalog number C988400) (Taipale et al., 2000) as described previously (Karlstrom et al., 2003) (see also section 4.2) with the following modifications. Cyclopamine stock (10 mM in 95% ethanol) was administered at a high (100 μM) or low (25 μM) concentration in E3 medium containing 0.5% DMSO. For controls, embryos were exposed to a high (1%) or low (0.25%) ethanol concentration. Embryos were exposed for ages as early as 3 hpf and as late as 48 hpf, depending on the experiment.

5.2.3   In situ hybridization, immunohistochemistry, and imaging

Synthesis of the digoxigenin- and fluorescein-labeled probes and single color whole-mount in situ hybridization were performed as previously described (Bingham et al., 2003; Chandrasekhar et al., 1997; Prince et al., 1998). Two-color in situ hybridizations were also carried out as previously described (Prince et al., 1998; Vanderlaan et al., 2005). The following in situ probes were used: *paired-homeobox 2a* (*phox2a*) (Guo et al., 1999); *engrailed-4* (*en4*) and *paired-homeobox 2.1* (*pax2.1*), kindly provided by Richard Dorsky; and *krox20* (Oxtoby and Jowett, 1993).

Whole-mount immunohistochemistry was performed as previously described (Bingham et al., 2002; Chandrasekhar et al., 1997). The following antibodies in the indicated dilutions were used: zn5/8 (Trevarrow et al., 1990; 1:10); islet (39.4D5, 1:200) (Korzh et al., 1993); BrdU (G3/G4, Developmental Studies Hybridoma Bank; 1:50); pH3-Ser10 (Upstate; 1:750); GFP (rabbit IgG; Invitrogen; 1:1000); GFP (mouse IgG; Chemicon; 1:750). For fluorescent immunohistochemistry (zn5/8, GFP, BrdU, pH3-Ser10, and GFP), species-appropriate AlexaFluor 488 (FITC)- or AlexaFluor 568 (RITC)-conjugated secondary antibodies (Molecular Probes / Invitrogen; 1:500) were used.

Embryos were de-yolked, mounted in glycerol, and examined with an Olympus BX60 microscope. In all comparisons, at least ten wild type, mutant or drug-treated embryos were examined. Confocal imaging was carried out on fixed embryos mounted in 70% glycerol. Images were captured on an Olympus IX70 microscope equipped with a BioRad Radiance 2000 confocal laser system.

5.2.4 BrdU incorporation and detection

Prior to BrdU administration, the chorions of embryos must be removed to facilitate equivocal chemical access to the embryo proper. Enzymatic dechorionation using Pronase E (Sigma, catalog number P5147) is preferred at these early ages as physical dechorionation methods involving forceps tend to pulverize the whole embryo. Briefly, prior to 2 hpf, a clutch of 20-30 embryos are exposed to 2 mg / ml Pronase E in embryonic medium (E3) inside a glass petri dish. Glass dishes are essential as live embryos will stick to plastic instruments. Exposure to Pronase E continues for roughly two minutes, with gentle swirling of the petri dishes, performed under a dissecting microscope. Enzymatic dechorionation is complete as soon as the first instance of an embryo's chorion becomes indented, as visualized under an Olympus SZX12 microscope. Dechorionated embryos are then gently submerged in a 250 ml glass beaker filled with embryonic medium (E3) and gently swirled to wash away excess enzyme. For retrieval of embryos, flame-polished glass pipettes are used to prevent accidental skewering of specimens.

At 2 hpf of development, Pronase-E dechorionated embryos were transferred to 1.2% agar coated Petri dishes and grown at 28.5°C. At desired developmental ages (9hpf to 27 hpf), embryos were transferred to glass cavity blocks containing 4 ml of 10 mM BrdU / 15% DMSO in E3 without methylene blue. BrdU treatment lasted for 30 minutes on ice and embryos were subsequently returned to E3 and grown until 36 hpf for fixation in 4%

paraformaldehyde in PBS. Fixed embryos were then shifted to methanol for 2 days at -20°C.

For detection of BrdU-incorporation, fluorescent immunolabeling was performed. Briefly, embryos were rehydrated to PBTx (1X phosphobuffered saline + 3% Triton-X), washed twice for 5 minutes in PBTx, rinsed in 2N HCl in PBTx twice for 5 minutes each, incubated in 2N HCl in PBTx for 30 minutes, and rinsed in PBTx twice for 5 minutes each. Embryos were then blocked for 5-7 hours in PBTxB (PBTx + 0.25% BSA). For simultaneous incubation with mouse anti-BrdU antibody (1:50) and rabbit anti-GFP IgG (1:1000), embryos were rocked gently overnight at 4°C. Embryos were then washed 8 times with PBTx for 30 minutes each, blocked in PBTxB for 30 minutes, and simultaneously incubated with goat anti-mouse AlexaFluor 568 (1:500) and goat anti-rabbit AlexaFluor 488 (1:500), overnight on a 4°C rocker in the dark. Embryos were then washed three times in 1X PBS, fixed for 45 minutes in 4% paraformaldehyde, and washed three more times in 1X PBS.

Imaging of BrdU-treated samples was performed on an Olympus IX70 microscope equipped with a BioRad Radiance 2000 confocal laser system, using the following settings: Z-step of 2.5 microns, 20X Uplanar objective, 512 x 512 resolution, 500 lps scan speed, and a Kahlman averaging value of two. Two permit cell counts, individual optical Z-sections were preserved for both BrdU (RITC) and *islet1*-GFP (FITC) channels.

5.2.5   Quantification

For quantification of confocal images, individual Z-planes (2.5 microns deep) from samples double stained with anti-BrdU and anti-GFP antibodies (for vendor and concentration info, see Table 1) were counted for both the total number of BMNs expressing the *islet1*-GFP transgene and also the total number of *islet*-GFP expressing BMNs which incorporated BrdU.   For each transgenic embryo exposed to BrdU, ratios between GFP_{BrdU}:GFP_{total} were calculated per optical Z-section per BMN subpopulation. BMN-specific ratios were then averaged and standard deviations generated using Graphpad InStat software for all embryos exposed to a given BrdU timepoint, with sample sizes of at least five embryos per timepoint. Quantification of islet immunohistochemical stains was performed as previously described (Chandrasekhar et al., 1999). A statistical software package (Graphpad InStat v3.2) employing one-way analysis of variance (Anova) with Bonferroni post tests was used for data analysis for both BrdU and islet immunohistochemistry experiments.

5.3   RESULTS

5.3.1   *phox2* genes are expressed by precursor and differentiated branchiomotor neurons.

Previous work has shown that *phox2* genes are necessary and sufficient for branchiomotor neuron differentiation in vertebrates (Dubreuil et al., 2002;

Dubreuil et al., 2000; Pattyn et al., 2000). In zebrafish, *phox2a* is expressed in branchiomotor neuron subpopulations, but does not seem necessary for their specification (Guo et al., 1999). As mouse *phox2b* appears to participate in early (neurogenesis) and late (motor neuron differentiation) events, we carefully examined the early and late expression patterns of the *phox2* gene family in zebrafish.

In wild type embryos at 30 hpf of development, *phox2a* labels the branchiomotor neurons in the head, while *olig2*, a bHLH-class transcription factor, is expressed in somatic motor neurons of the head and trunk (Figure 29A, D). By 36 hpf, although the various characteristic branchiomotor neuron subpopulations clearly express *phox2a* (Figure 29E), in zebrafish *phox2a/soulless* mutant embryos, *islet1*-expressing branchiomotor neurons form normally (Figure 29F) (Guo et al., 1999). Thus, although not necessary for specification, *phox2a* expression demarcates differentiated branchiomotor neurons.

As some motor neurons appear to be specified by Hh signaling at ages earlier than 30 hpf (see Chapter 4, Figure 26D-I), we next examined the early expression pattern of *phox2a* in the hindbrain. In 12 hpf wild type embryos, *phox2a* is expressed primarily at the midline and lateral margins of r2 and subtly in r4 (Figure 29B). By 15 hpf, *phox2a* expression is excluded from the midline and confined to the lateral neural tube (Figure 29C). A hallmark feature of neural tube cells located near the midline (and hence, within the ventricular zone) is the

FIGURE 29. *Phox2a* and *phox2b* together label branchiomotor neurons and progenitors, while *olig2* labels somatic motor neurons in zebrafish.

Panels A, L, M, and Q are lateral views. Panels B-K, N-P are dorsal views of the hindbrain. In all images, anterior is to the left, except for G-J where anterior is top.

(A) At 30 hpf, all zebrafish motor neurons are labeled by *phox2a* and *olig2*. Expression of *phox2a* (red) is found from nV trigeminal (white triangle) to nX vagal branchiomotor neurons (black arrow). Expression of *olig2* is found in somatic motor neuron subpopulations, such as the nVI abducens (white arrows) in r5 and r6, and the spinal motor neurons (asterisk) of the trunk.

(B-C): At early ages, *phox2a* expression is found in putative motor neuron progenitors in r2 and r4. *krox20* expression labels rhombomeres 3 and 5. At 12 hpf, *phox2a* expression is found near the midline primarily in r2 and weakly in r3 and r4 (B). By 15 hpf, all *phox2a* expression is refined to cell clusters occupying the lateral margins of r2 and r4 (C). *phox2a* expression is excluded from midline tissues in these rhombomeres. **(D-E):** By 30 hpf (D) and 36 hpf (E), *phox2a* expression is found in a stereotypic pattern resembling the various branchiomotor neuron subpopulations. **(F):** *islet1*-expressing motor neurons form normally in the zebrafish *soulless* (*phox2a⁻*) mutant hindbrain. **(G-J):** *phox2a*-expressing putative motor neuron progenitors are no longer mitotic after 16 hpf. From 9-12 hpf, some cells (white arrows) within the *phox2a* expression domain (red) coexpress the pH3 (green) mitotic marker (G, H). At 16 hpf or 21 hpf, all *phox2a*-expressing cells are post-mitotic evidenced by the lack of pH3 coexpression (I, J). **(K-M):** In the zebrafish hindbrain, *phox2b* expression is found in the ventral and dorsal aspects of the neural tube. At 12 hpf, *phox2b* is expressed in a cluster of cells near the midline (K). By 16 hpf, *phox2b* expression is found primarily in ventral (black arrows) and dorsal (white arrow) cells of the neural tube (L). In 30 hpf embryos, *phox2b* expression is expanded dramatically in both the dorsal (white arrow) and ventral (black arrow) neural tube, and may also label the nX vagal (asterisk) branchiomotor neurons (M). **(N-Q):** The *olig2*-GFP transgene is expressed in somatic motor neurons of the head and trunk. At 48 hpf, the somatic motor nuclei (white arrows) of the nVI abducens coexpress alcam (zn5/8, red) and GFP driven by the *olig2* enhancer element (N).

246

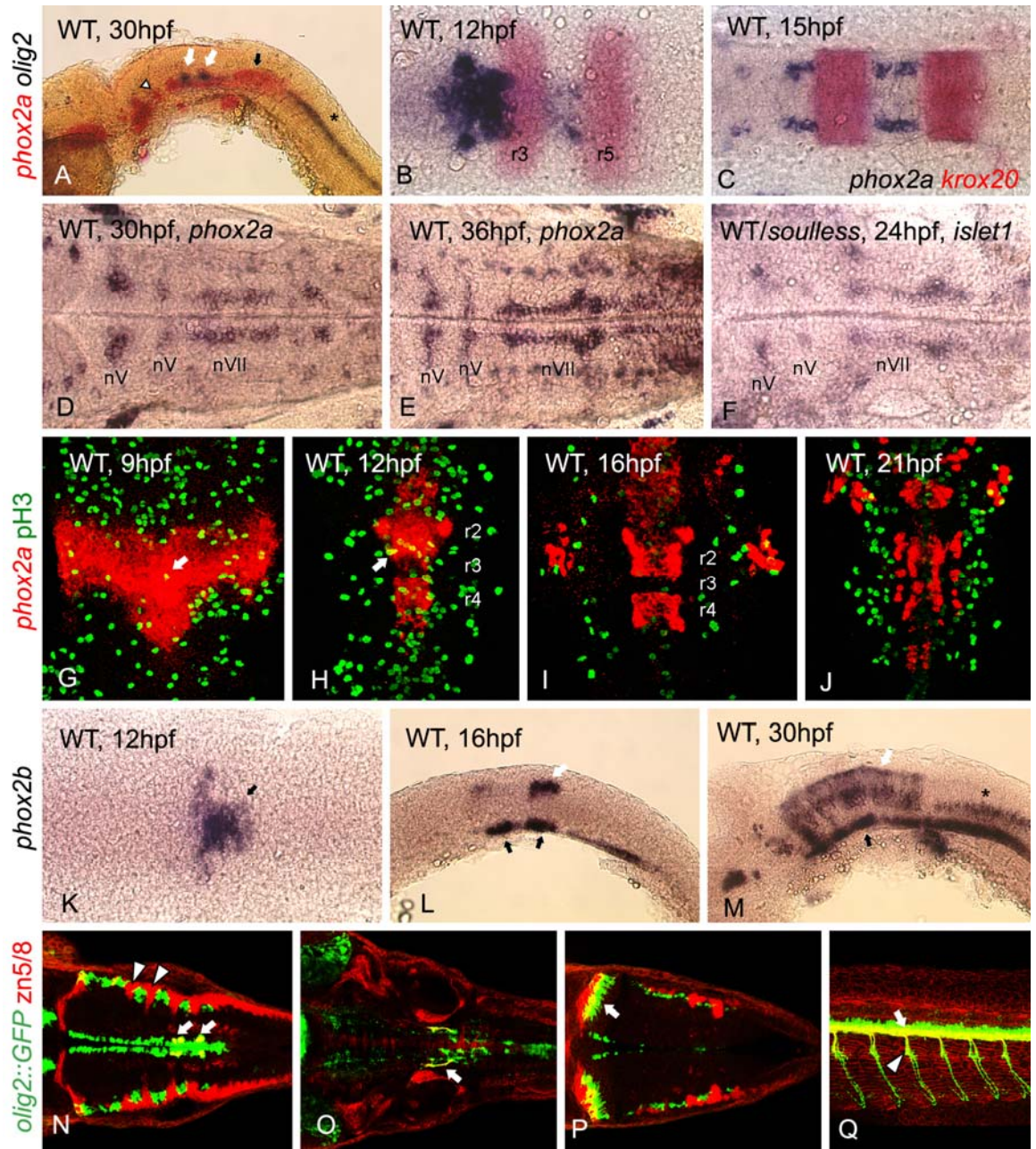**FIGURE 29. (CONTINUED)** *Phox2a* and *phox2b* together label branchiomotor neurons and progenitors, while *olig2* labels somatic motor neurons in zebrafish.

In the same embryo as in (N), a deeper confocal plane reveals that the motor axons (white arrows) of the nVI abducens coexpress alcam and *olig2*-GFP while projecting rostrally (O). In the trunk, the cell bodies (white arrow) and axons (arowhead) of secondary spinal motor neurons, a somatic subtype, also coexpress alcam and *olig2*-GFP (Q). In contrast, sensory commissural cell bodies never express both alcam and *olig2*-GFP; instead, cell bodies at rhombomere centers express alcam while nuclei at rhombomere boundaries (arrowheads) express *olig2*-GFP (N). Likewise, in the same embryo as in (N), cell bodies of cerebellar neurons (white arrows) primarily express either alcam or *olig2*-GFP, with little overlap (P). Abbreviations: nV, trigeminal branchiomotor neurons; nVII, facial branchiomotor neurons; nX, vagal branchiomotor neurons.

ability to divide and function as precursors for differentiated neurons. To determine whether *phox2a*-expressing cells might be progenitors, we examined whether *phox2a*-positive cells also coexpressed phospho-Histone3 (pH3), a mitotic marker. Mitotic cells expressing *phox2a* were found in the hindbrains of 9 and 12 hpf embryos, but by 16 and 21 hpf, all *phox2a*-expressing cells failed to coexpress pH3 (Figure 29G-J). Thus, at ages prior to neural tube formation, zebrafish *phox2a* appears to also be expressed in putative neuronal progenitors.

We next examined the early and late expression patterns of *phox2b*. Like *phox2a*, *phox2b* is expressed in a cluster of cells near the midline of the zebrafish hindbrain at 12 hpf (Figure 29K). However, *phox2b* expression is primarily clustered in r4, with weak levels of expression in r2, r3, and r5 (Figure 31E). By 16 hpf, *phox2b* is expressed in both dorsal and ventral domains of the neural tube (Figure 29L) and by 30 hpf, expression of *phox2b* nearly encompasses the entire breadth of the neural tube (Figure 29M). Taken together, the expression data of the *phox2* genes at ages in which Hh signaling appears to function for motor neuron specification suggests the possibility that zebrafish *phox2a* and *phox2b* function redundantly for branchiomotor neuron induction.

5.3.2 *olig2* is expressed in somatic motor neurons of the head and trunk.

In vertebrates, *olig2* is expressed in progenitors of spinal motor neurons, a somatic motor neuron subtype (Mizuguchi et al., 2001; Novitch et al., 2001; Park et al., 2004). Further, misexpression of *olig2* is sufficient to drive ectopic motor neuron formation in the dorsal neural tube (Mizuguchi et al., 2001; Novitch et al., 2001) and is essential for the formation of primary spinal motor neurons in zebrafish (Park et al., 2002). Given the importance of the *olig2* gene in neuronal specification (Park et al., 2004), we carefully examined the expression pattern of an *olig2*-GFP transgene in the zebrafish hindbrain. By 48 hpf, the somatic motor nuclei of the abducens (nVI) subpopulation coexpress *olig2*-GFP and alcam/Zn5 (Figure 29N, arrows) (Trevarrow et al., 1990). In adjacent optical cross-sections, both alcam/Zn5 and *olig2*-GFP also label the nVI axons as they project rostrally (Figure 29O). In the somatic motor neurons of the trunk, alcam/Zn5 and *olig2*-GFP is also found in both the soma (Figure 29Q, arrow) and axons (Figure 29Q, arrowhead) of secondary spinal motor neurons. Interestingly, we also observed that unlike the somatic motor neurons, some neurons express either *olig2*-GFP or alcam/Zn5, but not both; for instance, cell bodies of sensory commissural neurons located at rhombomere boundaries express only the *olig2*-GFP transgene, while those found at rhombomere centers express alcam/Zn5 (Figure 29N, arrowhead). Likewise, cell bodies of cerebellar neurons express either alcam/Zn5 or the *olig2*-GFP transgene, with little overlap (Figure 29P).

5.3.3 Putative neurons of the hindbrain are regulated by Notch signaling.

As many neuronal cell types, including interneurons, have yet to be described in the zebrafish hindbrain, we next examined the effects of perturbed Notch signaling for neurogenesis of various neuronal cell types. Mutations in *mind bomb* (*mib*), an E3 ligase, severely disrupt motor neuron differentiation (see Chapter 3, Figure 11A-B) (Itoh et al., 2003; Jiang et al., 1996). Similarly, *mib* mutants exhibited dramatic neurogenic phenotypes for expression of *phox2a* (control) and putative interneuronal markers *en4*, and *pax2.1* (Figure 30). In the spinal cord, misexpression of *gata2*-promoter traps has been shown to label ventral interneurons (Meng et al., 1997). We also observed that *en4* but not *pax2.1* is coexpressed with the *gata2*-GFP transgene in the hindbrain (Figure 30G-H). Thus, *en4* and *pax2.1*-expressing cells are regulated by Notch signaling and therefore neuronal in nature, and at least a subpopulation of *en4* cells are likely interneurons as they coexpress the *gata2*-GFP transgene.
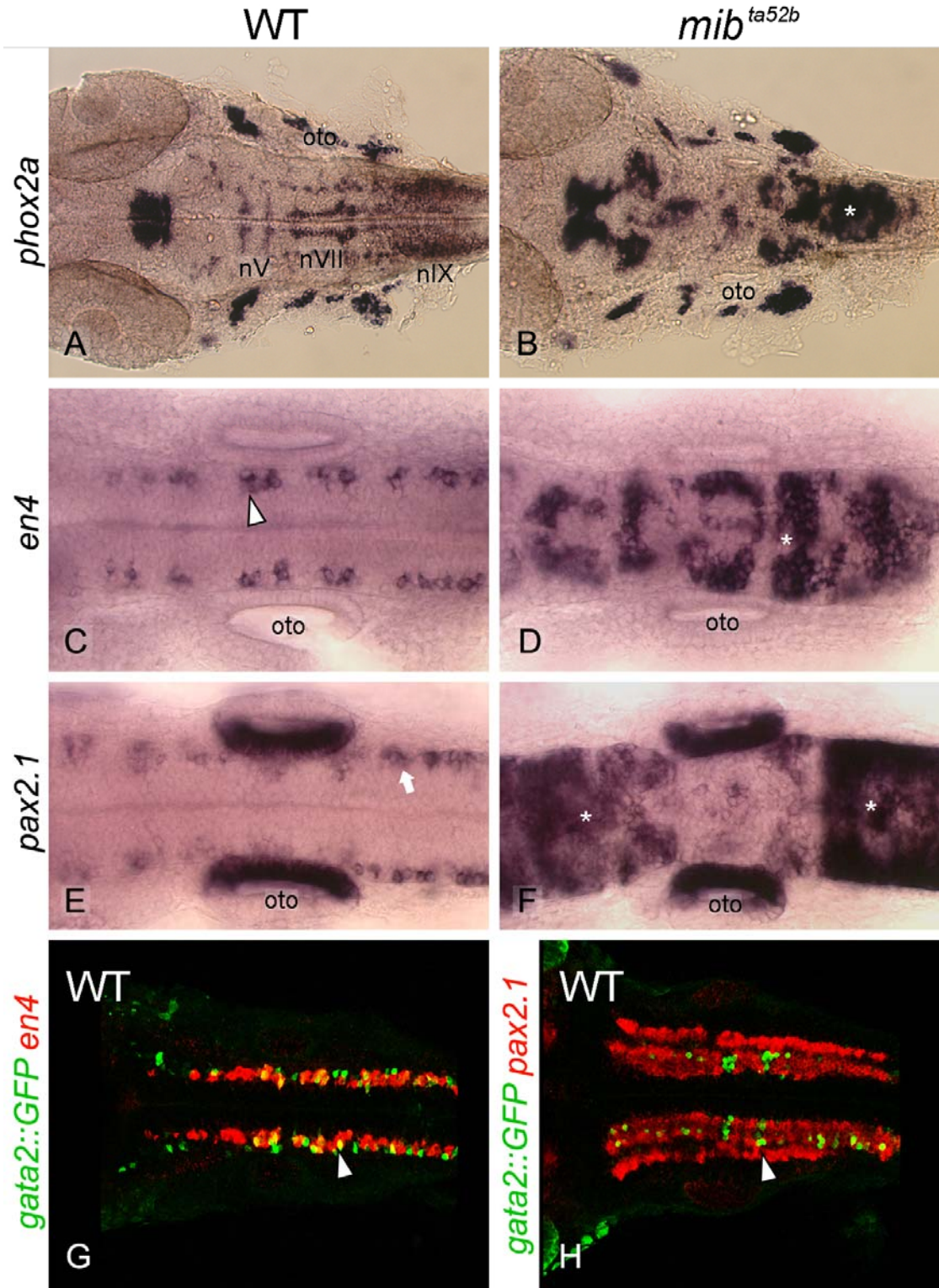
FIGURE 30. Notch signaling regulates timing of neuronal commitment by a compartmentalized mechanism.

All panels show dorsal views of the hindbrain, with anterior to the left. **(A, B):** *phox2a*-expressing branchiomotor neurons require Notch signaling for proper patterning. In a 36 hpf wild type embryo, *phox2a*-expressing branchiomotor neuron subpopulations (nV, nVII, and nIX) are found in characteristic locations (A). In *mib* mutants defective for Notch signaling, branchiomotor neurons (BMNs) expressing *phox2a* are fused at the midline in numerous rhombomeres (B). BMNs in the caudal hindbrain (asterisk) appear up-regulated, while those adjacent to the otocyst (oto) are mildly affected (B). **(C, D):** *en4*-expressing neurons also require Notch signaling for neuronal development. At 22 hpf, *en4*-expressing cell clusters (arrowhead) decorate the lateral margins of the neural tube (C). In a *mib*^{ta52b} mutant sibling, ectopic *en4*-expressing cells (asterisk) are found fused at the midline (D). **(E, F):** *pax2.1*-expressing neurons also require *mib* function for neuronal patterning. In a 24 hpf wild type embryo, expression of *pax2.1* is found in cells (arrow) removed from the midline (E). In *mib* mutants, supernumerary *pax2.1*-expressing neurons are found in rostral and caudal rhombomeres (asterisks), while very few are found in the rhombomere adjacent to the otic vesicle (F). **(G, H):** Neurons that express *en4*, but not *pax2.1*, also coexpress the *gata2*-GFP transgene. In a 22 hpf transgenic embryo, a subpopulation of *en4*-expressing cells (arrowhead) also express *gata2*-GFP (G). In a 30 hpf transgenic embryo, hindbrain neurons express either *pax2.1* or *gata2*-GFP, but never both (H).

5.3.4   Hedgehog signaling is necessary for expression of both *phox2a* and *phox2b* in the hindbrain.

Mouse *phox2b* is essential for branchiomotor neuron differentiation (Pattyn et al., 2000) while in all vertebrates, all motor neuron induction requires Hh signaling (Chandrasekhar et al., 1999; Chandrasekhar et al., 1998; Chen et al., 2001; Varga et al., 2001; Wijgerde et al., 2002) (see also Chapter 4, Figure 21). Therefore, if zebrafish *phox2a* and *phox2b* are truly expressed in branchiomotor neuron progenitors, loss of Hh signaling should eliminate their expression. To address this, we employed pharmacological and genetic approaches to disrupt Hh signal transduction and analyzed resulting changes in the expression of the *phox2* gene family at early ages, prior to neural tube formation. In control embryos treated with ethanol, *phox2a* expression at 12 hpf is found at the midline while at 15 hpf, *phox2a* is expressed along the lateral edges of the neural tube (Figure 31A, C). Application of cyclopamine, a pharmacological inhibitor of the Hh signaling pathway (Taipale et al., 2000), from as early as 3 hpf was sufficient to eliminate nearly all *phox2a* expression in r2-r4 (Figures 31B, D). Of particular interest, a small cluster of *phox2a*-expressing neurons located in rhombomere 2 (r2) appear to be refractory to cyclopamine treatment (Figures 31B, D) and may represent progenitors for the nV trigeminal BMNs.
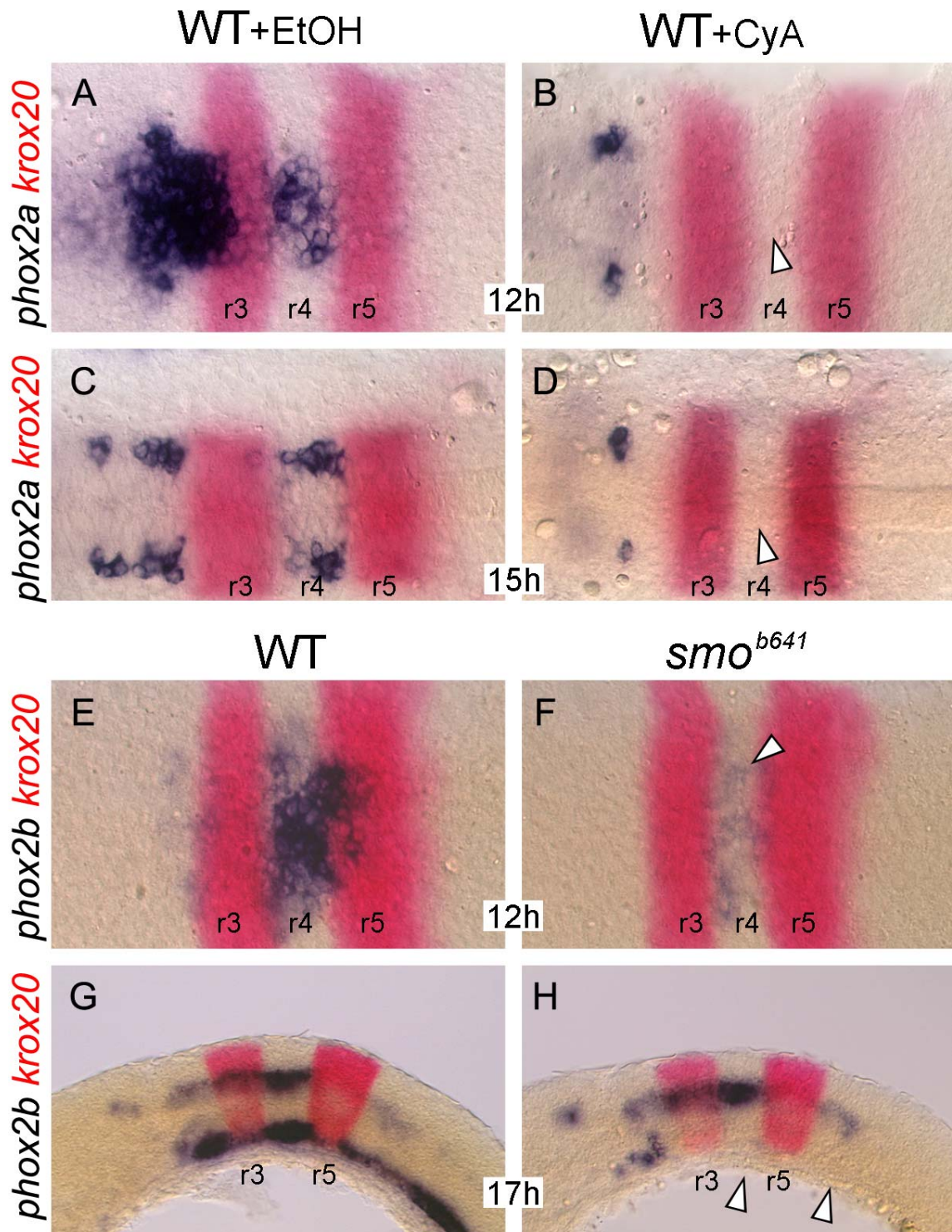
FIGURE 31. Hh signaling is essential for *phox2a* and *phox2b* expression in putative branchiomotor neuron progenitors.

Panels A-F show dorsal views of the hindbrain while panels G and H are lateral views. In all images, anterior is to the left and *krox20* expression (red) demarcates r3 and r5. **(A-D):** Pharmacological disruption of Hedghehog signaling eliminates most *phox2a*-expressing cells. In control embryos treated with ethanol, putative branchiomotor neuron progenitors expressing *phox2a* at 12 hpf are found in both the midline and lateral margins of r2 through r4 (A). By 15 hpf, *phox2a*-expressing neurons are confined to clusters lining the lateral edges of the neural tube (C). At 12 or 15 hpf, wild type embryos treated with the Hh pathway antagonist, cyclopamine, exhibit severe reductions in all putative *phox2a*-positive BMN progenitors (B, arrowhead) and putative BMNs (D, arrowhead). Interestingly, a few laterally-located *phox2a*-expressing cells in r2 are unaffected by cyclopamine-mediated disruption of the Hh signaling pathway (B, D). **(E-H):** Genetic disruption of Hh signal transduction severely reduces *phox2b* expression. In 12 hpf wild type embryos, *phox2b* expression is primarily located in r4 (E). In *smo* mutant siblings, *phox2b* expression is eliminated in r5, and greatly reduced in r4 (F, arrowhead). By 17 hpf, *phox2b* expression is found in the dorsal and ventral neural tube of wild type embryos (G). In *smo* mutants, only *phox2b* expression in the ventral neural tube is abolished (arrowheads), with the exception of a few cells in r2 (H).

We next examined the role of Hh signaling for *phox2b* expression in the hindbrain. In control embryos, *phox2b* expression is found primarily in r4 at 12 hpf (Figure 31E), and at later ages, *phox2b* is expressed in two distinct ventral and dorsal domains in the neural tube (Figure 31G). In *smo* mutant siblings however, *phox2b* expression is severely reduced in putative progenitors of r4 (Figure 31F), while only the ventral *phox2b* expression domain is lost by 17 hpf of development (Figure 31H). Of particular interest, a small patch of *phox2b*-expressing cells was observed in rhombomere 2 (r2) of *smo* mutants (Figure 31H). Taken together, Hh signaling is essential in the ventral neural tube for the expression of *phox2* genes in putative BMN progenitors.

5.3.5   Different branchiomotor neuron subpopulations have different temporal requirements for Hedgehog signaling.

As motor neuron determinants of the *phox2* gene family are expressed in a Hh-dependent manner in neuronal progenitors prior to neural tube closure, we hypothesized that ages when *phox2* genes are expressed might correlate with times in which the Hh signaling pathway is necessary for BMN induction. We therefore exposed wild type embryos to cyclopamine, starting as early as 6 hpf and at every 3 hour time point afterwards until 27 hpf, to determine the temporal requirement by which Hh signaling specified various branchiomotor neuron subpopulations. To our surprise, we found that trigeminal (nV) motor neurons in r2 are completely specified by 15 hpf (Figure 32, compare orange to red line),

256

while nV BMNs located in a single adjacent segment, r3, require Hh signaling until as late as 24 hpf (Figure 32, compare light blue to dark blue line) (Table 10, Figure 37). In zebrafish, the facial (nVII) branchiomotor neurons are born in r4 and migrate during development to r6 and r7 (Bingham et al., 2002; Chandrasekhar et al., 1997). We examined the role of Hh signaling for nVII BMN induction by quantifying the number of islet-expressing motor neurons found in r4-r7 of both ethanol-treated control and cyclopamine-treated embryos (Figure 33, Table 10). Facial (nVII) BMN specification required Hh signaling over a long period of time, beginning as early as 9 hpf to as late as 21 hpf (Figures 33 and 37, see also Table 10). Thus, Hh signaling is required at different times and durations for at least three different subpopulations of branchiomotor neurons, with r2 nV BMNs specified earliest.

nV trigeminal motor neurons

Avg # of Islet⁺ cells per rhombomere

Onset of CyA treatment (hpf)

Legend:
- r2+EtOH (red)
- r2+CyA (orange)
- r3+EtOH (blue)
- r3+CyA (teal)

258
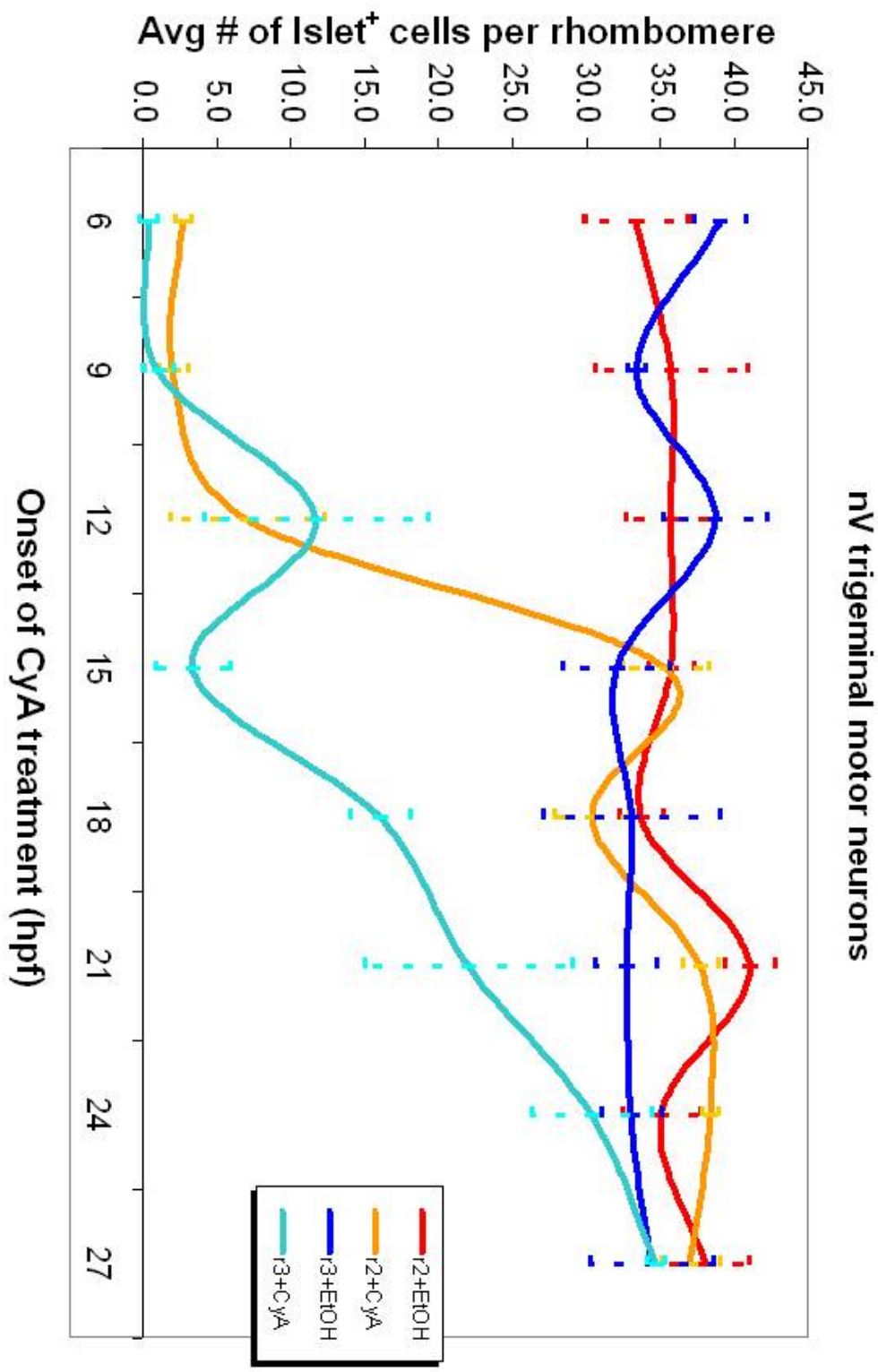
FIGURE 32. Different branchiomotor neuron subpopulations have different temporal requirements for Hh signaling.

In control embryos, the number of Islet-expressing trigeminal (nV) branchiomotor neurons in r2 and r3 remains constant and unaffected by time of treatment (red, blue lines, respectively). Cyclopamine (CyA)-mediated disruption of Hh signaling beginning as early as 6, 9, or 12 hpf eliminates most or all nV motor neurons in rhombomere 2 (r2; orange line). CyA treatment beginning from 15 hpf onwards has no effect on nV motor neurons in r2 (orange line). In r3, trigeminal motor neurons are affected by onset of CyA treatment from 6 hpf to 21 hpf, returning to normal numbers by 24 hpf (light blue line).

nVII facial motor neurons

260
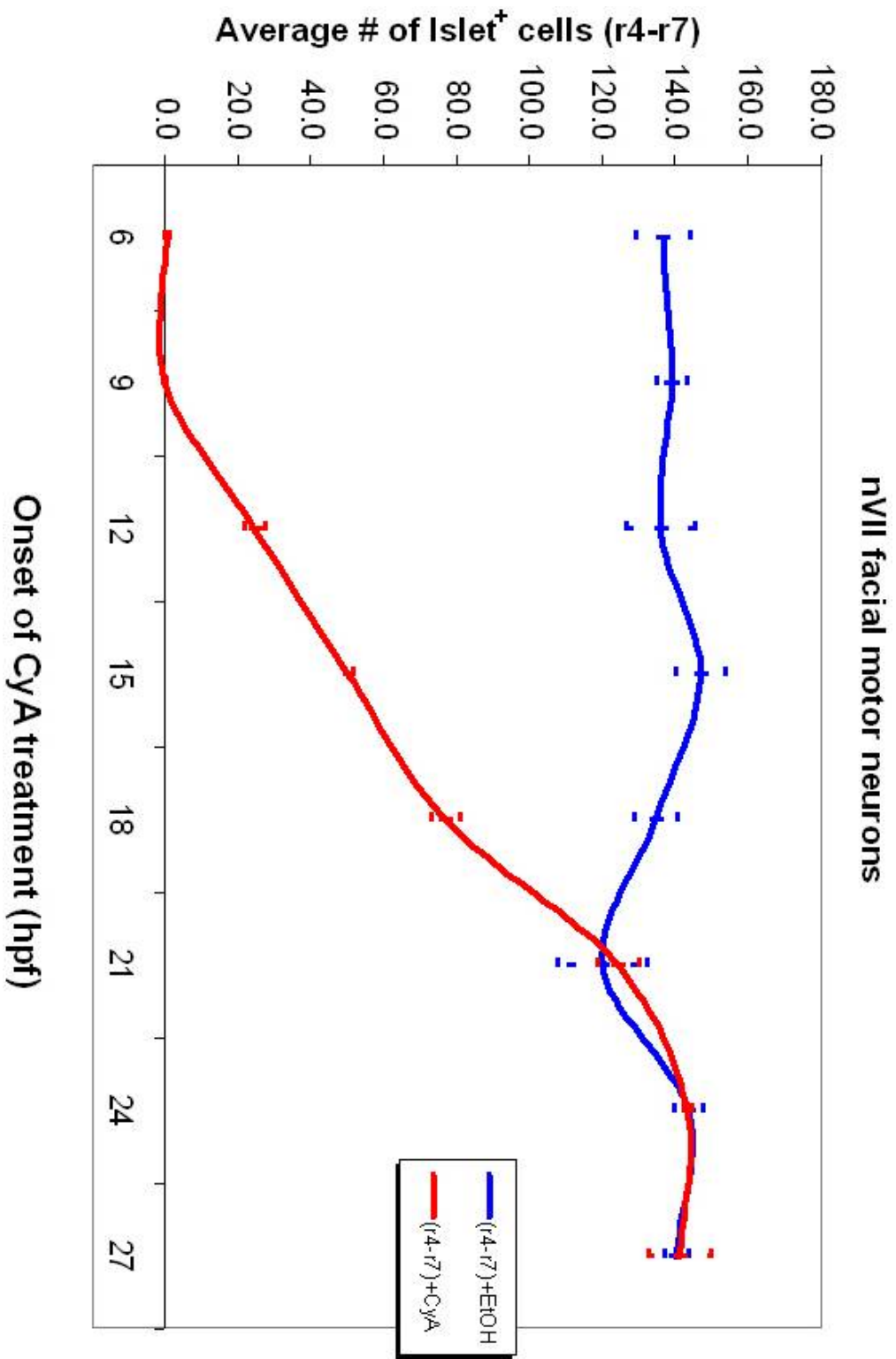
FIGURE 33. Facial (nVII) branchiomotor neurons require Hh signaling across a lengthy period for specification.

In r4-r7, the average number of Islet-expressing facial (nVII) branchiomotor neurons remains relatively constant at about 125 cells in embryos treated with ethanol at different ages (blue line). Following CyA treatment, the nVII BMNs are eliminated at 6 and 9 hpf, and are progressively more abundant from 12 hpf through 18 hpf, returning to normal cell numbers by 21 hpf of treatment (red line).

5.3.6 Hedgehog signaling is required over a long period for somatic motor neuron specification.

We next examined whether a different class of motor neurons would have different Hh temporal requirements for specification compared to those of BMNs. In control embryos treated with ethanol at 12 hpf, the somatic motor neuron subtype, nVI abducens, are specified normally (Figure 34A). However, cyclopamine treatment at 12 hpf completely eliminates all nVI cell bodies (Figure 34B). Most nVI cranial motor neurons are refractory to cyclopamine treatment by 16 hpf, while nVI abducens no longer require Hh signaling by 21 hpf (compare Figure 34A to C and D). In the trunk, the secondary spinal motor neurons also represent a somatic motor neuron subpopulation. As the mechanism of motor neuron induction differs dramatically between the head and the trunk (Chandrasekhar et al., 1999) (see also Chapter 4, Figure 28), we examined whether temporal Hh signaling requirements might act as contributing factors for somatic motor neuron development along the anterior-posterior axis. In control embryos (Figure 34E), secondary spinal motor neurons and their axons are found as a row of cells (yellow), just below oligodendrocytes (green) (Park et al., 2004). Following cyclopamine treatment at 12 or 16 hpf, all secondary spinal motor neurons are eliminated (Figures 34F, G). However, cyclopamine administration at 21 hpf is insufficient to eliminate secondary spinal motor neuron induction (Figure 34H). We next examined, in greater temporal resolution, the requirement of Hh signaling for all somatic motor neurons in the spinal cord. The islet antibody (Korzh et al., 1993) labels both primary and secondary spinal motor

262

The text labels visible in the figure:

- A: +EtoH @ 12 hpf
- B: +CyA @ 12 hpf
- *olig2::GFP* Zn5
- oto
- C: +CyA @ 16 hpf
- D: +CyA @ 21 hpf
- *olig2::GFP* Zn5
- oto
- E: +EtoH @ 12 hpf
- F: +CyA @ 12 hpf
- *olig2::GFP* Zn5
- G: +CyA @ 16 hpf
- H: +CyA @ 21 hpf
- *olig2::GFP* Zn5
- HEAD
- TRUNK
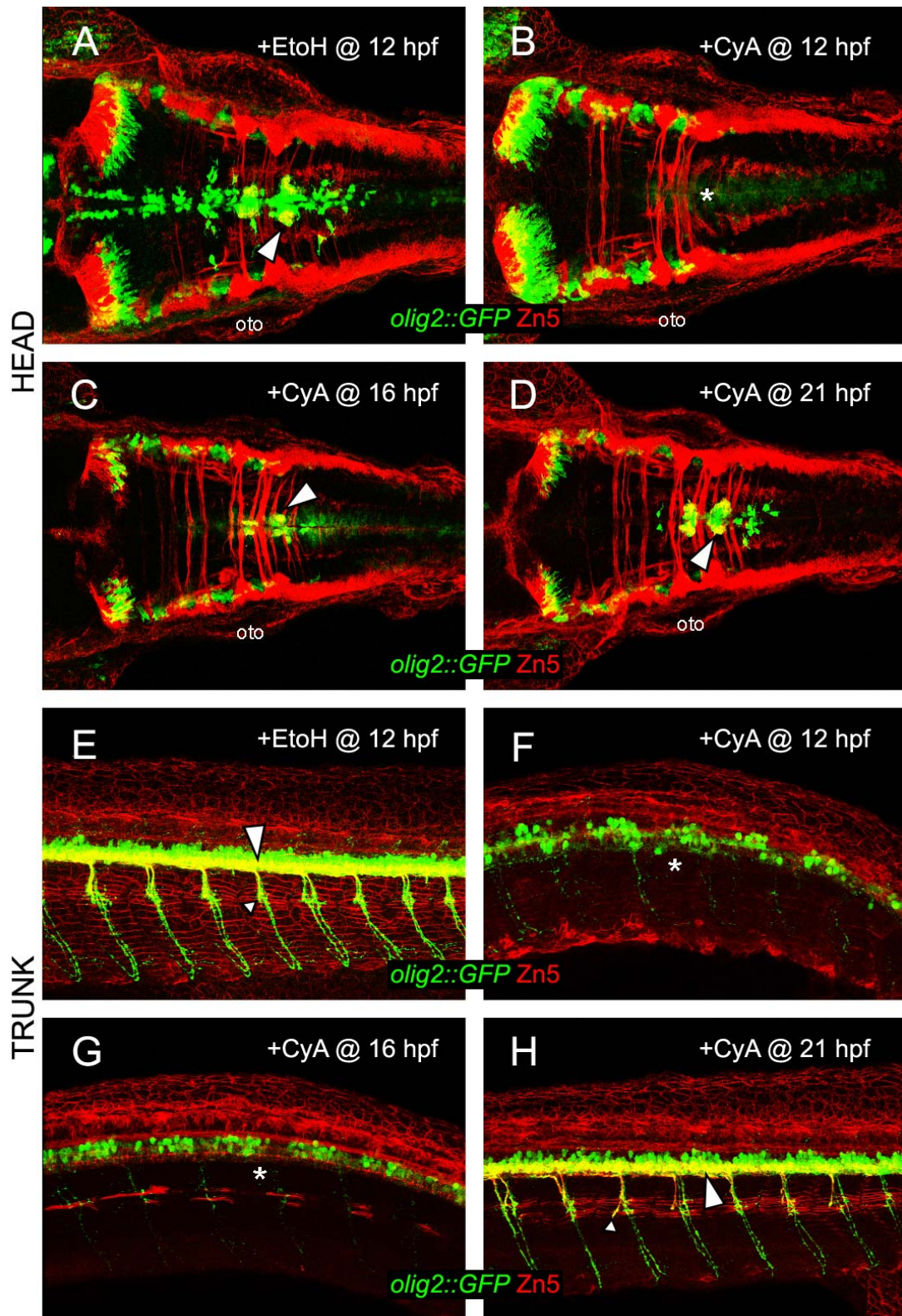
FIGURE 34. Somatic motor neuron specification at all axial levels requires Hh signaling prior to 21 hpf.

Panels A-D are dorsal views of the hindbrain, while panels E-H show lateral views of the spinal cord. In all images, anterior is to the left. **(A-D):** Hh signaling is necessary between 12-21 hpf for abducens (nVI) somatic motor neuron induction. In control transgenic embryos treated with ethanol at 12 hpf, *olig2*-GFP is expressed in oligodendrocytes (green) while coexpressed with alcam (Zn5, red) in nuclei (yellow) of nVI abducens (A, arrowhead). Following CyA treatment from 12-48 hpf, nearly all transgenic GFP driven by the *olig2* enhancer is eliminated, especially in the nuclei of the abducens somatic motor neurons (B, asterisk). CyA-mediated inhibition of Hh signaling from 16-48 hpf eliminates all *olig2*-GFP rostral to r5, while nVI abducens (yellow) appear to be slightly reduced in r5 and r6 (C). Inhibition of Hh signaling from 21-48 hpf is still sufficient to eliminate *olig2*-GFP expression rostral to r5, while nuclei (arrowhead) of nVI abducens somatic motor neurons appear normal (D). **(E-H):** Hh signaling is required prior to 21 hpf for induction of the secondary spinal motor neurons, a somatic motor neuron subtype. By 48 hpf, in transgenic control embryos treated with ethanol at 12 hpf, cell bodies (large arrowhead) and axons (small arrowhead) of secondary spinal motor neurons coexpress *olig2*-GFP and alcam/Zn5 (E). In these control embryos, oligodendrocytes and primary spinal motor neurons express *olig2*-GFP but not alcam/Zn5 (E). Following CyA treatment from 12-48 hpf, all secondary spinal motor neurons are eliminated and *olig2*-GFP expression is dramatically reduced, and slightly mispatterned (F). CyA treatment from 16-48 hpf is still sufficient to inhibit secondary spinal motor neuron specification while severely affecting *olig2*-GFP expression (G). CyA treatment 21-48 hpf is not sufficient to inhibit the majority of secondary spinal motor neurons, although *olig2*-GFP expression is still slightly reduced, presumably in oligodendrocytes (H). Abbreviations: EtOH, ethanol; CyA, cyclopamine; nV, trigeminal; nVI, abducens; nVII, facial; BMN, branchiomotor neuron; SMN, somatomotor neuron; GFP, green fluorescent protein; hpf, hours post fertilization.

neuron subpopulations. We therefore examined the consequences of Hh

pathway blockade on all spinal motor neurons for every 3 hour interval beginning

at 6 hpf of development. In control embryos treated with ethanol, an average

number of ~30 islet-positive cells per hemisegment was observed for each age

group (Figure 35). In cyclopamine-treated embryos, spinal motor neuron

induction was severely affected (50% loss) by as late as 21 hpf, and not

completely recovered until 27 hpf of development (Figure 35, Table 10). Taken

together, these findings demonstrate that different somatic motor neuron

subtypes require Hh signaling at different times for their specification.

5.3.7   Progenitors of different branchiomotor neuron subpopulations enter terminal S-phases at different times.

Previous work has shown that motor neurons undergo a terminal mitosis

upon expressing islet for the first time (Ericson et al., 1996). We hypothesized

that if different motor neuron subpopulations require Hh signaling at different

times, this effect might be produced from different progenitors of motor neuron

subtypes existing at different stages of the motoneuronal program. One method

to assess stages of a motoneuronal program is to identify the time by which

neuronal progenitors exit the cell cycle and adopt a post-mitotic differentiation

fate. We chose to compare two different BMN subpopulations, the nV

(trigeminal) in r2 and the nVII (facial) in r4-r7, due to dramatic differences in

Spinal motor neurons

Avg # of Islet⁺ cells per hemisegment

Onset of CyA treatment (hpf)

SMN+EtOH

SMN+CyA

266
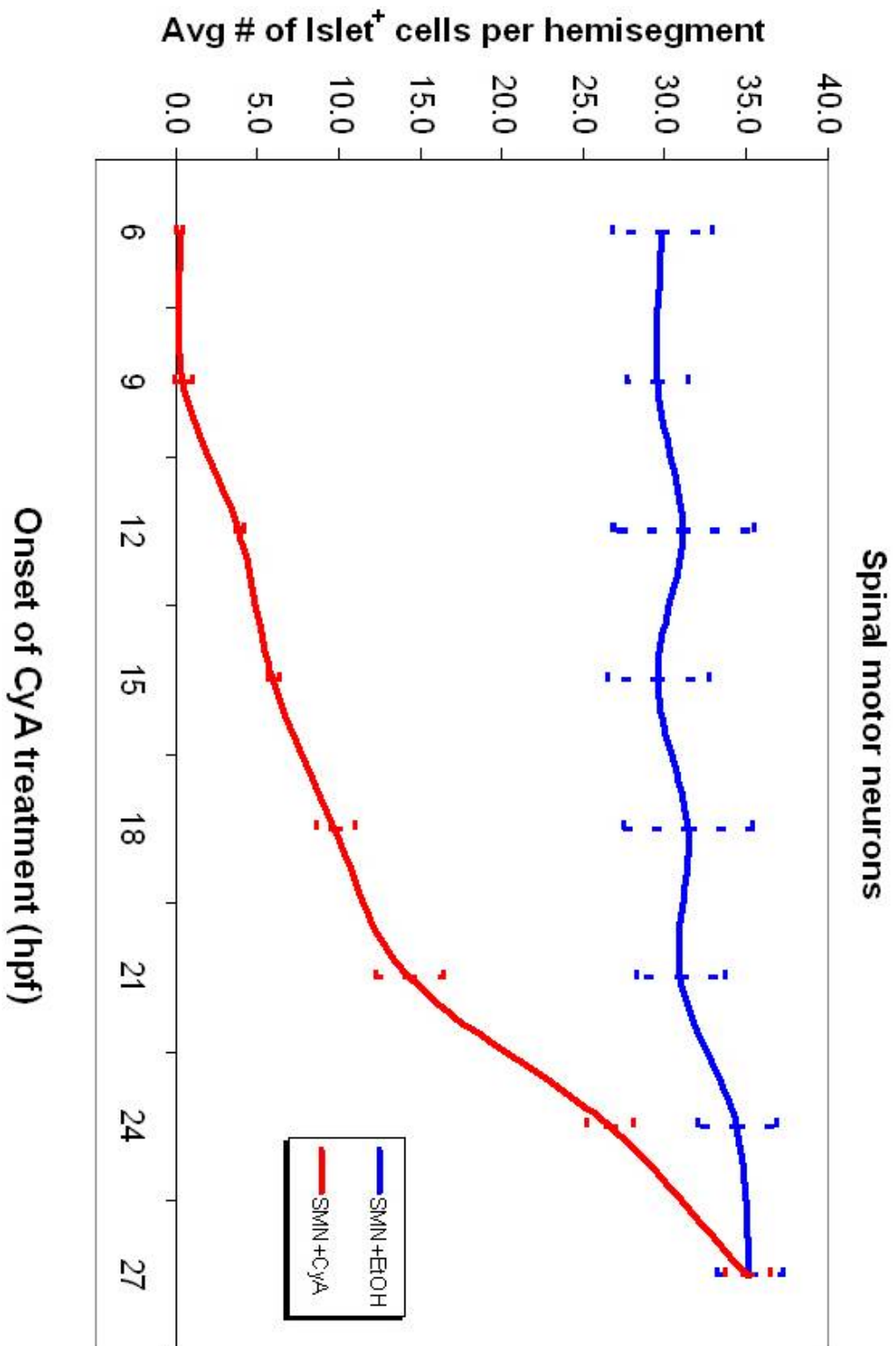
FIGURE 35. For proper induction, secondary spinal motor neurons, a somatic subtype, require Hh signaling across a long duration.

In the trunk, the average number of Islet-expressing spinal motor neurons, a somatomotor neuron population, is about 32 cells per hemisegment in ethanol-treated control embryos (blue line). CyA inhibition of Hh signaling at 6 and 9 hpf eliminates all spinal motor neuron induction (red line). From 12 hpf through 24 hpf of CyA treatment, cell number progressively increases, returning to normal by 27 hpf (red line).

TABLE 10. Temporal requirements for Hh-mediated motor neuron induction in the hindbrain and spinal cord.

Phenotype[@]	Number of islet antibody-labeled neurons		
	Hindbrain (nV neurons)$^{\varphi}$	Hindbrain (nVII neurons)$^{\lambda}$	Ventral spinal cord (motor neurons)$^{\xi}$
WT+EtOH (9hpf)	35.7±5.1	139.0±4.4	29.5±1.9
+CyA (9hpf)	2.0±1.0	0.0±0.0	0.4±0.5
Ratio	0.06***	0.00***	0.01***
WT+EtOH (18hpf)	33.7±1.5	134.7±5.9	31.4±4.0
+CyA (18hpf)	30.3±2.5	77.0±4.0	9.7±1.2
Ratio	0.90^{NS}	0.57***	0.31***
WT+EtOH (27hpf)	38.0±3.0	140.3±3.2	35.2±2.0
+CyA (27hpf)	37.0±2.0	141.3±8.5	35.1±1.4
Ratio	0.97^{NS}	1.01^{NS}	1.00^{NS}

TABLE 10. Temporal requirements for Hh-mediated motor neuron induction in the hindbrain and spinal cord.

$^{@}$n=3 embryos

φTotal number of labeled cells in rhombomere 2

λTotal number of labeled cells in rhombomeres 4-7

ξAverage number of labeled cells per hemisegment

***Strong statistical significance, P value < 0.001

^{NS} No statistical significance, P value > 0.05

temporal requirements for Hh signaling (Figures 32, 33, and 37). *Islet1*-GFP

transgenic embryos were treated with BrdU beginning as early as 9 hpf and for

every 3 hour interval until 27 hpf. BrdU incorporation in differentiated motor

neurons was then assessed at 36 hpf of development. We observed a subtle,

but statistically significant, difference in the terminal S-phases of these two BMN

subtypes. For nV trigeminal BMNs in r2, progenitors incorporated BrdU for the

last time at 18 hpf while nVII BMNs still incorporated BrdU by 21 hpf of

development (Figure 36). Thus, the terminal S-phase of nV BMN progenitors

found in r2 occurs 3 hours prior to that of nVII facial BMN progenitors. The fact

that r2 nV BMN progenitors are still in S-phase at 18 hpf (Figure 36) is also

somewhat surprising as r2 nV BMNs no longer require Hh signaling by 15 hpf

(Figure 32).

5.4   DISCUSSION

5.4.1   Expression of *phox2* genes represents the earliest

readout for BMN induction.

In mouse, *phox2b* serves to function as a molecular integrator of Notch

and Hedgehog signaling pathways, for neurogenesis and branchiomotor neuron

specification (Dubreuil et al., 2002; Dubreuil et al., 2000). Given the pivotal role

of *phox2b*, we examined the expression patterns of *phox2a* and *phox2b* in the

zebrafish hindbrain. For *phox2a*, we showed that expression coincided with

mitotic activity at very early ages, suggesting that *phox2a*-expressing cells might

271
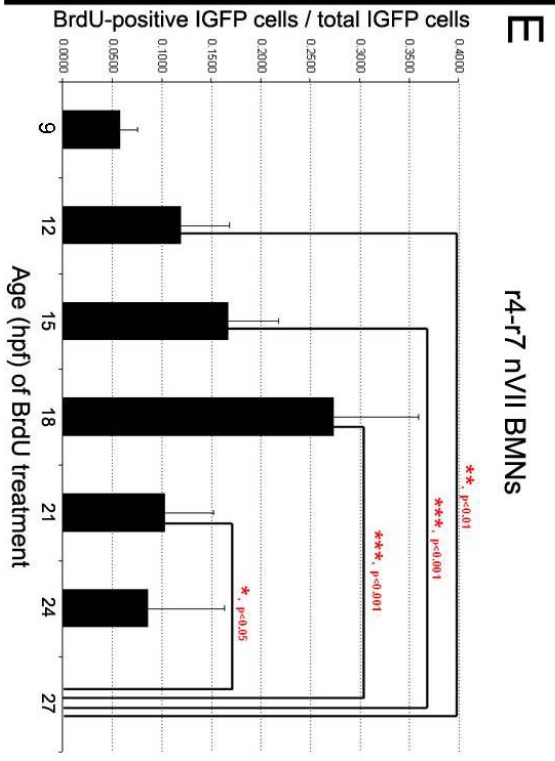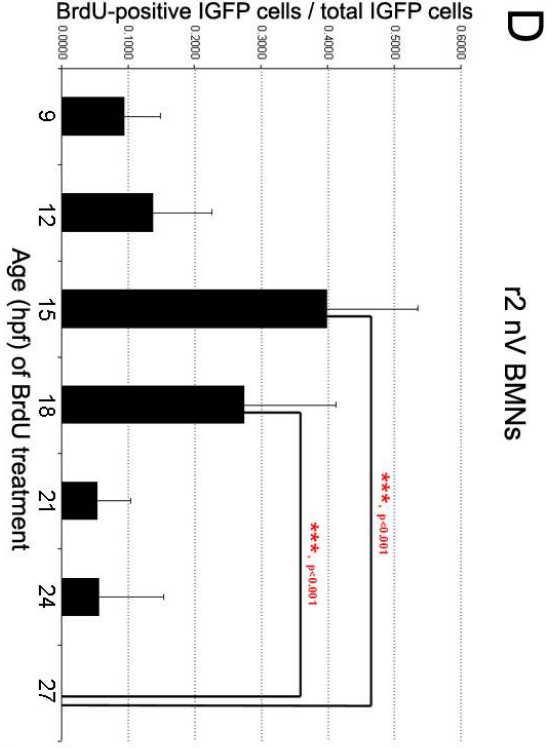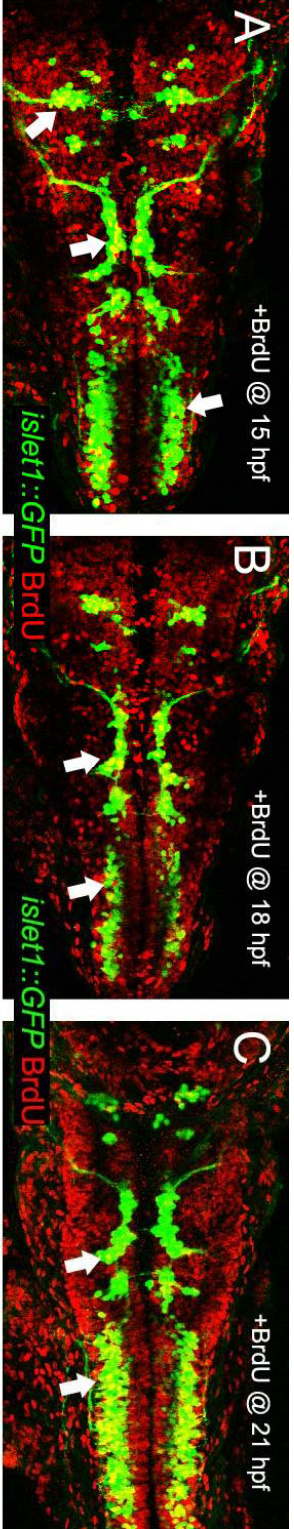
FIGURE 36. Progenitors of different branchiomotor subpopulations enter

S-phase en masse at different times.

Panels A-C show dorsal views of the hindbrain with anterior to the left. **(A-C):** Transgenic *islet*1-

GFP embryos show expression of GFP at 36 hpf in stereotypically-located BMN subpopulations

in the zebrafish head. Administration of BrdU at selected ages labels motor neuron progenitor

cells (white arrows) that were in S-phase at time of incorporation (A-C). **(D, E):**

The majority of trigeminal (nV) motor neuron progenitors from r2 enter a terminal S-phase by 18

hpf ($p < 0.001$) (D). nVII facial branchiomotor neuron progenitors enter terminal S-phase as late

as 21 hpf of development ($p < 0.05$) (E).

be BMN progenitors. Consistent with this, at early ages such as 12 hpf, strong

phox2a and *phox2b* expression was found in cell clusters at the midline, a site

where progenitors are found. The expression patterns of the *phox2* genes at

these early ages are also highly suggestive of functional divisions for zebrafish

BMN differentiation. In the ventral neural tube at 12 hpf, expression of *phox2a* is

located mainly in r2, while *phox2b* is found primarily in r4. However, although

such complementary expression patterns in r2 and r4 might predict subtype

specific phenotypes for *phox2* loss-of-function conditions, we did not observe any

deficits for nV BMNs in r2 of *soulless/phox2a* mutant hindbrains (see also Guo et

al., 1999). This might be due to functional redundancy between *phox2a* and

phox2b genes. Future experiments targeting knockdown of Phox2b translation in

wild type or *soulless* mutant embryos should address this issue. In any case,

expression of the *phox2* genes, especially *phox2a*, is dependent on Hh signaling

and to our knowledge serves as the earliest markers for putative BMN

progenitors in zebrafish.

5.4.2   Different motor neuron subpopulations are induced by Hh

signaling at different times and for different durations.

In vitro, Hh signaling has been shown to drive the formation of various

ventral neural tube cell types, including motor neurons, at different

concentrations and for different durations of ligand exposure (Ericson et al.,

1996; Jessell, 2000). Similarly, application of cyclopamine at different

MOTOR NEURON TYPE

Somatic

Branchial

AGE (hpf)

0 3 6 9 12 15 18 21 24 27

1° + 2° SMNs

2° SMNs

nVI

nVII

r3 nV

r2 nV
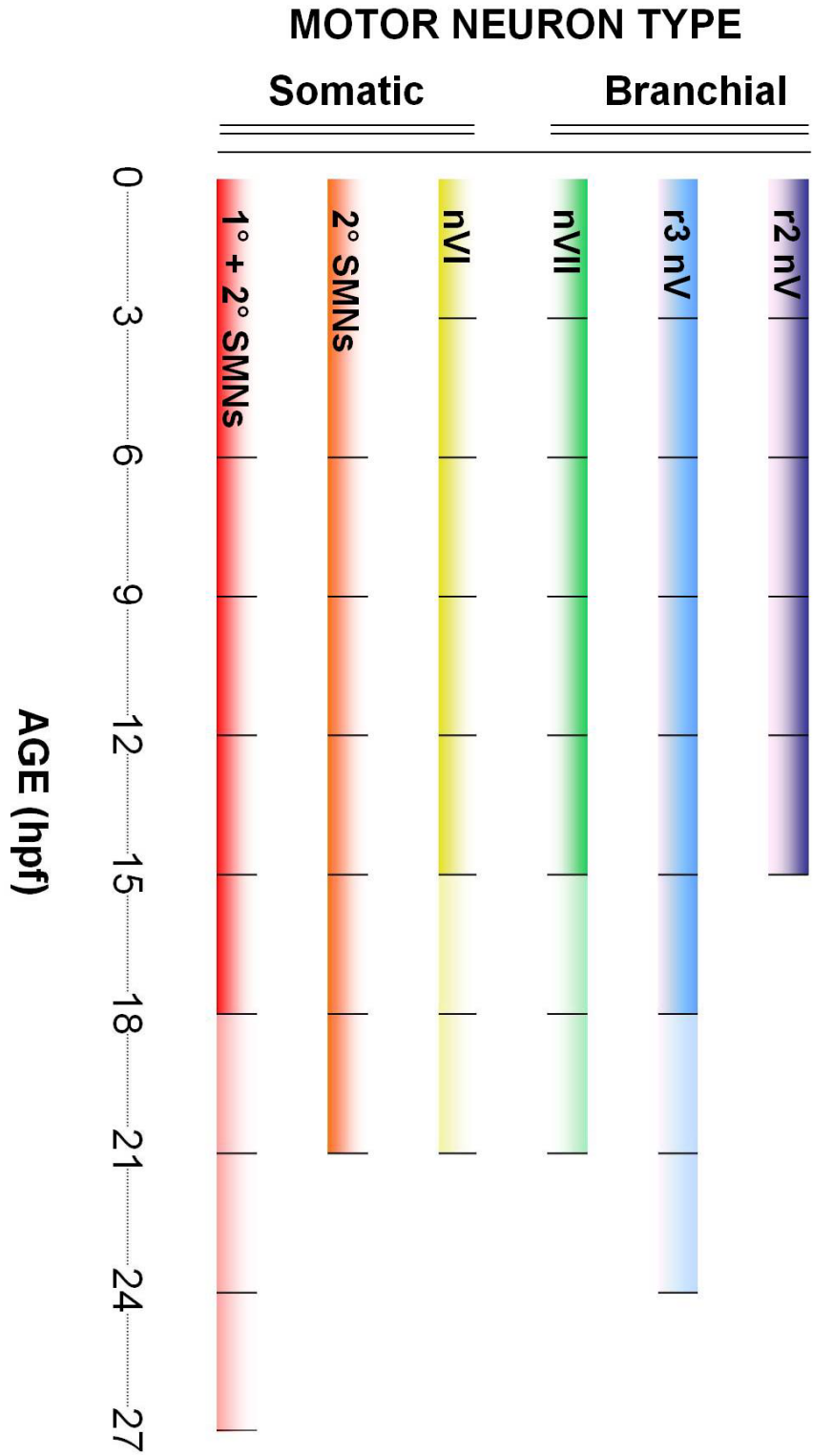
FIGURE 37. Different motor neuron subpopulations are sensitive to Hh pathway blockade at slightly different times.

Critical period offsets for branchiomotor neurons (BMNs) are shown in top three bars (purple, blue, and green) while bottom three bars represent those for somatic motor neurons (yellow, orange, and red). Lightly shaded bars denote ages in which greater than 2/3rd of motor neuron cell number are present. Hedgehog signaling is required at similar ages for the specification of most motor neurons, irregardless or subtype. Remarkably, specification of trigeminal (nV) motor neurons in r2 is complete by 15 hpf (purple bar). For all other motor neurons, Hh signaling is required until 21 hpf (nVII, green bar; nVI, yellow bar), 24 hpf (r3 nV, blue bar), or 27 hpf (all spinal motor neurons). Abbreviations: BMN, branchiomotor neuron; SMN, spinal motor neuron; r2, rhombomere 2; nV, trigeminal BMN; nVII, facial BMN; nVI, abducens cranial motor neuron; 1° SMN, primary spinal motor neuron; 2° SMN, secondary spinal motor neuron.

concentrations or durations reveals critical periods and sensitivities to pharmacological blockade of Hh signaling for motor neuron induction (Cooper et al., 1998; Incardona et al., 1998; Park et al., 2004). We examined whether Hh signaling regulated induction of all motor neuron subtypes at the same time (Figure 37). We did not detect a timing mechanism that favored one motor neuron type over another, but we did observe differences in temporal requirements within subpopulations of a particular type. For instance, nV BMNs in r2 no longer require Hh signaling at 15 hpf of age, while r3 nV BMNs require Hh signaling until as late as 24 hpf (Figure 37). Such differences might be due to the different times at which rhombomeres form (Maves et al., 2002). However, an explanation for temporal differences in Hh requirements based solely on timing of rhombomere formation would be inadequate as r4 is the earliest completed compartment, and nVII facial BMNs require Hh signaling over a very lengthy period (Maves et al., 2002). More likely, different BMN subpopulations are produced by different stochastic mechanisms, which impact the duration by which Hh signaling is required for their induction. In addition, duration of competence to Hh signaling likely refines this process.

5.4.3 Cell-cycle status of BMN progenitors correlates with temporal Hh signaling requirements.

Recent evidence links the Hh signaling pathway to cell cycle regulation in the vertebrate neural tube (Lobjois et al., 2004). Misexpression of Shh in the

chick spinal cord is sufficient to drive *cyclinD1* expression, while cyclopamine-mediated disruption of the Hh signaling pathway eliminates all *cyclinD1* in chick neural tubes (Lobjois et al., 2004). Since the Hh pathway appears to be necessary and sufficient to regulate expression of at least one cell cycle gene, we examined whether we might detect differences in terminal S-phase acquisition among different BMN subpopulations which require Hh signaling at different times. We found that a correlation does exist between the time that BMN subpopulations enter terminal S-phases first and the earliest time at which BMNs no longer require Hh signaling. Thus, Hh signaling appears to drive BMN specification by a compartmentalized mechanism, and acquisition of post-mitotic status in BMN progenitor cells might serve as an early, reliable predictor of Hh signaling.

5.5   ACKNOWLEDGEMENTS

CHAPTER 6

FUTURE DIRECTIONS

Our work has elucidated the molecular players driving motor neuron specification at head and trunk levels of the developing zebrafish embryo. We have also investigated the timing requirements by which Hh signal transduction generates various motor neuron subpopulations, from somatic to branchiomotor neurons. However, as many elements of the motor neuron development story remain unsolved, the zebrafish model organism will serve as an ideal platform to test future hypotheses.

6.1 Do zebrafish *phox2* genes have a role in motor neuron differentiation?

Although zebrafish *phox2a* is not essential for cranial motor neuron induction (Guo et al., 1999) Chapter 5), *phox2a* expression in the ventral neural tube faithfully labels the same motor neuron subpopulations that express *islet1*, a transcription factor essential for motor neuron development (Chandrasekhar et al., 1997; Pfaff et al., 1996). Further, while mouse *phox2b* is necessary for cranial motor neuron induction (Pattyn et al., 2000), the role of zebrafish *phox2b* has not yet been described. At early ages in which Hh signaling is required for

motor neuron induction, *phox2b* is expressed only in putative nVII progenitors (see Chapter 5). Thus, it is quite possible that zebrafish *phox2a* and *phox2b* cooperate for cranial motor neuron specification, at least in rhombomere 4. To examine a role for *phox2* genes in motor neuron induction, we will generate double loss-of-function conditions by injecting *soulless* (*phox2a*) mutants with *phox2b* morpholinos, followed by islet immunohistochemistry and motor neuron quantification.

6.2   Does a Gli-activator / Gli-repressor ratio code exist for motor neuron specification?

Recent work has demonstrated that varying Gli activity is sufficient for the generation of different ventral neural tube cell types in chicken embryos (Stamataki et al., 2005). However, the ability to acquire a fate upon forced Gli-activator expression in no way dictates a requirement nor distribution of endogenous Gli activity codes. We will address the distribution of a potential Gli activity code by first generating antibodies directed against N- and C-termini of Gli1, Gli2, and Gli3. Alternatively, we will construct dual-fluorescent YFP/RFP Gli fusion proteins (YFP-^{N}Gli^C-RFP) for the *in vivo* monitoring of full length versus truncated Gli isoforms (precedence for C-terminal Gli-GFP fusions in mouse limb bud cultures has been set by Haycraft et al., 2005). In the case of dual-fluorescent Gli fusions, we will ensure function is not lost due to fluorophore

presence by misexpressing Gli fusion proteins in zebrafish *gli1* morphants and screening for constructs which rescue expression of Hh-regulated genes. Dual-fluorescent Gli fusion constructs will then be expressed in wild type embryos carrying the *islet1-GFP* transgene, permitting an *in vivo* analysis of the distribution of full-length versus truncated Gli isoforms in differentiated motor neurons. Further, if available, dual-fluorescent Gli fusion constructs will be misexpressed in *phox2a-GFP* transgenic embryos and analyzed at early ages (9 hpf – 15 hpf) for Gli isoform distribution in cranial motor neurons prior to mitotic exit. In doing these experiments, we will detect a putative Gli isoform code, a ratio of full-length Gli isoforms to truncated Gli isoforms. By performing these experiments in transgenic GFP lines reporting both progenitor (*phox2a-GFP*) and differentiation (*islet1-GFP*) status, we can then make the comparison of Gli isoform codes found within *phox2a*-expressing motor neuron progenitors versus *islet1*-expressing differentiated motor neurons. As the *islet1*-GFP transgene is continually expressed over many days, we will also track the persistence of Gli isoforms in the head and trunk motor neurons. Similar experiments can also be performed using the *olig2*-GFP transgenic line and YFP-^{N}Gli^{C}-RFP misexpression to determine whether a Gli isoform code exists specific to somatic versus branchiomotor neurons. These experiments are particularly exciting as they will address whether Gli isoform ratios change from BMN progenitors to differentiated BMNs, and whether any difference exists between differentiated BMNs and somatic motor neurons.

6.3 What is the molecular latency between ligand and transcription factors in mediating Hh signal transduction for motor neuron specification?

Our pharmacological studies have shown that Hh signaling is required for most motor neurons between 10-27 hpf of development, with some branchiomotor neuron populations no longer requiring Hh signaling by 15 hpf (see Chapter 5). It would be interesting to examine a critical period in which Gli function was required for motor neuron specification. Our characterization of the *yot* (*gli2^{ty119}*) mutant allele demonstrated that mutant Gli2^{ty119} functions to dominantly repress Hh signaling for motor neuron specification (see Chapter 4) (Karlstrom et al., 2003). The next step might involve generation of a transgenic line in which dominant negative *gli2^{ty119}* expression is driven by a heat-inducible promoter (*hsp70*) (Halloran et al., 2000). The *hsp70::gli2^{ty119}* transgene would provide an understanding of the *in vivo* temporal Gli requirement necessary for motor neuron specification. As cyclopamine inhibits Hh signaling at the level of Smoothened (Taipale et al., 2000), we might then compare differences between critical periods for both branchiomotor and somatomotor neurons in the head and the trunk. Direct comparisons between pharmacological inhibition (see Chapter 5) and genetic disruption might be difficult to interpret due to differential latencies derived from promoter activation versus drug incorporation. However, misexpression of a dominant-negative form of *patched1$^{\Delta L2}$* is sufficient to reduce motor neuron formation in the chick neural tube at the level of the Hh receptor (Briscoe et al., 2001). Construction then of a second transgenic line

281

($hsp70$::$patched1^{\Delta L2}$) would permit a direct genetic comparison between ligand-regulated versus Gli-regulated critical periods.

6.4 Do primary cilia have a role in Hh signal transduction for zebrafish motor neuron specification?

Primary cilia has been described lining the lumenal surfaces of neural progenitor cells in the mouse neural tube (Huangfu and Anderson, 2005) and mutations in intraflagellar transport components which eliminate primary cilia formation also disrupt motor neuron development in mice (Huangfu and Anderson, 2005; Huangfu and Anderson, 2006; Huangfu et al., 2003; Scholey and Anderson, 2006). Our cyclopamine data suggests that for some branchiomotor neurons, Hh signaling is required prior to neural tube formation, between neural plate and neural keel stages (see Chapter 5). Therefore, if primary cilia have a role in mediating Hh signal transduction, it might occur as early 9 hpf – 15 hpf (see Chapter 5). To locate primary cilia in zebrafish, wild type embryos at early ages will be processed by immunohistochemistry for acetylated-tubulin and analyzed by confocal microscopy. If available, *phox2a*-GFP transgenic embryos will also be stained for acetylated-tubulin to determine whether putative BMN progenitors contain primary cilium.

Intraflagellar transport (IFT) machinery, including anterograde Kinesin-II motor activity, is essential for primary cilium formation in mouse (Huangfu et al.,

2003). To investigate a role for Kinesin-II in the formation of identified zebrafish primary cilia, we will misexpress a dominant-negative form of Kinesin-II (dn-Kinesin-II) which lacks motor domains. dn-Kinesin-II misexpression in Xenopus embryos is sufficient to repress motor activity and induce retinal degeneration (Le Bot et al., 1998; Lin-Jones et al., 2003; Tuma et al., 1998). We will examine the consequences of dn-Kinesin-II transient overexpression on motor neuron specification in the head and the trunk of zebrafish embryos. Differential requirements for motor proteins in mediating Hh signaling along the anterior-posterior axis are entirely possible as mouse *Dnchc2* mutants for the IFT retrograde motor lack motor neurons only in the rostral half of the spinal cord (Huangfu and Anderson, 2005). Further, the finding of a differential Kinesin-II requirement along the rostral-caudal axis would be particularly exciting as a potential mechanistic link to the zebrafish *gli1* motor neuron phenotype (Chandrasekhar et al., 1999).

6.5 Does Hedgehog signaling regulate Gli isoform localization to the primary cilium of motor neuron progenitors?

In cell cultures of mouse limb buds, all full-length Gli isoforms localize to the distal tips of primary cilia (Haycraft et al., 2005), while Gli repressor isoforms remain cytosolic. Further, in MDCK cells, Hh signaling is essential for the

localization of Smoothened protein to primary cilia (Corbit et al., 2005). Localization of Gli isoforms as a consequence of Hh signaling has not yet been described *in vitro* or *in vivo*. In various mutants (e.g. *smo*, *dtr*) of the Hh signaling pathway carrying the *phox2a*-GFP transgene, we will misexpress dual fluorescent YFP-^{N}Gli^C-RFP constructs. Samples will then be fixed at early ages (9-15 hpf), and processed for acetylated-tubulin staining (Far Red) of primary cilium in motor neuron progenitors. Multi-channel confocal imaging will permit an analysis of the role of Hh signaling in the distribution of full-length versus truncated Gli proteins. Further, if dn-Kinesin-II misexpression is sufficient to inhibit motor neuron differentiation (see section 6.4), we will also examine the role of Kinesin-II function in regulating Gli isoformation. As dn-Kinesin-II contains a functional GFP fusion in place of the motor domain (Le Bot et al., 1998; Lin-Jones et al., 2003; Tuma et al., 1998), we will misexpress, in wild type embryos carrying the *phox2a*-GFP transgene, both dn-Kinesin-II and YFP-^{N}Gli^C-RFP constructs to determine the *in vivo* distribution of Gli activator and repressor isoforms. To conditionally attenuate the Hh signaling pathway, similar experiments involving YFP-^{N}Gli^C-RFP misexpression and either *hsp70*::*patched1*$^{\Delta L2}$ or *hsp70*::*gli2*^{ty119} will be performed to address the temporal role by which Hh signaling regulates ongoing Gli activity codes. Further, in all experiments, embryos will also be fixed at 36 hpf and processed for islet antibody staining to form a direct correlation between Gli activator / repressor ratios and BMN induction. Alternatively, a similar, albeit technically simpler, experiment can be performed to address the role of Hh signaling in the distribution of Gli

isoforms. Cyclopamine-treated embryos carrying the *phox2a*-GFP transgene will be fixed at various ages (9 hpf – 21 hpf) and immunostained for primary cilia (acetylated tubulin) and N- and C-terminal specific endogenous Gli antibodies. If endogenous antibodies are unavailable, wild type embryos will be injected with dual epitope tagged *gli* fusion constructs and later treated with cyclopamine, followed by fixation and triple immunohistochemistry.

These experiments are particularly exciting as they would determine the specific Gli activity codes generated by global or real-time changes in the Hh signaling pathway. More importantly, knowledge of such codes would drive future hypotheses directed towards code manipulation when such advanced tools become available.

REFERENCES

Amieux, P. S. and McKnight, G. S. (2002). The essential role of RI alpha in the maintenance of regulated PKA activity. *Ann N Y Acad Sci* **968**, 75-95.

Ang, S. L. and Rossant, J. (1994). HNF-3 beta is essential for node and notochord formation in mouse development. *Cell* **78**, 561-74.

Appel, B. and Eisen, J. S. (1998). Regulation of neuronal specification in the zebrafish spinal cord by Delta function. *Development* **125**, 371-80.

Appel, B., Fritz, A., Westerfield, M., Grunwald, D. J., Eisen, J. S. and Riley, B. B. (1999). Delta-mediated specification of midline cell fates in zebrafish embryos. *Curr Biol* **9**, 247-56.

Appel, B., Korzh, V., Glasgow, E., Thor, S., Edlund, T., Dawid, I. B. and Eisen, J. S. (1995). Motoneuron fate specification revealed by patterned LIM homeobox gene expression in embryonic zebrafish. *Development* **121**, 4117-25.

Artavanis-Tsakonas, S., Rand, M. D. and Lake, R. J. (1999). Notch signaling: cell fate control and signal integration in development. *Science* **284**, 770-6.

Aza-Blanc, P., Lin, H. Y., Ruiz i Altaba, A. and Kornberg, T. B. (2000). Expression of the vertebrate Gli proteins in Drosophila reveals a distribution of activator and repressor activities. *Development* **127**, 4293-301.

Aza-Blanc, P., Ramirez-Weber, F. A., Laget, M. P., Schwartz, C. and Kornberg, T. B. (1997). Proteolysis that is inhibited by hedgehog targets Cubitus interruptus protein to the nucleus and converts it to a repressor. *Cell* **89**, 1043-53.

Bai, C. B., Auerbach, W., Lee, J. S., Stephen, D. and Joyner, A. L. (2002). Gli2, but not Gli1, is required for initial Shh signaling and ectopic activation of the Shh pathway. *Development* **129**, 4753-61.

Bai, C. B. and Joyner, A. L. (2001). Gli1 can rescue the *in vivo* function of Gli2. *Development* **128**, 5161-72.

Bai, C. B., Stephen, D. and Joyner, A. L. (2004). All mouse ventral spinal cord patterning by hedgehog is Gli dependent and involves an activator function of Gli3. *Dev Cell* **6**, 103-15.

Baker, N. E. (2000). Notch signaling in the nervous system. Pieces still missing from the puzzle. *Bioessays* **22**, 264-73.

Barresi, M. J., Stickney, H. L. and Devoto, S. H. (2000). The zebrafish slow-muscle-omitted gene product is required for Hedgehog signal transduction and the development of slow muscle identity. *Development* **127**, 2189-99.

Barth, K. A. and Wilson, S. W. (1995). Expression of zebrafish nk2.2 is influenced by sonic hedgehog/vertebrate hedgehog-1 and demarcates a zone of neuronal differentiation in the embryonic forebrain. *Development* **121**, 1755-68.

Begemann, G., Marx, M., Mebus, K., Meyer, A. and Bastmeyer, M. (2004). Beyond the neckless phenotype: influence of reduced retinoic acid signaling on motor neuron development in the zebrafish hindbrain. *Dev Biol* **271**, 119-29.

Bellaiche, Y., The, I. and Perrimon, N. (1998). Tout-velu is a Drosophila homologue of the putative tumour suppressor EXT-1 and is needed for Hh diffusion. *Nature* **394**, 85-8.

Belloni, E., Muenke, M., Roessler, E., Traverso, G., Siegel-Bartelt, J., Frumkin, A., Mitchell, H. F., Donis-Keller, H., Helms, C., Hing, A. V., Heng, H. H., Koop, B., Martindale, D., Rommens, J. M., Tsui, L. C. and Scherer, S. W. (1996). Identification of Sonic hedgehog as a candidate gene responsible for holoprosencephaly. *Nature Genetics* **14**, 353-6.

Bingham, S., Chaudhari, S., Vanderlaan, G., Itoh, M., Chitnis, A. and Chandrasekhar, A. (2003). Neurogenic phenotype of mind bomb mutants leads to severe patterning defects in the zebrafish hindbrain. *Dev Dyn* **228**, 451-63.

Bingham, S., Higashijima, S., Okamoto, H. and Chandrasekhar, A. (2002). The Zebrafish trilobite gene is essential for tangential migration of branchiomotor neurons. *Dev Biol* **242**, 149-60.

Bingham, S., Nasevicius, A., Ekker, S. C. and Chandrasekhar, A. (2001). Sonic hedgehog and tiggy-winkle hedgehog cooperatively induce zebrafish branchiomotor neurons. *Genesis* **30**, 170-4.

Bitgood, M. J., Shen, L. and McMahon, A. P. (1996). Sertoli cell signaling by Desert hedgehog regulates the male germline. *Curr Biol* **6**, 298-304.

Bose, J., Grotewold, L. and Ruther, U. (2002). Pallister-Hall syndrome phenotype in mice mutant for Gli3. *Hum Mol Genet* **11**, 1129-35.

Bouwmeester, T., Kim, S., Sasai, Y., Lu, B. and De Robertis, E. M. (1996). Cerberus is a head-inducing secreted factor expressed in the anterior endoderm of Spemann's organizer. *Nature* **382**, 595-601.

Brand, M., Heisenberg, C. P., Jiang, Y. J., Beuchle, D., Lun, K., Furutani-Seiki, M., Granato, M., Haffter, P., Hammerschmidt, M., Kane, D. A., Kelsh,

R. N., Mullins, M. C., Odenthal, J., van Eeden, F. J. and Nusslein-Volhard, C. (1996a). Mutations in zebrafish genes affecting the formation of the boundary between midbrain and hindbrain. *Development* **123**, 179-90.

Brand, M., Heisenberg, C. P., Warga, R. M., Pelegri, F., Karlstrom, R. O., Beuchle, D., Picker, A., Jiang, Y. J., Furutani-Seiki, M., van Eeden, F. J., Granato, M., Haffter, P., Hammerschmidt, M., Kane, D. A., Kelsh, R. N., Mullins, M. C., Odenthal, J. and Nusslein-Volhard, C. (1996b). Mutations affecting development of the midline and general body shape during zebrafish embryogenesis. *Development* **123**, 129-42.

Brandon, E. P., Idzerda, R. L. and McKnight, G. S. (1997). PKA isoforms, neural pathways, and behaviour: making the connection. *Curr Opin Neurobiol* **7**, 397-403.

Briscoe, J., Chen, Y., Jessell, T. M. and Struhl, G. (2001). A hedgehog-insensitive form of patched provides evidence for direct long-range morphogen activity of sonic hedgehog in the neural tube. *Mol Cell* **7**, 1279-91.

Briscoe, J., Pierani, A., Jessell, T. M. and Ericson, J. (2000). A homeodomain protein code specifies progenitor cell identity and neuronal fate in the ventral neural tube. *Cell* **101**, 435-45.

Brou, C., Logeat, F., Gupta, N., Bessia, C., LeBail, O., Doedens, J. R., Cumano, A., Roux, P., Black, R. A. and Israel, A. (2000). A novel proteolytic cleavage involved in Notch signaling: the role of the disintegrin-metalloprotease TACE. *Molecular Cell* **5**, 207-16.

Bulgakov, O. V., Eggenschwiler, J. T., Hong, D. H., Anderson, K. V. and Li, T. (2004). FKBP8 is a negative regulator of mouse sonic hedgehog signaling in neural tissues. *Development* **131**, 2149-59.

Burke, R., Nellen, D., Bellotto, M., Hafen, E., Senti, K. A., Dickson, B. J. and Basler, K. (1999). Dispatched, a novel sterol-sensing domain protein dedicated to the release of cholesterol-modified hedgehog from signaling cells. *Cell* **99**, 803-15.

Carpenter, E. M., Goddard, J. M., Chisaka, O., Manley, N. R. and Capecchi, M. R. (1993). Loss of Hox-A1 (Hox-1.6) function results in the reorganization of the murine hindbrain. *Development* **118**, 1063-75.

Caspary, T., Garcia-Garcia, M. J., Huangfu, D., Eggenschwiler, J. T., Wyler, M. R., Rakeman, A. S., Alcorn, H. L. and Anderson, K. V. (2002). Mouse Dispatched homolog1 is required for long-range, but not juxtacrine, Hh signaling. *Curr Biol* **12**, 1628-32.

Cau, E., Gradwohl, G., Fode, C. and Guillemot, F. (1997). Mash1 activates a cascade of bHLH regulators in olfactory neuron progenitors. *Development* **124**, 1611-21.

Chamoun, Z., Mann, R. K., Nellen, D., von Kessler, D. P., Bellotto, M., Beachy, P. A. and Basler, K. (2001). Skinny hedgehog, an acyltransferase required for palmitoylation and activity of the hedgehog signal. *Science* **293**, 2080-4.

Chandrasekhar, A. (2004). Turning heads: development of vertebrate branchiomotor neurons. *Dev Dyn* **229**, 143-61.

Chandrasekhar, A., Moens, C. B., Warren, J. T., Jr., Kimmel, C. B. and Kuwada, J. Y. (1997). Development of branchiomotor neurons in zebrafish. *Development* **124**, 2633-44.

Chandrasekhar, A., Schauerte, H. E., Haffter, P. and Kuwada, J. Y. (1999). The zebrafish detour gene is essential for cranial but not spinal motor neuron induction. *Development* **126**, 2727-37.

Chandrasekhar, A., Warren, J. T., Jr., Takahashi, K., Schauerte, H. E., van Eeden, F. J., Haffter, P. and Kuwada, J. Y. (1998). Role of sonic hedgehog in branchiomotor neuron induction in zebrafish. *Mech Dev* **76**, 101-15.

Chen, C. H., von Kessler, D. P., Park, W., Wang, B., Ma, Y. and Beachy, P. A. (1999). Nuclear trafficking of Cubitus interruptus in the transcriptional regulation of Hedgehog target gene expression. *Cell* **98**, 305-16.

Chen, M. H., Li, Y. J., Kawakami, T., Xu, S. M. and Chuang, P. T. (2004a). Palmitoylation is required for the production of a soluble multimeric Hedgehog protein complex and long-range signaling in vertebrates. *Genes Dev* **18**, 641-59.

Chen, W., Burgess, S. and Hopkins, N. (2001). Analysis of the zebrafish smoothened mutant reveals conserved and divergent functions of hedgehog activity. *Development* **128**, 2385-96.

Chen, W., Ren, X. R., Nelson, C. D., Barak, L. S., Chen, J. K., Beachy, P. A., de Sauvage, F. and Lefkowitz, R. J. (2004b). Activity-dependent internalization of smoothened mediated by beta-arrestin 2 and GRK2. *Science* **306**, 2257-60.

Chen, Y., Gallaher, N., Goodman, R. H. and Smolik, S. M. (1998). Protein kinase A directly regulates the activity and proteolysis of cubitus interruptus. *Proc Natl Acad Sci USA* **95**, 2349-54.

Chen, Y., Goodman, R. H. and Smolik, S. M. (2000). Cubitus interruptus requires Drosophila CREB-binding protein to activate wingless expression in the Drosophila embryo. *Mol Cell Bioll* **20**, 1616-25.

Chiang, C., Litingtung, Y., Lee, E., Young, K. E., Corden, J. L., Westphal, H. and Beachy, P. A. (1996). Cyclopia and defective axial patterning in mice lacking Sonic hedgehog gene function. *Nature* **383**, 407-13.

Chitnis, A., Henrique, D., Lewis, J., Ish-Horowicz, D. and Kintner, C. (1995). Primary neurogenesis in Xenopus embryos regulated by a homologue of the Drosophila neurogenic gene Delta. *Nature* **375**, 761-6.

Coffman, C. R., Skoglund, P., Harris, W. A. and Kintner, C. R. (1993). Expression of an extracellular deletion of Xotch diverts cell fate in Xenopus embryos. *Cell* **73**, 659-71.

Concordet, J. P., Lewis, K. E., Moore, J. W., Goodrich, L. V., Johnson, R. L., Scott, M. P. and Ingham, P. W. (1996). Spatial regulation of a zebrafish patched homologue reflects the roles of sonic hedgehog and protein kinase A in neural tube and somite patterning. *Development* **122**, 2835-46.

Cooke, J., Moens, C., Roth, L., Durbin, L., Shiomi, K., Brennan, C., Kimmel, C., Wilson, S. and Holder, N. (2001). Eph signalling functions downstream of Val to regulate cell sorting and boundary formation in the caudal hindbrain. *Development* **128**, 571-80.

Cooper, A. F., Yu, K. P., Brueckner, M., Brailey, L. L., Johnson, L., McGrath, J. M. and Bale, A. E. (2005). Cardiac and CNS defects in a mouse with targeted disruption of suppressor of fused. *Development* **132**, 4407-17.

Cooper, M. K., Porter, J. A., Young, K. E. and Beachy, P. A. (1998). Teratogen-mediated inhibition of target tissue response to Shh signaling. *Science* **280**, 1603-7.

Cooper, M. S., D'Amico, L. A. and Henry, C. A. (1999). Confocal microscopic analysis of morphogenetic movements. *Methods in Cell Biology* **59**, 179-204.

Copp, A. J., Greene, N. D. and Murdoch, J. N. (2003). The genetic basis of mammalian neurulation. *Nat Rev Genet* **4**, 784-93.

Corbit, K. C., Aanstad, P., Singla, V., Norman, A. R., Stainier, D. Y. and Reiter, J. F. (2005). Vertebrate Smoothened functions at the primary cilium. *Nature* **437**, 1018-21.

Cordes, S. P. and Barsh, G. S. (1994). The mouse segmentation gene kr encodes a novel basic domain-leucine zipper transcription factor. *Cell* **79**, 1025-34.

Cox, W. G. and Hemmati-Brivanlou, A. (1995). Caudalization of neural fate by tissue recombination and bFGF. *Development* **121**, 4349-58.

Criley, B. B. (1969). Analysis of embryonic sources and mechanims of development of posterior levels of chick neural tubes. *J Morphol* **128**, 465-501.

Currie, P. D. and Ingham, P. W. (1996). Induction of a specific muscle cell type by a hedgehog-like protein in zebrafish. *Nature* **382**, 452-5.

Curtin, J. A., Quint, E., Tsipouri, V., Arkell, R. M., Cattanach, B., Copp, A. J., Henderson, D. J., Spurr, N., Stanier, P., Fisher, E. M., Nolan, P. M., Steel, K. P., Brown, S. D., Gray, I. C. and Murdoch, J. N. (2003). Mutation of Celsr1 disrupts planar polarity of inner ear hair cells and causes severe neural tube defects in the mouse. *Curr Biol* **13**, 1129-33.

Dai, P., Akimaru, H., Tanaka, Y., Maekawa, T., Nakafuku, M. and Ishii, S. (1999). Sonic Hedgehog-induced activation of the Gli1 promoter is mediated by GLI3. *J Biol Chem* **274**, 8143-52.

Davis, L. G., Kuehl, M., and Battey, J. F. (1986). Basic Methods in Molecular Biology. University of Pennsylvania. Pennsylvania, Philadelphia: McGraw-Hill Professional.

de la Pompa, J. L., Wakeham, A., Correia, K. M., Samper, E., Brown, S., Aguilera, R. J., Nakano, T., Honjo, T., Mak, T. W., Rossant, J. and Conlon, R. A. (1997). Conservation of the Notch signalling pathway in mammalian neurogenesis. *Development* **124**, 1139-48.

De Strooper, B., Annaert, W., Cupers, P., Saftig, P., Craessaerts, K., Mumm, J. S., Schroeter, E. H., Schrijvers, V., Wolfe, M. S., Ray, W. J., Goate, A. and Kopan, R. (1999). A presenilin-1-dependent gamma-secretase-like protease mediates release of Notch intracellular domain. *Nature* **398**, 518-22.

Deblandre, G. A., Lai, E. C. and Kintner, C. (2001). Xenopus neuralized is a ubiquitin ligase that interacts with XDelta1 and regulates Notch signaling. *Dev Cell* **1**, 795-806.

Denef, N., Neubuser, D., Perez, L. and Cohen, S. M. (2000). Hedgehog induces opposite changes in turnover and subcellular localization of patched and smoothened. *Cell* **102**, 521-31.

Deshaies, R. J. (1999). SCF and Cullin/Ring H2-based ubiquitin ligases. *Annu Rev Cell Dev Biol* **15**, 435-67.

Ding, Q., Motoyama, J., Gasca, S., Mo, R., Sasaki, H., Rossant, J. and Hui, C. C. (1998). Diminished Sonic hedgehog signaling and lack of floor plate differentiation in Gli2 mutant mice. *Development* **125**, 2533-43.

Dubreuil, V., Hirsch, M. R., Jouve, C., Brunet, J. F. and Goridis, C. (2002). The role of Phox2b in synchronizing pan-neuronal and type-specific aspects of neurogenesis. *Development* **129**, 5241-53.

Dubreuil, V., Hirsch, M. R., Pattyn, A., Brunet, J. F. and Goridis, C. (2000). The Phox2b transcription factor coordinately regulates neuronal cell cycle exit and identity. *Development* **127**, 5191-201.

Durston, A. J., Timmermans, J. P., Hage, W. J., Hendriks, H. F., de Vries, N. J., Heideveld, M. and Nieuwkoop, P. D. (1989). Retinoic acid causes an anteroposterior transformation in the developing central nervous system. *Nature* **340**, 140-4.

Edlich, F. and Fischer, G. (2006). Pharmacological targeting of catalyzed protein folding: the example of peptide bond cis/trans isomerases. *Handb Exp Pharmacol*, 359-404.

Eggenschwiler, J. T. and Anderson, K. V. (2000). Dorsal and lateral fates in the mouse neural tube require the cell-autonomous activity of the open brain gene. *Dev Biol* **227**, 648-60.

Eggenschwiler, J. T., Bulgakov, O. V., Qin, J., Li, T. and Anderson, K. V. (2006). Mouse Rab23 regulates hedgehog signaling from smoothened to Gli proteins. *Dev Biol* **290**, 1-12.

Eggenschwiler, J. T., Espinoza, E. and Anderson, K. V. (2001). Rab23 is an essential negative regulator of the mouse Sonic hedgehog signalling pathway. *Nature* **412**, 194-8.

Eisen, J. S. (1991). Motoneuronal development in the embryonic zebrafish. *Development* **Suppl 2**, 141-7.

Ekker, S. C., Ungar, A. R., Greenstein, P., von Kessler, D. P., Porter, J. A., Moon, R. T. and Beachy, P. A. (1995). Patterning activities of vertebrate hedgehog proteins in the developing eye and brain. *Curr Biol* **5**, 944-55.

Entchev, E. V., Schwabedissen, A. and Gonzalez-Gaitan, M. (2000). Gradient formation of the TGF-beta homolog Dpp. *Cell* **103**, 981-91.

Episkopou, V., Arkell, R., Timmons, P. M., Walsh, J. J., Andrew, R. L. and Swan, D. (2001). Induction of the mammalian node requires Arkadia function in the extraembryonic lineages. *Nature* **410**, 825-30.

Ericson, J., Morton, S., Kawakami, A., Roelink, H. and Jessell, T. M. (1996). Two critical periods of Sonic Hedgehog signaling required for the specification of motor neuron identity. *Cell* **87**, 661-73.

Ericson, J., Thor, S., Edlund, T., Jessell, T. M. and Yamada, T. (1992). Early stages of motor neuron differentiation revealed by expression of homeobox gene Islet-1. *Science* **256**, 1555-60.

Fashena, D. and Westerfield, M. (1999). Secondary motoneuron axons localize DM-GRASP on their fasciculated segments. *J Comp Neurol* **406**, 415-24.

Fode, C., Gradwohl, G., Morin, X., Dierich, A., LeMeur, M., Goridis, C. and Guillemot, F. (1998). The bHLH protein NEUROGENIN 2 is a determination factor for epibranchial placode-derived sensory neurons. *Neuron* **20**, 483-94.

Fraser, S., Keynes, R. and Lumsden, A. (1990). Segmentation in the chick embryo hindbrain is defined by cell lineage restrictions. *Nature* **344**, 431-5.

Fuse, N., Maiti, T., Wang, B., Porter, J. A., Hall, T. M., Leahy, D. J. and Beachy, P. A. (1999). Sonic hedgehog protein signals not as a hydrolytic enzyme but as an apparent ligand for patched. *Proc Natl Acad Sci USA* **96**, 10992-9.

Gale, E., Prince, V., Lumsden, A., Clarke, J., Holder, N. and Maden, M. (1996). Late effects of retinoic acid on neural crest and aspects of rhombomere. *Development* **122**, 783-93.

Gale, E., Zile, M. and Maden, M. (1999). Hindbrain respecification in the retinoid-deficient quail. *Mech Dev* **89**, 43-54.

Garcia-Garcia, M. J., Eggenschwiler, J. T., Caspary, T., Alcorn, H. L., Wyler, M. R., Huangfu, D., Rakeman, A. S., Lee, J. D., Feinberg, E. H., Timmer, J. R. and Anderson, K. V. (2005). Analysis of mouse embryonic patterning and morphogenesis by forward genetics. *Proc Natl Acad Sci USA* **102**, 5913-9.

Geldmacher-Voss, B., Reugels, A. M., Pauls, S. and Campos-Ortega, J. A. (2003). A 90-degree rotation of the mitotic spindle changes the orientation of mitoses of zebrafish neuroepithelial cells. *Development* **130**, 3767-80.

Giguere, V. (1994). Retinoic acid receptors and cellular retinoid binding proteins: complex interplay in retinoid signaling. *Endocr Rev* **15**, 61-79.

Goodrich, L. V., Milenkovic, L., Higgins, K. M. and Scott, M. P. (1997). Altered neural cell fates and medulloblastoma in mouse patched mutants. *Science* **277**, 1109-13.

Graper, L. (1913). Die Rhombomeren und ihre Nervenbeziehungen. *Arch. Mikr. Anat.* **83**.

Gray, M., Moens, C. B., Amacher, S. L., Eisen, J. S. and Beattie, C. E. (2001). Zebrafish deadly seven functions in neurogenesis. *Dev Biol* **237**, 306-23.

Gridley, T. (1997). Notch signaling in vertebrate development and disease. *Mol & Cell Neuro* **9**, 103-8.

Griffith, C. M., Wiley, M. J. and Sanders, E. J. (1992). The vertebrate tail bud: three germ layers from one tissue. *Anat Embryol (Berl)* **185**, 101-13.

Gritli-Linde, A., Lewis, P., McMahon, A. P. and Linde, A. (2001). The whereabouts of a morphogen: direct evidence for short- and graded long-range activity of hedgehog signaling peptides. *Dev Biol* **236**, 364-86.

Guo, S., Brush, J., Teraoka, H., Goddard, A., Wilson, S. W., Mullins, M. C. and Rosenthal, A. (1999). Development of noradrenergic neurons in the zebrafish hindbrain requires BMP, FGF8, and the homeodomain protein soulless/Phox2a. *Neuron* **24**, 555-66.

Guthrie, S., Prince, V. and Lumsden, A. (1993). Selective dispersal of avian rhombomere cells in orthotopic and heterotopic grafts. *Development* **118**, 527-38.

Haddon, C., Jiang, Y. J., Smithers, L. and Lewis, J. (1998a). Delta-Notch signalling and the patterning of sensory cell differentiation in the zebrafish ear: evidence from the mind bomb mutant. *Development* **125**, 4637-44.

Haddon, C., Smithers, L., Schneider-Maunoury, S., Coche, T., Henrique, D. and Lewis, J. (1998b). Multiple delta genes and lateral inhibition in zebrafish primary neurogenesis. *Development* **125**, 359-70.

Halloran, M. C., Sato-Maeda, M., Warren, J. T., Su, F., Lele, Z., Krone, P. H., Kuwada, J. Y. and Shoji, W. (2000). Laser-induced gene expression in specific cells of transgenic zebrafish. *Development* **127**, 1953-60.

Halpern, M. E., Thisse, C., Ho, R. K., Thisse, B., Riggleman, B., Trevarrow, B., Weinberg, E. S., Postlethwait, J. H. and Kimmel, C. B. (1995). Cell-autonomous shift from axial to paraxial mesodermal development in zebrafish floating head mutants. *Development* **121**, 4257-64.

Hamblet, N. S., Lijam, N., Ruiz-Lozano, P., Wang, J., Yang, Y., Luo, Z., Mei, L., Chien, K. R., Sussman, D. J. and Wynshaw-Boris, A. (2002). Dishevelled 2 is essential for cardiac outflow tract development, somite segmentation and neural tube closure. *Development* **129**, 5827-38.

Hamilton, G. S. and Steiner, J. P. (1998). Immunophilins: beyond immunosuppression. *J Med Chem* **41**, 5119-43.

Hammerschmidt, M., Bitgood, M. J. and McMahon, A. P. (1996). Protein kinase A is a common negative regulator of Hedgehog signaling in the vertebrate embryo. *Genes Dev* **10**, 647-58.

Han, C., Belenkaya, T. Y., Wang, B. and Lin, X. (2004). Drosophila glypicans control the cell-to-cell movement of Hedgehog by a dynamin-independent process. *Development* **131**, 601-11.

Hansen, C. S., Marion, C. D., Steele, K., George, S. and Smith, W. C. (1997). Direct neural induction and selective inhibition of mesoderm and epidermis inducers by Xnr3. *Development* **124**, 483-92.

Hatta, K. (1992). Role of the floor plate in axonal patterning in the zebrafish CNS. *Neuron* **9**, 629-42.

Haycraft, C. J., Banizs, B., Aydin-Son, Y., Zhang, Q., Michaud, E. J. and Yoder, B. K. (2005). Gli2 and Gli3 localize to cilia and require the intraflagellar transport protein polaris for processing and function. *PLoS Genet* **1**, e53.

Hemmati-Brivanlou, A., Kelly, O. G. and Melton, D. A. (1994). Follistatin, an antagonist of activin, is expressed in the Spemann organizer and displays direct neuralizing activity. *Cell* **77**, 283-95.

Hicke, L. (2001). Protein regulation by monoubiquitin. *Nature Reviews* **2**, 195-201.

Higashijima, S., Hotta, Y. and Okamoto, H. (2000). Visualization of cranial motor neurons in live transgenic zebrafish expressing green fluorescent protein under the control of the islet-1 promoter/enhancer. *J Neurosci* **20**, 206-18.

Hirano, S., Fuse, S. and Sohal, G. S. (1991). The effect of the floor plate on pattern and polarity in the developing central nervous system. *Science* **251**, 310-3.

Hirokawa, N., Tanaka, Y., Okada, Y. and Takeda, S. (2006). Nodal flow and the generation of left-right asymmetry. *Cell* **125**, 33-45.

Holley, S. A., Geisler, R. and Nusslein-Volhard, C. (2000). Control of her1 expression during zebrafish somitogenesis by a delta-dependent oscillator and an independent wave-front activity. *Genes Dev* **14**, 1678-90.

Holley, S. A., Julich, D., Rauch, G. J., Geisler, R. and Nusslein-Volhard, C. (2002). her1 and the notch pathway function within the oscillator mechanism that regulates zebrafish somitogenesis. *Development* **129**, 1175-83.

Hooper, J. E. and Scott, M. P. (2005). Communicating with Hedgehogs. *Nature Reviews* **6**, 306-17.

Hsu, D. R., Economides, A. N., Wang, X., Eimon, P. M. and Harland, R. M. (1998). The Xenopus dorsalizing factor Gremlin identifies a novel family of secreted proteins that antagonize BMP activities. *Mol Cell* **1**, 673-83.

Huang, Y., Roelink, H. and McKnight, G. S. (2002). Protein kinase A deficiency causes axially localized neural tube defects in mice. *J Biol Chem* **277**, 19889-96.

Huangfu, D. and Anderson, K. V. (2005). Cilia and Hedgehog responsiveness in the mouse. *Proc Natl Acad Sci USA* **102**, 11325-30.

Huangfu, D. and Anderson, K. V. (2006). Signaling from Smo to Ci/Gli: conservation and divergence of Hedgehog pathways from Drosophila to vertebrates. *Development* **133**, 3-14.

Huangfu, D., Liu, A., Rakeman, A. S., Murcia, N. S., Niswander, L. and Anderson, K. V. (2003). Hedgehog signalling in the mouse requires intraflagellar transport proteins. *Nature* **426**, 83-7.

Hui, C. C. and Joyner, A. L. (1993). A mouse model of greig cephalopolysyndactyly syndrome: the extra-toesJ mutation contains an intragenic deletion of the Gli3 gene. *Nat Genet* **3**, 241-6.

Hui, C. C., Slusarski, D., Platt, K. A., Holmgren, R. and Joyner, A. L. (1994). Expression of three mouse homologs of the Drosophila segment polarity gene cubitus interruptus, Gli, Gli-2, and Gli-3, in ectoderm- and mesoderm-derived tissues suggests multiple roles during postimplantation development. *Dev Biol* **162**, 402-13.

Hutchinson, S. A. and Eisen, J. S. (2006). Islet1 and Islet2 have equivalent abilities to promote motoneuron formation and to specify motoneuron subtype identity. *Development* **133**, 2137-47.

Hynes, M., Stone, D. M., Dowd, M., Pitts-Meek, S., Goddard, A., Gurney, A. and Rosenthal, A. (1997). Control of cell pattern in the neural tube by the zinc finger transcription factor and oncogene Gli-1. *Neuron* **19**, 15-26.

Hynes, M., Ye, W., Wang, K., Stone, D., Murone, M., Sauvage, F. and Rosenthal, A. (2000). The seven-transmembrane receptor smoothened cell-autonomously induces multiple ventral cell types. *Nat Neurosci* **3**, 41-6.

Incardona, J. P., Gaffield, W., Kapur, R. P. and Roelink, H. (1998). The teratogenic Veratrum alkaloid cyclopamine inhibits sonic hedgehog signal transduction. *Development* **125**, 3553-62.

Incardona, J. P., Gruenberg, J. and Roelink, H. (2002). Sonic hedgehog induces the segregation of patched and smoothened in endosomes. *Curr Biol* **12**, 983-95.

Ingham, P. W. (1995). Signalling by hedgehog family proteins in Drosophila and vertebrate development. *Curr Opin Gen Dev* **5**, 492-8.

Ingham, P. W. (2001). Hedgehog signaling: a tale of two lipids. *Science* **294**, 1879-81.

Ingham, P. W. and McMahon, A. P. (2001). Hedgehog signaling in animal development: paradigms and principles. *Genes Dev* **15**, 3059-87.

Itoh, M., Kim, C. H., Palardy, G., Oda, T., Jiang, Y. J., Maust, D., Yeo, S. Y., Lorick, K., Wright, G. J., Ariza-McNaughton, L., Weissman, A. M., Lewis, J., Chandrasekharappa, S. C. and Chitnis, A. B. (2003). Mind bomb is a ubiquitin ligase that is essential for efficient activation of Notch signaling by Delta. *Dev Cell* **4**, 67-82.

Jessell, T. M. (2000). Neuronal specification in the spinal cord: inductive signals and transcriptional codes. *Nat Rev Genet* **1**, 20-9.

Jessen, J. R., Topczewski, J., Bingham, S., Sepich, D. S., Marlow, F., Chandrasekhar, A. and Solnica-Krezel, L. (2002). Zebrafish trilobite identifies new roles for Strabismus in gastrulation and neuronal movements. *Nat Cell Biol* **4**, 610-5.

Jia, J., Amanai, K., Wang, G., Tang, J., Wang, B. and Jiang, J. (2002). Shaggy/GSK3 antagonizes Hedgehog signalling by regulating Cubitus interruptus. *Nature* **416**, 548-52.

Jia, J., Tong, C. and Jiang, J. (2003). Smoothened transduces Hedgehog signal by physically interacting with Costal2/Fused complex through its C-terminal tail. *Genes Dev* **17**, 2709-20.

Jiang, J. (2002). Degrading Ci: who is Cul-pable? *Genes Dev* **16**, 2315-21.

Jiang, J. and Struhl, G. (1995). Protein kinase A and hedgehog signaling in Drosophila limb development. *Cell* **80**, 563-72.

Jiang, Y. J., Brand, M., Heisenberg, C. P., Beuchle, D., Furutani-Seiki, M., Kelsh, R. N., Warga, R. M., Granato, M., Haffter, P., Hammerschmidt, M., Kane, D. A., Mullins, M. C., Odenthal, J., van Eeden, F. J. and Nusslein-Volhard, C. (1996). Mutations affecting neurogenesis and brain morphology in the zebrafish, Danio rerio. *Development* **123**, 205-16.

Kanki, J. P., Chang, S. and Kuwada, J. Y. (1994). The molecular cloning and characterization of potential chick DM-GRASP homologs in zebrafish and mouse. *J Neurobiology* **25**, 831-45.

Karlstrom, R. O., Talbot, W. S. and Schier, A. F. (1999). Comparative synteny cloning of zebrafish you-too: mutations in the Hedgehog target gli2 affect ventral forebrain patterning. *Genes Dev* **13**, 388-93.

Karlstrom, R. O., Trowe, T., Klostermann, S., Baier, H., Brand, M., Crawford, A. D., Grunewald, B., Haffter, P., Hoffmann, H., Meyer, S. U., Muller, B. K., Richter, S., van Eeden, F. J., Nusslein-Volhard, C. and Bonhoeffer, F. (1996). Zebrafish mutations affecting retinotectal axon pathfinding. *Development* **123**, 427-38.

Karlstrom, R. O., Tyurina, O. V., Kawakami, A., Nishioka, N., Talbot, W. S., Sasaki, H. and Schier, A. F. (2003). Genetic analysis of zebrafish gli1 and gli2 reveals divergent requirements for gli genes in vertebrate development. *Development* **130**, 1549-64.

Kawakami, T., Kawcak, T., Li, Y. J., Zhang, W., Hu, Y. and Chuang, P. T. (2002). Mouse dispatched mutants fail to distribute hedgehog proteins and are defective in hedgehog signaling. *Development* **129**, 5753-65.

Keeler, R. F. (1969). Teratogenic compounds of Veratrum californicum (Durand). VII. The structure of the glycosidic alkaloid cycloposine. *Steroids* **13**, 579-88.

Kengaku, M. and Okamoto, H. (1995). bFGF as a possible morphogen for the anteroposterior axis of the central nervous system in Xenopus. *Development* **121**, 3121-30.

Kidd, S. and Lieber, T. (2002). Furin cleavage is not a requirement for Drosophila Notch function. *Mech Dev* **115**, 41-51.

Kim, C. H., Ueshima, E., Muraoka, O., Tanaka, H., Yeo, S. Y., Huh, T. L. and Miki, N. (1996). Zebrafish elav/HuC homologue as a very early neuronal marker. *Neurosci Lett* **216**, 109-12.

Kimmel, C. B., Ballard, W. W., Kimmel, S. R., Ullmann, B. and Schilling, T. F. (1995). Stages of embryonic development of the zebrafish. *Dev Dyn* **203**, 253-310.

Kimmel, C. B., Metcalfe, W. K. and Schabtach, E. (1985). T reticular interneurons: a class of serially repeating cells in the zebrafish hindbrain. *The J Comp Neuro* **233**, 365-76.

Kimmel, C. B., Warga, R. M. and Kane, D. A. (1994). Cell cycles and clonal strings during formation of the zebrafish central nervous system. *Development* **120**, 265-76.

Kimmel, C. B. and Westerfield, M. (1990). Primary neurons of the zebrafish. New York: Wiley Interscience.

Kinto, N., Iwamoto, M., Enomoto-Iwamoto, M., Noji, S., Ohuchi, H., Yoshioka, H., Kataoka, H., Wada, Y., Yuhao, G., Takahashi, H. E., Yoshiki, S. and Yamaguchi, A. (1997). Fibroblasts expressing Sonic hedgehog induce osteoblast differentiation and ectopic bone formation. *FEBS Lett* **404**, 319-23.

Klingensmith, J., Ang, S. L., Bachiller, D. and Rossant, J. (1999). Neural induction and patterning in the mouse in the absence of the node and its derivatives. *Dev Biol* **216**, 535-49.

Knecht, A. K., Good, P. J., Dawid, I. B. and Harland, R. M. (1995). Dorsal-ventral patterning and differentiation of noggin-induced neural tissue in the absence of mesoderm. *Development* **121**, 1927-35.

Koebernick, K. and Pieler, T. (2002). Gli-type zinc finger proteins as bipotential transducers of Hedgehog signaling. *Differentiation* **70**, 69-76.

Korzh, V., Edlund, T. and Thor, S. (1993). Zebrafish primary neurons initiate expression of the LIM homeodomain protein Isl-1 at the end of gastrulation. *Development* **118**, 417-25.

Koudijs, M. J., den Broeder, M. J., Keijser, A., Wienholds, E., Houwing, S., van Rooijen, E. M., Geisler, R. and van Eeden, F. J. (2005). The Zebrafish Mutants dre, uki, and lep Encode Negative Regulators of the Hedgehog Signaling Pathway. *PLoS Genet* **1**, 223-234.

Krauss, S., Concordet, J. P. and Ingham, P. W. (1993). A functionally conserved homolog of the Drosophila segment polarity gene hh is expressed in tissues with polarizing activity in zebrafish embryos. *Cell* **75**, 1431-44.

Krishnan, V., Pereira, F. A., Qiu, Y., Chen, C. H., Beachy, P. A., Tsai, S. Y. and Tsai, M. J. (1997). Mediation of Sonic hedgehog-induced expression of COUP-TFII by a protein phosphatase. *Science* **278**, 1947-50.

Kurata, T., Nakabayashi, J., Yamamoto, T. S., Mochii, M. and Ueno, N. (2001). Visualization of endogenous BMP signaling during Xenopus development. *Differentiation* **67**, 33-40.

Lai, E. C., Deblandre, G. A., Kintner, C. and Rubin, G. M. (2001). Drosophila neuralized is a ubiquitin ligase that promotes the internalization and degradation of delta. *Dev Cell* **1**, 783-94.

Lamb, T. M. and Harland, R. M. (1995). Fibroblast growth factor is a direct neural inducer, which combined with noggin generates anterior-posterior neural pattern. *Development* **121**, 3627-36.

Lanzetti, L., Rybin, V., Malabarba, M. G., Christoforidis, S., Scita, G., Zerial, M. and Di Fiore, P. P. (2000). The Eps8 protein coordinates EGF receptor signalling through Rac and trafficking through Rab5. *Nature* **408**, 374-7.

Lauderdale, J. D., Davis, N. M. and Kuwada, J. Y. (1997). Axon tracts correlate with netrin-1a expression in the zebrafish embryo. *Mol & Cell Neuro* **9**, 293-313.

Le Bot, N., Antony, C., White, J., Karsenti, E. and Vernos, I. (1998). Role of xklp3, a subunit of the Xenopus kinesin II heterotrimeric complex, in membrane transport between the endoplasmic reticulum and the Golgi apparatus. *J Cell Biol* **143**, 1559-73.

Lee, J., Platt, K. A., Censullo, P. and Ruiz i Altaba, A. (1997). Gli1 is a target of Sonic hedgehog that induces ventral neural tube development. *Development* **124**, 2537-52.

Lee, J. D. and Treisman, J. E. (2001). Sightless has homology to transmembrane acyltransferases and is required to generate active Hedgehog protein. *Curr Biol* **11**, 1147-52.

Lee, J. J., Ekker, S. C., von Kessler, D. P., Porter, J. A., Sun, B. I. and Beachy, P. A. (1994). Autoproteolysis in hedgehog protein biogenesis. *Science* **266**, 1528-37.

Lee, K. J. and Jessell, T. M. (1999). The specification of dorsal cell fates in the vertebrate central nervous system. *Annu Rev Neurosci* **22**, 261-94.

Lei, Q., Zelman, A. K., Kuang, E., Li, S. and Matise, M. P. (2004). Transduction of graded Hedgehog signaling by a combination of Gli2 and Gli3 activator functions in the developing spinal cord. *Development* **131**, 3593-604.

Lewis, K. E. and Eisen, J. S. (2001). Hedgehog signaling is required for primary motoneuron induction in zebrafish. *Development* **128**, 3485-95.

Lin-Jones, J., Parker, E., Wu, M., Knox, B. E. and Burnside, B. (2003). Disruption of kinesin II function using a dominant negative-acting transgene in Xenopus laevis rods results in photoreceptor degeneration. *Invest Ophthalmol Vis Sci* **44**, 3614-21.

Lin, X. and Perrimon, N. (1999). Dally cooperates with Drosophila Frizzled 2 to transduce Wingless signalling. *Nature* **400**, 281-4.

Linville, A., Gumusaneli, E., Chandraratna, R. A. and Schilling, T. F. (2004). Independent roles for retinoic acid in segmentation and neuronal differentiation in the zebrafish hindbrain. *Dev Biol* **270**, 186-99.

Litingtung, Y. and Chiang, C. (2000). Specification of ventral neuron types is mediated by an antagonistic interaction between Shh and Gli3. *Nat Neurosci* **3**, 979-85.

Liu, A., Wang, B. and Niswander, L. A. (2005). Mouse intraflagellar transport proteins regulate both the activator and repressor functions of Gli transcription factors. *Development* **132**, 3103-11.

Lobjois, V., Benazeraf, B., Bertrand, N., Medevielle, F. and Pituello, F. (2004). Specific regulation of cyclins D1 and D2 by FGF and Shh signaling coordinates cell cycle progression, patterning, and differentiation during early steps of spinal cord development. *Dev Biol* **273**, 195-209.

Logeat, F., Bessia, C., Brou, C., LeBail, O., Jarriault, S., Seidah, N. G. and Israel, A. (1998). The Notch1 receptor is cleaved constitutively by a furin-like convertase. *Proc Natl Acad Sci USA* **95**, 8108-12.

Lowery, L. A. and Sive, H. (2004). Strategies of vertebrate neurulation and a re-evaluation of teleost neural tube formation. *Mech Dev* **121**, 1189-97.

Lum, L. and Beachy, P. A. (2004). The Hedgehog response network: sensors, switches, and routers. *Science* **304**, 1755-9.

Lumsden, A. (1990). The cellular basis of segmentation in the developing hindbrain. *Trends Neurosci* **13**, 329-35.

Lumsden, A. and Keynes, R. (1989). Segmental patterns of neuronal development in the chick hindbrain. *Nature* **337**, 424-8.

Lyons, D. A., Guy, A. T. and Clarke, J. D. (2003). Monitoring neural progenitor fate through multiple rounds of division in an intact vertebrate brain. *Development* **130**, 3427-36.

Ma, Q., Chen, Z., del Barco Barrantes, I., de la Pompa, J. L. and Anderson, D. J. (1998). neurogenin1 is essential for the determination of neuronal precursors for proximal cranial sensory ganglia. *Neuron* **20**, 469-82.

Ma, Y., Erkner, A., Gong, R., Yao, S., Taipale, J., Basler, K. and Beachy, P. A. (2002). Hedgehog-mediated patterning of the mammalian embryo requires transporter-like function of dispatched. *Cell* **111**, 63-75.

Maden, M., Gale, E., Kostetskii, I. and Zile, M. (1996). Vitamin A-deficient quail embryos have half a hindbrain and other neural defects. *Curr Biol* **6**, 417-26.

Manzanares, M., Cordes, S., Kwan, C. T., Sham, M. H., Barsh, G. S. and Krumlauf, R. (1997). Segmental regulation of Hoxb-3 by kreisler. *Nature* **387**, 191-5.

Manzanares, M., Trainor, P. A., Nonchev, S., Ariza-McNaughton, L., Brodie, J., Gould, A., Marshall, H., Morrison, A., Kwan, C. T., Sham, M. H., Wilkinson, D. G. and Krumlauf, R. (1999). The role of kreisler in segmentation during hindbrain development. *Dev Biol* **211**, 220-37.

Marigo, V., Davey, R. A., Zuo, Y., Cunningham, J. M. and Tabin, C. J. (1996). Biochemical evidence that patched is the Hedgehog receptor. *Nature* **384**, 176-9.

Marshall, H., Nonchev, S., Sham, M. H., Muchamore, I., Lumsden, A. and Krumlauf, R. (1992). Retinoic acid alters hindbrain Hox code and induces transformation of rhombomeres 2/3 into a 4/5 identity. *Nature* **360**, 737-41.

Marshall, H., Studer, M., Popperl, H., Aparicio, S., Kuroiwa, A., Brenner, S. and Krumlauf, R. (1994). A conserved retinoic acid response element required for early expression of the homeobox gene Hoxb-1. *Nature* **370**, 567-71.

Marszalek, J. R., Ruiz-Lozano, P., Roberts, E., Chien, K. R. and Goldstein, L. S. (1999). Situs inversus and embryonic ciliary morphogenesis defects in mouse mutants lacking the KIF3A subunit of kinesin-II. *Proc Natl Acad Sci USA* **96**, 5043-8.

Marti, E., Bumcrot, D. A., Takada, R. and McMahon, A. P. (1995). Requirement of 19K form of Sonic hedgehog for induction of distinct ventral cell types in CNS explants. *Nature* **375**, 322-5.

Masai, I., Lele, Z., Yamaguchi, M., Komori, A., Nakata, A., Nishiwaki, Y., Wada, H., Tanaka, H., Nojima, Y., Hammerschmidt, M., Wilson, S. W. and

Okamoto, H. (2003). N-cadherin mediates retinal lamination, maintenance of forebrain compartments and patterning of retinal neurites. *Development* **130**, 2479-94.

Matise, M. P., Epstein, D. J., Park, H. L., Platt, K. A. and Joyner, A. L. (1998). Gli2 is required for induction of floor plate and adjacent cells, but not most ventral neurons in the mouse central nervous system. *Development* **125**, 2759-70.

Maves, L., Jackman, W. and Kimmel, C. B. (2002). FGF3 and FGF8 mediate a rhombomere 4 signaling activity in the zebrafish hindbrain. *Development* **129**, 3825-37.

Maynard, T. M., Jain, M. D., Balmer, C. W. and LaMantia, A. S. (2002). High-resolution mapping of the Gli3 mutation extra-toes reveals a 51.5-kb deletion. *Mamm Genome* **13**, 58-61.

McGinnis, W. and Krumlauf, R. (1992). Homeobox genes and axial patterning. *Cell* **68**, 283-302.

Mendelson, B. (1986). Development of reticulospinal neurons of the zebrafish. I. Time of origin. *J Comp Neuro* **251**, 160-71.

Meng, A., Tang, H., Ong, B. A., Farrell, M. J. and Lin, S. (1997). Promoter analysis in living zebrafish embryos identifies a cis-acting motif required for neuronal expression of GATA-2. *Proc Natl Acad Sci USA* **94**, 6267-72.

Methot, N. and Basler, K. (2000). Suppressor of fused opposes hedgehog signal transduction by impeding nuclear accumulation of the activator form of Cubitus interruptus. *Development* **127**, 4001-10.

Micchelli, C. A., The, I., Selva, E., Mogila, V. and Perrimon, N. (2002). Rasp, a putative transmembrane acyltransferase, is required for Hedgehog signaling. *Development* **129**, 843-51.

Mizuguchi, R., Sugimori, M., Takebayashi, H., Kosako, H., Nagao, M., Yoshida, S., Nabeshima, Y., Shimamura, K. and Nakafuku, M. (2001). Combinatorial roles of olig2 and neurogenin2 in the coordinated induction of pan-neuronal and subtype-specific properties of motoneurons. *Neuron* **31**, 757-71.

Moens, C. B., Cordes, S. P., Giorgianni, M. W., Barsh, G. S. and Kimmel, C. B. (1998). Equivalence in the genetic control of hindbrain segmentation in fish and mouse. *Development* **125**, 381-91.

Moens, C. B. and Fritz, A. (1999). Techniques in neural development. *Methods in Cell Biology* **59**, 253-72.

Moens, C. B. and Prince, V. E. (2002). Constructing the hindbrain: insights from the zebrafish. *Dev Dyn* **224**, 1-17.

Moens, C. B., Yan, Y. L., Appel, B., Force, A. G. and Kimmel, C. B. (1996). valentino: a zebrafish gene required for normal hindbrain segmentation. *Development* **122**, 3981-90.

Mohler, J. and Vani, K. (1992). Molecular organization and embryonic expression of the hedgehog gene involved in cell-cell communication in segmental patterning of Drosophila. *Development* **115**, 957-71.

Motoyama, J., Milenkovic, L., Iwama, M., Shikata, Y., Scott, M. P. and Hui, C. C. (2003). Differential requirement for Gli2 and Gli3 in ventral neural cell fate specification. *Dev Biol* **259**, 150-61.

Murcia, N. S., Richards, W. G., Yoder, B. K., Mucenski, M. L., Dunlap, J. R. and Woychik, R. P. (2000). The Oak Ridge Polycystic Kidney (orpk) disease gene is required for left-right axis determination. *Development* **127**, 2347-55.

Murdoch, J. N., Doudney, K., Paternotte, C., Copp, A. J. and Stanier, P. (2001). Severe neural tube defects in the loop-tail mouse result from mutation of Lpp1, a novel gene involved in floor plate specification. *Hum Mol Genet* **10**, 2593-601.

Murdoch, J. N., Henderson, D. J., Doudney, K., Gaston-Massuet, C., Phillips, H. M., Paternotte, C., Arkell, R., Stanier, P. and Copp, A. J. (2003). Disruption of scribble (Scrb1) causes severe neural tube defects in the circletail mouse. *Hum Mol Genet* **12**, 87-98.

Nakano, Y., Kim, H. R., Kawakami, A., Roy, S., Schier, A. F. and Ingham, P. W. (2004). Inactivation of dispatched 1 by the chameleon mutation disrupts Hedgehog signalling in the zebrafish embryo. *Dev Biol* **269**, 381-92.

Nie, J., McGill, M. A., Dermer, M., Dho, S. E., Wolting, C. D. and McGlade, C. J. (2002). LNX functions as a RING type E3 ubiquitin ligase that targets the cell fate determinant Numb for ubiquitin-dependent degradation. *EMBO J* **21**, 93-102.

Nilsson, M., Unden, A. B., Krause, D., Malmqwist, U., Raza, K., Zaphiropoulos, P. G. and Toftgard, R. (2000). Induction of basal cell carcinomas and trichoepitheliomas in mice overexpressing GLI-1. *Proc Natl Acad Sci USA* **97**, 3438-43.

Nonaka, S., Shiratori, H., Saijoh, Y. and Hamada, H. (2002). Determination of left-right patterning of the mouse embryo by artificial nodal flow. *Nature* **418**, 96-9.

Nonaka, S., Tanaka, Y., Okada, Y., Takeda, S., Harada, A., Kanai, Y., Kido, M. and Hirokawa, N. (1998). Randomization of left-right asymmetry due to loss of nodal cilia generating leftward flow of extraembryonic fluid in mice lacking KIF3B motor protein. *Cell* **95**, 829-37.

Novitch, B. G., Chen, A. I. and Jessell, T. M. (2001). Coordinate regulation of motor neuron subtype identity and pan-neuronal properties by the bHLH repressor Olig2. *Neuron* **31**, 773-89.

Novitch, B. G., Wichterle, H., Jessell, T. M. and Sockanathan, S. (2003). A requirement for retinoic acid-mediated transcriptional activation in ventral neural patterning and motor neuron specification. *Neuron* **40**, 81-95.

Nusslein-Volhard, C. and Wieschaus, E. (1980). Mutations affecting segment number and polarity in Drosophila. *Nature* **287**, 795-801.

Nybakken, K. E., Turck, C. W., Robbins, D. J. and Bishop, J. M. (2002). Hedgehog-stimulated phosphorylation of the kinesin-related protein Costal2 is mediated by the serine/threonine kinase fused. *J Biol Chem* **277**, 24638-47.

Oro, A. E., Higgins, K. M., Hu, Z., Bonifas, J. M., Epstein, E. H., Jr. and Scott, M. P. (1997). Basal cell carcinomas in mice overexpressing sonic hedgehog. *Science* **276**, 817-21.

Osumi, N., Hirota, A., Ohuchi, H., Nakafuku, M., Iimura, T., Kuratani, S., Fujiwara, M., Noji, S. and Eto, K. (1997). Pax-6 is involved in the specification of hindbrain motor neuron subtype. *Development* **124**, 2961-72.

Ou, C. Y., Lin, Y. F., Chen, Y. J. and Chien, C. T. (2002). Distinct protein degradation mechanisms mediated by Cul1 and Cul3 controlling Ci stability in Drosophila eye development. *Genes Dev* **16**, 2403-14.

Oxtoby, E. and Jowett, T. (1993). Cloning of the zebrafish krox-20 gene (krx-20) and its expression during hindbrain development. *Nucleic Acids Res* **21**, 1087-95.

Papan, C. and Campos-Ortega, J. A. (1993). On the formation of the neural keel and neural tube in the zebrafish Danio (Brachydanio rerio). *Roux's Arch. Dev. Biol.* **203**, 178-186.

Park, H. C. and Appel, B. (2003). Delta-Notch signaling regulates oligodendrocyte specification. *Development* **130**, 3747-55.

Park, H. C., Mehta, A., Richardson, J. S. and Appel, B. (2002). olig2 is required for zebrafish primary motor neuron and oligodendrocyte development. *Dev Biol* **248**, 356-68.

Park, H. C., Shin, J. and Appel, B. (2004). Spatial and temporal regulation of ventral spinal cord precursor specification by Hedgehog signaling. *Development* **131**, 5959-69.

Park, H. L., Bai, C., Platt, K. A., Matise, M. P., Beeghly, A., Hui, C. C., Nakashima, M. and Joyner, A. L. (2000). Mouse Gli1 mutants are viable but have defects in SHH signaling in combination with a Gli2 mutation. *Development* **127**, 1593-605.

Parks, A. L., Klueg, K. M., Stout, J. R. and Muskavitch, M. A. (2000). Ligand endocytosis drives receptor dissociation and activation in the Notch pathway. *Development* **127**, 1373-85.

Pattyn, A., Hirsch, M., Goridis, C. and Brunet, J. F. (2000). Control of hindbrain motor neuron differentiation by the homeobox gene Phox2b. *Development* **127**, 1349-58.

Pavletich, N. P. and Pabo, C. O. (1993). Crystal structure of a five-finger GLI-DNA complex: new perspectives on zinc fingers. *Science* **261**, 1701-7.

Pavlopoulos, E., Pitsouli, C., Klueg, K. M., Muskavitch, M. A., Moschonas, N. K. and Delidakis, C. (2001). neuralized Encodes a peripheral membrane protein involved in delta signaling and endocytosis. *Dev Cell* **1**, 807-16.

Penzel, R., Oschwald, R., Chen, Y., Tacke, L. and Grunz, H. (1997). Characterization and early embryonic expression of a neural specific transcription factor xSOX3 in Xenopus laevis. *Int J Dev Biol* **41**, 667-77.

Pepinsky, R. B., Zeng, C., Wen, D., Rayhorn, P., Baker, D. P., Williams, K. P., Bixler, S. A., Ambrose, C. M., Garber, E. A., Miatkowski, K., Taylor, F. R., Wang, E. A. and Galdes, A. (1998). Identification of a palmitic acid-modified form of human Sonic hedgehog. *J Biol Chem* **273**, 14037-45.

Persson, M., Stamataki, D., te Welscher, P., Andersson, E., Bose, J., Ruther, U., Ericson, J. and Briscoe, J. (2002). Dorsal-ventral patterning of the spinal cord requires Gli3 transcriptional repressor activity. *Genes Dev* **16**, 2865-78.

Pfaff, S. L., Mendelsohn, M., Stewart, C. L., Edlund, T. and Jessell, T. M. (1996). Requirement for LIM homeobox gene Isl1 in motor neuron generation reveals a motor neuron-dependent step in interneuron differentiation. *Cell* **84**, 309-20.

Placzek, M. (1995). The role of the notochord and floor plate in inductive interactions. *Curr Opin Genet Dev* **5**, 499-506.

Placzek, M., Tessier-Lavigne, M., Yamada, T., Jessell, T. and Dodd, J. (1990). Mesodermal control of neural cell identity: floor plate induction by the notochord. *Science* **250**, 985-8.

Porter, J. A., Ekker, S. C., Park, W. J., von Kessler, D. P., Young, K. E., Chen, C. H., Ma, Y., Woods, A. S., Cotter, R. J., Koonin, E. V. and Beachy, P. A. (1996). Hedgehog patterning activity: role of a lipophilic modification mediated by the carboxy-terminal autoprocessing domain. *Cell* **86**, 21-34.

Porter, J. A., von Kessler, D. P., Ekker, S. C., Young, K. E., Lee, J. J., Moses, K. and Beachy, P. A. (1995). The product of hedgehog autoproteolytic cleavage active in local and long-range signalling. *Nature* **374**, 363-6.

Preat, T., Therond, P., Lamour-Isnard, C., Limbourg-Bouchon, B., Tricoire, H., Erk, I., Mariol, M. C. and Busson, D. (1990). A putative serine/threonine protein kinase encoded by the segment-polarity fused gene of Drosophila. *Nature* **347**, 87-9.

Price, M. A. and Kalderon, D. (1999). Proteolysis of cubitus interruptus in Drosophila requires phosphorylation by protein kinase A. *Development* **126**, 4331-9.

Price, M. A. and Kalderon, D. (2002). Proteolysis of the Hedgehog signaling effector Cubitus interruptus requires phosphorylation by Glycogen Synthase Kinase 3 and Casein Kinase 1. *Cell* **108**, 823-35.

Prince, V. E., Moens, C. B., Kimmel, C. B. and Ho, R. K. (1998). Zebrafish hox genes: expression in the hindbrain region of wild type and mutants of the segmentation gene, valentino. *Development* **125**, 393-406.

Pujic, Z. and Malicki, J. (2001). Mutation of the zebrafish glass onion locus causes early cell-nonautonomous loss of neuroepithelial integrity followed by severe neuronal patterning defects in the retina. *Dev Biol* **234**, 454-69.

Qi, M., Zhuo, M., Skalhegg, B. S., Brandon, E. P., Kandel, E. R., McKnight, G. S. and Idzerda, R. L. (1996). Impaired hippocampal plasticity in mice lacking the Cbeta1 catalytic subunit of cAMP-dependent protein kinase. *Proc Natl Acad Sci USA* **93**, 1571-6.

Qiu, L., Joazeiro, C., Fang, N., Wang, H. Y., Elly, C., Altman, Y., Fang, D., Hunter, T. and Liu, Y. C. (2000). Recognition and ubiquitination of Notch by Itch, a hect-type E3 ubiquitin ligase. *J Biol Chem* **275**, 35734-7.

Rand, M. D., Grimm, L. M., Artavanis-Tsakonas, S., Patriub, V., Blacklow, S. C., Sklar, J. and Aster, J. C. (2000). Calcium depletion dissociates and activates heterodimeric notch receptors. *Mol Cell Biol* **20**, 1825-35.

307

Ribisi, S., Jr., Mariani, F. V., Aamar, E., Lamb, T. M., Frank, D. and Harland, R. M. (2000). Ras-mediated FGF signaling is required for the formation of posterior but not anterior neural tissue in Xenopus laevis. *Dev Biol* **227**, 183-96.

Riley, B. B., Chiang, M., Farmer, L. and Heck, R. (1999). The deltaA gene of zebrafish mediates lateral inhibition of hair cells in the inner ear and is regulated by pax2.1. *Development* **126**, 5669-78.

Robbins, D. J., Nybakken, K. E., Kobayashi, R., Sisson, J. C., Bishop, J. M. and Therond, P. P. (1997). Hedgehog elicits signal transduction by means of a large complex containing the kinesin-related protein costal2. *Cell* **90**, 225-34.

Roelink, H., Augsburger, A., Heemskerk, J., Korzh, V., Norlin, S., Ruiz i Altaba, A., Tanabe, Y., Placzek, M., Edlund, T., Jessell, T. M. and et al. (1994). Floor plate and motor neuron induction by vhh-1, a vertebrate homolog of hedgehog expressed by the notochord. *Cell* **76**, 761-75.

Roelink, H., Porter, J. A., Chiang, C., Tanabe, Y., Chang, D. T., Beachy, P. A. and Jessell, T. M. (1995). Floor plate and motor neuron induction by different concentrations of the amino-terminal cleavage product of sonic hedgehog autoproteolysis. *Cell* **81**, 445-55.

Rowitch, D. H., B, S. J., Lee, S. M., Flax, J. D., Snyder, E. Y. and McMahon, A. P. (1999). Sonic hedgehog regulates proliferation and inhibits differentiation of CNS precursor cells. *J Neurosci* **19**, 8954-65.

Ruiz i Altaba, A. (1998). Combinatorial Gli gene function in floor plate and neuronal inductions by Sonic hedgehog. *Development* **125**, 2203-12.

Ruiz i Altaba, A. (1999). Gli proteins encode context-dependent positive and negative functions: implications for development and disease. *Development* **126**, 3205-16.

Sander, M., Paydar, S., Ericson, J., Briscoe, J., Berber, E., German, M., Jessell, T. M. and Rubenstein, J. L. (2000). Ventral neural patterning by Nkx homeobox genes: Nkx6.1 controls somatic motor neuron and ventral interneuron fates. *Genes Dev* **14**, 2134-9.

Sasai, Y., Lu, B., Steinbeisser, H. and De Robertis, E. M. (1995). Regulation of neural induction by the Chd and Bmp-4 antagonistic patterning signals in Xenopus. *Nature* **377**, 757.

Sasaki, H., Nishizaki, Y., Hui, C., Nakafuku, M. and Kondoh, H. (1999). Regulation of Gli2 and Gli3 activities by an amino-terminal repression domain:

implication of Gli2 and Gli3 as primary mediators of Shh signaling. *Development* **126**, 3915-24.

Sbrogna, J. L., Barresi, M. J. and Karlstrom, R. O. (2003). Multiple roles for Hedgehog signaling in zebrafish pituitary development. *Dev Biol* **254**, 19-35.

Schauerte, H. E., van Eeden, F. J., Fricke, C., Odenthal, J., Strahle, U. and Haffter, P. (1998). Sonic hedgehog is not required for the induction of medial floor plate cells in the zebrafish. *Development* **125**, 2983-93.

Schier, A. F., Neuhauss, S. C., Harvey, M., Malicki, J., Solnica-Krezel, L., Stainier, D. Y., Zwartkruis, F., Abdelilah, S., Stemple, D. L., Rangini, Z., Yang, H. and Driever, W. (1996). Mutations affecting the development of the embryonic zebrafish brain. *Development* **123**, 165-78.

Schmitz, B., Papan, C. and Campos-Ortega, J. (1993). Neurulation in the anterior trunk region of the zebrafish Brachydanio rerio. *Roux's Arch. Dev. Biol.* **202**, 250-259.

Schneider-Maunoury, S., Seitanidou, T., Charnay, P. and Lumsden, A. (1997). Segmental and neuronal architecture of the hindbrain of Krox-20 mouse mutants. *Development* **124**, 1215-26.

Schneider, L., Clement, C. A., Teilmann, S. C., Pazour, G. J., Hoffmann, E. K., Satir, P. and Christensen, S. T. (2005). PDGFRalphaalpha signaling is regulated through the primary cilium in fibroblasts. *Curr Biol* **15**, 1861-6.

Scholey, J. M. (2003). Intraflagellar transport. *Annu Rev Cell Dev Biol* **19**, 423-43.

Scholey, J. M. and Anderson, K. V. (2006). Intraflagellar transport and cilium-based signaling. *Cell* **125**, 439-42.

Sekimizu, K., Nishioka, N., Sasaki, H., Takeda, H., Karlstrom, R. O. and Kawakami, A. (2004). The zebrafish iguana locus encodes Dzip1, a novel zinc-finger protein required for proper regulation of Hedgehog signaling. *Development* **131**, 2521-32.

Shirasaki, R. and Pfaff, S. L. (2002). Transcriptional codes and the control of neuronal identity. *Annu Rev Neurosci* **25**, 251-81.

Sisson, J. C., Ho, K. S., Suyama, K. and Scott, M. P. (1997). Costal2, a novel kinesin-related protein in the Hedgehog signaling pathway. *Cell* **90**, 235-45.

Skalhegg, B. S., Huang, Y., Su, T., Idzerda, R. L., McKnight, G. S. and Burton, K. A. (2002). Mutation of the Calpha subunit of PKA leads to growth retardation and sperm dysfunction. *Mol Endocrinol* **16**, 630-9.

Sockanathan, S., Perlmann, T. and Jessell, T. M. (2003). Retinoid receptor signaling in postmitotic motor neurons regulates rostrocaudal positional identity and axonal projection pattern. *Neuron* **40**, 97-111.

Spemann, H. (1938). Embryonic Development and Induction. New Haven, Yale University Press; London, Oxford University Press.

St-Jacques, B., Hammerschmidt, M. and McMahon, A. P. (1999). Indian hedgehog signaling regulates proliferation and differentiation of chondrocytes and is essential for bone formation. *Genes Dev* **13**, 2072-86.

Stamataki, D., Ulloa, F., Tsoni, S. V., Mynett, A. and Briscoe, J. (2005). A gradient of Gli activity mediates graded Sonic Hedgehog signaling in the neural tube. *Genes Dev* **19**, 626-41.

Stegman, M. A., Vallance, J. E., Elangovan, G., Sosinski, J., Cheng, Y. and Robbins, D. J. (2000). Identification of a tetrameric hedgehog signaling complex. *J Biol Chem* **275**, 21809-12.

Stenmark, H., Parton, R. G., Steele-Mortimer, O., Lutcke, A., Gruenberg, J. and Zerial, M. (1994). Inhibition of rab5 GTPase activity stimulates membrane fusion in endocytosis. *EMBO J* **13**, 1287-96.

Stone, D. M., Hynes, M., Armanini, M., Swanson, T. A., Gu, Q., Johnson, R. L., Scott, M. P., Pennica, D., Goddard, A., Phillips, H., Noll, M., Hooper, J. E., de Sauvage, F. and Rosenthal, A. (1996). The tumour-suppressor gene patched encodes a candidate receptor for Sonic hedgehog. *Nature* **384**, 129-34.

Strahle, U., Blader, P., Henrique, D. and Ingham, P. W. (1993). Axial, a zebrafish gene expressed along the developing body axis, shows altered expression in cyclops mutant embryos. *Genes Dev* **7**, 1436-46.

Strahle, U., Fischer, N. and Blader, P. (1997). Expression and regulation of a netrin homologue in the zebrafish embryo. *Mech Dev* **62**, 147-60.

Streit, A., Berliner, A. J., Papanayotou, C., Sirulnik, A. and Stern, C. D. (2000). Initiation of neural induction by FGF signalling before gastrulation. *Nature* **406**, 74-8.

Studer, M., Popperl, H., Marshall, H., Kuroiwa, A. and Krumlauf, R. (1994). Role of a conserved retinoic acid response element in rhombomere restriction of Hoxb-1. *Science* **265**, 1728-32.

Supp, D. M., Brueckner, M., Kuehn, M. R., Witte, D. P., Lowe, L. A., McGrath, J., Corrales, J. and Potter, S. S. (1999). Targeted deletion of the ATP binding domain of left-right dynein confirms its role in specifying development of left-right asymmetries. *Development* **126**, 5495-504.

Supp, D. M., Witte, D. P., Potter, S. S. and Brueckner, M. (1997). Mutation of an axonemal dynein affects left-right asymmetry in inversus viscerum mice. *Nature* **389**, 963-6.

Taipale, J., Chen, J. K., Cooper, M. K., Wang, B., Mann, R. K., Milenkovic, L., Scott, M. P. and Beachy, P. A. (2000). Effects of oncogenic mutations in Smoothened and Patched can be reversed by cyclopamine. *Nature* **406**, 1005-9.

Taipale, J., Cooper, M. K., Maiti, T. and Beachy, P. A. (2002). Patched acts catalytically to suppress the activity of Smoothened. *Nature* **418**, 892-7.

Takke, C., Dornseifer, P., v Weizsacker, E. and Campos-Ortega, J. A. (1999). her4, a zebrafish homologue of the Drosophila neurogenic gene E(spl), is a target of NOTCH signalling. *Development* **126**, 1811-21.

Tanaka, Y., Okada, Y. and Hirokawa, N. (2005). FGF-induced vesicular release of Sonic hedgehog and retinoic acid in leftward nodal flow is critical for left-right determination. *Nature* **435**, 172-7.

Tashiro, S., Michiue, T., Higashijima, S., Zenno, S., Ishimaru, S., Takahashi, F., Orihara, M., Kojima, T. and Saigo, K. (1993). Structure and expression of hedgehog, a Drosophila segment-polarity gene required for cell-cell communication. *Gene* **124**, 183-9.

Tay, S. Y., Ingham, P. W. and Roy, S. (2005). A homologue of the Drosophila kinesin-like protein Costal2 regulates Hedgehog signal transduction in the vertebrate embryo. *Development* **132**, 625-34.

Tetzlaff, M. T., Yu, W., Li, M., Zhang, P., Finegold, M., Mahon, K., Harper, J. W., Schwartz, R. J. and Elledge, S. J. (2004). Defective cardiovascular development and elevated cyclin E and Notch proteins in mice lacking the Fbw7 F-box protein. *Proc Natl Acad Sci USA* **101**, 3338-45.

Thaeron, C., Avaron, F., Casane, D., Borday, V., Thisse, B., Thisse, C., Boulekbache, H. and Laurenti, P. (2000). Zebrafish evx1 is dynamically expressed during embryogenesis in subsets of interneurones, posterior gut and urogenital system. *Mech Dev* **99**, 167-72.

Therond, P. P., Knight, J. D., Kornberg, T. B. and Bishop, J. M. (1996). Phosphorylation of the fused protein kinase in response to signaling from hedgehog. *Proc Natl Acad Sci USA* **93**, 4224-8.

Trevarrow, B., Marks, D. L. and Kimmel, C. B. (1990). Organization of hindbrain segments in the zebrafish embryo. *Neuron* **4**, 669-79.

Tuma, M. C., Zill, A., Le Bot, N., Vernos, I. and Gelfand, V. (1998). Heterotrimeric kinesin II is the microtubule motor protein responsible for pigment dispersion in Xenopus melanophores. *J Cell Biol* **143**, 1547-58.

Tyurina, O. V., Guner, B., Popova, E., Feng, J., Schier, A. F., Kohtz, J. D. and Karlstrom, R. O. (2005). Zebrafish Gli3 functions as both an activator and a repressor in Hedgehog signaling. *Dev Biol* **277**, 537-56.

Ungar, A. R. and Moon, R. T. (1996). Inhibition of protein kinase A phenocopies ectopic expression of hedgehog in the CNS of wild type and cyclops mutant embryos. *Dev Biol* **178**, 186-91.

Vaage, S. (1969). The segmentation of the primitive neural tube in chick embryos (Gallus domesticus). A morphological, histochemical and autoradiographical investigation. *Ergeb Anat Entwicklungsgesch* **41**, 3-87.

van Eeden, F. J., Granato, M., Schach, U., Brand, M., Furutani-Seiki, M., Haffter, P., Hammerschmidt, M., Heisenberg, C. P., Jiang, Y. J., Kane, D. A., Kelsh, R. N., Mullins, M. C., Odenthal, J., Warga, R. M., Allende, M. L., Weinberg, E. S. and Nusslein-Volhard, C. (1996). Mutations affecting somite formation and patterning in the zebrafish, Danio rerio. *Development* **123**, 153-64.

van Straaten, H. W. and Hekking, J. W. (1991). Development of floor plate, neurons and axonal outgrowth pattern in the early spinal cord of the notochord-deficient chick embryo. *Anat Embryol (Berl)* **184**, 55-63.

Vanderlaan, G., Tyurina, O. V., Karlstrom, R. O. and Chandrasekhar, A. (2005). Gli function is essential for motor neuron induction in zebrafish. *Dev Biol* **282**, 550-70.

Varga, Z. M., Amores, A., Lewis, K. E., Yan, Y. L., Postlethwait, J. H., Eisen, J. S. and Westerfield, M. (2001). Zebrafish smoothened functions in ventral neural tube specification and axon tract formation. *Development* **128**, 3497-509.

Wang, B., Fallon, J. F. and Beachy, P. A. (2000a). Hedgehog-regulated processing of Gli3 produces an anterior/posterior repressor gradient in the developing vertebrate limb. *Cell* **100**, 423-34.

Wang, G., Amanai, K., Wang, B. and Jiang, J. (2000b). Interactions with Costal2 and suppressor of fused regulate nuclear translocation and activity of cubitus interruptus. *Genes Dev* **14**, 2893-905.

Wang, G. and Jiang, J. (2004). Multiple Cos2/Ci interactions regulate Ci subcellular localization through microtubule dependent and independent mechanisms. *Dev Biol* **268**, 493-505.

Wang, G., Wang, B. and Jiang, J. (1999). Protein kinase A antagonizes Hedgehog signaling by regulating both the activator and repressor forms of Cubitus interruptus. *Genes Dev* **13**, 2828-37.

Wang, Q., Pan, J. and Snell, W. J. (2006). Intraflagellar transport particles participate directly in cilium-generated signaling in chlamydomonas. *Cell* **125**, 549-62.

Wang, Q. T. and Holmgren, R. A. (1999). The subcellular localization and activity of Drosophila cubitus interruptus are regulated at multiple levels. *Development* **126**, 5097-106.

Wang, Q. T. and Holmgren, R. A. (2000). Nuclear import of cubitus interruptus is regulated by hedgehog via a mechanism distinct from Ci stabilization and Ci activation. *Development* **127**, 3131-9.

Waskiewicz, A. J., Rikhof, H. A. and Moens, C. B. (2002). Eliminating zebrafish pbx proteins reveals a hindbrain ground state. *Dev Cell* **3**, 723-33.

Wechsler-Reya, R. and Scott, M. P. (2001). The developmental biology of brain tumors. *Annu Rev Neurosci* **24**, 385-428.

Weissman, A. M. (2001). Themes and variations on ubiquitylation. *Nature Reviews* **2**, 169-78.

Westerfield, M. (1995). The Zebrafish Book. Eugene, OR: University of Oregon.

Wick, M. J., Ann, D. K. and Loh, H. H. (1995). Molecular cloning of a novel protein regulated by opioid treatment of NG108-15 cells. *Brain Res Mol Brain Res* **32**, 171-5.

Wijgerde, M., McMahon, J. A., Rule, M. and McMahon, A. P. (2002). A direct requirement for Hedgehog signaling for normal specification of all ventral progenitor domains in the presumptive mammalian spinal cord. *Genes Dev* **16**, 2849-64.

Wilbanks, A. M., Fralish, G. B., Kirby, M. L., Barak, L. S., Li, Y. X. and Caron, M. G. (2004). Beta-arrestin 2 regulates zebrafish development through the hedgehog signaling pathway. *Science* **306**, 2264-7.

Wilkinson, D. G., Bhatt, S., Chavrier, P., Bravo, R. and Charnay, P. (1989). Segment-specific expression of a zinc-finger gene in the developing nervous system of the mouse. *Nature* **337**, 461-4.

Wilson, S. I. and Edlund, T. (2001). Neural induction: toward a unifying mechanism. *Nat Neurosci* **4 Suppl**, 1161-8.

Wizenmann, A. and Lumsden, A. (1997). Segregation of rhombomeres by differential chemoaffinity. *Mol Cell Neurosci* **9**, 448-59.

Wolff, C., Roy, S. and Ingham, P. W. (2003). Multiple muscle cell identities induced by distinct levels and timing of hedgehog activity in the zebrafish embryo. *Curr Biol* **13**, 1169-81.

Wolff, C., Roy, S., Lewis, K. E., Schauerte, H., Joerg-Rauch, G., Kirn, A., Weiler, C., Geisler, R., Haffter, P. and Ingham, P. W. (2004). iguana encodes a novel zinc-finger protein with coiled-coil domains essential for Hedgehog signal transduction in the zebrafish embryo. *Genes Dev* **18**, 1565-76.

Wu, G., Lyapina, S., Das, I., Li, J., Gurney, M., Pauley, A., Chui, I., Deshaies, R. J. and Kitajewski, J. (2001). SEL-10 is an inhibitor of notch signaling that targets notch for ubiquitin-mediated protein degradation. *Mol Cell Biol* **21**, 7403-15.

Xie, J., Murone, M., Luoh, S. M., Ryan, A., Gu, Q., Zhang, C., Bonifas, J. M., Lam, C. W., Hynes, M., Goddard, A., Rosenthal, A., Epstein, E. H., Jr. and de Sauvage, F. J. (1998). Activating Smoothened mutations in sporadic basal-cell carcinoma. *Nature* **391**, 90-2.

Xu, Q., Mellitzer, G., Robinson, V. and Wilkinson, D. G. (1999). In vivo cell sorting in complementary segmental domains mediated by Eph receptors and ephrins. *Nature* **399**, 267-71.

Yamada, T., Placzek, M., Tanaka, H., Dodd, J. and Jessell, T. M. (1991). Control of cell pattern in the developing nervous system: polarizing activity of the floor plate and notochord. *Cell* **64**, 635-47.

Yoon, J. W., Liu, C. Z., Yang, J. T., Swart, R., Iannaccone, P. and Walterhouse, D. (1998). GLI activates transcription through a herpes simplex viral protein 16-like activation domain. *J Biol Chem* **273**, 3496-501.

Zeller, J., Schneider, V., Malayaman, S., Higashijima, S., Okamoto, H., Gui, J., Lin, S. and Granato, M. (2002). Migration of zebrafish spinal motor nerves into the periphery requires multiple myotome-derived cues. *Dev Biol* **252**, 241-56.

Zhang, X. M., Ramalho-Santos, M. and McMahon, A. P. (2001). Smoothened mutants reveal redundant roles for Shh and Ihh signaling including regulation of L/R symmetry by the mouse node. *Cell* **106**, 781-92.

VITA

Gary Vanderlaan was born in Las Vegas, Nevada, USA on September 3rd, 1978. In Las Vegas, Gary was educated in the public school system before pursuing a Bachelor's degree in Biology from Truman State University, Kirksville, Missouri, USA. In 2000, Gary obtained a B.S. in Biology and enrolled in graduate school at the University of Missouri-Columbia to pursue a Ph.D. in Biological Sciences. In 2006, Gary has accepted a post-doctoral position with Professor John Dowling at Harvard University's Molecular and Cellular Biology division, to study the roles of genetic factors regulating drug addiction in the nervous system of the developing larval zebrafish.